Conditional Many-Body Dynamics and Quantum Control of Ultracold Fermions and Bosons in Optical Lattices Coupled to Quantized Light

Gabriel Mazzucchi

Department of Physics

University of Oxford

This dissertation is submitted for the degree of

Doctor of Philosophy

Keble College | Trinity Term 2016

Ai miei genitori, con perenne gratitudine.

To my loving parents, with endless gratitude.

Acknowledgements

The work contained in this thesis would have not been possible without the help and support of numerous individuals. First, I would like to thank my supervisor Igor Mekhov for helping and encouraging me during these past four years in Oxford. He has been an excellent mentor for deepening my understanding of the topics in this work and developing my scientific career. A special thanks goes to Wojciech Kozlowski and Santiago Caballero Benitez for the stimulating discussions and the for the fruitful time we have spent together. Moreover, I would like to thank my co-authors Thomas Elliott and Denis Ivanov with whom I have collaborated during these years. I must also express my gratitude to Keble College and EPSRC for providing the means that allowed me to live and study in Oxford.

A big thanks goes to my parents and to Alex for the support they have showed me and for being always close to me despite of the distance that separates us. I dedicate this thesis to them with all my respect and gratitude. Last but not least, I express my gratitude and love to my wife Melanny. She has always been on my side and played a fundamental role in helping me to cope with the most stressful and frustrating moments of my PhD.

Oxford, September 2016

Conditional Many-Body Dynamics and Quantum Control of Ultracold Fermions and Bosons in Optical Lattices Coupled to Quantized Light

Gabriel Mazzucchi, Keble College
A thesis submitted for the degree of Doctor of Philosophy
Trinity Term 2016

Abstract

We study the atom-light interaction in the fully quantum regime, with the focus on off-resonant light scattering into a cavity from ultracold atoms trapped in an optical lattice. Because of the global coupling between the atoms and the light modes, observing the photons leaking from the cavity allows the quantum nondemolition (QND) measurement of quantum correlations of the atomic ensemble, distinguishing between different quantum states. Moreover, the detection of the photons perturbs the quantum state of the atoms via the so-called measurement backaction. This effect constitutes an unusual additional dynamical source in a many-body strongly correlated system and it is able to efficiently compete with its intrinsic short-range dynamics. This competition becomes possible due to the ability to change the spatial profile of a global measurement at a microscopic scale comparable to the lattice period, without the need of single site addressing. We demonstrate nontrivial dynamical effects such as large-scale multimode oscillations, breakup and protection of strongly interacting fermion pairs. We show that measurement backaction can be exploited for realizing quantum states with spatial modulations of the density and magnetization, thus overcoming usual requirement for a strong interatomic interactions. We propose detection schemes for implementing antiferromagnetic states and density waves and we demonstrate that such long-range correlations cannot be realized with local addressing. Finally, we describe how to stabilize these emerging phases with the aid of quantum feedback. Such a quantum optical approach introduces into many-body physics novel processes, objects, and methods of quantum engineering, including the design of many-body entangled environments for open systems and it is easily extendable to other systems promising for quantum technologies.

Supervisor: Dr. Igor B. Mekhov, University of Oxford.

DPhil Examination occurred at 3:00pm on Friday 9th December 2016.

Internal Examiner: Dr. Joshua Nunn, University of Oxford.

External Examiner: Prof. Helmut Ritsch, Institute for Theoretical Physics, University of Innsbruck.

Table of contents

List of figures **ix**

List of tables **xii**

1 Introduction **1**

1.1 Thesis overview 6

2 Quantum optics with quantum gases **9**

2.1 Light scattering from ultracold atoms 10

2.1.1 Optical lattices 10

2.1.2 Ultracold gases coupled to quantized light modes 12

2.2 QND probing of the atomic system 19

2.2.1 Quantum addition to the classical scattering pattern 25

2.2.2 Generation of spatial modes by global scattering 29

2.2.3 QND measurement in fermionic systems 30

2.2.4 3D Fermi gas in free space 32

2.2.5 Probing local fluctuations in the magnetization 37

2.3 Light mediated synthetic atom-atom interaction 40

2.3.1 One probe and one cavity 43

2.3.2 Multiple probes and one cavity 45

2.3.3 Multiple cavity modes and one probe 48

2.4 Discussion 51

3 Quantum measurement 53

3.1 Conditional dynamics of a quantum system 54

3.1.1 Quantum trajectories 54

3.1.2 Simulating quantum trajectories 59

3.2 Quantum state engineering via measurement backaction 61

3.2.1 Generation of number-squeezed states and Schrödinger cat states 65

3.3 Ensemble averages and master equation 70

3.3.1 Inefficient detection 74

3.4 Discussion 75

4 Measurement-induced dynamics in ultracold gases in optical lattices 77

4.1 Competition between tunneling and measurement 78

4.2 Effective dynamics of macroscopic spatial modes in bosonic systems . . . 80

4.3 Large-scale dynamics due to weak measurement 84

4.3.1 Probing the odd sites of the optical lattice 88

4.3.2 Case $J = 0$ 96

4.3.3 Case $J \neq 0$ 96

4.3.4 Effect of detector efficiency 102

4.3.5 Stochastic differential equations and measurement 104

4.4 Beyond non-interacting bosons 109

4.4.1 Fermi systems 111

4.4.2 Competition between tunneling, measurement and interactions . . 114

4.5 Extensions for multimode photonic systems 121

4.6 Discussion 123

5 Measurement-induced magnetic order and density modulations in ultracold Fermi gases in optical lattices 125

5.1 Monitoring Fermi systems 126

5.2 Measurement-induced antiferromagnetic ordering 128

5.3 Measurement-induced density ordering 132

5.4 Discussion 137

6 Quantum optical feedback control for creating strong correlations in many-body systems 139

6.1 Conditional dynamics of the atomic state in presence of feedback 140

6.2 Feedback-stabilized density waves and antiferromagnetic ordering 145

6.3 Discussion 151

Summary and Conclusions 153

References 157

List of figures

2.1 Examples of different optical lattices that can be obtained by combining more laser beams . . . 11
2.2 Schematic illustration of the measurement setup . . . 13
2.3 Classical diffraction patterns and quantum addition for fermions in an optical lattice . . . 32
2.4 Chemical potential and order parameter Δ for a 3D uniform Fermi gas . 37
2.5 Relative fluctuations for the detected photons in the forward direction as a function of the atomic interaction . . . 39
2.6 Relative fluctuations for the detected photons in the forward direction as a function of the Pippard length . . . 40
2.7 Synthetic light-mediated interactions using a single cavity and one probe beam . . . 44
2.8 Synthetic light-mediated interactions that can be engineered using traveling waves . . . 47
2.9 Schematic representation of a setup where atoms can scatter light to multiple quantized light modes . . . 49

3.1 Conditional dynamics in a single quantum trajectory for non-interacting fermions (I) . . . 68

3.2 Conditional dynamics in a single quantum trajectory for non-interacting fermions (II) . . . 70
3.3 Ensemble averages over many quantum trajectories . . . 73

4.1 Oscillatory dynamics in the absence of measurement starting from an imbalanced state . . . 85
4.2 Oscillatory dynamics induced by the measurement process in a single quantum trajectory for non-interacting bosons . . . 86
4.3 Effect of the quantum jumps on the atomic observables neglecting the non-Hermitian dynamics . . . 94
4.4 Close orbits around the stable point if quantum jumps and non-Hermitian dynamics are neglected . . . 95
4.5 Effect of the quantum jumps on the dynamics of the system around the stable point setting $\Gamma = 0$ . . . 98
4.6 Under-damped oscillations around the stable point if quantum jumps and non-Hermitian dynamics are neglected . . . 99
4.7 Conditional dynamics of a two-mode bosonic system in the weak measurement regime . . . 100
4.8 Over-damped oscillations in the strong measurment regime when the quantum jumps are neglected . . . 102
4.9 Conditional dynamics of a two-mode bosonic system in the strong measurement regime . . . 103
4.10 Effect of the detection efficiency on the conditional dynamics . . . 105
4.11 Oscillatory dynamics induced by the measurement process in Fermi systems 113
4.12 Squeezing due to backaction as a function of local interactions and measurement strength . . . 116
4.13 Effect of local interactions on the dynamics of single quantum trajectories 120

5.1 Measurement-induced AFM order in a single experimental run for non-interacting fermions 128
5.2 Measurement-induced AFM order in a single experimental run for interacting fermions 131
5.3 Conditional evolution of the local density in a single experimental run . . 133
5.4 Solution of the mean field equations for a single experimental run 137

6.1 Schematic representation of the experimental setup in presence of feedback 144
6.2 Effect of feedback on the probability distribution of $\hat{N}_{\text{odd}} - \hat{N}_{\text{even}}$ 146
6.3 Effects of measurement and feedback detecting the photons scattered in the diffraction minimum 148
6.4 Effect of measurement and feedback probing the staggered magnetization in a fermionic system 150

List of tables

2.1 Statistical quantities and quantum addition of typical quantum states for bosonic systems 28

Chapter 1

Introduction

It does no harm to the romance of the sunset to know a little bit about it.

Carl Sagan
Pale Blue Dot: A Vision of the Human Future in Space, 1994

Quantum physics is often portrayed as an "esoteric" discipline that concerns only with the microscopic world with few practical applications. This is obviously far from being true: for example, understanding the motion of electrons in a material allowed the semiconductor industries to develop the electronic devices that are permeating our lives today. We can now find that new restaurant without carrying a map, check our finances without going to the bank, take beautiful pictures without dealing with film, and, maybe, read this thesis on a screen without printing it on paper. In the next decades, a new generation of devices that are capable of creating and manipulating the quantum state of matter by exploiting entanglement and quantum superposition promises to enter in our lives. These new technical breakthroughs, usually referred as *quantum technologies*, will have a major impact on our world in the 21st century [1], revolutionizing vast sectors of our society, from finance to medicine to defence. The realization of these promises relies on two fundamental premises: (i) the possibility of building a quantum system that is sufficiently flexible and stable and (ii) understanding the effect of measurement on such a system. Because of their extreme tunablity, one of the most promising physical systems that could be used for implementing new quantum technologies are the so-called ultracold atomic gases. These systems allow to experimentally realize toy Hamiltonians with parameters that can be easily manipulated, opening the possibility of applications in quantum computing and quantum simulations [103].

The realization of the first Bose-Einstein condensate in 1995 [7, 23, 43] started this new field in atomic and molecular physics where the effects of interactions and quantum statistics dominate over single-particle properties. In the following years, many quantum mechanical effects were observed in these systems: from matter wave interference between two overlapping condensates [8] to quantized vortices [2, 104, 107]. At the same time, cooling techniques applied to alkali bosonic systems also began to be applied to the other class of quantum particles, fermions. Interest in these systems arises from the fact that interacting many-body quantum Fermi systems are the building blocks of visible matter. These include, for example, electrons in a metal, strongly correlated materials, superconductors, superfluid ^{3}He but also more exotic systems such as neutron stars, white dwarfs, atomic nuclei and the quark-gluon plasma present in the early universe. The first ultracold Fermi gas was realised in 1999 [44, 173, 183] while the phase transition between the Fermi sea and the superfluid state was first observed in 2004 [16, 22, 153, 196].

The introduction of optical lattices for trapping the atoms in a predetermined crystal-like structure, opened the possibility of using ultracold gases for mimicking Hamiltonians that were first formulated in condensed matter physics. For example, in 1998 [81] it was shown that a system of bosons loaded in an optical lattice can be described by the Bose-Hubbard model and that, by changing the value of the interaction parameter, the atoms undergo a quantum phase transition between a superfluid an Mott insulator state. This phenomenon was subsequently observed in 2002 [67], confirming that ultracold gases are a very convenient setting for studying many-body effects [20]. Loading ultracold attractive fermions in an optical lattice allows to investigate phenomena that are typical of solid state systems such as superconductivity and quantum magnetism. The first one considers the case of strong attractive interactions so that, at sufficiently low temperatures, atoms with opposite momentum form Cooper pairs [153] and an excitation gap opens in the spectrum [39], leading to superfluidity [195]. If the interatomic interactions are repulsive, the ground state of the system reduces to a configuration with very low entropy which exhibit antiferromagnetic (AFM) correlations that were recently observed [66, 73].

Although light is fundamental for trapping the atoms and manipulating their quantum state, its quantum properties are usually neglected. Quantum optics of quantum gases is a relatively new field of research that studies the regime where the quantum nature of both the electromagnetic field and the matter field are equally important. As a consequence, light and atoms become entangled and they develop nontrivial correlations between them. Such correlations have a dual effect on the dynamics of the system. On one hand, the quantum properties of the atoms are mapped on the scattered light allowing to perform quantum nondemolition measurement of the matter observables. On the other hand, the trapping potential becomes a dynamical quantum variable that needs to be determined self-consistently with the atomic state leading to the so-called quantum optical lattices. In the last few years, the interest of the experimental community in these systems grew considerably. Several laboratories were able to implement the building blocks for this proposal: light scattered from ultracold atoms in an optical lattice (without a cavity) has been detected [127, 188] and ultracold bosons have been trapped in an optical cavity (without an optical lattice) [17, 171, 191]. Moreover, very recent experimental breakethroughs were able to couple a system of ultracold bosons loaded in an optical lattice to the cavity modes of an optical cavity [87, 98], achieving the ultimate quantum level of light-matter interaction.

The study of quantum optics of quantum gases is indeed a very broad field of research because of many phenomena that emerge by focusing on the quantum properties of both light and matter. We can summarize it by considering three different areas with growing complexity [120].

Firstly, the coupling between light and matter defines a quantum non-demolition (QND) measurement [28] as the correlations of the quantum state of the atoms are mapped onto the scattered photons and can be observed in real-time. In contrast to the completely destructive measurement schemes that are usually used in ultracold atoms experiments (e. g. time-of-flight and absorption imaging), here observing the photons leaking from the cavity weakly perturbs the atomic state. Thus, it is not necessary to prepare a new atomic sample after each photodetection and many consecutive measurements can be realized on the same system. This approach allows to probe correlations in strongly correlated systems [50, 99] and to characterize their phase diagram identifying quantum phases such as superfluid state, Mott insulator and Bose glass [91]. Moreover, it can be applied to a vast range of physical systems such as bosons [42, 53, 71, 116, 157, 179], fermions [4, 53, 75, 160], spins [49, 89, 158] and complex molecules [114].

Secondly, coupling an ultracold atomic system to the quantized light modes of an optical cavity allows to study the dynamics of a many-body system conditioned to the outcome of the measurement process. Because of the entanglement between light and matter, detecting the photons escaping the optical cavity changes the quantum state of the atoms via the so-called measurement backaction. This typical quantum optical effect cannot be observed in conventional condensed matter systems because of their short coherence time but it is accessible in ultracold atomic systems [120]. Engineering the measurment operator, the perturbation due to its backaction can be exploited for tailoring correlations and preparing interesting quantum states [116]. This is analogous to cavity QED experiments [72, 185] where photonic states such as Fock and Schrödinger cat states were realized using measurement backaction. If the measurement is sufficiently strong, it can freeze the dynamics of the system in a subspace of the Hilbert space realizing the quantum Zeno regime [56]. This effect has been observed in the context of QED cavities [151, 152] and atomic systems [169, 175]. Furthermore, carefully choosing the spatial profile of the measurment operator, it is possible to project the state of the system into a quantum Zeno subspace where specific dynamical processes are enhanced or suppressed [90, 92, 93].

Thirdly, the cavity field mediates an effective long-range interaction between the atoms (usually referred as cavity backaction). This is because the optical cavity strongly enhances the coupling between matter and light so that the atoms scatter photons in a well-defined direction. The effect of the scattered light on the atoms depends on both the light-matter coupling constant and the scattered intensity so that its influence on the atomic system can be comparable to the one due to the probe light beams. Realizations of this effect have been proposed [131] and observed [17] in systems where a BEC is loaded in an optical cavity (without an optical lattice) and the light field induces a phase transition towards a supersolid phase, opening the possibility of studying self-organization for both bosons [94, 144, 155, 174] and fermions [38, 85, 145]. If the atoms are trapped in an optical lattice, the spatial profile of the light-mediated interaction can be easily tuned by changing the angle between the optical cavity and the probe beam. This extreme flexibility could be exploited for realizing novel many-body phases [32–35, 69] and designing long-range correlations. In this regime, the potential trapping the atoms is created by quantum light and thus it becomes a dynamical variable which must be determined self-consistently with the state of the atoms. Depending on the parameter of the system, this quantum trapping potential can shift the position of the quantum phase transition between superfluid and Mott insulator state [106].

In this thesis we will touch all of these three research directions but we will mainly focus on the second one, i. e. the effects of measurement backaction on many-body systems. The work contained in this thesis lead to six publications:

T. J. Elliott, G. Mazzucchi, W. Kozlowski, S. F. Caballero-Benitez, and I. B. Mekhov, "Probing and Manipulating Fermionic and Bosonic Quantum Gases with Quantum Light," *Atoms*, vol. 3, no. 3, pp. 392–406, 2015.

G. Mazzucchi, W. Kozlowski, S. F. Caballero-Benitez, T. J. Elliott, and I. B. Mekhov, "Quantum measurement-induced dynamics of many-body ultracold bosonic and fermionic systems in optical lattices," *Physical Review A*, vol. 93, 8 no. 2, p. 023632, 2016.

S. F. Caballero-Benitez, G. Mazzucchi, and I. B. Mekhov, "Quantum simulators based on the global collective light-matter interaction," *Physical Review A*, vol. 93, 33 p. 063632, 2016.

G. Mazzucchi, W. Kozlowski, S. F. Caballero-Benitez, and I. B. Mekhov, "Collective dynamics of multimode bosonic systems induced by weak quantum measurement," *New Journal of Physics*, vol. 18, no. 7, p. 073017, 2016.

G. Mazzucchi, S. F. Caballero-Benitez, and I. B. Mekhov, "Quantum measurement-induced antiferromagnetic order and density modulations in ultracold Fermi gases in optical lattices," *Scientific Reports*, vol. 6, p. 31196, 2016.

G. Mazzucchi, S. F. Caballero-Benitez, D. A. Ivanov, and I. B. Mekhov, "Quantum optical feedback control for creating strong correlations in many-body systems," *Optica*, vol. 3, no. 11, p. 1213-1219, 2016.

1.1 Thesis overview

The results that are presented in these thesis are based on the content of the publications listed in the previous section. The structure of the thesis is as follows.

- In Chapter 2 we present the quantum mechanical model for describing a system of ultracold atoms loaded in an optical lattice and coupled to the quantized light modes of an optical cavity. We demonstrate that by detecting the photons that leak from the cavity one can realize a quantum non-demolition measurement of the atomic correlations. We apply these ideas to a system of ultracold fermions and we show that the light field can be used for distinguishing different ground states. Moreover, the light field inside the cavity mediates an effective interaction between the atoms. By changing the geometry of the setup, it is possible to tailor the spatial profile of such coupling and realize long-range interactions without recurring to complex physical systems such as polar molecules and Rydberg atoms.

- In Chapter 3 we give a brief introduction on the theory of quantum measurement with special emphasis on the quantum trajectories technique. We illustrate few examples of different measurement configurations and we show that the measurement backaction can be exploited for engineering interesting many-body states such as Schrödinger cat states and squeezed states.

- In Chapter 4 we consider the effect of measurement backaction on bosons and fermions when the effective dynamics introduced by the detection process competes with the atomic tunneling and interactions. We develop an analytic description of the conditional dynamics of a bosonic system showing that the measurement induces collective macroscopic oscillations of the atomic population. Moreover, we demonstrate both the breakup and protection of strongly interacting fermion pairs by continuous monitoring.

- In Chapter 5 we focus on Fermi systems and we present a measurement scheme that allows to induce antiferromagnetic and density correlations on the atoms. We compare our approach to other works based on local addressing and we show that the global coupling between light and matter is crucial for obtaining the effects described in this thesis.

- In Chapter 6 we show how to incorporate feedback within the quantum trajectories formalism and we focus on the case where the depth of the optical lattice is changed depending on the number of photons leaving the optical cavity. We discuss how to use quantum control for exploiting measurement backaction in order to deterministically create quantum states characterized by density or magnetic ordering.

The thesis then concludes with a summary and an outline of future research directions.

The code we developed for simulating the quantum trajectories is available at the address http://github.com/gambero88/quantum_trajectories.

Chapter 2

Quantum optics with quantum gases

Ultracold atomic systems offer a unique tool for investigating the behavior of matter in the quantum degenerate regime, promising studies of a vast range of phenomena covering many disciplines from condensed matter to quantum information and particle physics [103]. Classical light fields are crucial ingredients for cooling, trapping and manipulating such systems. In this Chapter, we introduce a model that describes the coupling between quantized light modes and a cloud of ultracold atoms loaded in an optical lattice. This allows to observe phenomena where the quantum nature of both light and matter plays an equally important role. The experimental realization of such regime became feasible only recently [87, 98] where, for the first time, a quantum gas in an optical lattice was coupled to the quantized light modes of an optical cavity.

This chapter is structured as follows. We first introduce on a general model for describing the coupling between a many-body system of bosons and fermions and the quantized light field of an optical cavity (see [120] for a review). Then, we show that the scattering pattern arising from such quantum coupling is different from the usual classical diffraction pattern and can be exploited for performing quantum nondemolition measurements on the atomic state. We illustrate this by presenting several examples in lattice and free space. Finally, we show that the electromagnetic field inside the cavity mediates an effective interaction between the atoms that can be engineered by changing the geometric configuration of the setup.

2.1 Light scattering from ultracold atoms

2.1.1 Optical lattices

Classical laser beams can be used for trapping ultracold atomic gases into periodical potentials that closely resemble the crystal structure of condensed matter and solid state systems. The oscillating electric field couples to the dipole moment of the atoms and, in the far detuning limit, leads to the trapping potential

$$V_{OL}(\mathbf{r}) = -\mathbf{d} \cdot \mathbf{E}(\mathbf{r}) \propto \alpha(\omega_p) \left|\mathbf{E}(\mathbf{r})\right|^2 \tag{2.1}$$

where $\mathbf{d}$ is the atomic dipole moment, $\mathbf{E}(\mathbf{r})$ is the electric field, α the polarizability of the atoms and ω_p is the frequency of the laser beam. Therefore, the atoms experience a potential that is determined by the intensity of the laser beam and whose signed depends on the atomic detuning $\Delta_a = \omega_p - \omega_a$ (ω_a being the frequency of the atomic transition). Specifically, if the light beam is blue-detuned (i. e. $\Delta_a > 0$), the minima of the potential correspond to the regions with low light intensity and the atoms tend to occupy these points. On the contrary, if the laser is red-detuned (i. e. $\Delta_a < 0$), the potential pushes the atoms towards the maxima of the light field since these corresponds to the minima of $V_{OL}(\mathbf{r})$.

Combining more than one light beam allows to obtain a periodic potential whose geometry is determined by the interference pattern between the different beams. For example, considering the case of two counter-propagating traveling waves with wavelength λ, the resulting optical lattice potential is a standing wave profile which traps the atoms

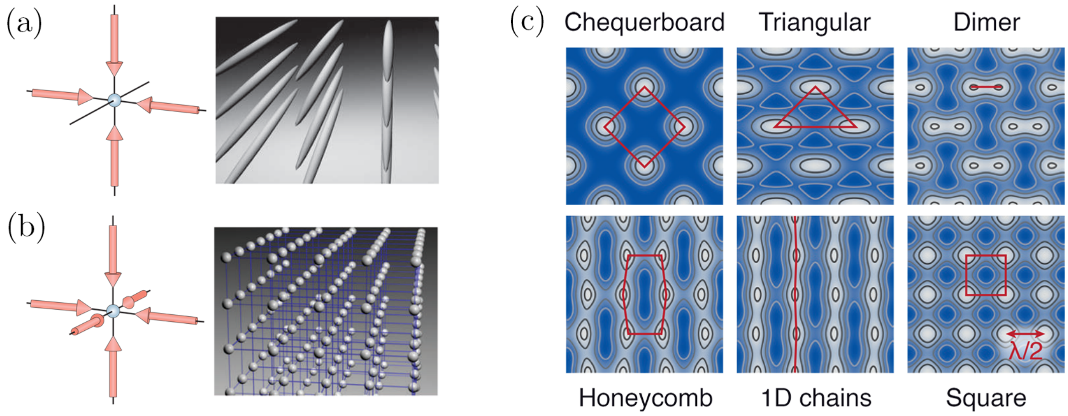

Fig. 2.1 Examples of different optical lattices that can be obtained by combining more laser beams. Using more than two laser beams at different angles it is possible to create periodic potentials in different dimensions and characterized by different lattice structure. From [20] and [180].

in a series of cigar-shaped regions [20]. By adding more laser beams, it is possible to obtain one-, two- or three-dimensional periodic potentials. Moreover, the geometry of such interference patterns can be easily tuned by changing the angles between the laser beams allowing to realize different lattices such as square, hexagonal and triangular [180] (Figure 2.1). Thus, optical lattices provide an extremely flexible tool for realizing periodic potentials in which atoms can move.

Time of flight imaging

One of the easiest and most common techniques for probing the state of an ultracold atomic gas loaded in an optical lattice is the so-called time of flight imaging. This method gives access to the momentum distribution of the matter system and, therefore, allows to distinguish different quantum phases. Although time-of-flight imaging is very popular, it represents a completely destructive measurement scheme since, after the image is taken, the atomic cloud is destroyed. The experimental procedure for realizing this technique consist in taking an absorption image of the atomic system after the trapping potential

(e. g. the optical lattice) is switched off and the atoms are let free to fall for a time t_{tof}. The resulting image represents the density of the system integrated over the direction of the beam used for imaging, i. e. the column-density operator. If the atomic system is not strongly interacting and if its density is not too large, we can consider the atoms to be in free fall and the position of an atom at the time when the image is taken is $\mathbf{r} = \hbar t_{\text{tof}}\mathbf{q}/m$ where m is the atomic mass and $\mathbf{q}$ is the momentum of the atom in the trapping potential. Therefore, one can process the data composing the image and obtain the probability distribution of the operator

$$\hat{n}(\mathbf{q}) = \int \hat{\Psi}^{\dagger}(\mathbf{q}, q')\hat{\Psi}(\mathbf{q}, q')\,\mathrm{d}q' \tag{2.2}$$

where q' is the projection of the momentum of the atoms along the direction perpendicular the plane of the image and $\hat{\Psi}^{\dagger}(\mathbf{q}, q')$ and $\hat{\Psi}(\mathbf{q}, q')$ are respectively the creation and annihilation operators of the matter field expressed in the Fourier domain. In order to obtain meaningful results, it is necessary to repeat this procedure several times and the atomic system has to be prepared again after each imaging session. By averaging over many shots, one has access to the average momentum distribution $\langle\hat{n}(\mathbf{q})\rangle$. This approach is fundamentally different from the one we will present in the following sections where we will show how to probe the atomic observables non-destructively.

2.1.2 Ultracold gases coupled to quantized light modes

We start by considering a system of ultracold bosons coupled to a quantized light field [120] (Figure 2.2). Specifically, we describe the light field in terms of its annihilation (creation) $\hat{a}_l$ ($\hat{a}_l^{\dagger}$) operators and the Hamiltonian

$$\hat{H}_l = \hbar\sum_l \hat{a}_l^{\dagger}\hat{a}_l - i\hbar\sum_l \left(\eta_l^*\hat{a}_l - \eta_l\hat{a}_l^{\dagger}\right) \tag{2.3}$$

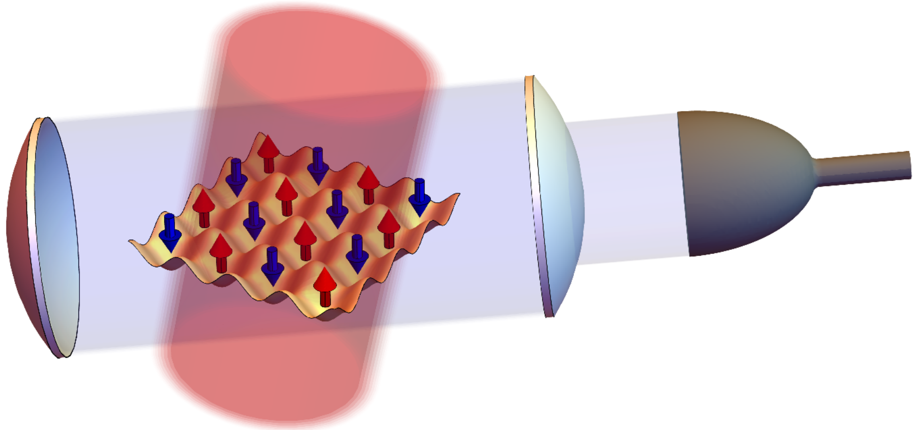

Fig. 2.2 Experimental setup. An ultracold quantum gas is loaded inside an optical cavity and it is probed with a coherent light beam (red). The scattered light (blue) is collected and enhanced by a leaky cavity, allowing the detection of the escaped photons.

where the sum over l runs over the light modes, ω_l is the frequency of the light mode l which can be pumped by a coherent field with amplitude η_l. We model the atomic cloud as an ensemble of N two-level atoms where the ground state is described by the bosonic field operators $\hat{\Psi}^\dagger(\mathbf{r})$ and $\hat{\Psi}(\mathbf{r})$ such that

$$\left[\hat{\Psi}(\mathbf{r}), \hat{\Psi}^\dagger(\mathbf{r}')\right] = \delta(\mathbf{r} - \mathbf{r}'). \tag{2.4}$$

The dynamics of the atomic system can be described taking into account three distinct contributions: (i) one body terms such as external potential and kinetic energy, (ii) interactions between the atoms and (iii) coupling between the matter field and the light. Specifically, the first two terms describe the usual dynamics of an ultracold atomic gas and are given by

$$\hat{H}_a = \int \hat{\Psi}^\dagger(\mathbf{r}) \left(-\frac{\hbar^2 \nabla^2}{2m} + V(\mathbf{r}) + \frac{\hbar\omega_a}{2}\sigma_z \right) \hat{\Psi}(\mathbf{r}) \,\mathrm{d}\mathbf{r} + U \int \hat{\Psi}^\dagger(\mathbf{r})\hat{\Psi}^\dagger(\mathbf{r})\hat{\Psi}(\mathbf{r})\hat{\Psi}(\mathbf{r}) \,\mathrm{d}\mathbf{r} \tag{2.5}$$

where m is the atomic mass, $V(\mathbf{r})$ an external trapping potential (which may include an optical lattice), U is the interaction energy between the atoms, ω_a is the frequency of the atomic transition between the ground state and the excited state and σ_z is the population difference operator between these two states. Importantly, the interaction term $U = 2\pi a_s \hbar^2/m$ is related to the s-wave scattering length a_s of the atoms considered and can be easily tuned by applying a magnetic field on the system. We consider the case where the light modes and the atomic system are coupled linearly so that the light-matter Hamiltonian is

$$\hat{H}_{al} = -i\hbar \sum_l \int \hat{\Psi}^\dagger(\mathbf{r}) \left(\sigma^+ g_l \hat{a}_l u_l(\mathbf{r}) - \text{h.c.}\right) \hat{\Psi}(\mathbf{r})\, \mathrm{d}\mathbf{r} \tag{2.6}$$

where $u_l(\mathbf{r})$ are the mode functions of the light field, g_l are the light-atom coupling constant for the mode l and σ^+ (σ^-) are the raising (lowering) operator. The Hamiltonian $\hat{H}_{al}$ is the main difference from standard problems in ultracold gases where classical light beams are used for manipulating, controlling and cooling the atoms. Here, we focus on the ultimate quantum regime where both light and matter are treated as quantum mechanical operators.

In this Thesis we consider the case of non-resonant interaction, i. e. the light-matter detunings $\Delta_a = \omega_l - \omega_a$ are much larger than the spontaneous emission rate and the Rabi frequencies $g_l \hat{a}_l$. In this limit, we can adiabatically eliminate the upper atomic level as its population is negligible ($\sigma_z = -1$). In order to do so, we compute the Heisenberg equations for the polarizations σ^+ and σ^- and we express these quantities in terms of the light fields $\hat{a}_l$. Within this approximation, the light-atoms Hamiltonian (2.6) can be replaced by

$$\hat{H}_{al} = \frac{\hbar}{\Delta_a} \sum_{l,m} \int \hat{\Psi}^\dagger(\mathbf{r}) u_l^*(\mathbf{r}) u_m(\mathbf{r}) g_l g_m \hat{a}_l^\dagger \hat{a}_m \hat{\Psi}(\mathbf{r})\, \mathrm{d}\mathbf{r} \tag{2.7}$$

where $\Delta_a = \omega_p - \omega_a$ is the detuning between the atomic transition and the probe beam. The physical meaning of this expression is transparent: the photons of the light mode m are scattered by the atomic density $\hat{\Psi}^\dagger(\mathbf{r})\hat{\Psi}(\mathbf{r})$ to the light mode l. This analogous to the linear dipole approximation for the atoms, i. e. the dipoles respond linearly to the light amplitude with a very small population of the excited states. If the atomic cloud is loaded in an optical lattice with M lattice sites, we can further simplify (2.7) by expanding the matter field in terms of localized Wannier functions. Introducing the operators $\hat{b}_i$ ($\hat{b}_i^\dagger$) which annihilates (creates) an atom at the lattice site i, we rewrite $\hat{\Psi}(\mathbf{r})$ as $\hat{\Psi}(\mathbf{r}) = \sum_{i=1}^{M} \hat{b}_i w(\mathbf{r} - \mathbf{r}_i)$. Inserting this expression in the complete light-atoms Hamiltonian $\hat{H} = \hat{H}_l + \hat{H}_a + \hat{H}_{al}$ we obtain

$$\hat{H} = \hat{H}_l + \sum_{i,j} J_{ij}^{\text{cl}} \hat{b}_i^\dagger \hat{b}_j + \frac{U}{2} \sum_i \hat{b}_i^\dagger \hat{b}_i (\hat{b}_i^\dagger \hat{b}_i - 1) + \frac{\hbar}{\Delta_a} \sum_{l,m} g_l g_m \hat{a}_l^\dagger \hat{a}_m \left(\sum_{i,j} J_{ij}^{lm} \hat{b}_i^\dagger \hat{b}_j \right) \tag{2.8}$$

where J_{ij}^{cl} is the tunneling amplitude describing the motion of atoms between the lattice sites i and j and it is given by

$$J_{ij}^{\text{cl}} = \int w(\mathbf{r} - \mathbf{r}_i) \left(-\frac{\hbar^2 \nabla^2}{2m} + V(\mathbf{r}) \right) w(\mathbf{r} - \mathbf{r}_j) \, \mathrm{d}\mathbf{r}. \tag{2.9}$$

This quantity is essentially determined by the overlap of the Wannier functions centered at different lattice sites. For this reason, J_{ij}^{cl} can be safely neglected if the sites i and j are not nearest neighbors (or $i = j$). For a homogeneous system, these coefficients do not depend on the lattice site index so that we can define $J_0 = J_{ii}^{\text{cl}}$ and $J = -J_{i,i\pm1}^{\text{cl}}$. While J_0 is only a constant shift for the chemical potential of the system and can be neglected, J represents the tunneling amplitude between nearest neighbor lattice sites and determines the dynamics of the atoms. Moreover, the interplay between J and the local interaction $U = 4\pi a_s \hbar^2 / m_a \int |w(\mathbf{r})|^4 \mathrm{d}\mathbf{r}$ is essential for describing the phase diagram of the Bose-Hubbard model. The Hamiltonian (2.8) is an extension of this model as it includes an additional term describing the photons scattered by the atoms. The effect of the coupling between light and matter depends on both the Wannier functions and the spatial profile of the light amplitude (i. e. the mode functions $u_l(\mathbf{r})$) an it is described by

$$J_{ij}^{lm} = \int w(\mathbf{r} - \mathbf{r}_i) u_l^*(\mathbf{r}) u_m(\mathbf{r}) w(\mathbf{r} - \mathbf{r}_j) \, d\mathbf{r}. \tag{2.10}$$

Again, these coefficients depend on the overlap of the Wannier functions, so that J_{ij}^{lm} can be neglected unless the indexes i and j refer to the same site ($i = j$) or nearest neighbors sites. Within this approximation, we introduce the local density operator $\hat{n}_i = \hat{b}_i^\dagger \hat{b}_i$ and define $\hat{F}_{lm}$ as

$$\hat{F}_{lm} = \hat{D}_{lm} + \hat{B}_{lm} \tag{2.11}$$

where

$$\hat{D}_{lm} = \sum_i J_{ii}^{lm} \hat{n}_i \qquad \text{and} \qquad \hat{B}_{lm} = \sum_{\langle i,j \rangle} J_{ij}^{lm} \hat{b}_i^\dagger \hat{b}_j \tag{2.12}$$

where $\langle i, j \rangle$ denotes nearest neighboring lattice sites. Thus, the Hamiltonian (2.8) reduces to (up to constant terms)

$$\hat{H} = \hat{H}_l - J \sum_{\langle i,j \rangle} \hat{b}_i^\dagger \hat{b}_j + \frac{U}{2} \sum_i \hat{n}_i(\hat{n}_i - 1) + \frac{\hbar}{\Delta_a} \sum_{l,m} g_l g_m \hat{a}_l^\dagger \hat{a}_m \hat{F}_{lm}. \tag{2.13}$$

From this expression we can obtain the Heisenberg equations for the light field as

$$\dot{\hat{a}}_l = -i \left(\omega_l + \frac{g_l^2}{\Delta_a} \hat{F}_{ll} \right) \hat{a}_l - i \frac{g_l}{\Delta_a} \sum_{m \neq l} g_m \hat{a}_m \hat{F}_{lm} + \eta_l - \kappa_l \hat{a}_l \tag{2.14}$$

where we introduced phenomenologically the decay rate κ_l for describing the photons leaking from the cavity mirrors. Importantly, this expression does not contain any

Langevin noise term since we will be interested in normal-ordered quantities only [121]. Moreover, equation (2.14) highlights the physical meaning of the various terms in the Hamiltonian (2.13). In analogy to the classical Maxwell's equations for the light amplitude of a cavity mode, the first term describes the free evolution of the electromagnetic field and its phase shift due to the presence of the atoms (non-resonant dispersion) while the second term models the scattering from all the light modes to the mode $\hat{a}_l$. This second effect has two contributions as photons can be scattered from the on-site atomic density ($\hat{D}_{lm}$) or from the coherence between neighboring sites ($\hat{B}_{lm}$). The Heisenberg equations for the matter operators read

$$\begin{aligned}\dot{\hat{b}}_i = &-\frac{i}{\Delta_a}\left(\sum_{l,m} g_l g_m \hat{a}_l^\dagger \hat{a}_m J_{ii}^{lm} + U\hat{n}_i\right)\hat{b}_i \\ &-\frac{i}{\hbar}\sum_{j:i}\left(-J + \frac{\hbar}{\Delta_a}\sum_{l,m} g_l g_m \hat{a}_l^\dagger \hat{a}_m J_{ij}^{lm}\right)\hat{b}_j \end{aligned} \tag{2.15}$$

where the symbol $j : i$ indicates that the sum runs over all the nearest neighbors of the lattice site i. The first line of this expression describes the evolution of the phase of the matter field at the site i while the second line is relative to the coupling to the nearest neighbors. These equations highlights the fact that the Hamiltonian (2.13) introduces long-range correlations in the system as all lattice sites are coupled to the light modes $\hat{a}_l$. The cavity field mediates an infinite-range interaction between the atoms. The spatial structure of such non-local coupling is determined by the coefficients J_{ij}^{lm} which play a crucial role in determining the property of the system. This effect is essential for obtaining new many-body effects beyond the standard Bose-Hubbard model.

Generalization to fermionic atoms

The model described in the previous paragraphs can be generalized to a system of fermionic atoms by introducing the light polarization as additional degree of freedom for the electromagnetic field. We describe the matter as two distinct two-level systems that are not coupled to each other where the two lower energy states represent different degenerate hyperfine levels of a fermionic atom corresponding to the $\uparrow$ or $\downarrow$ spin species. Because of selection rules, the transitions between these two low energy states and the excited ones can occur only if a photon with specific (circular) polarization is absorbed/emitted. The field operators modeling the lowest energy levels of the matter field are $\Psi_\sigma(\mathbf{r})$ and $\Psi^\dagger_\sigma(\mathbf{r})$ ($\sigma =\uparrow, \downarrow$) and they fulfill the anticommutation relations

$$\left\{\Psi_\sigma(\mathbf{r}), \Psi^\dagger_{\sigma'}(\mathbf{r}')\right\} = \delta_{\sigma,\sigma'}\delta(\mathbf{r}-\mathbf{r}'). \tag{2.16}$$

The Hamiltonian describing the dynamics of the atoms is given by

$$\begin{aligned}\hat{H}_a = &\sum_{\sigma=\uparrow,\downarrow} \int \hat{\Psi}^\dagger_\sigma(\mathbf{r}) \left(-\frac{\hbar^2\nabla^2}{2m} + V(\mathbf{r}) + \frac{\hbar\omega_a}{2}\sigma_z^{(\sigma)}\right) \hat{\Psi}_\sigma(\mathbf{r})\, \mathrm{d}\mathbf{r} \\ &+ U \int \hat{\Psi}^\dagger_\uparrow(\mathbf{r})\hat{\Psi}^\dagger_\downarrow(\mathbf{r})\hat{\Psi}_\downarrow(\mathbf{r})\hat{\Psi}_\uparrow(\mathbf{r})\, \mathrm{d}\mathbf{r}\end{aligned} \tag{2.17}$$

where $\sigma_z^{(\uparrow)}$ and $\sigma_z^{(\downarrow)}$ are the population differences between the ground states and the excited states for each spin species. This expression is somehow analogous to (2.5) with the notable difference that, because of the Pauli exclusion principle, the contact interaction between the atoms is possible only between atoms with opposite spin. Adiabatically eliminating the upper energy levels, the Hamiltonian describing the coupling between the atoms and the light modes is

$$\hat{H}_{al} = \frac{\hbar}{\Delta_a} \sum_{\sigma=\uparrow,\downarrow} \sum_{l} \int \hat{\Psi}^\dagger_\sigma(\mathbf{r}) u_l^*(\mathbf{r}) u_m(\mathbf{r}) g_l g_m \hat{a}^\dagger_{l\sigma} \hat{a}_{m\sigma} \hat{\Psi}_\sigma(\mathbf{r})\, \mathrm{d}\mathbf{r} \tag{2.18}$$

where the light operators are expressed in the circular polarization basis and $\sigma =\uparrow$ ($\downarrow$) corresponds to left (right) circularly polarized light. In analogy to the bosonic case, we can expand the field operators in terms of the Wannier functions of the lattice, i. e.

$\hat{\Psi}_\sigma(\mathbf{r}) = \sum_{i=1}^{M} \hat{f}_{i\sigma} w(\mathbf{r}-\mathbf{r}_i)$ where $\hat{f}_{i\sigma}$ ($\hat{f}_{i\sigma}^\dagger$) annihilates (creates) a fermion with spin σ at the lattice site i. Therefore, the Hamiltonian describing the light-matter system resembles a generalization of the Hubbard Hamiltonian and it is given by

$$\hat{H} = \hat{H}_l - J \sum_{\sigma=\uparrow,\downarrow} \sum_{\langle i,j \rangle} \hat{f}_{i\sigma}^\dagger \hat{f}_{j\sigma} + U \sum_i \hat{n}_{i\uparrow}\hat{n}_{i\downarrow} + \frac{\hbar}{\Delta_a} \sum_{\sigma=\uparrow,\downarrow} \sum_{l,m} g_l g_m \hat{a}_{l\sigma}^\dagger \hat{a}_{m\sigma} \hat{F}_{lm}^{(\sigma)} \tag{2.19}$$

and

$$\hat{F}_{lm}^{(\sigma)} = \hat{D}_{lm}^{(\sigma)} + \hat{B}_{lm}^{(\sigma)} \tag{2.20}$$

where

$$\hat{D}_{lm}^{(\sigma)} = \sum_i J_{ii}^{lm} \hat{n}_{i\sigma} \qquad \text{and} \qquad \hat{B}_{lm}^{(\sigma)} = \sum_{\langle i,j \rangle} J_{ij}^{lm} \hat{f}_{i\sigma}^\dagger \hat{f}_{j\sigma}. \tag{2.21}$$

2.2 QND probing of the atomic system

In the previous section, we pointed out that one of the consequences of treating both light and matter as quantum mechanical operators is the emergence of correlations and entanglement between them. It has been shown that this property can be exploited for probing important characteristic of the atomic quantum state by analyzing the light scattered from the quantum gas [120]. We will now focus on this idea and, in the interest of clarity, we present an example from the literature where a bosonic system is considered [122]. The matter field is coupled to two different light modes: a classical coherent probe a_0 and the scattered light mode $\hat{a}_1$. Moreover, we consider the regime where the atomic dynamics defined by the tunneling between neighboring sites is much slower that the light scattering. In other words, the quantum properties of the atomic state are defined by the tunneling amplitude J and the interatomic interaction U and do not change during the measuring process so that the dynamics described by $\hat{H}_a$ can be neglected. Therefore, the Hamiltonian of the light-atom system reduces to

$$\begin{aligned}\hat{H} =& \hbar\left(\omega_1 + U_{11}\hat{F}_{11}\right)\hat{a}_1^\dagger\hat{a}_1 + \hbar U_{10}\left(a_0^*\hat{a}_1\hat{F}_{01} + \hat{a}_1^\dagger a_0\hat{F}_{10}\right) + \hbar U_{00}|a_0|^2\hat{F}_{00}+ \\ &- i\hbar\left(\eta_1^*\hat{a}_1 - \eta_1\hat{a}_1^\dagger\right)\end{aligned} \tag{2.22}$$

where we assumed that the probe is a coherent beam represented by the c-number a_0, $U_{lm} = g_l g_m/\Delta_a$ and η_1 is the amplitude of a probing through a mirror at frequency ω_p (if present). The first term in (2.22) describes the shift of the cavity resonance induced by the presence of the atoms. The second one illustrates the scattering of the photons of the probe a_0 into the optical cavity $\hat{a}_1$. Importantly, these two terms retain their quantum-mechanical character (i. e. they are operators) and lead to different light scattering amplitude depending on the quantum state of the atoms.

Probing the number of photons leaving the optical cavity ($\hat{a}_1^\dagger\hat{a}_1$) or other quantitites related to the light amplitude $\hat{a}_1$ fullfills the conditions describing a QND measurment of the atomic variable $\hat{F}_{lm}$ [27]. In general, a QND measurement of the "signal" observable $\hat{A}_S$ can be performed by detecting the "probe" observable $\hat{A}_P$ if the following requirements hold:

(i) the Hamiltonian that couples signal and probe and describes the measurement process ($\hat{H}_{SP}$) is a function of the signal observables, i. e. $\partial\hat{H}_{SP}/\partial\hat{A}_S \neq 0$;

(ii) the evolution of the signal observable is not affected by its coupling to $\hat{A}_P$ during the measurement so that $\left[\hat{H}_{SP}, \hat{A}_S\right] = 0$. This ensure that the free evolution of $\hat{A}_S$ remains unperturbed;

(iii) the commutator $\left[\hat{H}_{SP}, \hat{A}_P\right]$ is different from zero so that it is possible to measure $\hat{A}_S$ using $\hat{A}_P$;

(iv) because of the measurement backaction, the conjugate variable of $\hat{A}_S$ (i. e. $\hat{A}_S^c$), is altered in an uncontrollable way after the SP interaction takes place. In order to avoid an uncontrollable subsequent perturbation in the evolution of $\hat{A}_S$, the Hamiltonian describing the signal observable should not be a function of $\hat{A}_S^c$.

The Hamiltonian (2.22) fulfills all these conditions if we identify the probe observable with the photon number operator $\hat{a}_1^\dagger \hat{a}_1$ and the signal observables with the atomic operators $\hat{F}_{lm}$. Moreover, equation (2.22) allows us to compute the Heisenberg equations for the scattered light amplitude

$$\dot{\hat{a}}_1 = -i\left(\omega_1 + U_{11}\hat{F}_{11}\right)\hat{a}_1 - iU_{10}\hat{F}_{10}a_0 + \eta_1 - \kappa\hat{a}_1 \tag{2.23}$$

where we dropped the index from the cavity decay κ. The solution of this equation can be computed by rewriting the scattered light amplitude as $\hat{a}_1 = \hat{\tilde{a}}_1 e^{-i\omega_p}$ where $\hat{\tilde{a}}_1$ is a slowly varying operator, i. e. we assume that $\hat{a}_1$ oscillates with the same frequency as the probe beam (ω_p). Within this ansatz, we can take the derivative $\dot{\hat{a}}_1$ and neglect the term $\propto \hat{\tilde{a}}_1$ so that the stationary solution of (2.23) becomes

$$\hat{a}_1 = \frac{\eta_1 - iU_{10}a_0\hat{F}_{10}}{i(U_{11}\hat{F}_{11} - \Delta_p) + \kappa} \tag{2.24}$$

where $\Delta_p = \omega_p - \omega_1$ is the cavity-probe detuning. Note that the denominator in this expression is an operator and represents the inverse $\left[i(U_{11}\hat{F}_{11} - \Delta_p) + \kappa\right]^{-1}$ (applied on the left hand side). Equation (2.24) gives a direct relation between the *operators* describing the light field and the quantum state of the atoms. In general, this relation is non-linear since the $\hat{F}_{lm}$ operator appear in both numerator and denominator. Following [120], we can further simplify this expression specializing to two different optical configurations:

(i) **Transverse probing**

If the dispersive frequency shift is smaller than κ and the cavity-probe detuning Δ_p, we can neglect the term $U_{11}\hat{F}_{11}$ in (2.24) and the denominator of this expression becomes a c-number. Focusing on the case where only one transverse probe a_0 is present ($\eta_1 = 0$), the amplitude of the scattered light is directly proportional to the atomic operator $\hat{F}_{10}$:

$$\hat{a}_1 = C\hat{F}_{10} \quad \text{and} \qquad C = \frac{U_{10}a_0}{\Delta_p + i\kappa} \tag{2.25}$$

As a consequence, the correlations of the quantum state of the atoms are directly mapped on the light intensity $n_\phi = \langle \hat{a}_1^\dagger \hat{a}_1 \rangle$ since this is sensitive to the square of $\hat{F}_{10}$. Note that higher moments of the photon number operator (e. g. its variance $\langle \hat{a}_1^\dagger \hat{a}_1 \hat{a}_1^\dagger \hat{a}_1 \rangle - \langle \hat{a}_1^\dagger \hat{a}_1 \rangle^2$) carry information about higher order correlations such as four-points correlation functions.

(ii) **Probing through a mirror**

In this case, there is no transverse probe beam (a_0) and the electromagnetic field inside the optical cavity is sustained by an optical pump. Therefore, the light amplitude $\hat{a}_1$ is essentially determined by the dispersive frequency shift. In contrast to the previous example, the coupling between $\hat{a}_1$ and the atomic operators is non-linear and allows to measure the full probability distribution function of $\hat{F}_{11}$ without addressing higher moments of n_ϕ [115, 123]. The presence of resonances in the transmission spectrum of the optical cavity allows to distinguish between different quantum phases and to determine important atomic statistical quantities.

In this Thesis we will focus on the configuration (i) and we will assume that the dispersive frequency shift is smaller than κ and Δ_p and can be neglected. Moreover, for deep optical lattices, the contribution to the operator $\hat{F}_{lm}$ due to $\hat{D}_{lm}$ dominates over the one due to $\hat{B}_{lm}$ which can be neglected. However, by carefully engineering the mode functions of the light field it is possible to completely suppress $\hat{D}_{lm}$ so that the light scattering is sensitive solely to $\hat{B}_{lm}$ [93, 110]. The coefficients J_{jj} determine the spatial profile of the measurement operator and, for well-localized atoms, reduce to $J_{jj}^{lm} = u_l^*(\mathbf{r}_j)u_m(\mathbf{r}_j)$. Therefore, the observable that is probed non-destructively by collecting the photons escaping the optical cavity is

$$\hat{D}_{10} = \sum_j u_1^*(\mathbf{r}_j)u_0(\mathbf{r}_j)\,\hat{n}_j. \tag{2.26}$$

For fermions, the polarization of the probe beam plays a crucial role for addressing density and magnetic correlations. If only two light modes are present, the coupling between the probe $a_{0\sigma}$ and the scattered light $\hat{a}_1$ reads

$$\begin{aligned}\hat{H}_{al} =& \hbar \sum_{\sigma=\uparrow,\downarrow} \left(\omega_1 + U_{11}\hat{F}_{11}^{(\sigma)}\right)\hat{a}_1^\dagger\hat{a}_1 + \hbar \sum_{\sigma=\uparrow,\downarrow} U_{10}\left(a_{0\sigma}^*\hat{a}_1\hat{F}_{01}^{(\sigma)} + \hat{a}_1^\dagger a_{0\sigma}\hat{F}_{10}^{(\sigma)}\right) \\ &+ \hbar \sum_{\sigma=\uparrow,\downarrow} U_{00}|a_{0\sigma}|^2\hat{F}_{00}^{(\sigma)}.\end{aligned} \tag{2.27}$$

where we used the index $\sigma =\uparrow,\downarrow$ to indicate both the spin species and the light polarization. Again, the second term of this expression is the most interesting one as it describe the scattering from the probe beam to the optical cavity. Depending on the polarization of the probe beam, this coupling has different forms. Starting from the light modes expressed in the circular polarization basis, we can define the annihilation operators for linearly polarized light as

$$\hat{a}_x = \frac{\hat{a}_L + \hat{a}_R}{\sqrt{2}} \qquad \text{and} \qquad \hat{a}_y = -i\frac{\hat{a}_R - \hat{a}_L}{\sqrt{2}} \tag{2.28}$$

so that the second term in (2.27) can be rewritten as

$$\hbar \sum_{\sigma=\uparrow,\downarrow} U_{10}\left(a_{0\sigma}^*\hat{a}_1\hat{F}_{01}^{(\sigma)} + \hat{a}_1^\dagger a_{0\sigma}\hat{F}_{10}^{(\sigma)}\right) =$$

$$
\begin{aligned}
&= \hbar\frac{U_{10}}{\sqrt{2}}\Big[(a_{0x}^* + i a_{0y}^*)\hat{a}_1\hat{F}_{01}^{(\uparrow)} + \hat{a}_1^\dagger(a_{0x} - i a_{0y})\hat{F}_{10}^{(\uparrow)} \\
&\qquad + (a_{0x}^* - i a_{0y}^*)\hat{a}_1\hat{F}_{01}^{(\downarrow)} + \hat{a}_1^\dagger(a_{0x} + i a_{0y})\hat{F}_{10}^{(\downarrow)}\Big] \\
&= \hbar\frac{U_{10}}{\sqrt{2}}\Big[a_{0x}^*\hat{a}_1(\hat{F}_{01}^{(\uparrow)} + \hat{F}_{01}^{(\downarrow)}) + \hat{a}_1^\dagger a_{0x}(\hat{F}_{10}^{(\uparrow)} + \hat{F}_{10}^{(\downarrow)}) \\
&\qquad + i a_{0y}^*\hat{a}_1(\hat{F}_{01}^{(\uparrow)} - \hat{F}_{10}^{(\downarrow)}) - i\hat{a}_1^\dagger a_{0y}(\hat{F}_{10}^{(\uparrow)} - \hat{F}_{01}^{(\downarrow)})\Big] \\
&= \hbar\frac{U_{10}}{\sqrt{2}}\left(a_{0x}^*\hat{a}_1\hat{F}_{01}^{(x)} + \hat{a}_1^\dagger a_{0x}\hat{F}_{10}^{(x)} + i a_{0y}^*\hat{a}_1\hat{F}_{10}^{(y)} - i\hat{a}_1^\dagger a_{0y}\hat{F}_{01}^{(y)}\right). \qquad (2.29)
\end{aligned}
$$

Despite of being equivalent to (2.27), this expression highlights the fact that if the probe beam is linearly polarized (i. e. either a_{0x} or a_{0y} are equal to zero), the scattered light performs a QND measurement of $\hat{F}_{lm}^{(x)}$ or $\hat{F}_{lm}^{(y)}$. If the optical lattice is sufficiently deep and the contribution to light scattering from the $B-$operators can be neglected, the $F-$operators reduce to the corresponding $D-$operators. In the case of a linearly polarized probe, the measurement operators are

$$\hat{D}_{lm}^{(x)} = \sum_j u_1^*(\mathbf{r}_j)u_0(\mathbf{r}_j)\,\hat{\rho}_j \qquad (2.30)$$

$$\hat{D}_{lm}^{(y)} = \sum_j u_1^*(\mathbf{r}_j)u_0(\mathbf{r}_j)\,\hat{m}_j \qquad (2.31)$$

where $\hat{\rho}_j = \hat{n}_{j\uparrow} + \hat{n}_{j\downarrow}$ and $\hat{m}_j = \hat{n}_{j\uparrow} - \hat{n}_{j\downarrow}$. Therefore, probing the atomic system with linearly polarized light it is possible to address different linear combinations of the $\uparrow$ and $\downarrow$ spin densities. This allows to investigate density and magnetic properties that are particularly relevant especially in systems that reproduce condensed matter phenomena such as density waves, Cooper pairing and antiferromagnetism.

From the Hamiltonian (2.22) and in analogy to the bosonic case, we can compute the stationary solution of the Heisenberg equation for the cavity light mode operator $\hat{a}_1$ as

$$\hat{a}_1 = \frac{\eta_1 - iU_{10}(a_{0L}\hat{D}_{10}^{(\uparrow)} + a_{0R}\hat{D}_{10}^{(\downarrow)})}{i\left[U_{11}(\hat{D}_{11}^{(\uparrow)} + \hat{D}_{11}^{(\downarrow)}) - \Delta_p\right] + \kappa}. \qquad (2.32)$$

If the atomic system is not probed through a mirror and neglecting the cavity dispersive shift, the annihilation operator for the scattered light becomes

$$\hat{a}_1 = \sum_{\sigma=\uparrow,\downarrow} C_\sigma \hat{D}_{10}^{(\sigma)} \quad \text{where} \qquad C_\sigma = \frac{U_{10}a_{0\sigma}}{\Delta_p + i\kappa} \tag{2.33}$$

In the previous sections, we focused on the limit where the detuning between the probe and the atomic transition is very large. However, this is not the only way to achieve a direct mapping between the properties of the scattered light and the density/magnetization correlations of the atomic system. Specifically, it is possible to probe the magnetic property of an ultracold gas by setting the detuning of the light field to be half way between the two hyperfine states that correspond to different spin species [68, 101, 113, 130, 164–166]. In this case, the phase shift experienced by the light in both the L polarization and the R polarization due to the atom ensemble is the same but opposite in sign. In other words, for a specific choice of the frequency of the probe beam, the two atomic spin states will have different polarizabilities, and the local refractive index will depend on a linear combination of the density operators for $\uparrow$ and $\downarrow$ states. Moreover, if the light probe frequency is exactly between the two hyperfine levels, the refractive index is proportional to the magnetization. This allows to determine the fluctuations of the local magnetization by measuring the so-called speckle pattern.

2.2.1 Quantum addition to the classical scattering pattern

Depending on the mode functions of the light modes and on the angles between the optical lattice, the cavity and the probe, it is possible to address different linear combinations of the local atomic densities. Focusing on a one-dimensional atomic chain along the z axis and considering traveling waves as mode functions (so that $u_l(\mathbf{r}) = e^{i\mathbf{k}_l\cdot\mathbf{r}}$) the coefficients J_{jj}^{lm} describe the usual diffraction from a periodic grating. If only two light modes are present, we find that $J_{jj}^{10} = e^{i(\mathbf{k}_0-\mathbf{k}_1)\cdot\mathbf{r}_j} = e^{i\delta j}$, where $\delta = (k_{0,z} - k_{1,z})d$ and the subscript

z represents the projection along the z axis so that $k_{l,z} = |\mathbf{k}_l| \cos\theta_l$, $l = 0, 1$. Simply adjusting the angles θ_0 and θ_1 allows us to probe different linear combinations of the atomic density without changing the wavelength of the probe beam or requiring single-site resolution. For example, by collecting the light scattered in the diffraction maximum (where all atoms scatter light in phase and $u_1^*(\mathbf{r}_j)u_0(\mathbf{r}_j) = 1$), the photon annihilation operator reduces to $\hat{a}_1 = C\sum_{i=1}^{K} \hat{n}_i$ where $K \leq M$ is the number of illuminated lattice sites [121, 122]. In this case, the QND measurement is sensitive to the total number of atoms $\hat{N}_K$ that occupy the region of the optical lattice addressed by the probe beam. Although different quantum state with the same local density lead to the same amplitude for the scattered light $\hat{a}_1$, their quantum correlations are imprinted onto the light intensity $\hat{a}_1^\dagger\hat{a}_1$ which allows to distinguish them. Specifically, the number of photons leaving the optical cavity depends linearly on the two-points correlation functions as

$$\hat{a}_1^\dagger\hat{a}_1 = |C|^2\hat{D}_{10}^*\hat{D}_{10} = |C|^2\sum_{i,j}(J_{ii}^{10})^* J_{jj}^{10}\hat{n}_i\hat{n}_j. \tag{2.34}$$

Note that this mapping between the electromagnetic field and the atomic correlations requires that the light is treated as a quantum variable. In fact, we can compare (2.34) to its classical analogous where the intensity of the scattered light is computed by squaring its amplitude:

$$|\langle\hat{a}_1\rangle|^2 = |C|^2|\langle\hat{D}_{10}\rangle|^2 = |C|^2\sum_{i,j}(J_{ii}^{10})^* J_{jj}^{10}\langle\hat{n}_i\rangle\langle\hat{n}_j\rangle. \tag{2.35}$$

In order to quantify the difference between the contributions to light scattering described by (2.34) and (2.35), we compute the quantum addition to the classical scattering pattern as (bosonic case)

$$R(\theta_0, \theta_1) \equiv \langle\hat{a}_1^\dagger\hat{a}_1\rangle - |\langle\hat{a}_1\rangle|^2$$

$$= |C|^2 \left[\langle\hat{D}^*\hat{D}\rangle - |\langle\hat{D}\rangle|^2\right]$$
$$= |C|^2 \sum_{i,j}(J_{ii})^* J_{jj} \left[\langle\hat{n}_i\hat{n}_j\rangle - \langle\hat{n}_i\rangle\langle\hat{n}_j\rangle\right] \tag{2.36}$$

where we dropped the light mode indexes from the $D-$operator and the J_{ij} coefficients. This quantity allows to distinguish different quantum states even if their classical scattering pattern is the same [120]. In order to clarify this, let us consider the case of forward scattering where the light mode functions are traveling waves that probe the number of atoms occupying K contiguous lattice sites of the optical lattice so that $\hat{a}_1 = C\sum_{i=1}^{K}\hat{n}_i = C\hat{N}_K$. Focusing on a bosonic system composed by N atoms loaded in an optical lattice with M lattice sites, we can compare the value of $R(0,0) = |C|^2\sum_{i,j}(\langle\hat{n}_i\hat{n}_j\rangle - \langle\hat{n}_i\rangle\langle\hat{n}_j\rangle)$ for three different ground states: Mott insulator (MI), superfluid (SF) and coherent state (COH). Importantly, since all these states have the same local density $\langle\hat{n}_i\rangle = n = N/M$, the classical contribution to the light scattering is

$$|\hat{a}_1|^2 = |C|^2\left|\sum_{i=1}^{K}\langle\hat{n}_i\rangle\right|^2 = |C|^2 n^2 K^2 \tag{2.37}$$

and cannot distinguish between MI, SF and COH [121, 122]. However, these quantum states have very different correlations that are imprinted on the quantum addition to the classical scattering pattern (see Table 2.1), allowing to differentiate them. The MI state is characterized by the absence of density fluctuations as all the lattice sites are occupied by an exact number of atoms. Consequently, the light scattered from this state coincide with the classical case and the quantum addition R is zero in all directions. The COH state is an approximation for the ground state of a non-interacting Bose gas (the particle number is not fixed exactly) and the fluctuations of its local density are Poissonian, i. e. $\langle(\hat{n}_i - n)^2\rangle_{\text{COH}} = n$. In contrast, in the case of the SF state the density fluctuations are

	Mott insulator	superfluid	coherent
quantum state	$\prod_{i=1}^{M} \hat{b}_i^\dagger \lvert 0\rangle_i$	$\frac{1}{\sqrt{M^N N!}}\left(\sum_{i=1}^{M} \hat{b}_i^\dagger\right)^N \lvert 0\rangle$	$e^{-N/2}\prod_{i=1}^{M} e^{\sqrt{N/M}\hat{b}_i^\dagger}\lvert 0\rangle_i$
$\langle \hat{n}_i^2\rangle$	n^2	$n^2(1-1/N)+n$	n^2+n
$\langle \hat{n}_i \hat{n}_j\rangle$, $i\neq j$	n^2	$n^2(1-1/N)$	n^2
$\langle \hat{n}_i^2\rangle - \langle \hat{n}_i\rangle^2$	0	$n(1-1/M)$	n
$\langle \hat{N}_K^2\rangle$	n^2K^2	$n^2K^2(1-1/N)+nK$	n^2K^2+nK
$R(0,0)$	0	$\lvert C\rvert^2 nK(1-K/M)$	$\lvert C\rvert^2 nK$

Table 2.1 Statistical quantities and quantum addition of typical quantum states for bosonic systems. From [121].

sub-Poissonian ($\langle(\hat{n}_i - n)^2\rangle_{\mathrm{SF}} = n(1-1/M)$). Therefore, the quantum addition $R(0,0)$ for these two quantum states do not vanish and they can be easily distinguished.

If the atomic system is probed using traveling waves, the quantum addition to the classical light scattering is given by

$$R(\theta_0,\theta_1) = |C|^2 \sum_{i,j} e^{-i(\mathbf{k}_0-\mathbf{k}_1)\cdot(\mathbf{r}_i-\mathbf{r}_j)}\left(\langle \hat{n}_i\hat{n}_j\rangle - \langle \hat{n}_i\rangle\langle \hat{n}_j\rangle\right) \tag{2.38}$$

which is proportional to the structure factor. This quantity is crucial for describing the many-body properties of condensed matter systems and quantum gases as it captures the (eventual) presence of long-range order and correlations. Here, we provide a way to measure this non-destructively and with an extremely flexible setup which resembles Bragg scattering. Moreover, a setup similar to the one described in these paragraphs has been recently realized [97], albeit without having an optical lattice. In this experiment, an ultracold atomic gas is coupled to the vacuum field inside a high finesse optical cavity which allows to measure non-destructively the dynamic structure factor in real time across a structural phase transition.

2.2.2 Generation of spatial modes by global scattering

The coefficients J_{ij} determine the spatial profile of the $D-$operator, making our setup extremely flexible. Depending on the mode functions of the light modes and on the angles between the optical lattice, the cavity and the probe, it is possible to address different observables. For example, if we consider the case of a one-dimensional optical lattice along the z axis which is probed with a coherent beam a_0 and assuming that the light mode functions are travelling waves (so that $u_l(\mathbf{r}) = e^{i\mathbf{k}\cdot\mathbf{r}}$), the coefficients J_{jj} are given by $J_{jj} = e^{i(\mathbf{k}_0-\mathbf{k}_1)\cdot\mathbf{r}_j} = e^{i(k_{0,z}-k_{1,z})jd}$, where $\delta = (k_{0,z} - k_{1,z})d$ and the subscript z represents the projection along the z axis so that $k_{l,z} = |\mathbf{k}_l|\cos\theta_l$, $l = 0, 1$. Crucially, if the value of J_{jj} is the same on a subset of sites of the optical lattice, atoms in this region scatter light with the same phase and are therefore indistinguishable by the measurement [52]. As a consequence, the detection process divides the optical lattice in different spatial modes composed by non-contiguous lattice sites that show long-range entanglement and correlations. Since the measurement process is only sensitive to global observables, the dynamics of the modes preserves quantum superpositions and can entangle distant lattice sites by enhancing specific dynamical processes [110], relaxing the requirements for single-site or other spatial resolution necessary to obtain various important effects [10, 186]. With reference to the previous example, if $\delta = 2\pi s/R$ ($s, R \in \mathbb{Z}^+$) the lattice is partitioned in R spatial modes since atoms separated by R lattice sites scatter light with the same phase and amplitude, making them indistinguishable to the measurement. Therefore, the scattered light operator reduces from being a sum of numerous microscopic contributions from individual sites to the sum of smaller number of macroscopically occupied regions ($a_1 \propto \sum_{m=1}^{R} e^{i2\pi sm/R}\hat{N}_m$). In general, the partitioning in R spatial modes is not unique and can be achieved in several different configurations. For example, the case $R = 2$ can be obtained by placing the cavity along the lattice direction (i. e. $\theta_1 = 0$) and the probe beam is perpendicular to them (i. e. $\theta_0 = \pi/2$) so that $J_{ii} = (-1)^i$ [114, 115, 117–119].

Another way to divide the optical lattice in two macroscopically occupied spatial modes is to use standing waves ($u_i(\mathbf{r}) = \cos(\mathbf{k}_i \cdot \mathbf{r})$) crossed at such angles to the lattice that $\mathbf{k}_0 \cdot \mathbf{r}$ is equal to $\mathbf{k}_1 \cdot \mathbf{r}$ and shifted such that the even sites are placed in the maxima of the light interference pattern, while the even sites are positioned at the interference zeros and do not scatter light. In this way the coefficient J_{ii} are such that $J_{ii} = 1$ for i odd while $J_{ii} = 0$ for i even. Note that both the measurement scheme we illustrated here do not require single-site resolution since the coefficients J_{ii} are determined by the projections of the probe/cavity wave vectors on the direction of the optical lattice and not by their wavelengths.

2.2.3 QND measurement in fermionic systems[1]

We now go beyond the bosonic case presented in [121, 122] and we focus on the diffraction pattern of a system of ultracold fermions. In the classical case, this is analogous to the bosons and it is essentially determined by the local atomic density. However, the quantum addition to the scattered light in this case depends on the polarization of the probe beam and makes it sensitive to different atomic variables. Therefore, we need to distinguish between four different R functions:

$$\begin{aligned} R_\sigma(\theta_0, \theta_1) &= |C|^2 \left(\langle \hat{D}^{(\sigma)*} \hat{D}^{(\sigma)} \rangle - \left| \hat{D}^{(\sigma)} \right|^2 \right) \\ &= |C|^2 \sum_{i,j} (J_{ii})^* J_{jj} \left(\langle \hat{n}_{i\sigma} \hat{n}_{j\sigma} \rangle - \langle \hat{n}_{i\sigma} \rangle \langle \hat{n}_{j\sigma} \rangle \right), \quad \sigma = \uparrow, \downarrow \qquad (2.39) \\ R_x(\theta_0, \theta_1) &= |C|^2 \left(\langle \hat{D}^{(x)*} \hat{D}^{(x)} \rangle - \left| \hat{D}^{(x)} \right|^2 \right) \\ &= |C|^2 \sum_{i,j} (J_{ii})^* J_{jj} \left(\langle \hat{\rho}_{i\sigma} \hat{\rho}_{j\sigma} \rangle - \langle \hat{\rho}_{i\sigma} \rangle \langle \hat{\rho}_{j\sigma} \rangle \right) \qquad (2.40) \\ R_y(\theta_0, \theta_1) &= |C|^2 \left(\langle \hat{D}^{(y)*} \hat{D}^{(y)} \rangle - \left| \hat{D}^{(y)} \right|^2 \right) \end{aligned}$$

[1] The results presented in this section are published in [53].

$$= |C|^2 \sum_{i,j} (J_{ii})^* J_{jj} \left(\langle \hat{m}_{i\sigma} \hat{m}_{j\sigma} \rangle - \langle \hat{m}_{i\sigma} \rangle \langle \hat{m}_{j\sigma} \rangle \right) \tag{2.41}$$

where we dropped the indexes lm characterizing the light modes. These quantities depends both on the geometry of the system (via the coefficients J_{ii}) and on the many-body atomic correlations (via the expectation values). If the mode functions of the probe and scattered light are traveling waves with wave-vectors $\mathbf{k}_0$ and $\mathbf{k}_1$, the quantum addition R is proportional to a structure factor, i. e., the Fourier transform of the density-density correlations. Figure 2.3 compares the classical diffraction pattern and quantum additions R_x and R_y for fermions in a one-dimensional optical lattice at half filling. The scattering patterns were calculated for the ground state, obtained via imaginary time evolution using the TNT library [5]. In particular, we focus on the ground state of the system in two different regimes: non-interacting ($U/J = 0$) and strongly-attractive interactions ($U/J = 10$). Note that in both cases, the local magnetization of the system is zero ($\langle \hat{m}_i \rangle = 0$), and as a consequence, the classical diffraction probing the system with linear-y polarized light vanishes, i.e., $\langle \hat{a}_1 \rangle = 0$. Nevertheless, the quantum addition R_y is non-zero and depends on the quantum state of the system. In particular, we find that R_y decreases with increasing values of U/J, as the attraction between the atoms favors doubly-occupied sites, i. e., the formation of pairs of fermions with opposite spin, which suppress the fluctuations in the magnetization. Furthermore, the classical diffraction pattern due to the atomic density does not depend on U/J, as the local density is independent of the interaction for a translationally-invariant optical lattice ($\langle \hat{\rho}_i \rangle = 1$). However, the presence of doubly-occupied sites increases the fluctuations in the atom number, leading to a stronger signal for R_x. In general, the scheme we propose allows direct probing of the phase diagram for the superfluid-Mott insulator-Bose glass phases in the one-dimensional Bose–Hubbard model [91] and the detection of different quantum states of atomic systems such as dimers [33], density waves and magnetic order.

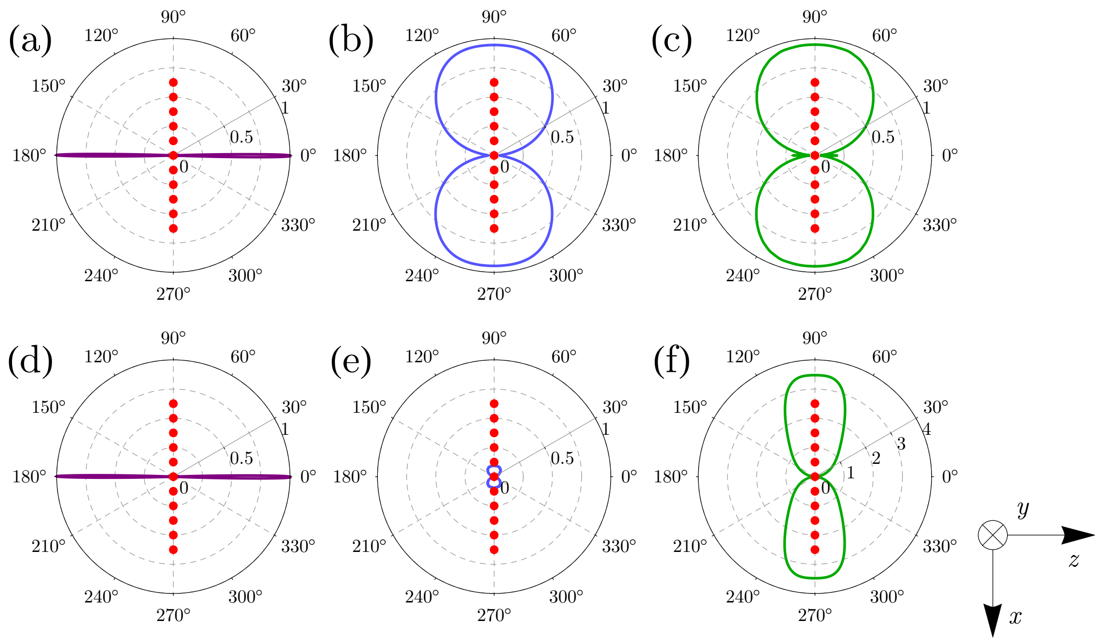

Fig. 2.3 Classical diffraction patterns (normalized to N^2) and quantum additions (normalized to N) for N fermions in a one-dimensional optical lattice (45 sites, half filling) in the non-interacting regime (first row) and for $U/J = 10$ (second row). The lattice extends into the vertical direction, and the probe is along the horizontal, i. e., the angle marked with 0° indicates the light intensity in the forward direction. The classical diffraction patterns (a,d) do not depend on the interaction while the quantum additions R_y (b,e) and R_x (c,f) distinguish between different ground states. Note that the scale in (f) is different from (a–e): the fluctuations in the atom number increase as the attraction between the atoms favors doubly-occupied sites. Red circles indicate the orientation of the lattice (not to scale).

2.2.4 3D Fermi gas in free space

We will now consider the example of a three-dimensional uniform atomic cloud with balanced spin population that is not loaded in an optical lattice, i. e. the atoms are free to move in space so that their positions are represented by real coordinates. If this is the case, we can generalize the $D-$operators to the continuum case by replacing the sums with integrals in the previous expressions. This approach is equivalent to the one presented in [160] and we report it in the next paragraphs with more details and analytic insight. In this case, the quantum addition to the light scattering R_σ becomes

$$R_\sigma(\theta_0,\theta_1) = |C|^2 \int\int J^*(\mathbf{r})J(\mathbf{r}')\left[\langle \hat{n}_\sigma(\mathbf{r})\hat{n}_\sigma(\mathbf{r}')\rangle - \langle \hat{n}_\sigma(\mathbf{r})\rangle\langle \hat{n}_\sigma(\mathbf{r}')\rangle\right] \mathrm{d}\mathbf{r}\,\mathrm{d}\mathbf{r}' \tag{2.42}$$

where $J(\mathbf{r}) = u_0^*(\mathbf{r})u_1(\mathbf{r})$. Focussing on the case of attractive interactions ($U < 0$), we compute the wavefunction of the atomic system by applying a Hartree-Fock mean field approximation equivalent to BCS theory [181]. Specifically, the interaction term in (2.17) is replaced by single particle operator (up to constant terms):

$$\begin{aligned}
&\hat{\Psi}^\dagger_\uparrow(\mathbf{r})\hat{\Psi}^\dagger_\downarrow(\mathbf{r})\hat{\Psi}_\downarrow(\mathbf{r})\hat{\Psi}_\uparrow(\mathbf{r}) \approx \\
&\qquad \langle\hat{\Psi}^\dagger_\uparrow(\mathbf{r})\hat{\Psi}^\dagger_\downarrow(\mathbf{r})\rangle\hat{\Psi}_\downarrow(\mathbf{r})\hat{\Psi}_\uparrow(\mathbf{r}) + \langle\hat{\Psi}_\downarrow(\mathbf{r})\hat{\Psi}_\uparrow(\mathbf{r})\rangle\hat{\Psi}^\dagger_\uparrow(\mathbf{r})\hat{\Psi}^\dagger_\downarrow(\mathbf{r}) + \\
&\qquad + \langle\hat{\Psi}^\dagger_\uparrow(\mathbf{r})\hat{\Psi}_\uparrow(\mathbf{r})\rangle\hat{\Psi}^\dagger_\downarrow(\mathbf{r})\hat{\Psi}_\downarrow(\mathbf{r}) + \langle\hat{\Psi}^\dagger_\downarrow(\mathbf{r})\hat{\Psi}_\downarrow(\mathbf{r})\rangle\hat{\Psi}^\dagger_\uparrow(\mathbf{r})\hat{\Psi}_\uparrow(\mathbf{r}) + \\
&\qquad - \langle\hat{\Psi}^\dagger_\uparrow(\mathbf{r})\hat{\Psi}_\downarrow(\mathbf{r})\rangle\hat{\Psi}^\dagger_\downarrow(\mathbf{r})\hat{\Psi}_\uparrow(\mathbf{r}) - \langle\hat{\Psi}^\dagger_\downarrow(\mathbf{r})\hat{\Psi}_\uparrow(\mathbf{r})\rangle\hat{\Psi}^\dagger_\uparrow(\mathbf{r})\hat{\Psi}_\downarrow(\mathbf{r}),
\end{aligned} \tag{2.43}$$

where the $\langle \ldots \rangle$ is the expectation value computed for the ground state of the system. In order to simplify the problem, we enforce some symmetry constraints on the approximated Hamiltonian resulting from this decomposition:

- translational symmetry is preserved, i. e. the system is homogeneous so that the local density does not depend on the position vector $\mathbf{r}$;
- spin-rotational symmetry is preserved (there is no magnetic order), so

$$\langle\hat{\Psi}^\dagger_\downarrow(\mathbf{r})\hat{\Psi}_\uparrow(\mathbf{r})\rangle = \langle\hat{\Psi}^\dagger_\uparrow(\mathbf{r})\hat{\Psi}_\downarrow(\mathbf{r})\rangle = 0 \tag{2.44}$$

- global spin balance. The two local spin densities are both given by

$$\langle\hat{\Psi}^\dagger_\sigma(\mathbf{r})\hat{\Psi}_\sigma(\mathbf{r})\rangle = n. \tag{2.45}$$

- global U(1) symmetry can be broken so that we can define the order parameter

$$U\langle\hat{\Psi}^{\dagger}_{\uparrow}(\mathbf{r})\hat{\Psi}^{\dagger}_{\downarrow}(\mathbf{r})\rangle = \Delta^{*} \tag{2.46}$$

$$U\langle\hat{\Psi}_{\downarrow}(\mathbf{r})\hat{\Psi}_{\uparrow}(\mathbf{r})\rangle = \Delta, \tag{2.47}$$

where Δ could be different from zero, depending on the value of the interaction parameter U, the particle density n and, in general, the temperature. Note that one can choose a real value for Δ assuming that any complex phase is absorbed by the creation and annihilation operators of the matter field. Moreover, this parameter is related to the gap of the excitation spectrum of the system state [181].

Taking the Fourier transform (FT) of the matter field operators

$$\hat{\Psi}_{\sigma}(\mathbf{r}) = \left(\frac{1}{2\pi}\right)^{3/2}\int e^{i\mathbf{k}\cdot\mathbf{r}}\hat{f}_{\mathbf{k}\sigma}\,\mathrm{d}\mathbf{k} \tag{2.48}$$

and defining the non-interacting single particle spectrum $\epsilon(\mathbf{k}) = k^2/2m$, the mean field Hamiltonian describing the atomic system becomes

$$\hat{H}_{\mathrm{MF}} - \mu\hat{N} = \frac{1}{(2\pi)^3}\int\sum_{\sigma}\tilde{\epsilon}(\mathbf{k})\hat{f}^{\dagger}_{\mathbf{k}\sigma}\hat{f}_{\mathbf{k}\sigma} - \Delta\left(\hat{f}^{\dagger}_{\mathbf{k}\uparrow}\hat{f}^{\dagger}_{\mathbf{k}\downarrow} + \hat{f}_{\mathbf{k}\downarrow}\hat{f}_{\mathbf{k}\uparrow}\right)\mathrm{d}\mathbf{k}. \tag{2.49}$$

where we introduced the chemical potential μ in order to fix the average number of particles in the system (i. e. we work in the grand-canonical ensemble) and $\tilde{\epsilon}(\mathbf{k}) = \epsilon(\mathbf{k}) - \mu - Un/2$. This operator can be easily diagonalised performing a Bogoliubov transformation [6] of the matter field. Importantly, this mean field approach is equivalent to BCS theory since the Bogoliubov coefficients $u_{\mathbf{k}}$ and $v_{\mathbf{k}}$ can be used for defining the variational wavefunction

$$|\Psi_{BCS}\rangle = \prod_{\mathbf{k}}\left(u_{\mathbf{k}} + v_{\mathbf{k}}\hat{f}^{\dagger}_{\mathbf{k}\uparrow}\hat{f}^{\dagger}_{-\mathbf{k}\downarrow}\right)|0\rangle, \tag{2.50}$$

where $|0\rangle$ is the particle vacuum and

$$\begin{cases} |v_{\mathbf{k}}|^2 = \dfrac{1}{2}\left(1 - \dfrac{\epsilon(\mathbf{k}) - \mu}{\sqrt{(\epsilon(\mathbf{k}) - \mu)^2 + |\Delta|^2}}\right) \\ |u_{\mathbf{k}}|^2 = \dfrac{1}{2}\left(1 + \dfrac{\epsilon(\mathbf{k}) - \mu}{\sqrt{(\epsilon(\mathbf{k}) - \mu)^2 + |\Delta|^2}}\right) \end{cases} \tag{2.51}$$

Within this formulation, the physical meaning of $u_{\mathbf{k}}$ and $v_{\mathbf{k}}$ becomes transparent: they allow the wavefunction to be *flexible* in order to describe both the superconducting and the normal state. For example, if the order parameter Δ is zero, one has $u_{\mathbf{k}} = 0$ and $v_{\mathbf{k}} = 1$ if $|\mathbf{k}| \leq k_{\mathrm{F}}$ while $u_{\mathbf{k}} = 1$ and $v_{\mathbf{k}} = 0$ if $|\mathbf{k}| > k_{\mathrm{F}}$ where k_{F} is the Fermi vector $k_F = (3\pi^2 n)^{1/3}$. In this case, the $|\Psi_{BCS}\rangle$ coincides with the Fermi sea. Moreover, we can use the wavefunction (2.50) for calculating the quantum addition to the scattering light in the case of an attractive Fermi gas. Focusing on the cases of R_x and R_y, we need to compute the two-points functions

$$\begin{aligned} \langle \hat{\rho}(\mathbf{r})\hat{\rho}(0)\rangle &= \langle (\hat{n}_\uparrow(\mathbf{r}) + \hat{n}_\uparrow(\mathbf{r}))\,(\hat{n}_\uparrow(0) + \hat{n}_\uparrow(0))\rangle \\ &= n^2 + n\,\delta(\mathbf{r}) - 2\,|\alpha(\mathbf{r})|^2 + 2\,|\beta(\mathbf{r})|^2 \end{aligned} \tag{2.52}$$

$$\begin{aligned} \langle \hat{m}(\mathbf{r})\hat{m}(0)\rangle &= \langle (\hat{n}_\uparrow(\mathbf{r}) - \hat{n}_\uparrow(\mathbf{r}))\,(\hat{n}_\uparrow(0) - \hat{n}_\uparrow(0))\rangle \\ &= n\,\delta(\mathbf{r}) - 2\,|\alpha(\mathbf{r})|^2 - 2\,|\beta(\mathbf{r})|^2 \end{aligned} \tag{2.53}$$

where the functions $\alpha(\mathbf{r})$ and $\beta(\mathbf{r})$ are given by

$$\alpha(\mathbf{r}) = \frac{1}{(2\pi)^3}\int e^{i\mathbf{k}\cdot\mathbf{r}}|v_{\mathbf{k}}|^2\,\mathrm{d}\mathbf{k} \tag{2.54}$$

$$\beta(\mathbf{r}) = \frac{1}{(2\pi)^3}\int e^{i\mathbf{k}\cdot\mathbf{r}}u_{\mathbf{k}}v_{\mathbf{k}}^*\,\mathrm{d}\mathbf{k} \tag{2.55}$$

Therefore, in order to compute R_x and R_y it is necessary to find the order parameter Δ and the chemical potential μ so that it is possible to estimate $u_{\mathbf{k}}$ and $v_{\mathbf{k}}$. This can be achieved by minimizing the energy of the atomic system for given values of the interaction strength U and the atomic density n, leading to a system of two self-consistent equations:

$$\begin{cases} \dfrac{2}{U} = \dfrac{1}{(2\pi)^3} \displaystyle\int \frac{\mathrm{d}\mathbf{k}}{\sqrt{(\epsilon(\mathbf{k})-\mu)^2+|\Delta|^2}} \\ n = \dfrac{1}{(2\pi)^3} \displaystyle\int \left[1 - \frac{\epsilon(\mathbf{k})-\mu}{\sqrt{(\epsilon(\mathbf{k})-\mu)^2+|\Delta|^2}}\right] \mathrm{d}\mathbf{k} \end{cases} \tag{2.56}$$

Because of the peculiar nature of the contact interaction chosen in (2.17) (i. e. there is no cut-off frequency if the interaction is expressed in momentum space), attempting to solve these expressions directly leads to inevitable divergences. For this reason, the coupling constant U has to be renormalized. Importantly, a BCS-like cutoff (e. g. Debye frequency) cannot be used in the strong coupling BEC regime: all the fermions are affected by the interaction, not just those occupying the Fermi surface. Therefore, we choose the renormalization

$$\frac{m}{4\pi a} = -\frac{1}{U} + \frac{1}{(2\pi)^3} \int_{|\mathbf{k}|<\Lambda} \frac{\mathrm{d}\mathbf{k}}{2\epsilon(\mathbf{k})} \tag{2.57}$$

where a is the s-wave scattering length [143] and Λ is a cut-off frequency. Using this expression and making use of the rotational symmetry, the system (2.56) reduces to two coupled one-dimensional integral equations

$$\begin{cases} \dfrac{1}{ak_F} = \dfrac{2}{\pi} \displaystyle\int_0^\infty \left(1 - \frac{x^2}{\sqrt{(x^2-\mu)^2+|\Delta|^2}}\right) \mathrm{d}x \\ 1 = \dfrac{3}{2} \displaystyle\int_0^\infty x^2 \left(1 - \frac{x^2-\mu}{\sqrt{(x^2-\mu)^2+|\Delta|^2}}\right) \mathrm{d}x \end{cases} \tag{2.58}$$

These equations must be solved numerically up to self-consistency for given values of ak_F, to determine the order parameter Δ, and the chemical potential μ (see Figure 2.4).

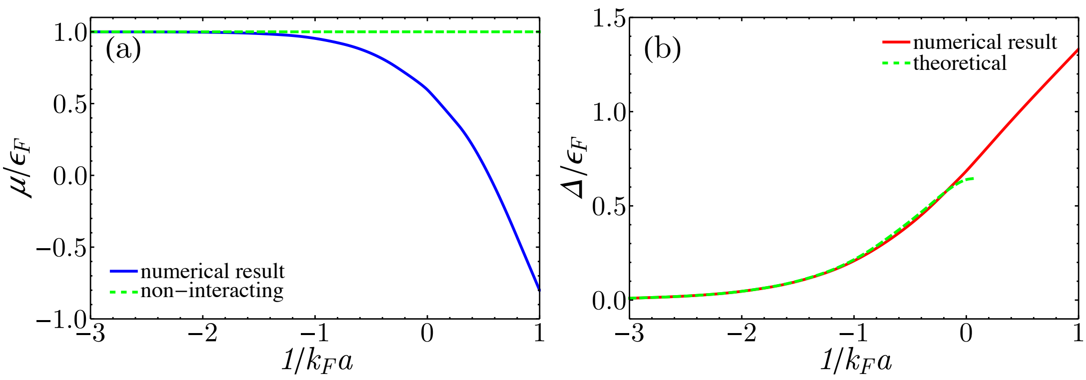

Fig. 2.4 Chemical potential and order parameter Δ for a 3D uniform Fermi gas. The analytical prediction represented by the green dashed line in the right plot is obtained expanding (2.58) for small Δ as in [181].

Note that, because of the rotational symmetry of the system, both α and β depend solely on $r = |\mathbf{r}|$. Moreover, one can proove that the function $\beta(\mathbf{r})$ diverges like $\sim 1/r$ if $r \to 0$: this is an artefact of the zero-range interaction between the fermions, and can not be eliminated using a renormalisation procedure as we did for the interaction strength U [187].

2.2.5 Probing local fluctuations in the magnetization

The approach described in the previous paragraphs is particularly convenient for probing the magnetic properties of the atomic system. If the mode functions of the light field are traveling waves and the whole atomic cloud is illuminated, i. e. $u_l(\mathbf{r}) = e^{i\mathbf{k}_l\cdot\mathbf{r}}$, the quantum addition R_x (R_y) coincides with the Fourier transform of the density (magnetization) correlations which reduces to a one-dimensional integral

$$R_x(\theta_0, \theta_1) = |C|^2 \left[N - 8\pi\Omega \int_0^{+\infty} \frac{r\sin(ar)}{a} \left(|\alpha(r)|^2 - |\beta(r)|^2 \right) \mathrm{d}r \right] \tag{2.59}$$

$$R_y(\theta_0, \theta_1) = |C|^2 \left[N - 8\pi\Omega \int_0^{+\infty} \frac{r\sin(ar)}{a} \left(|\alpha(r)|^2 + |\beta(r)|^2 \right) \mathrm{d}r \right] \tag{2.60}$$

where $a = |\mathbf{k}_0 - \mathbf{k}_1|/k_{\mathrm{F}}$ and Ω is the volume occupied by the atomic cloud. In analogy to the bosonic case, we can compute the *total* fluctuations of the particle number or the magnetization by focusing on the case of forward scattering ($\mathbf{k}_1 = \mathbf{k}_0$). Since we solved the mean field problem in the grand-canonical ensemble, the number of the BCS state is analogous to the coherent state in the bosonic case and the number of particles is not fixed so that $R_x(0,0) = N$. Moreover, the BCS wavefunction (2.50) is an eigenstate of the total magnetisation operator and therefore the quantum addition $R_y(0,0)$ vanishes [124]. Probing the system in this geometry is not particularly interesting since it does not give us any particular insight on the physics of the system. In order to investigate the *local* fluctuations in the magnetization, we examine the case of a probe with a Gaussian profile and we focus on forward-scattering. Specifically, we considered the mode functions

$$u_0(\mathbf{r}) = e^{-\frac{x^2+y^2}{2\sigma^2}} e^{ikz} \qquad \text{and} \qquad u_1(\mathbf{r}) = e^{-\frac{x^2+y^2}{2\sigma^2}} e^{ikz} \tag{2.61}$$

so the quantum addition sensitive to the magnetization is

$$R_y(0,0) = \frac{N}{2\Omega}\pi\sigma^2 L\left(1 + \frac{2\Omega}{N}(2\pi)^{3/2}k_F\sigma\int_0^{+\infty}\mathrm{d}x\, x\,\xi(x)\,\mathrm{Im}\left[w\left(-\frac{x}{\sqrt{2}\sigma k_F}\right)\right]\right) \tag{2.62}$$

where $\xi(x) = |\alpha(r)|^2 + |\beta(r)|^2$, $w(x)$ is the Faddeeva function [3]

$$w(x) = e^{-x^2}\left(1 + \frac{2i}{\sqrt{\pi}}\int_0^z e^{t^2}\mathrm{d}t\right) \tag{2.63}$$

and L the dimension of the atomic cloud along the z direction. Figure 2.5 shows the value of R_y/N as a function of the interaction strength for various beam waists of the Gaussian probe. The fluctuations in the magnetization are directly mapped on the radiation field: the quantum fluctuations are suppressed when the characteristic size of a Cooper pair is comparable to the width of the Gaussian probe. If this is the case, the pair is contained in the illuminated area, so the magnetization in the region probed by the laser does not fluctuate. In order to confirm this result we computed the so-called Pippard length ξ_P which characterizes the size of a Cooper pair in the BCS theory. This length scale is given by $\xi_P = 1/(\pi k_{\mathrm{F}}|\Delta|)$. Figure 2.6 shows the relative fluctuations of the detected light as a function of the Pippard length for various beam waists. Again, fluctuations are strongly suppressed when the size of a pair is comparable to the width of the Gaussian probe. The main experimental difficulty in this setup is that in order to explore the full range of fluctuations one should consider $\sigma k_{\mathrm{F}} \sim 1$. In typical experiments ($n \sim 10^{13}\,\mathrm{cm}^{-3}$) the Fermi wavevector is $k_{\mathrm{F}} \sim 150\,\mathrm{nm}^{-1}$ and therefore a very tightly focused laser is required for observing the effects we illustrated. For this reason, it is more convenient to consider the case where the gas is loaded in an optical lattice.

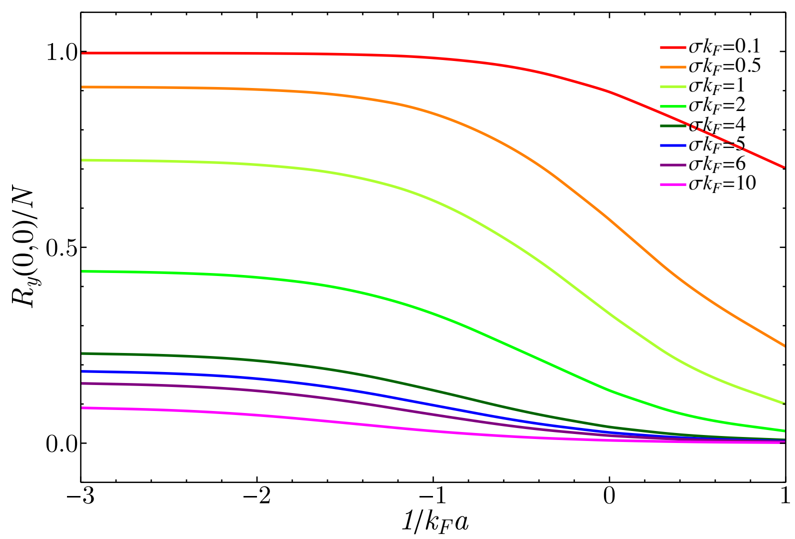

Fig. 2.5 Relative fluctuations for the detected photons in the forward direction. Note that these are decreasing as a function of the interaction (tighter pairs) and the beam waist. These results can be compared to [160].

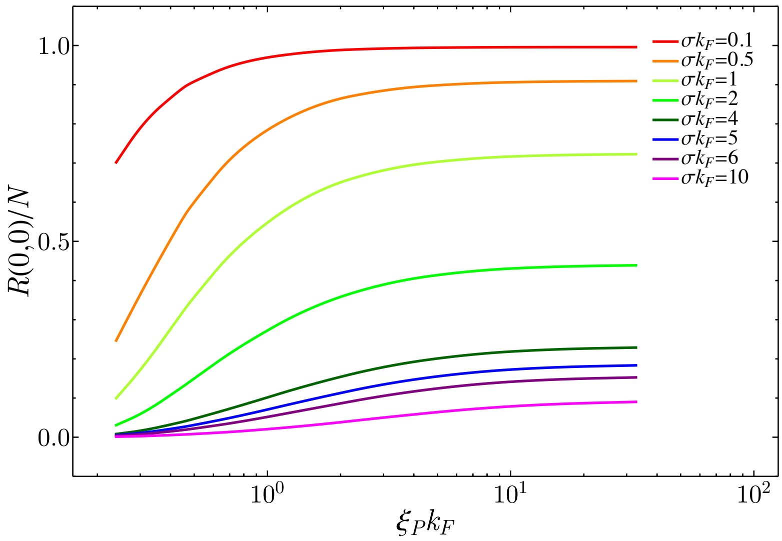

Fig. 2.6 Relative fluctuations for the detected photons in the forward direction as a function of the Pippard length for various beam widths. Note that fluctuations are suppressed when $\xi_P k_F$ is less than ~ 1.

2.3 Light mediated synthetic atom-atom interaction[2]

Typical experiments with ultracold atoms in optical lattices allow to experimentally realize effective Hamiltonians which contain short-range physical processes such as tunneling between neighboring lattice sites and on-site interactions. The implementation of long-range interactions that extend over many lattice sites is an extremely challenging task since it requires the use of more complex systems such as polar molecules [14, 96] or Rydberg atoms [64, 137, 148]. Moreover, the spatial structure of the interaction itself is fixed by the physical system used (e.g. dipole-dipole interaction for molecules and Van der Waals interaction for Rydberg atoms) and cannot be changed.

In this section, we show that loading an optical lattice inside a cavity allows to engineer synthetic many-body interactions with an arbitrary spatial profile [35]. These interactions are mediated by the light field and do not depend on fundamental processes,

[2]The results presented in this section are published in [35].

making them extremely tunable and suitable for realizing quantum simulations of many-body long-range Hamiltonians. In contrast to other proposals based on light-mediated interactions [26, 48, 135, 150, 177], we suggest a novel approach, where the shortening of the a priori infinitely long-range (global) light-induced interaction does not degrade the collective light-matter interaction, but rather benefits from it. In contrast to other proposals, where shortening of the interaction length requires increasing the number of light modes, in our case, rather short-range interactions can be simulated with a small number of light modes. Moreover, even a single mode cavity is enough to simulate some finite-range interactions. As a result, the quantum phase of matter possesses properties of systems with both short-range and global collective interactions. The effective Hamiltonians can be an acceptable representation of an otherwise experimentally hard-to-achieve quantum degenerate system with finite range interactions.

The coupling between the light field and the atoms described by the Hamiltonian (2.8) leads to a rather complicated structure of the Hilbert space of the system since light and matter become entangled. However, in the good cavity limit $|\Delta_p| \gg \kappa$, while $|\Delta_p| \gg |U|$ and $|\Delta_p| \gg |J|$ the light field can be adiabatically eliminated. In this section, we will focus on the effective interatomic interaction that is mediated by the cavity field. In general, the problem of reconstruction of the effective matter Hamiltonian is hard, and there are several alternatives for this reconstruction as shown in [32, 57, 106]. Thus, the light field becomes enslaved by the matter and vice versa, we refer to this as cavity backaction. This leads to the effective Hamiltonian:

$$\hat{H}_{\text{eff}} = \hat{H}_a + \sum_c \sum_{p,q} \left(\frac{g_{\text{eff}}^{pqc}}{2} \hat{F}_{pc}^\dagger \hat{F}_{qc} + \frac{(g_{\text{eff}}^{pqc})^*}{2} \hat{F}_{pc}^\dagger \hat{F}_{qc} \right) \tag{2.64}$$

where the effective coupling constant is

$$g_{\text{eff}}^{pqc} = g_c^* g_q / (\Delta_{qc} + i\kappa_c) \tag{2.65}$$

where we defined the detuning $\Delta_{qc} = \omega_q - \omega_c$. Note that, in order to distinguish between cavity modes and probe beams, in this section we will use a slightly different notation where the index c refers to the cavity modes (for a multimode cavity or several cavities), p and q refer to the probe beams. The new terms in (2.64) are the by-product of the cavity backaction of light and matter: an effective structured interaction that depends on the form of coefficients given by the effective interaction couplings g_{eff}^{pqc}. Careful analysis [32] shows that beyond the adiabatic limit, additional terms modify the effective Hamiltonian due to the non-commuting nature between light induced processes with the original matter Hamiltonian and higher order photon processes. In what follows we will always consider the adiabatic limit. Recalling that the $F-$operator can be expressed as $\hat{F}_{pc} = \hat{D}_{pc} + \hat{B}_{pc}$, the new terms beyond the atomic Hamiltonian $\hat{H}_a$ give rise to effective long-range light-induced interaction which is characterized by three different kinds of terms: density-density interactions ($\sim \hat{D}_{pc}\hat{D}_{qc}$), bonds-bonds interactions ($\sim \hat{B}_{pc}\hat{B}_{qc}$) and density-bond interactions ($\sim \hat{D}_{pc}\hat{B}_{qc}$). Moreover, each of these terms depends on the geometry of the cavity modes and light pumps injected into the system which determine the emergent phases in the system. The coefficients J_{ij}^{pc} together with the effective interaction couplings g_{eff}^{pqc} give an unprecedented ability to design an arbitrary interaction profile between the atoms. The new terms from (2.64) provide the system with a plethora of new possibilities [32, 34, 35].

In principle one can design arbitrary interaction patterns by choosing the geometry of the light: modifying angles, pump amplitudes, detunings and cavity parameters. Certainly, the potential of this to enrich cold atomic systems in terms of the simulation and design of interactions is vast. In what follows, we will discuss some simple examples of how the above Hamiltonian can be used to generate synthetic interactions for quantum simulation, i.e. the couplings between the atoms is not a consequence of fundamental physical processes but are mediated by the light field and depend on the geometrical arrangement of the probe beam and the optical cavity.

2.3.1 One probe and one cavity

For a deep optical lattice, the $B-$contribution to the $F-$operator can be neglected. If only one probe and one optical cavity are present, the effective atom-atom interaction can be re-written as:

$$\hat{H}_{\text{int}} = g_{\text{eff}} \sum_{i,j} W_{ij} \hat{n}_i \hat{n}_j. \tag{2.66}$$

with $g_{\text{eff}} = \text{Re}[g_{\text{eff}}^{111}]/2 = \Delta_{11}|g_1|^2/(\Delta_{11}^2 + \kappa_1^2)$, thus the effective interaction strength factors out. The specific dependence of the functions J_{ii}^{11} defines the spatial profile of the interaction between the atoms via the interaction matrix $W_{ij} = 2\,\text{Re}\left[(J_{ii}^{11})^* J_{jj}^{11}\right]$. In order to illustrate this, we focus on a one-dimensional lattice and we consider traveling waves as mode functions for the light modes (i. e. $u_c(\mathbf{r}) = e^{i\mathbf{k}_c\cdot\mathbf{r}}$ and $J_{jj}^{11} = e^{i(\mathbf{k}_{c_1} - \mathbf{k}_{p_1})\cdot\mathbf{r}_j}$) so that W_{ij} becomes:

$$W_{ij} = \cos\left[(\mathbf{k}_{c_1} - \mathbf{k}_{p_1}) \cdot (\mathbf{r}_i - \mathbf{r}_j)\right]. \tag{2.67}$$

The cavity induces a periodic interaction between the atoms and, depending on the projection of $\mathbf{k}_{c_1} - \mathbf{k}_{p_1}$ along the lattice direction $\hat{e}_{\mathbf{r}_i}$, its spatial period can be tuned to be commensurate or incommensurate to the lattice spacing. Specifically, if $J_{jj}^{11} = e^{i2\pi j/R}$ and $R \in \mathbb{Z}$, atoms separated by R lattice sites scatter light with the same phase and intensity and the optical lattice is partitioned in R macroscopically occupied regions (spatial modes) composed by non-adjacent lattice sites [52] (see §2.2.2). The specific geometric configuration of the light beams is determined by the angles θ_{c_1,p_1} between the

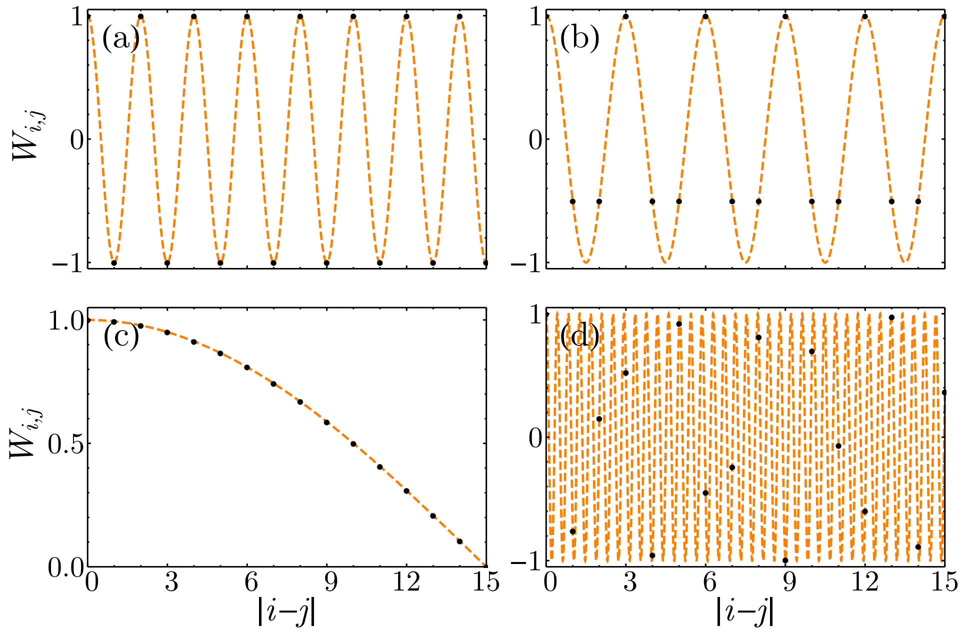

Fig. 2.7 Different interactions that can be implemented using a single cavity mode and a single probe for $L = 16$ lattice sites and using traveling waves as mode functions. The panels illustrate the value of $W_{i,j}$ as a function of $|i-j|$ (normalized). Panels (a) and (b): interaction strength in presence of $R = 2$ ($\theta_{c_1} = 0$, $\theta_{p_1} = \pi/2$, $\lambda = 2a$) and 3 ($\theta_{c_1} = 0$, $\cos\theta_{p_1} = 1/3$, $\lambda = 2a$) spatial modes. The value of $W_{i,j}$ depends solely on the mode distance. Panel (c): increasing the number of atomic modes leads to long-range interactions with a well-defined spatial profile ($\theta_{c_1} = 0$, $\cos\theta_{p_1} = 7/8$, $\lambda = 2a$). Panel (d): the periodicity of $W_{i,j}$ is incommensurate to the lattice spacing, resulting in a "disordered" interaction.

wavevectors $\mathbf{k}_{c_1,p_1}$ and $e_{\mathbf{r}_i}$: in order to have R spatial modes, one has to set

$$\cos\theta_{p_1} = \cos\theta_{c_1} - \frac{\lambda}{a}\frac{1}{R} \tag{2.68}$$

where λ is the wavelength of the light modes. If this relation is fulfilled, W_{ij} has periodicity R lattice sites and, defining the operator $\hat{N}_j$ to be the population of the mode j, the interaction strength between two atoms belonging to the different modes i and j depends solely on their *mode distance* ($(i-j)\mathrm{mod}R$) and not their actual separation. In this case, we find that the mode-mode interaction Hamiltonian is given by

$$\hat{H}_{\text{int}} = 2g_{\text{eff}} \sum_{i,j=1}^{R} \cos\left[\frac{2\pi}{R}(i-j)\right] \hat{N}_i \hat{N}_j. \tag{2.69}$$

The case $R = 2$ has been recently realized [98], showing that new light-mediated interaction heavily affects the ground state of the Bose-Hubbard model inducing a new supersolid phase. Simply changing the angle between the cavity and the optical lattice, one can increase the number of spatial modes and therefore implement more complicated long-range interactions that cannot be obtained using molecules or Rydberg atoms (see Figure 2.7). If the period of W_{ij} is incommensurate to the lattice spacing, the spatial modes are not well-defined since each lattice sites scatters light with a different phase and amplitude. Therefore, the value of the interaction matrix is no longer periodic and resembles disorder [70]. This behavior is analogous to the potential generated by the superposition of two incommensurate optical lattices [163] which has been used for generating controllable disordered potential, allowing the observation of Anderson localization and new quantum phases (Bose glass) in ultracold gases [46, 156]. Here, we move a step further and we create synthetic random interactions between the atoms, generalizing the Anderson model where disorder affects only the local potential and/or the tunneling amplitude [62, 133].

2.3.2 Multiple probes and one cavity

The previous simple case where only one cavity and one probe are present allows to realize interactions that resemble a cosine profile. We know turn to a different monitoring scheme where the atoms are probed with R different classical pumps and scatter light to a single optical cavity. In addition to the previous paragraphs, where the light mode of the cavity has contributions from all the sites of the optical lattice, all the probe beams contribute to the value of the light field inside the cavity and the effective atom-atom interaction is

$$\hat{H}_{\text{int}} = \sum_{p,q=1}^{R} \left(\frac{g_{\text{eff}}^{pq1}}{2} \hat{D}_{p1}^{\dagger} \hat{D}_{q1} + \text{h.c.} \right) \tag{2.70}$$

The spatial profile of the interaction described by (2.70) can be tuned changing the light mode functions or/and the intensity and phase of the probe beams. As in the previous examples, we consider traveling waves as mode functions for the light and we note that

$$\hat{H}_{\text{int}} = \gamma_{\text{eff}} \sum_{l,m=1}^{R} \sum_{i,j} \left(g_l^* g_m e^{-i(\mathbf{k}_{c_1} - \mathbf{k}_{p_l})\cdot \mathbf{r}_i} \, e^{i(\mathbf{k}_{c_1} - \mathbf{k}_{p_m})\cdot \mathbf{r}_j} \hat{n}_i \hat{n}_j + \text{h.c.} \right) \tag{2.71}$$

with $\gamma_{\text{eff}} = \Delta_{pc}/(\Delta_{pc}^2 + \kappa_c^2)$, as the pumps have the same wavelength $\lambda_{p_l} = \lambda_{p_m}$, such that all the detunings are the same: $\Delta_{p_l c} = \Delta_{p_m c} = \Delta_{pc}$. This is equivalent to the product of two Discrete Fourier Transforms (DFT) if $a(\mathbf{k}_{c_1} - \mathbf{k}_{p_l}) \cdot \hat{e}_{\mathbf{r}_i} = 2\pi l/R$ for all the probe beams $l = 1, 2, ...R$, and $\hat{e}_{\mathbf{r}_i}$ is the unit vector of $\mathbf{r}_i$ and a the lattice spacing. Importantly, these conditions fix only the directions of the probe beams ($\cos\theta_{p_l} = \cos\theta_{c_1} - \frac{\lambda}{a}\frac{l}{R}$) and not their intensities or phases, i. e. the coefficients g_p. Furthermore, the probe beams divide the optical lattice in R macroscopically occupied spatial modes which interact according to the Hamiltonian

$$\hat{H}_{\text{int}} = \gamma_{\text{eff}} \sum_{i,j=1}^{R} \left(V_i^* V_j \hat{N}_i \hat{N}_j + h.c. \right), \tag{2.72}$$

where $V_j = \sum_{m=1}^{R} g_m e^{i\frac{2\pi m j}{R}}$ describes the strength of the interaction between the *spatial modes* defined by the light scattering. Tuning the probe intensities and their relative phase, the function V_j can be modified to design to any spatial profile, as illustrated in Figure 2.8. Importantly, (2.69) implies that the coupling between the modes i and j is $W_{ij} \propto V_i^* V_j$ and therefore the interaction matrix W_{ij} does not depend on the *distance* between the spatial modes. This is in contrast to the usual solid state physics scenarios

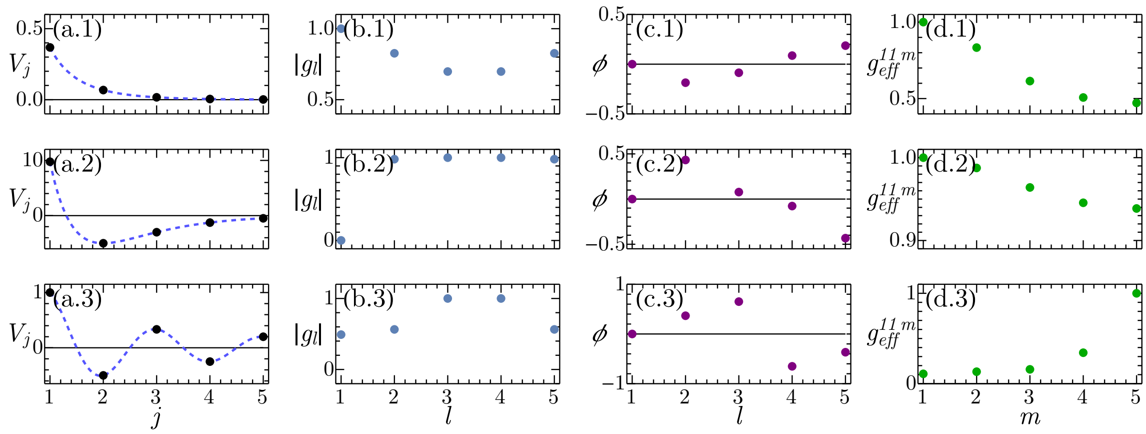

Fig. 2.8 Examples different synthetic interactions that can be implemented using traveling waves as mode functions. Panel (a) represents the effective synthetic interaction potential V_j. We show a Yukawa potential ($V_j = V_j = e^{-j}/j$) in panel (1), a Morse potential in panel (2)$\left(V_j = 5\left[(1-e^{-(j-2)})^2 - 1\right]\right)$ and a Bessel potential in panel (3) ($V_j = \pi y_0(\pi x)$), where y_0 is the Bessel function of the second kind. Panels (b) and (c) show the parameters using a single cavity and five probes described by the effective intensity $|g_l|$ (normalized) and the phase $\phi = \mathrm{Arg}(g_l)$, the effective interaction is $W_{ij} \propto V_i^* V_j$ ($\theta_{c_1} = 0$, $\cos\theta_{p_l} = 1 - 2l/5$, $\lambda = 2a$). Panel (d) shows the effective couplings for five cavity modes and one probe corresponding to (a), the effective interaction is $W_{ij} \propto V_{|i-j|}$ ($\theta_{p_1} = 0$, $\cos\theta_{c_l} = 1 - l/5$, $\lambda = 2a$).

where interactions do not depend on the specific position of two particles but only on their distance. This interaction is akin to multicomponent interactions due to different spin projections in a BEC. Here, the interaction coefficients between each light induced mode have an arbitrary coupling that links all the elements in the manifold. The scheme we propose opens the possibility of studying new classes of interactions and effects not observable in conventional systems. It is worth mentioning that there is only one distance-dependent interaction function that can be realized with this setup: a cosine profile. Specifically, one has $W_{ij} = W_{|i-j|}$ only if V_j is a pure phase (which can be obtained with one probe and one cavity).

In this paragraph, we assumed the light mode functions to be traveling waves which allowed us to give a simple description of the synthetic interactions in terms of DFT. Importantly, the definition of the spatial modes does not rely on this assumption but only on the fact that the coefficients J_{jj} can have the same value on different lattice sites so that atoms in these positions scatter light with the same phase and intensity. For example, it is possible to realize the case $R = 2$ by considering standing waves ($u_i(\mathbf{r}) = \cos(\mathbf{k}_i \cdot \mathbf{r})$) crossed at such angles to the lattice that $\mathbf{k}_0 \cdot \mathbf{r}$ is equal to $\mathbf{k}_1 \cdot \mathbf{r}$ and shifted such that all even sites are positioned at the nodes, so $J_{ii} = 1$ for i odd while $J_{ii} = 0$ for i even or the $R = 3$ case by imposing $\mathbf{k}_{1,0} \cdot \mathbf{r} = \pi/4$ so that the coefficients J_{ii} are $J_{ii} = [1, 1/2, 0, 1/2, 1, 1/2, 0...]$. If the light mode functions are not traveling waves, the general form of the interaction between the modes follows $V_j = \sum_{m=1}^{R} g_m J_{jj}$ where J_{jj} is not a simple phase factor. Therefore, in order to engineer a given long range interaction it is not possible to use the simple DFT formalism for computing the coefficients g_m but one has to resort to numerical methods.

2.3.3 Multiple cavity modes and one probe

In order to obtain an interaction that depends solely on the distance between the atoms (or the modes), we turn to the case of one classical probe which scatters photons to R light modes. This scheme can be realized using multiple cavities crossing at specific angles or a multi mode cavity. In this case, the atoms scatter ligth from the probe beam to more than one quantized light mode whihch mediates long-range interactions. Although this setup is more challenging to realize than the previous ones that we have described, recent experiments succeeded in trapping a BEC at the intersection of two optical cavities [102] (see Figure 2.9) and observed the formation of a supersolid quantum phase.

Considering only the events when light is scattered by the atoms from the probe beam to one of the cavities and neglecting the photon scattering between different cavities, we

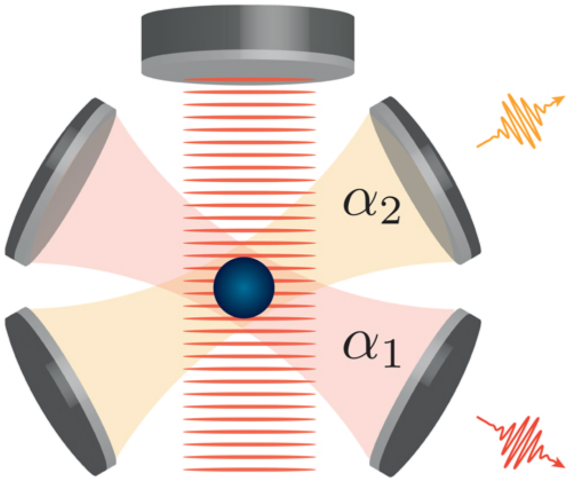

Fig. 2.9 Schematic representation of a interaction between an atomic system (blue), a single probe beam (red stripes) and two optical cavities (α_1 and α_2). Photons scattered by the atoms populate the two cavity modes and mediate a long-range interaction that leads to a supersolid phase. From [102].

find that the atom-atom interaction follows

$$\hat{H}_{\text{int}} = \sum_{m=1}^{R} \left(\frac{g_{\text{eff}}^{11m}}{2} \hat{D}^{\dagger}_{1m} \hat{D}_{1m} + \text{h.c.} \right) \tag{2.73}$$

where $g_{\text{eff}}^{11m} = \Delta_{1m}|g_1|^2/(\Delta_{1m}^2 + \kappa_{1m}^2)$. Eq. (2.73) is fundamentally different from (2.70) since here only one sum is present and the interaction does not mix $D-$operators with different indexes. This allows to engineer long-range interactions that depend on the distance between the lattice sites and are analogous to the usual two-body interactions studied in condensed matter systems. We illustrate this by considering traveling waves as mode functions for the light and (2.73) becomes:

$$\hat{H}_{\text{int}} = \sum_{m=1}^{R} \sum_{i,j} \left(g_{\text{eff}}^{11m} e^{-i(\mathbf{k}_{p_1} - \mathbf{k}_{c_m})\cdot(\mathbf{r}_i - \mathbf{r}_j)} \hat{n}_i \hat{n}_j + \text{h.c.} \right) \tag{2.74}$$

Fixing the the direction of the wave vectors of the cavity modes so that $a(\mathbf{k}_{p_1} - \mathbf{k}_{c_m}) \cdot \hat{e}_{\mathbf{r}_i} = \pi l/R$ for all $l = 1, 2, ...R$ (corresponding to the angles fulfilling $\cos\theta_{c_l} = \cos\theta_{p_1} - \frac{\lambda}{2a}\frac{l}{R}$), the light scattering process defines R spatial modes and we can perform a DFT analysis. However, instead we have a Discrete Cosine Transform. Specifically, (2.74) reduces to

$$\hat{H}_{\text{int}} = 2\sum_{i,j} V_{|i-j|}\hat{N}_i\hat{N}_j, \tag{2.75}$$

where $V_j = \sum_{m=1}^{R} g_{\text{eff}}^{11m}\cos(\frac{\pi m j}{R})$. In contrast to the scheme we considered in the previous paragraphs, here the interaction between mode i and mode j depends solely on the distance between the modes $(i-j)$ and can be shaped to any V_j profile changing the detunings and the decay coefficients of the cavities. Therefore, this scheme allows to realize quantum simulators that are able to mimic long-range interactions with an arbitrary spatial profile, such that $W_{i,j} \propto V_{|i-j|}$.

As we see, the global (infinitely long-range) light-matter interaction allows to simulate systems with rather short-range and tunable interactions. Moreover, simulating short-range interaction requires just a small number of light modes. Indeed, the price for this is that we do not simulate an original problem of interacting atoms at sites, but replace it by an effective one, simulating the interaction between the global modes. The effective mode Hamiltonians can be an acceptable representation of an otherwise experimentally hard to achieve quantum degenerate system with finite range interaction. Such a global but spatially structured interaction, can still compete with intrinsic short-range processes leading to non-trivial phases. As a result, the quantum phases will have properties of systems due to both short-range and global processes, thus directly benefiting from the collective enhancement of the light-matter coupling [35].

2.4 Discussion

Quantum optics and quantum gases are rather separate fields: The former deals with delicate quantum effects such as quantum measurement, but in systems without strong correlations and interactions. The latter typically deals with truly many-body systems, but with classical light only. The study of quantum optical effects in ultracold atomic systems is a rather recent research direction. Nevertheless, this should not be considered as a mere theoretical *Gedankenexperiment*: new experimental breakthrough realized the setup we describe in this Chapter [87, 98] and several other groups are working on achieving the ultimate quantum regimes of light-matter interactions where ultracold atoms, optical lattices and cavities are combined together. We can drawn an analogy with famous cavity QED experiments [72], where the quantum light states in a cavity were probed and projected by measuring atoms. Here, light and matter are reversed and we probe matter-fields with light. A striking advancement is that the number of quantum matter waves (sites with trapped atoms) can be easily scaled from few to thousands by changing the number of illuminated sites, while scaling cavities is a challenge [72].

We showed that, by taking into account the quantum nature of the light field, it is possible to map the correlations of the quantum state of the atoms to the angular distribution of the scattered light. We applied these ideas to a system of ultracold fermions and we found that by detecting the photons escaping the optical cavity one can distinguish between different ground states of the atomic system. For example, probing the atomic cloud with linearly polarized light allows to measure the local fluctuations of the magnetization and to determine the spatial extension of Cooper pairs. The setup we considered is extremely flexible and opens new opportunities for probing and distinguishing different quantum phases non-destructively [91]. Moreover, because of the global coupling between the light field and the atoms, if some lattice sites scatter light with the same phase and intensity the measurement defines macroscopically occupied spatial modes. Depending on the number of probe beams and optical cavities and on their geometric orientations, the light field mediates an effective long-range interaction between different light modes. In contrast to usual ultracold atoms experiments, where the spatial profile of the coupling is determined by fundamental physical processes, in this Chapter we presented a way to realize synthetic long-range interactions without recurring to complex systems such as polar molecules [14, 96] or Rydberg atoms [64, 137, 148]. This opens an additional path for implementing quantum simulations of phenomena from several disciplines such as condensed matter, high energy physics and biological systems.

Chapter 3

Quantum measurement

We have shown that the coupling between the quantized light modes of an optical cavity and an ultracold atomic system allows to extract information on the quantum state of the atoms. The correlations of the matter field are mapped onto the scattered light and can be used for distinguishing quantum phases and fluctuations in different quantities. In order to apply this scheme experimentally, it is necessary to perform multiple measurements on the quantum state of the system. This is the usual approach adopted in experiments with ultracold gases: the same experimental sequence is repeated several times after restoring the initial state of the system. The results are then averaged over many realizations and quantum mechanical expectation values are computed as ensemble averages. However, this approach completely ignores the subtle effects of measurement that are visible in a single experimental run. In this Chapter, we will focus on the *conditional* evolution of the atomic state in a single experimental realization without considering any averaging procedure. We show that measurement backaction can play a crucial role in the dynamics of the system and allows to engineer different quantum states that are not easy to obtain with conventional methods.

3.1 Conditional dynamics of a quantum system

The Hamiltonians (2.22) and (2.27) describe the evolution of the system when measuring the scattered light from the atomic system. Because of the coupling between light and matter, these two become entangled. Thus, a measurement performed on one of the two subsystems (i. e. light) will inevitably affect the other one via the so-called measurement backaction. This is one of the most fundamental manifestations of quantum mechanics and it is usually treated as an unwanted perturbation that modifies the state of the system. In contrast to this, here we show that this effect induces an effective dynamics for the quantum system. Although this conditional evolution follows a stochastic process, it is possible to identify several features that are common to all the experimental runs but disappear when averaging over many realizations. Most of the results that we present in this thesis rely on the description of the conditional dynamics of a quantum system under continuous monitoring. We will now introduce a very powerful and relatively simple mathematical tool for achieving this, i. e. the quantum trajectories approach for modeling quantum measurement.

3.1.1 Quantum trajectories

Let us consider a quantum system described by the Hamiltonian operator $\hat{H}$. If the state of the system at a given time is known, we can compute its dynamics at all future (and past) times by solving the Schrödinger equation

$$\frac{\mathrm{d}}{\mathrm{d}t}|\psi(t)\rangle = -i\hat{H}|\psi(t)\rangle. \tag{3.1}$$

Since this is a first order linear differential equation, the evolution of the system is continuous and deterministic. Measurement drastically changes this and introduces *discontinuities* in the dynamics of the quantum system. Traditionally, this effect is described as a projection: if we perform a measurement of the observable $\hat{O}$, the result is one of the eigenvalues of $\hat{O}$ (say o) and the state of the system collapses to an eigenstate of $\hat{O}$ (say $|o\rangle$) with probability $|\langle o|\psi(t)\rangle|^2$. Although this representation of measurement can be extended to continuous variables and to mixed states, it is quite inadequate for describing real experiments for many reasons. Firstly, it assumes that the detection apparatus does not introduce classical noise to the measurement results. Secondly, there are many schemes in which the state of the system after the measurement event is not an eigenstate of the measured quantity. For example, if we detect the photons escaping an optical cavity until this is empty, the final state of the system is the vacuum state and not the eigenstate of the photon number operator corresponding to the n photocounts we recorded. Lastly, but more importantly, a measurement that is performed in a real experiment never addresses directly the system of interest, but rather its interaction with the environment. For example, if we want to observe an electron transitioning between two atomic energy levels, we will choose a detector that couples to the electromagnetic fields around the atom and can “click” when a photon is emitted. One could argue that this generates an infinite chain where the electromagnetic filed is coupled to the electronic circuits inside the detector, which are coupled to the computer monitor showing the results, which is coupled to the observer’s retina, which is coupled to her/his brain and so on. In order to give a description of the physical world, we need to cut this chain and decide where to apply the projection postulate for modeling the measurement process. Because of the rapid decoherence time of macroscopic objects such as a photodetector, we stop this chain by assuming that the measurement of the light field is indeed projective. This allows us to formulate an accurate description of the atomic dynamics: since the field interacted with the atom, their quantum states are entangled and a measurement of the light field is effectively a measurement of the atomic state, although not a projective one.

Let us consider a quantum system initialized in the pure state $|\psi(t)\rangle$ and coupled to a *meter* with initial state $|\theta(t)\rangle$. The initial state of the composite quantum system is

$$|\Psi(t)\rangle = |\theta(t)\rangle|\psi(t)\rangle. \tag{3.2}$$

Since these two quantum systems are coupled, the unitary time evolution $\hat{U}(T_1)$ will entangle them so that

$$|\Psi(t+T_1)\rangle = \hat{U}(T_1)|\theta(t)\rangle|\psi(t)\rangle. \tag{3.3}$$

cannot be factorized as a product state. If a projective measurement is performed on the meter over a time interval T_2 and assuming that the evolution of the system and meter over this time is negligible, the final state of the full quantum system is

$$|\Psi(t+T)\rangle = \frac{|r\rangle\langle r|\hat{U}(T_1)|\theta(t)\rangle|\psi(t)\rangle}{\sqrt{\mathcal{P}_r}}. \tag{3.4}$$

where $T = T_1 + T_2$, r denotes the measured value of the observable $\hat{R}$ that has eigenstates $\{|r\rangle\}_r$ forming an orthonormal basis for the meter Hilbert space. Moreover, $\mathcal{P}_r$ is the probability of obtaining r as a result of the measurement, i. e.

$$\mathcal{P}_r = \langle\psi(t)|\langle\theta(t)|\hat{U}(T_1)\left[|r\rangle\langle r| \otimes \mathbf{1}\right]\hat{U}(T_1)|\theta(t)\rangle|\psi(t)\rangle \tag{3.5}$$

where we highlighted the fact that the projector $|r\rangle\langle r|$ is acting only on the Hilbert space of the meter. Importantly, the measurement process disentangles the system and the meter so that the state (3.4) can be written as

$$|\Psi(t+T)\rangle = |r\rangle\frac{\hat{M}_r|\psi(t)\rangle}{\sqrt{\mathcal{P}_r}}. \tag{3.6}$$

where we defined the *measurement operator* $\hat{M}_r = \langle r|\hat{U}(T_1)|\theta(t)\rangle$. Following this definition, the probability $\mathcal{P}_r$ can be condensed as

$$\mathcal{P}_r = \langle\psi(t)|\hat{M}_r^\dagger \hat{M}_r|\psi(t)\rangle \tag{3.7}$$

We now apply this formalism to a quantum system subjected to continuous monitoring. Specifically, we consider an ultracold gas inside an optical cavity where the meter system is represented by the light field which is used for probing the state of the atoms. In this case, the observable $\hat{R}$ describes the photocount process. Since there are only two possible outcomes for this process (either a photon is detected or it is not), we model the detection using only two measurement operators ($\hat{M}_1$ and $\hat{M}_0$). Importantly, for each small time interval $\mathrm{d}t$, the sum of the probabilities of detecting and not detecting a photon, $\mathcal{P}_0 + \mathcal{P}_1$, has to be equal to one. Therefore, the operators $\hat{M}_1$ and $\hat{M}_0$ fulfill the completeness relation

$$\hat{M}_0^\dagger(\mathrm{d}t)\hat{M}_0(\mathrm{d}t) + \hat{M}_1^\dagger(\mathrm{d}t)\hat{M}_1(\mathrm{d}t) = \mathbf{1}. \tag{3.8}$$

Moreover, one can prove that the operator $\hat{M}_0(\mathrm{d}t)$ is given by [190]

$$\hat{M}_0(\mathrm{d}t) = \mathbf{1} - \left(\frac{\hat{c}^\dagger \hat{c}}{2} + i\hat{H}\right)\mathrm{d}t \tag{3.9}$$

where $\hat{H}$ is the Hamiltonian describing the light-matter system and we introduced the *jump operator* $\hat{c}$ such that $\hat{R} = \hat{c}^\dagger\hat{c}$. Finally, from the completeness condition (3.8) we find

$$\hat{M}_1(\mathrm{d}t) = \sqrt{\mathrm{d}t}\,\hat{c}. \tag{3.10}$$

These two operators allow us to describe the conditional dynamics for the atomic system in a single experimental run. The specific sequence of phototcounts identifies a single realization of the measurement process and characterizes each *quantum trajectory*. Defining $N(t)$ as the number of photodetections up to time t in a single experimental run, the increment $\mathrm{d}N(t)$ is a stochastic variable (Itô formalism) which obeys

$$\mathrm{d}N(t)^2 = \mathrm{d}N(t) \tag{3.11}$$

$$\mathrm{E}[\mathrm{d}N(t)] = \langle \hat{M}_1^\dagger(\mathrm{d}t)\hat{M}_1(\mathrm{d}t)\rangle = \langle\psi(t)|\hat{c}^\dagger\hat{c}|\psi(t)\rangle\mathrm{d}t \tag{3.12}$$

where $\mathrm{E}[\dots]$ denotes the expectation value of the stochastic process (ensemble average) and $\langle\dots\rangle$ is the usual quantum expectation value. The physical meaning of the first expression is that the photocount increment $\mathrm{d}N$ in an infinitesimal time $\mathrm{d}t$ can be either zero or one. The second equation gives the expectation value of $\mathrm{d}N$, which is equal to the probability $\mathcal{P}_1$ of detecting a photon in a time interval $\mathrm{d}t$. At each time t, the quantum state of the system evolves according to the result of the measurement: if a photon is detected ($\mathrm{d}N = 1$), the state of the system changes as

$$|\psi_1(t+\mathrm{d}t)\rangle = \frac{\hat{M}_1(\mathrm{d}t)|\psi(t)\rangle}{\sqrt{\langle\psi(t)|\hat{M}_1^\dagger(\mathrm{d}t)\hat{M}_1(\mathrm{d}t)|\psi(t)\rangle}} = \frac{\hat{c}|\psi(t)\rangle}{\sqrt{\langle\psi(t)|\hat{c}^\dagger\hat{c}|\psi(t)\rangle}} \tag{3.13}$$

i. e. the annihilation operator for the light field is applied to $|\psi_1(t)\rangle$ and the state vector is normalized. This process describes the collapse of the quantum state of the system and we will refer to it as a *quantum jump*. Importantly, if there is no detection ($\mathrm{d}N(t) = 0$) the evolution does not follow the unitary dynamics generated by $\hat{H}$ but it is given by

$$\begin{aligned}|\psi_0(t+\mathrm{d}t)\rangle &= \frac{\hat{M}_0(\mathrm{d}t)|\psi(t)\rangle}{\sqrt{\langle\psi(t)|\hat{M}_0^\dagger(\mathrm{d}t)\hat{M}_0(\mathrm{d}t)|\psi(t)\rangle}}\\ &= \left[\mathbf{1} - \mathrm{d}t\left(i\hat{H} + \tfrac{1}{2}\hat{c}^\dagger\hat{c} - \tfrac{1}{2}\langle\hat{c}^\dagger\hat{c}\rangle(t)\right)\right]|\psi(t)\rangle \end{aligned} \tag{3.14}$$

where we expanded the denominator at first order in $\mathrm{d}t$. The additional term in this expression takes into account the information about the state of the system that is recovered when no photons are detected. The stochastic evolution described by (3.13) and (3.14) can be summarized in the stochastic Schrödinger equation (SSE)

$$\begin{aligned} \mathrm{d}|\psi(t)\rangle = \Bigg\{ & \mathrm{d}N(t) \left(\frac{\hat{c}}{\sqrt{\langle \psi(t)|\hat{c}^\dagger \hat{c}|\psi(t)\rangle}} - \mathbf{1} \right) \\ & + [\mathbf{1} - N(t)]\, \mathrm{d}t \left(\frac{\langle \hat{c}^\dagger \hat{c}\rangle(t)}{2} - \frac{\hat{c}^\dagger \hat{c}}{2} - i\hat{H} \right) \Bigg\} |\psi(t)\rangle. \end{aligned} \tag{3.15}$$

Moreover, this expression can be further simplified by noting that the product $\mathrm{d}N\mathrm{d}t$ is negligible with respect to $\mathrm{d}t$. Thus, (3.15) becomes

$$\mathrm{d}|\psi(t)\rangle = \left[\mathrm{d}N(t) \left(\frac{\hat{c}}{\sqrt{\langle \psi(t)|\hat{c}^\dagger \hat{c}|\psi(t)\rangle}} - \mathbf{1} \right) + \mathrm{d}t \left(\frac{\langle \hat{c}^\dagger \hat{c}\rangle(t)}{2} - \frac{\hat{c}^\dagger \hat{c}}{2} - i\hat{H} \right) \right] |\psi(t)\rangle. \tag{3.16}$$

3.1.2 Simulating quantum trajectories

In general, one can consider a setup where the system is monitored by using more than one measurement channel (for example two different light polarizations or multiple cavities). In this case, the conditional dynamics is generated by an equal number of jump operators $\hat{c}_\mu$ and the SSE (3.16) generalizes to

$$\mathrm{d}|\psi(t)\rangle = \sum_\mu \left[\mathrm{d}N_\mu(t) \left(\frac{\hat{c}_\mu}{\sqrt{\langle \psi(t)|\hat{c}_\mu^\dagger \hat{c}_\mu|\psi(t)\rangle}} - \mathbf{1} \right) + \mathrm{d}t \left(\frac{\langle \hat{c}_\mu^\dagger \hat{c}_\mu\rangle(t)}{2} - \frac{\hat{c}_\mu^\dagger \hat{c}_\mu}{2} - i\hat{H} \right) \right] |\psi(t)\rangle. \tag{3.17}$$

where the increments in the counts for each channel are such that $\mathrm{E}[\mathrm{d}N_\mu(t)] = \langle \psi(t)|\hat{c}_\mu^\dagger \hat{c}_\mu|\psi(t)\rangle \mathrm{d}t$ and $\mathrm{d}N_\mu(t)\mathrm{d}N_\nu(t) = \mathrm{d}N_\mu(t)\delta_{\mu\nu}$.

The easiest way to simulate conditional dynamics of a quantum system under continuous monitoring is to solve equation (3.17) by replacing all the differentials with small finite differences δ and discretizing the time t. For each time interval δt, one has to generate a random number r uniformly distributed in $[0, 1]$ and compare it with the probability of a quantum jump

$$p_{\text{jump}} = \delta t \sum_{\mu} \langle \psi(t) | \hat{c}_{\mu}^{\dagger} \hat{c}_{\mu} | \psi(t) \rangle. \tag{3.18}$$

If $r < p_{\text{jump}}$ a jump occurs (i. e. a photon is emitted) and one of the possible measurement channels is chosen randomly using the same (or another) random number and assigning the weight $\langle \psi(t) | \hat{c}_{\mu}^{\dagger} \hat{c}_{\mu} | \psi(t) \rangle$ to each jump operator. The appropriate increment δN_{μ} is then set to 1 (while all others are set to zero) and $\delta | \psi(t) \rangle$ is calculated using (3.17).

Although this method can be used for solving the SSE (3.17), it is not the most efficient way to do so since it requires to find δt so that only one quantum jumps occurs for each time interval. Moreover, because of (3.18), the time interval between two consecutive quantum jumps strongly depends on the state of the system and therefore it is more convenient to use an algorithm that does not require to discretize time in intervals with predetermined length. Therefore, instead of solving (3.17) directly, the following method is usually implemented:

(i) at the initial time t_i, generate a random number r uniformly distributed in $[0, 1]$;

(ii) solve the non-unitary Schrödinger equation

$$\frac{\mathrm{d}}{\mathrm{d}t} | \psi(t) \rangle = - \left(\sum_{\mu} \tfrac{1}{2} \hat{c}_{\mu}^{\dagger} \hat{c}_{\mu} + i \hat{H} \right) | \psi(t) \rangle \tag{3.19}$$

until it reaches the time t_j such that $\langle \psi(t_j) | \psi(t_j) \rangle = r$. This condition defines when the system undergoes a quantum jump;

(iii) generate another uniformly distributed random number in order to decide which jump operator is applied to the quantum state of the system according to the weights $\langle \psi(t) | \hat{c}_{\mu}^{\dagger} \hat{c}_{\mu} | \psi(t) \rangle$;

(iv) the relevant collapse operator is applied to the state of the system which is then normalized, i. e.

$$|\psi(t_j)\rangle \rightarrow \frac{\hat{c}_\mu|\psi(t_j)\rangle}{\sqrt{\langle\psi(t_j)|\hat{c}_\mu^\dagger\hat{c}_\mu|\psi(t_j)\rangle}}; \tag{3.20}$$

(v) set $t_i = t_j$ and repeat from (i).

Since (3.19) is an ordinary linear differential equation, there are several efficient libraries that are capable of solving it. Moreover, it is possible to compute iteratively t_j (for example with an event-detection function) without imposing a predetermined time step δt and taking advantage of adaptive-step methods such as Runge-Kutta. Crucially, the decay in the norm of the state of the system describes its evolution when there are no photocounts, i. e. the repeated action of the operator $\hat{M}_0(\mathrm{d}t)$. We will refer to the non-Hermitian Hamiltonian in (3.19) as the *effective* Hamiltonian of the system.

3.2 Quantum state engineering via measurement backaction[1]

We will now apply the theory introduced in the previous section in order to present some results regarding ultracold fermions loaded in an optical lattice and subjected to continuous monitoring. In this case, the measurement process consists in recording the photons leaking from an optical cavity. Moreover, we consider the case of transverse probing so that we can set $\eta_1 = 0$. If the atomic dynamics can be neglected, i. e. the tunneling rate between neighboring sites is much slower than the light scattering, the

[1]The results in this section are published in [53].

effective Hamiltonian describing the light-matter system is

$$\hat{H}_{\text{eff}} = \hbar \sum_{\sigma=\uparrow,\downarrow} \left(\omega_1 + U_{11}\hat{D}_{11}^{(\sigma)}\right) \hat{a}_1^\dagger \hat{a}_1 + \hbar U_{10} \sum_{\sigma=\uparrow,\downarrow} \left(a_{0\sigma}^* \hat{a}_1 \hat{D}_{01}^{(\sigma)} + \hat{a}_1^\dagger a_{0\sigma} \hat{D}_{10}^{(\sigma)}\right) - i\kappa \hat{a}_1^\dagger \hat{a}_1 \tag{3.21}$$

where we assumed that the contribution to the light scattering due to the operator $\hat{D}$ dominates over the one due to $\hat{B}$. Note that the evolution described by this Hamiltonian is non-unitary because of the non-Hermitian term $i\kappa\hat{a}_1^\dagger\hat{a}_1$ which describes the photons leaking from the optical cavity. In analogy to the previous section, this operator models the dynamics of the system in between two consecutive photodetections. Thus, we can identify the operator $\hat{c}$ in (3.19) as $\hat{c} = \sqrt{2\kappa}\hat{a}_1$. However, since $\hat{c}$ and $\hat{a}_1$ are proportional, we will refer to both of them as jump operator (the proportionality constant disappears when the state is normalized). The initial state of the system can be written as

$$|\Psi(0)\rangle = \sum_{\mathbf{k},\mathbf{q}} c_{\mathbf{qk}}^{(0)} |\mathbf{q}\uparrow, \mathbf{k}\downarrow\rangle |\alpha_{\mathbf{qk}}(0)\rangle \tag{3.22}$$

where $|\mathbf{q}\sigma\rangle$ are the Fock states for fermions of species σ and $|\alpha_{\mathbf{qk}}(0)\rangle$ is the coherent state of the light field inside the optical cavity. Since at this stage we are neglecting the effect of the atomic tunneling, both the Hamiltonian (3.21) and the quantum jumps do not mix different Fock states. This simplifies the problem significantly and allows to compute an analytic expression for the conditional dynamics $|\Psi_c(t)\rangle$. Importantly, if a coherent probe illuminates the classical atomic configuration $\mathbf{qk}$ (such as the one described by a Fock state), the cavity field remains in a coherent state that can be written as $e^{i\Phi_{\mathbf{qk}}(t)}|\alpha_{\mathbf{qk}}(t)\rangle$ [61, 80, 116]. The specific form of the prefactor and the coherent state $|\alpha_{\mathbf{qk}}(t)\rangle$ can be computed by taking the expectation value of $\hat{H}_{\text{eff}}$ on the state $|\mathbf{q}\uparrow, \mathbf{k}\downarrow\rangle$ and solving the resulting Schrödinger equation (3.19) for each atomic configuration $|\mathbf{q}\sigma\rangle$. Thus, the complete expression of $|\Psi_c(t)\rangle$ will then be given by the superposition of those solutions.

Solving the differential equation for the light amplitude $\alpha_{\mathbf{qk}}(t)$ assuming that the light amplitude is varying slowly we find

$$\alpha_{\mathbf{qk}}(t) = Ae^{-i\omega_p t} + (\alpha_{\mathbf{qk}}(0) - A)\, e^{-i\left[\omega_1 + U_{11}\sum_\sigma D_{11}^{(\sigma)}(\mathbf{qk})\right]t - \kappa t} \tag{3.23}$$

where

$$A = \frac{-iU_{10}\sum_\sigma a_{0\sigma} D_{10}^{(\sigma)}(\mathbf{qk})}{i\left[U_{11}\sum_\sigma D_{11}^{(\sigma)}(\mathbf{qk}) - \Delta_p\right] + \kappa}, \tag{3.24}$$

$$D_{lm}^{(\sigma)}(\mathbf{qk}) = \langle \mathbf{q}\uparrow, \mathbf{k}\downarrow | \hat{D}_{lm}^{(\sigma)} | \mathbf{q}\uparrow, \mathbf{k}\downarrow \rangle. \tag{3.25}$$

The function $\Phi_{\mathbf{qk}}(t)$ that appears in the prefactor of $e^{i\Phi_{\mathbf{qk}}(t)}|\alpha_{\mathbf{qk}}(t)\rangle$ is given by

$$\Phi_{\mathbf{qk}}(t) = -\int_0^t \left\{ \frac{iU_{10}}{2} \sum_{\sigma=\uparrow,\downarrow} \left[a_{0\sigma} D_{01}^{(\sigma)}(\mathbf{qk}) \alpha_{\mathbf{qk}}^*(s) + a_{0\sigma}^* D_{10}^{(\sigma)}(\mathbf{qk}) \alpha_{\mathbf{qk}}(s) \right] - \kappa \left| \alpha_{\mathbf{qk}}(s) \right|^2 \right\} \mathrm{d}s \tag{3.26}$$

The physical meaning of equation (3.23) is the following: the first term describes the oscillations of the light field at the probe frequency ω_p while the second term gives the transient process with decay κ and oscillation frequency $\omega_1 + U_{11}\sum_\sigma D_{11}^{(\sigma)}$, i. e. the cavity frequency shifted by the dispersive shift due to the atoms. This expression allows to model the non-Hermitian evolution of the system generated by the Schrödinger equation (3.19). However, this is not the only process contributing to the dynamics of the system since the backaction due to the photodetections is equally important and cannot be ignored. If a photon escapes the optical cavity, the corresponding annihilation operator is applied to the quantum state as

$$|\Psi_c(t)\rangle \to \frac{\hat{a}_1|\Psi_c(t)\rangle}{\langle\Psi_c(t)|\hat{a}_1^\dagger \hat{a}_1|\Psi_c(t)\rangle} \tag{3.27}$$

Therefore, the state of the quantum system after m quantum jumps happening at the times $t_1, t_2 \dots t_m$ can be written as

$$|\Psi_c(m,t)\rangle = \frac{1}{F(t)} \sum_{\mathbf{qk}} \alpha_{\mathbf{qk}}(t_1)\alpha_{\mathbf{qk}}(t_2)\dots\alpha_{\mathbf{qk}}(t_m)e^{i\Phi_{\mathbf{qk}}(t)}c^{(0)}_{\mathbf{qk}}|\mathbf{q}\uparrow,\mathbf{k}\downarrow\rangle|\alpha_{\mathbf{qk}}(t)\rangle \qquad (3.28)$$

where $F(t)$ is the normalization factor

$$F(t) = \sqrt{\sum_{\mathbf{qk}} |\alpha_{\mathbf{qk}}(t_1)|^2 |\alpha_{\mathbf{qk}}(t_2)|^2 \dots |\alpha_{\mathbf{qk}}(t_m)|^2 \left|e^{i\Phi_{\mathbf{qk}}(t)}\right|^2 \left|c^{(0)}_{\mathbf{qk}}\right|^2}. \qquad (3.29)$$

We further simplify these expressions by noting that for $t > 1/\kappa$ all the factors $\alpha_{\mathbf{qk}}(t_j)$ reach the constant value $\alpha_{\mathbf{qk}}(t_j) = A \equiv \alpha_{\mathbf{qk}}$. Furthermore, the phase factor $\Phi_{\mathbf{qk}}(t)$ becomes

$$\Phi_{\mathbf{qk}}(t) = -\kappa |\alpha_{\mathbf{qk}}|^2 t - \frac{itU_{10}}{2} \sum_{\sigma=\uparrow,\downarrow} \left[a_{0\sigma} D^{(\sigma)}_{01}(\mathbf{qk})\alpha^*_{\mathbf{qk}} + a^*_{0\sigma} D^{(\sigma)}_{10}(\mathbf{qk})\alpha_{\mathbf{qk}}\right] \qquad (3.30)$$

and

$$|\Psi_c(m,t)\rangle = \frac{1}{\tilde{F}(t)} \sum_{\mathbf{qk}} \alpha^m_{\mathbf{qk}} e^{i\Phi_{\mathbf{qk}}(t)} c^{(0)}_{\mathbf{qk}} |\mathbf{q}\uparrow,\mathbf{k}\downarrow\rangle|\alpha_{\mathbf{qk}}\rangle \qquad (3.31)$$

where the normalization coefficient is

$$\tilde{F}(t) = \sqrt{\sum_{\mathbf{qk}} |\alpha_{\mathbf{qk}}|^{2m} e^{-2\kappa|\alpha_{\mathbf{qk}}|^2 t} \left|c^{(0)}_{\mathbf{qk}}\right|^2}. \qquad (3.32)$$

Due to the steady state in all of the light amplitudes $\alpha_{\mathbf{qk}}$, this solution does not depend on the specific times t_j. Importantly, the solution (3.31) highlights the fact that as result of the measurement process, light and matter become entangled and the quantum state of the system cannot be expressed as a product state. Moreover, the conditional evolution induced by the measurement process changes the distribution of the atoms in the optical lattice since the probability of the Fock state configuration $|\mathbf{q}\uparrow, \mathbf{k}\downarrow\rangle$ is given by

$$P_{\mathbf{qk}}(m,t) = \frac{1}{\tilde{F}^2(t)} |\alpha_{\mathbf{qk}}|^{2m} \left|c^{(0)}_{\mathbf{qk}}\right|^2 e^{-\kappa|\alpha_{\mathbf{qk}}|^2 t}. \tag{3.33}$$

Note that this quantity is affected by both the photodetection events (via the $\alpha_{\mathbf{qk}}$ factor) and the effective non-Hermitian evolution in between two consecutive quantum jumps (via the exponential decay). Finally, since the terms $\alpha_{\mathbf{qk}}$ depend on the configuration of both $\uparrow$ and $\downarrow$ fermions, the cavity introduces an effective interaction between the two spin species.

3.2.1 Generation of number-squeezed states and Schrödinger cat states

We will now focus on the properties of the atomic system and we will analyze their evolution in a single quantum trajectory. We consider the case of non-interacting N fermions loaded in an optical lattice and we assume that the mode functions of the coherent probe beam and the scattered light are traveling waves so that $J^{lm}_{jj} = e^{i(\mathbf{k}_l - \mathbf{k}_m)\cdot \mathbf{r}_j}$. Moreover, we probe the atoms by illuminating K lattice sites and therefore the jump operator describing the measurement process is $\hat{a}_1 = \sum_\sigma C_\sigma \hat{N}_{K\sigma}$ where $\hat{N}_{K\sigma}$ is the number of fermions with spin σ occupying the illuminated region of the lattice. Instead of directing our attention to the huge number of probability distributions $P_{\mathbf{qk}}(m,t)$ describing each Fock state, we will focus on the probability distribution of having z_σ fermions with spin σ in the region that is probed by the light. Therefore $P_c(z_\uparrow, z_\downarrow, m, t)$ evolves as

$$P_c(z_\uparrow, z_\downarrow, m, t) = \frac{1}{\tilde{F}^2(t)} |C_\uparrow z_\uparrow + C_\downarrow z_\downarrow|^{2m} \exp\left(-2\kappa t\, |C_\uparrow z_\uparrow + C_\downarrow z_\downarrow|^2\right) P^{(0)}(z_\uparrow) P^{(0)}(z_\downarrow) \tag{3.34}$$

where the constants C_σ were defined in (2.33) and $P^{(0)}(z_\sigma)$ are the initial probability distributions. In general, these are calculated by summing the absolute values of the coefficients of all of the configurations $\mathbf{q}'\mathbf{k}'$ with the same z_σ, i. e. $P^{(0)}(z_\sigma) = \sum_{\mathbf{q}'\mathbf{k}'} \left|c^{(0)}_{\mathbf{q}'\mathbf{k}'}\right|^2$. Although it is relatively easy to compute this quantity in the case of a BEC [121], the fermionic case is more challenging because of the highly non-trivial phase relations between different Fock states. In general, the ground state of a non-interacting Fermi gas in an optical lattice is the Fermi Sea which is usually written as

$$|FS\rangle = \prod_{\mathbf{k}:|\mathbf{k}|<k_\mathrm{F}} \hat{f}^\dagger_{\mathbf{k}\uparrow}\hat{f}^\dagger_{\mathbf{k}\downarrow}|0\rangle \tag{3.35}$$

where k_F is the Fermi wavevector, $\hat{f}^\dagger_{\mathbf{k}\sigma}$ creates a fermion with momentum $\mathbf{k}$ and spin σ and $|0\rangle$ is the vacuum state. Since the observables probed by the measurement setup are expressed in position space and not in momentum space, one could take the Fourier Transform (FT) of the operator $\hat{f}^\dagger_{\mathbf{k}\sigma}$ and obtain the coefficients $c^{(0)}_{\mathbf{q}'\mathbf{k}'}$ describing all possible atomic configurations. However, this would generate a very large number of terms since the FT of the product (3.35) is a Slater determinant containing $N!$ factors with well-defined phase relations between them. In order to give an approximate description, we instead model $P^{(0)}(z_\sigma)$ as a Gaussian distribution with variance $\sigma^2 = \langle \hat{N}^2_{K\sigma}\rangle - \langle \hat{N}_{K\sigma}\rangle^2$ where the expectation values are computed on $|FS\rangle$. Focusing on a half-filled optical lattice with L lattice sites, we find

$$\langle FS|\hat{N}_{K\sigma}|FS\rangle = \frac{K}{2} \tag{3.36}$$
$$\langle FS|\hat{N}^2_{K\sigma}|FS\rangle = \frac{K^2}{4} + \sum_{\mathbf{p}:|\mathbf{p}|<k_\mathrm{F}} \sum_{\mathbf{m}:|\mathbf{m}|>k_\mathrm{F}} |g(\mathbf{p}-\mathbf{m})|^2 \tag{3.37}$$

where

$$g(\mathbf{p}) = \frac{1}{L}\sum_{j=1}^{K} e^{-i\mathbf{p}\cdot\mathbf{r}_j}. \tag{3.38}$$

These expressions can be easily evaluated numerically and allow to calculate the initial probability distribution $P^{(0)}(z_\sigma)$ as illustrated in Figure 3.1a.

If the probe beam is circularly polarized, the measurement process addresses only one of the two spin species (e. g. the $\uparrow$ fermions) and the resulting conditional evolution is given by

$$P_c(z_\uparrow, z_\downarrow, m, t) = \frac{1}{\tilde{F}^2(t)} z_\uparrow^{2m} \exp\left(-\tau z_\uparrow^2\right) P^{(0)}(z_\uparrow) P^{(0)}(z_\downarrow) \tag{3.39}$$

where $\tau = 2\left|C_\uparrow\right|^2 \kappa t$ defines the typical timescale of the interval between two consecutive quantum jumps. The relation between m and t follows a stochastic process which defines a single quantum trajectory. The measurement process strongly modifies the probability distributions of $z_\uparrow$ but leaves the one for $z_\downarrow$ unchanged. Specifically, the quantum jumps and the non-Hermitian dynamics have opposite effect on the expectation value of the number of $\uparrow$ fermions in the illuminated area: while the quantum jumps tend to increase $z_\uparrow$, the exponential decay favors small values of $z_\uparrow$. Although these two effects compete for determining the expectation value of $z_\uparrow$, they both tend to reduce its uncertainty and squeeze its probability distribution. In the large time limit, quantum jumps and non-Hermitian evolution balance each other and $P_c(z_\uparrow, m, t)$ shrinks around the value $z_\uparrow = \sqrt{m/\tau}$ (Figure 3.1b). The width of the distribution can be found by calculating the full-width-half-maximum (FWHM) of (3.39) around its peak, i. e. $\delta z_\uparrow \sim \sqrt{2\ln 2/\tau}$. Importantly, $z_\uparrow$ and $z_\downarrow$ are not conjugate variables and therefore it is possible to squeeze only one of theme leaving the other one unperturbed.

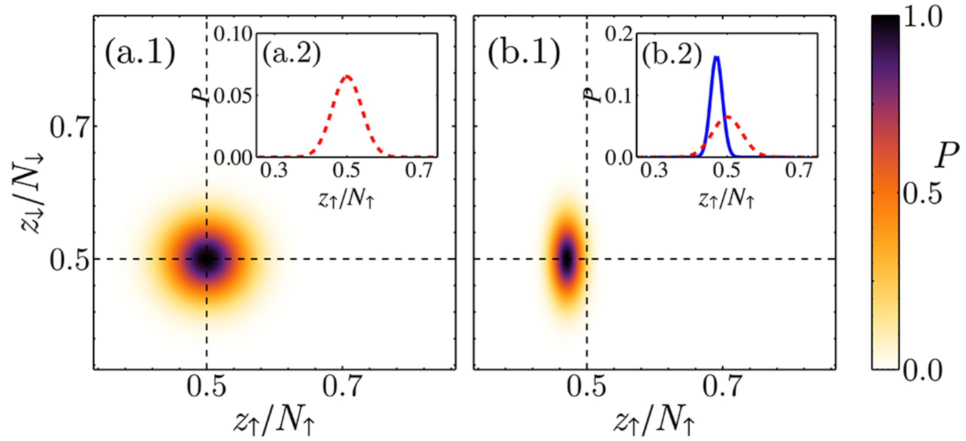

Fig. 3.1 Effects of the conditional dynamics on the atomic variables in a single quantum trajectory. The color maps show the joint probability distribution $P_c(z_\uparrow, z_\downarrow, m, t)$. (a) Initial state of the system. The inset illustrate the distribution $P^{(0)}(z_\uparrow)$. (b) Only the $\uparrow$ fermions are affected by the measurement processes. Their probability distribution is squeezed while the one for the $\downarrow$ fermions does not change. (b.2) Probability $P_c(z_\uparrow)$ (solid line) and $P^{(0)}(z_\uparrow)$ (dashed line). Note that $P^{(0)}(z_\uparrow)$ coincides with $P_c(z_\downarrow)$. Measurement backaction allows to squeeze only one of the spin species.

The setup we presented in this work is extremely flexible and it allows to probe different observables by changing the angles between the cavity , the probe beam and the optical lattice. In the case of fermions, changing the polarization of the lasers illuminating the atomic sample provides another route for tailoring the measurement operator. In general, the conditional probability distribution of $z_\uparrow$ and $z_\downarrow$ evolves as (3.34). The behavior of this quantity is essentially determined by the function

$$f(z_\uparrow, z_\downarrow, m, t) = |C_\uparrow z_\uparrow + C_\downarrow z_\downarrow|^{2m} \exp\left(-2\kappa t \, |C_\uparrow z_\uparrow + C_\downarrow z_\downarrow|^2\right) \tag{3.40}$$

which describes the dynamics induced by the quantum jumps and the non-Hermitian dynamics. By differentiating this expression, we find that the distribution $P_c(z_\uparrow, z_\downarrow, m, t)$

has a stationary point that fulfills the condition

$$|C_\uparrow z_\uparrow + C_\downarrow z_\downarrow|^2 = \frac{m}{2\kappa t}. \tag{3.41}$$

Therefore, the monitoring process squeezes the atomic occupations $z_\uparrow$ and $z_\downarrow$ along the direction perpendicular to the *line* defined by the (3.41) which can be easily tuned by changing the polarization or the intensity of the probe beam(s). For example, if only one $x-$linearly polarized probe is present so that the measurement is sensitive to the total number of atoms in the illuminated area, i. e. $\hat{a}_1 = C_x(\hat{N}_{K\uparrow} + \hat{N}_{K\downarrow})$, equation (3.41) reduces to $z_\uparrow + z_\downarrow = \sqrt{m/\tau}$ where $\tau = 2\kappa t\,|C_x|^2$. Therefore, the conditional dynamics diminishes the uncertainty of $z_\uparrow + z_\downarrow$ which corresponds to squeezing $P_c(z_\uparrow, z_\downarrow, m, t)$ along a 45° lines in the $(z_\uparrow, z_\downarrow)$ plane as shown in Figure (3.2)b.

The simple representation of the atomic evolution in terms of squeezing along a given direction breaks down if $C_\uparrow z'_\uparrow + C_\downarrow z'_\downarrow = 0$ for some values of $z'_\uparrow$ and $z'_\downarrow$. If this is the case, when the first photon is detected the probability distribution becomes bimodal as the probability of all the configurations with $C_\uparrow z'_\uparrow + C_\downarrow z'_\downarrow = 0$ collapses to zero. In order to illustrate this, we consider a $y-$linearly polarized probe beam so that the scattered light carries information about the magnetization of the illuminated area, i. e. $\hat{a}_1 = C_y(\hat{N}_{K\uparrow} - \hat{N}_{K\downarrow})$. Therefore, the conditional dynamics of the probability distribution of the magnetization is given by

$$P_c(z_\uparrow, z_\downarrow, m, t) = \frac{1}{\tilde{F}^2(t)}\,|z_\uparrow - z_\downarrow|^{2m} \exp\left(-\tau\,|z_\uparrow - z_\downarrow|^2\right) P^{(0)}(z_\uparrow)P^{(0)}(z_\downarrow), \tag{3.42}$$

where $\tau = 2\kappa t\,|C_y|^2$. When the first quantum jump occurs, all the atomic states with $\langle \hat{N}_{K\uparrow} - \hat{N}_{K\downarrow}\rangle = 0$ are forbidden since $P_c(z_\uparrow, z_\uparrow, m > 0, t) = 0$. As a consequence, $P_c(z_\uparrow, z_\downarrow, m, t)$ splits in two peaks around the values $\pm\sqrt{m/\tau}$ whose width decreases with time. Thus, the final state of the system has a well-defined absolute magnetization as

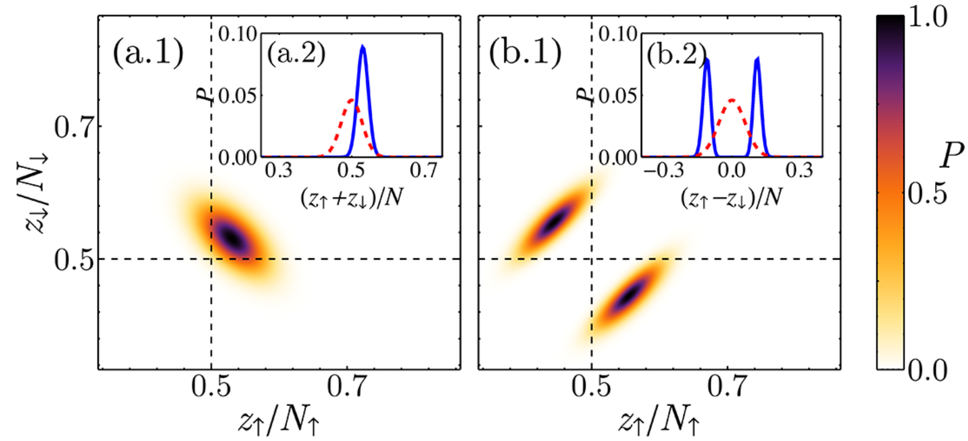

Fig. 3.2 Effects of the conditional dynamics on the atomic variables in a single quantum trajectory. (a.1) The measurement addresses the quantity $z_\uparrow + z_\downarrow$ and the distribution $P(z_\uparrow, z_\downarrow, m, t)$ is squeezed along a 45° line. (a.2) Probability distribution of $z_\uparrow + z_\downarrow$ for the final state (solid line) and the initial state (dashed line). (b.1) Joint probability distribution $P_c(z_\uparrow, z_\downarrow, m, t)$ when the magnetization is measured. (b.2) Probability distribution of $z_\uparrow - z_\downarrow$ for the final state (solid line) and the initial state (dashed line). Measurement backaction can be used for squeezing the atomic state along different directions and for creating Schrödinger cat states.

the measurement process projects the atomic state to a superposition of two states with magnetization M and $-M$: a Schrödinger cat state. This multicomponent structure emerges as a consequence of the degeneracy of the photon number operator $\hat{a}_1^\dagger \hat{a}_1$ and can be exploited to realize non-trivial quantum superpositions by detecting photons at different angles [120] or by engineering the coefficients J_{ii} using different light mode functions [52, 109–111].

3.3 Ensemble averages and master equation

In the previous paragraphs, we studied the effect of detection on a fermionic ultracold gas coupled to quantum light in a single experimental realization. We found that the quantum state of the atoms is strongly affected by the measurement and leads to an effective evolution even in the absence of atomic tunneling. Because of these effects, one may argue that it is not possible to probe the initial state of the system since each experimental run irremediably modifies it. It is indeed impossible to to determine $|\Psi(t = 0)\rangle$ by observing a single quantum trajectory since by performing many realizations of the same experiment one may obtain different results for each of them. However, by taking *ensemble averages* over the several quantum trajectories, it is possible to calculate *quantum mechanical expectation values* on the initial state of the system (only if the atomic dynamics can be neglected). We will now show that this corresponds to solving the master equation describing the dynamics of the atomic system.

The SSE (3.17) can be used for describing the conditional dynamics of a quantum system only if its quantum state is pure, i. e. it can be expressed using the vector $|\psi(t)\rangle$. If this is not the case, the state of system has to be represented using a density matrix. Defining the projector $\hat{\pi}(t) = |\psi(t)\rangle\langle\psi(t)|$, we can calculate an equation that models the conditional evolution of a mixed state in a single quantum trajectory by computing the differential $\mathrm{d}\hat{\pi}$ and making use of the SSE (3.17) . Following this procedure, one can prove that

$$\mathrm{d}\hat{\pi}(t) = \Big(\mathrm{d}N(t)\mathcal{G}[\hat{c}] - \mathrm{d}t\mathcal{H}\Big[i\hat{H} + \tfrac{1}{2}\hat{c}^\dagger\hat{c}\Big]\Big)\,\hat{\pi}(t) \tag{3.43}$$

where $\mathcal{G}[\dots]$ and $\mathcal{H}[\dots]$ are the non-linear superoperators

$$\mathcal{G}[\hat{w}]\,\hat{\pi} = \frac{\hat{w}\hat{\pi}\hat{w}^\dagger}{\mathrm{Tr}[\hat{w}\hat{\pi}\hat{w}^\dagger]} - \hat{\pi} \tag{3.44}$$

$$\mathcal{H}[\hat{w}]\,\hat{\pi} = \hat{w}\hat{\pi} + \hat{\pi}\hat{w}^\dagger - \mathrm{Tr}\Big[\hat{w}\hat{\pi} + \hat{\pi}\hat{w}^\dagger\Big]\,\hat{\pi}. \tag{3.45}$$

and $\mathrm{Tr}\Big[\hat{O}\Big]$ is the trace of $\hat{O}$. Expressions like the SSE (3.16) and (3.43) (but especially (3.16)) have been used extensively for computing numerically the solution of the master equation. Specifically, we identify the expectation value of the projector $\hat{\pi}(t)$ over an ensemble containing several quantum trajectories as the density matrix $\hat{\rho}$ that describes the evolution of a dissipative system, i. e. $\mathrm{E}[\hat{\pi}(t)] = \hat{\rho}$. Moreover, one can prove that the rule (3.12) can be generalized to any function g of the projector $\hat{\pi}(t)$ as

$$\mathrm{E}[\mathrm{d}N(t)\, g(\hat{\pi}(t))] = \mathrm{d}t\, \mathrm{E}\Big[\mathrm{Tr}\Big[\hat{\pi}(t)\hat{c}^\dagger\hat{c}\Big]\, g(\hat{\pi}(t))\Big] \,. \tag{3.46}$$

Applying this result, the density matrix $\hat{\rho}$ evolves according to

$$\mathrm{d}\hat{\rho} = -i\,\mathrm{d}t\left[\hat{H},\hat{\rho}\right] + \mathrm{d}t\,\mathcal{D}[\hat{c}]\,\hat{\rho} \tag{3.47}$$

where the superoperator $\mathcal{D}[\dots]$ is given by

$$\mathcal{D}[\hat{w}]\,\hat{\rho} = \hat{w}\hat{\rho}\hat{w}^\dagger - \tfrac{1}{2}\left(\hat{w}\hat{w}^\dagger\hat{\rho} + \hat{\rho}\hat{w}^\dagger\hat{w}\right). \tag{3.48}$$

In order to demonstrate that taking the average over many trajectories allows us to reconstruct the initial state of the system, we apply these results to the examples we illustrated in the previous section. Specifically, we consider two distinct detection setups: in the first one the measurement is sensitive to the total density $z_\uparrow + z_\downarrow$ while in the second one we probe the magnetization $z_\uparrow - z_\downarrow$. As illustrated in Figure 3.3, in both cases it is possible to recover the probability distribution of the initial state $P(z_\uparrow, z_\downarrow, 0, 0)$ by averaging several quantum trajectories.

The main advantage of solving the SSE (3.16) instead of the master equation (3.47) is strictly numerical. If N is the dimension of the Hilbert space of the system, then it is necessary to store N^2 complex numbers in order to represent the density matrix $\hat{\rho}$ accurately while the memory needed for storing the state vector $|\psi\rangle$ scales as N. Moreover, for large N, the time required for computing the evolution of $\hat{\rho}$ is proportional to N^4.

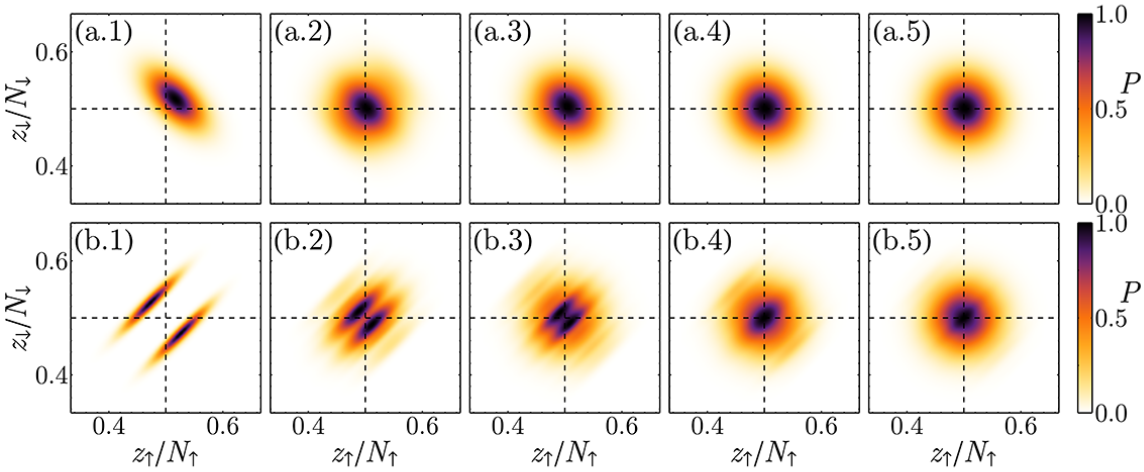

Fig. 3.3 Ensemble averages over several quantum trajectories when measuring the total density [(a)] or the magnetization [(b)] of the illuminated areas. Panels 1,2,3,4 and 5 show respectively the probability distribution $P_c(z_\uparrow, z_\downarrow, m, t)$ averaged over 1, 20, 100, 500 and 2000 quantum trajectories. Since the atomic dynamics is neglected, it is possible to measure the initial distribution $P(z_\uparrow, z_\downarrow, 0, 0)$ performing several experimental runs.

This should be compared to the time needed for computing an ensemble average of M quantum trajectories for $|\psi\rangle$ which scales as N^2M. In addition to this, computing different quantum trajectories is a task that can be easily parallelized on different processors since the different realizations of the conditional dynamics are completely independent from each other. Even though in order to obtain a good representation of $\hat{\rho}$ from the expectation value $\mathrm{E}[|\psi(t)\rangle\langle\psi(t)|]$ one should set $M \gg 1$, it is often very convenient to use this approach since reasonably accurate results can be achieved with $M \ll N^2$. Finally, if N is so large that it is not feasible to store the state vector at all times, it is still possible to compute the expectation value of observables by calculating the ensemble average over many quantum trajectories, i. e.

$$\langle\hat{O}(t)\rangle = \mathrm{E}\Big[\langle\psi(t)|\hat{O}|\psi(t)\rangle\Big] = \mathrm{Tr}\Big[\hat{\rho}(t)\hat{O}\Big]\,. \tag{3.49}$$

3.3.1 Inefficient detection

In the previous sections, we implicitly made two key assumptions: (i) the atoms do not scatter photons outside the optical cavity (free space photons) and that (ii) the experimental apparatus monitoring the quantum system by counting the number of quantum jumps (e. g. a photocounter) has perfect efficiency. Both these effects lead to dephasing and may destroy the effects that we will describe in the following chapters. Using an optical cavity with high Q factor allows to suppress the number of photons scattered in free space by several orders of magnitudes. Therefore, the dephasing due to the photons scattered outside the cavity mode can be neglected [17] and we can safely assume that (i) holds.

In order to describe the loss of coherence due to detector inefficiency we formulate a more accurate description of the conditional evolution by taking into account the effect of "missed" quantum jumps. If the detector is not ideal, a SSE describing the dynamics of the system does not exist because the conditioned state will become mixed even if the initial state is pure. This reflects the fact that the observer does not have access to perfect information about the quantum system, leading to a density matrix description. Modeling the state of the system with the matrix $\hat{\pi}(t)$, one can prove that its evolution in a single experimental run can be computed by solving the stochastic master equation (SME) [190]

$$\mathrm{d}\hat{\pi}(t) = \left\{\mathrm{d}N\,\mathcal{G}[\sqrt{\eta}\,\hat{c}] - \mathrm{d}t\,\mathcal{H}\left[\frac{\eta}{2}\hat{c}^\dagger\hat{c} + i\hat{H}\right] + \mathrm{d}t\,(1-\eta)\mathcal{D}[\hat{c}]\right\}\hat{\pi}(t), \tag{3.50}$$

where $\eta \in [0,1]$ is the detection efficiency and $\mathrm{d}N$ is the stochastic Itô increment such that $\mathrm{E}[\mathrm{d}N] = \eta\mathrm{Tr}\left[\hat{c}\hat{\pi}\hat{c}^\dagger\right]\mathrm{d}t$. Note that in the limit $\eta \to 1$ this equation reduces to the SSE (3.16) (if the initial state is pure) while it reduces to the unconditioned master equation (3.47) if the information from the quantum jumps is completely discarded ($\eta \to 0$).

3.4 Discussion

In this Chapter, we briefly introduced the quantum trajectory formalism for describing the conditional dynamics of a quantum system subjected to continuous monitoring. Within this picture, measurement backaction plays a crucial role in the evolution of the atomic state in a single experimental realization. Coupling a system of ultracold atoms to the quantized modes of an optical cavity offers an extremely flexible way for exploiting measurement backaction in order to engineer interesting quantum states. Simply changing the angle between probe and scattered beam or their polarization, it is possible to map different atomic observables onto the light field. If the atomic tunneling processes are slower that the light scattering, the dynamics of the system is determined by the competition between quantum jumps and effective non-Hermitian Hamiltonian. We illustrated this by focusing on the case of a Fermi gas loaded in an optical lattice when addressing its density. In this case, the measurement squeezes the probability distribution of the two spin species along a specific line in the $(z_\uparrow, z_\downarrow)$ plane which is precisely determined by the structure of the measurement operator. Moreover, we showed that by changing the polarization of the probe beam, the monitoring process is sensitive to the magnetization of the atomic system and it is not capable to distinguish between states with opposite values of this quantity. As a consequence, the quantum state of the matter becomes a Schrödinger cat state. Although the preparation of such interesting configurations follows a stochastic process, it is possible to follow it in real-time by monitoring number of photons escaping the optical cavity and offers important applications in quantum information and quantum technologies. The results presented in this Chapter are somehow analogous to previous works on spin squeezing [30, 75, 89]. However, the setup we consider here is more flexible and allows to address different observables (i. e. linear combinations of the atomic density of atoms with different spins) with the same experimental setup. This can be achieved by changing the angle between the optical cavity and the probe beam, without the need of quantum feedback.

Chapter 4

Measurement-induced dynamics in ultracold gases in optical lattices[1]

Ultracold gases trapped in optical lattices created by classical laser beams represent a successful interdisciplinary field: Atomic systems allow quantum simulations of phenomena predicted in condensed matter and particle physics, and find applications in quantum information processing [103]. Coupling quantum gases to quantized light [120, 155] broadens the field even further with opportunities to obtain novel quantum phases and light-matter entanglement [32–34, 37, 129]. Recent experimental breakthroughs [87, 98] succeeded in realizing the ultimate regimes where the quantum nature of both matter and light is equally important. As we have seen in Chapter 2, the coupling between an ultracold atomic system and quantized light modes can be exploited for mapping atomic properties (such as correlations and fluctuations) onto the light field and defines a QND measurement scheme. Although there are several examples of this approach in the literature [50, 53, 75, 91, 116, 157, 160, 162, 179], they all neglect either the many-body dynamics or measurement backaction. In this Chapter, we focus on the conditional dynamics of a many-body atomic system subjected to continuous monitoring. Specifically,

[1]The results presented in this chapter are published in [110] and [111].

we use the quantum trajectory formalism for describing the evolution of an ultracold gas when both atomic tunneling and measurement backaction are taken into account.

Quantum measurement is one of the most intriguing aspects of quantum mechanics. Many of its unusual manifestations have been already demonstrated, which include quantum jumps and the quantum Zeno effect. In particular, intriguing quantum states of light such as Fock and Schrödinger cat states were prepared using measurement backaction [72, 185]. In these scenarios, continuous measurement projects the quantum state of the system to a well-defined state. Here, we show that it is possible to preserve quantum superpositions by addressing the atomic system globally. Depending on the spatial profile of the measurement operator, its backaction competes with the standard short-range dynamical processes due to the atomic tunneling between nearest neighbor lattice sites. For bosons, the measurement induces dynamical macroscopic superpositions (multimode Schrödinger cat states). The resulting states have both oscillating density-density correlations with nontrivial spatial periods and long-range coherence, thus having properties of the supersolid state [17], but in the essentially dynamical version. For strongly interacting fermions, we demonstrate how to destroy and protect fermion pairs, clearly showing the interplay between many-body dynamics of fermions and the quantum measurement backaction.

4.1 Competition between tunneling and measurement

In the previous Chapter, we studied how measurement backaction affects key atomic properties of a system of ultracold fermions loaded in an optical lattice. However, in this description we completely neglected the atomic dynamics that may occur between two consecutive photocounts and the evolution of the system was dictated by the balance between quantum jumps and the effect of a non-Hermitian term in the Hamiltonian of the system. If the atomic tunneling cannot be ignored, the effective Hamiltonian of the system is given by

$$\hat{H}_{\text{eff}} = \hat{H}_a - i\hbar\frac{1}{2}\hat{c}^\dagger\hat{c} \tag{4.1}$$

where $\hat{c} = \sqrt{2\kappa}\hat{a}_1 = \sqrt{2\kappa}C\hat{D}$ is the jump operator and $\hat{H}_a$ is the Hamiltonian modeling the motion of the atoms in the absence of measurement. For bosons, we consider the Bose-Hubbard Hamiltonian

$$\hat{H}_a = -J\sum_{\langle i,j\rangle}\hat{b}_i^\dagger\hat{b}_j + \frac{U}{2}\sum_i\hat{n}_i(\hat{n}_i - 1) \tag{4.2}$$

while for fermions we take

$$\hat{H}_a = -J\sum_{\sigma=\uparrow,\downarrow}\sum_{\langle i,j\rangle}\hat{f}_{i\sigma}^\dagger\hat{f}_{j\sigma} + U\sum_i\hat{n}_{i\uparrow}\hat{n}_{i\downarrow}. \tag{4.3}$$

Importantly, the measurement introduces a new energy and time scale $\gamma = |C|^2\kappa$ which competes with the two other standard scales responsible for the unitary dynamics of a closed system (tunneling amplitude J and on-site interaction U). The non-Hermitian term in (4.1) couples all the sites of the optical lattice and leads to an effective cavity-mediated interaction between the atoms. This is a crucial feature of our setup and it is a direct consequence of the global addressing. If atoms scatter light independently, independent jump operators c_j would be applied to each site, projecting the atomic system to a state, where the long-range coherence degrades [146]. This is a typical scenario for spontaneous emission [146, 167], or rather analogous local [18, 40, 86, 178, 184] and fixed-range [13, 55] addressing and interactions. Additionally, if the light is scattered without a cavity, i.e. in uncontrolled directions, we lose the ability to choose the measurement operator and the jump operator applied would depend on the direction of the detected photon. In contrast, here we consider global coherent scattering, where the single global jump operator c is given by the sum over all sites, and the local coefficients J_{jj} (see § 2.2.2) responsible for the atom-environment coupling (via the light mode $\hat{a}$) can be engineered by optical geometry. Thus, atoms are coupled to the environment globally, and atoms that scatter light with the same phase are indistinguishable to light scattering (i.e. there is no "which-path information"). As a striking consequence, the long-range quantum superpositions are strongly preserved in the final projected states.

4.2 Effective dynamics of macroscopic spatial modes in bosonic systems

We start by considering the conditional evolution of a quantum gas with N bosons initially in the superfluid state

$$|\Phi(N)\rangle = \frac{1}{\sqrt{M^N N!}} \left(\sum_{i=1}^{N} \hat{b}_i^\dagger \right)^N |0\rangle \tag{4.4}$$

where $|0\rangle$ is the vacuum state for the operators $\hat{b}_i$. We continuously monitor this system using traveling waves as mode functions for the probe and scattered light beams. In this case, it is possible to tune the probe and scattered angles in such a way that the measurement scheme defines R macroscopically occupied spatial modes and the jump operator is $\hat{c} \propto \hat{a}_1 = C \sum_{j=1}^{R} e^{i2\pi j/R} \hat{N}_j$ where $\hat{N}_j$ is the occupation of the mode j (see § 2.2.2). Making use of the multinomial expansion for the sum in equation (4.4) and assuming that each mode has the same number of lattice sites, we can group the creation operators that act on the same mode so that $|\Phi(N)\rangle$ can be rewritten as

$$|\Phi(N)\rangle = \sqrt{\frac{N!}{R^N}} \sum_{\sum_i N_i = N} \sqrt{\frac{1}{N_1! N_2! \dots N_R!}} \prod_{i=1}^{R} |\Phi_i(N_i)\rangle. \tag{4.5}$$

where $|\Phi_i(N_i)\rangle$ is a superfluid in the spatial mode i with N_i atoms. In other words, we decompose a superfluid state in a linear combination of “smaller” superfluids that are defined in each spatial mode. This choice is particularly convenient because the states $\prod_{i=1}^{R}|\Phi_i(N_i)\rangle$ are eigenvectors of the jump operator

$$\hat{c}\prod_{i=1}^{R}|\Phi_i(N_i)\rangle = \sqrt{2\kappa}C\left(\sum_{j=1}^{R}e^{i2\pi j/R}N_j\right)\prod_{i=1}^{R}|\Phi_i(N_i)\rangle. \tag{4.6}$$

Therefore, defining $\mathcal{S}_R$ to be the subspace of the Hilbert space that is spanned by the vectors $\left\{\prod_{i=1}^{R}|\Phi_i(N_i)\rangle\right\}_{N_i}$, the dynamics due to the quantum jumps is internal to $\mathcal{S}_R$. This property enables us to formulate an effective description of the atomic evolution, greatly reducing the computational cost of each quantum trajectory and allowing us to formulate an analytic solvable model.

Carefully engineering the coefficients J_{jj}, we can partition the optical lattice in two spatial modes depending on the parity of the lattice sites. This can be achieved using traveling waves as mode functions for the probe and the cavity (i. e. $u_l(\mathbf{r}) = e^{i\mathbf{k}_l\cdot\mathbf{r}}$) where the wave vectors $\mathbf{k}_0$ and $\mathbf{k}_1$ are orthogonal, corresponding to the detection of the photons scattered in the diffraction minimum and the operator $\hat{a}_1 = C(\hat{N}_{\text{even}} - \hat{N}_{\text{odd}})$ [115, 117–119, 122]. Alternatively, one can obtain the same spatial mode structure considering standing waves (i. e. $u_l(\mathbf{r}) = \cos(\mathbf{k}_l\cdot\mathbf{r})$) crossed in such a way that $\mathbf{k}_0$ and $\mathbf{k}_1$ have the same projections on the lattice direction and are shifted in such a way that the even sites of the optical lattice are positioned at the nodes, so that the scattered light operator is $\hat{a}_1 = C\hat{N}_{\text{odd}}$ [110]. In this case, we can decompose the initial state of the system (superfluid) as

$$|\Phi(N)\rangle = \sum_{j=1}^{N}\sqrt{\frac{N!}{2^N j!(N-j)!}}|\Phi_{\text{odd}}(j), \Phi_{\text{even}}(N-j)\rangle. \tag{4.7}$$

If the interaction between the atoms can be neglected ($U = 0$), the dynamics resulting from the competition between the measurement process and the usual nearest-neighbors tunneling preserves the mode structure and it is possible to describe the system in terms of collective variables. To clarify this, we rewrite the tunneling term in equation (4.2) as

$$\sum_{\langle i,j\rangle} \hat{b}_j^\dagger \hat{b}_i = \sum_{i\in\text{odd}} \sum_{j:i} \hat{b}_j^\dagger \hat{b}_i + \sum_{i\in\text{even}} \sum_{j:i} \hat{b}_j^\dagger \hat{b}_i \tag{4.8}$$

where $j : i$ indicates that the sites j and i are nearest neighbors. The dynamics generated by this expression and the non-Hermitian term is internal to the space $\mathcal{S}_2$ if the initial state of the system belongs to $\mathcal{S}_2$. In fact, by applying $\hat{H}_{\text{eff}}$ to the product of two superfluid states one has

$$\begin{aligned}\hat{H}_{\text{eff}}|\Phi_{\text{odd}}(l), \Phi_{\text{even}}(m)\rangle &= -\hbar J\sqrt{l(m+1)}|\Phi_{\text{odd}}(l-1), \Phi_{\text{even}}(m+1)\rangle \\ &- \hbar J\sqrt{m(l+1)}|\Phi_{\text{odd}}(l+1), \Phi_{\text{even}}(m-1)\rangle \\ &- i\hbar\frac{\gamma}{2}|\beta_1 l + \beta_2 m|^2|\Phi_{\text{odd}}(l), \Phi_{\text{even}}(m)\rangle, \end{aligned} \tag{4.9}$$

where β_1 and β_2 depend on the measurement scheme ($\beta_1 = -\beta_2 = 1$ for probing in the diffraction minimum while $\beta_1 = 1$ and $\beta_2 = 0$ if only the odd sites are addressed). Therefore, the quantum state of the atoms can be expressed as $|\psi\rangle = \sum_{j=0}^{N} \alpha_j|\Phi_{\text{odd}}(j), \Phi_{\text{even}}(N-j)\rangle$ where $\alpha_j \in \mathbb{C}$ at all times. This allows us to reformulate the conditional dynamics of the system in terms of an effective double-well problem where the occupation of the two wells corresponds to the population of the spatial modes. However, this approach does not allow us to compute any spatial correlations for the system considered: only "collective" properties can be calculated.

The generalization of (4.9) to the case of R modes is straightforward: from the spatial structure of the jump operator one can compute the amplitude of the tunneling processes between different spatial modes and build an effective $R-$wells problem. Moreover, the coupling between the effective wells can be tuned by changing the spatial structure of the measurement operator, allowing us to go beyond simple double-well systems [161, 190]. For example, considering the case of $R = 3$ spatial modes generated by a measurement scheme where the light mode functions are traveling waves and the jump operator is $\hat{c} \propto \sum_{j=1}^{3} e^{i2\pi j/3}\hat{N}_j$, one has that the modes alternates across the lattice as $RGBRGB\ldots$. Therefore, each lattice site belonging to the mode R is connected to one site of mode G and one of mode B (indices can be cycled) so that tunneling processes are allowed between all the modes. This reduces the system to a three-wells problem where a specific linear combination of the atomic populations $\hat{N}_j$ is monitored while the atoms are free to hop between the three different wells. Importantly, this is not the only possible way to divide the optical lattice into three modes: if probe and scattered light are standing waves such that $\mathbf{k}_{1,0} \cdot \mathbf{r} = \pi/4$, the resulting J_{jj} coefficients are $[0, 1/2, 1, 1/2, 0, \ldots]$ and the modes alternates as $RGBGRGBGR\ldots$. In this case, tunneling is not allowed between mode R and B and the coupling between the effective three-wells describing the conditional dynamics must take this into account by forbidding atomic transfer between two of the effective wells.

The local interaction term in Eq. (4.2) tends to localize the atoms on each lattice site and cannot be included exactly in the approximation we presented. This is because the dynamics described by the interaction operator $\sum_i \hat{n}_i(\hat{n}_i - 1)$ is not internal to the subspace $\mathcal{S}_R$. For weak interactions and assuming that the measurement scheme partitions the optical lattice in R spatial modes, we find that the interaction energy U is rescaled by the number of lattice sites belonging to each mode (M_j) so that

$$\frac{\hbar U}{2}\sum_{i=1}^{M}\hat{n}_j(\hat{n}_j - 1) \approx \frac{\hbar}{2}\sum_{j=1}^{R}\frac{U}{M_j}\hat{N}_j(\hat{N}_j - 1). \tag{4.10}$$

Note that this expression is approximate and does not allow to describe the strong interacting limit where the atoms form a Mott insulator state. Despite this limitation, the model we presented allows to describe interacting systems where synthetic interactions mediated by the light field couple different spatial modes [35], as we discussed in § 2.3.

4.3 Large-scale dynamics due to weak measurement

If $\gamma \ll J$, the measurement is weak compared to the usual atomic dynamics and it is not able to project the state of the system to one of the eigenstates of the jump operator $\hat{c}$ and therefore quantum Zeno dynamics cannot take place [56, 151, 152, 169, 175]. However, even in this regime, the measurement backaction strongly affects the atomic evolution and cannot be neglected. We find that the continuous monitoring process actively competes with the dynamics due to the atomic tunneling between nearest neighboring lattice sites and such competition can be exploited for realizing interesting quantum states such as NOON states and multicomponent Schrödinger states. For non-interacting bosons, the measurement leads to giant oscillations of particle number between the spatial modes. Without continuous monitoring, the probability distribution of this quantity would spread out significantly and the average number of atoms would oscillate with an amplitude proportional to the initial imbalance, i.e. tiny oscillations for a tiny initial imbalance (Figure 4.1). In contrast, here we observe

(i) full exchange of atoms between the modes independent of the initial state and even in the absence of initial imbalance;

(ii) the distributions consist of a small number of well-defined components;

(iii) these components are squeezed even by weak measurement.

These effects are a consequence of the fact that addressing the system globally preserves long range coherence. Moreover, the spatial structure of the jump operator determines the conditional dynamics: the eventual degeneracy of the light intensity $\langle \hat{a}_1^\dagger \hat{a}_1 \rangle$ is imprinted

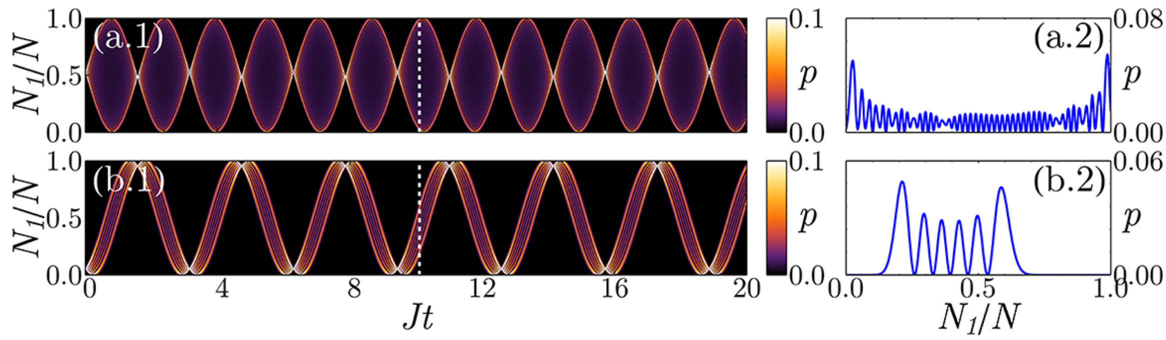

Fig. 4.1 Oscillatory dynamics in the absence of measurement starting from an imbalanced state. Panel (a) shows the probability distribution for the occupation of the odd sites of the optical lattice if the initial state has imbalance $(N_{\text{odd}} - N_{\text{even}})/N = 0.02$ while for panel (b) $(N_{\text{odd}} - N_{\text{even}})/N = 0.95$. Panels (1) illustrate the full probability distribution for all times while panels (2) focuses on the time indicated by the dashed vertical line. The probability distribution spreads over several components and the average occupation oscillates with amplitude proportional to the initial state. $\gamma/J = 0$, $N = 100$.

on the state of the atoms and can lead to a multicomponent structure. For example, if one detects the photons scattered in the diffraction minimum, so that the measurement addresses the difference in the population of the two spatial modes defined by the odd and even lattice sites, i. e. $\hat{D} = \hat{N}_{\text{even}} - \hat{N}_{\text{odd}}$, the photon number operator is not sensitive to the sign of this difference. This is because states with opposite $\langle \hat{N}_{\text{even}} - \hat{N}_{\text{odd}} \rangle$ scatter light with different phase but with the same intensity. As a consequence of the measurement backaction, the atomic state becomes a superposition of two macroscopically occupied components: a Schrödinger cat state. If the monitoring scheme defines more than two degenerate modes, the conditional evolution leads to an atomic wavefunction that can be expressed as a superposition of multiple macroscopically occupied components. If the light mode functions are traveling waves at an angle such that they define R distinct spatial modes, the $D-$operator is $\hat{D} = \sum_{l=1}^{R} \hat{N}_l e^{i2\pi l/R}$ $(R \in \mathbb{Z})$. In this case, the number of components of the atomic state, i.e. the degeneracy of $\hat{a}_1^\dagger \hat{a}_1$, can be computed from the eigenvalues of $\hat{D}$ noting that they can be represented as the sum of vectors on the complex plane with phases that are integer multiples of $2\pi/R$: $N_1 e^{i2\pi/R}, N_2 e^{i4\pi/R}, \ldots N_R$. Since

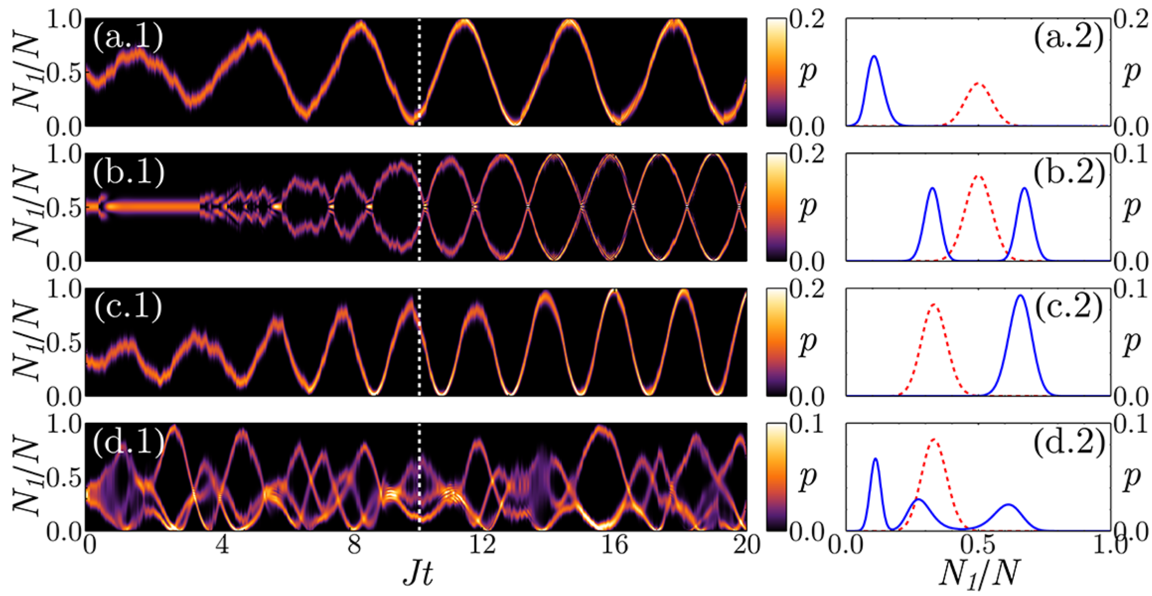

Fig. 4.2 Oscillatory dynamics induced by the measurement process in a single quantum trajectory for non-interacting bosons ($U = 0$). Atom number distributions $P(N_l)$ in one of the modes when the optical lattice is partitioned in two (a)-(b) or three spatial modes (c)-(d). Panels (1) illustrate the full probability distribution for all times while panels (2) focuses on the time indicated by the dashed vertical line (blue) and the initial state (red). Depending on the spatial structure of the jump operator, the detection process can lead to macroscopic superpositions of well-squeezed components. (a) $\gamma/J = 0.02$, $N = 100, /, J_{jj} = [1, 0, 1, 0, 1\ldots]$, (b) $\gamma/J = 0.02$, $N = 100, /, J_{jj} = (-1)^j$, (c) $\gamma/J = 0.02$, $N = 99, /, J_{jj} = [0, 1/2, 1, 1/2, 0\ldots]$, (d) $\gamma/J = 0.02$, $N = 99, /, J_{jj} = e^{i2\pi j/3}$. The initial state is a superfluid.

the sum of these vectors is invariant under rotations by $2\pi l/R$, $l \in \mathbb{Z}$ and reflection in the real axis, the state of the system is 2-fold degenerate for $R = 2$ and $2R$-fold degenerate for $R > 2$. Importantly, this property is a consequence of the spatial structure of the jump operator and does not only depend on the number of modes defined by the measurement. For example, considering the case of three modes arranged as $RGBRGB\ldots$ ($J_{jj=}e^{i2\pi j/3}$), the photon number $\langle \hat{a}_1^\dagger \hat{a}_1 \rangle$ is invariant under the exchange of any two spatial modes and, as a consequence, the probability distribution of the population of each mode presents three oscillating peaks, indicating that the atomic state conditioned to the measurement is a 6−modes Schrödinger cat state. However, if the spatial modes have a different structure such as $RGBGRGBGR\dots$ ($J_{jj} = [0, 1/2, 1, 1/2, 0, \dots]$) this is not the case: only the modes B and G can be exchanged without affecting the intensity of the detected light. Therefore, in this case the probability distribution of the occupation of the mode R has a single peak while the ones for modes G and B are bimodal (Figure 4.2).

Quantum states characterized by superposition of multiple components are useful in quantum metrology and information since this structure is a purely quantum effect. The multimode dynamics may recover the semiclassical character [100], when the number of modes is reduced to one. The method we propose does not require external control [78, 79, 142] for preparing these states: continuously monitoring the light intensity it is possible to determine when the splitting in the components reaches its maximum value (corresponding to the maximal macroscopicity [59]) and further oscillatory dynamics can be stopped by ramping up the lattice depth. Note that for $R > 1$ spatial modes each photocount changes the phase difference between the various components of the atomic state, making it fragile to photon losses. However, the measurement setup can be modified to make these states more robust [116]. In addition, the example in Figure 4.2a consists of only one component (here N_{odd} is measured directly) and is therefore insensitive to decoherence due to photon losses.

It is interesting to note, that the oscillating state we have described shows spatial periodicity in the density-density correlation function depending on the measurement configuration. For R modes the spatial period is Rd (d is the lattice period). Moreover, the state also has long-range coherence between distant sites. Therefore, it has properties of the supersolid state [17], but with a nontrivial period, and it exists in the essentially dynamical version.

4.3.1 Probing the odd sites of the optical lattice

In order to understand the origin of the oscillatory behavior illustrated in Figure 4.2, we now focus on the case when the measurement operator probes the population of the odd sites of the optical lattice, i. e. $\hat{a}_1 = C\hat{N}_{\text{odd}}$. Within this assumption, we can formulate an analytic description of the atomic dynamics [83]. In between the quantum jumps, the evolution of the system is deterministic and it is determined by the matrix elements of the non-Hermitian Hamiltonian (4.9):

$$\begin{aligned}\langle \Phi_{\text{odd}}(s), \Phi_{\text{even}}(N-s)|\hat{H}_{\text{eff}}|\psi\rangle &= -J\hbar\left(\alpha_{s-1}b_{s-1} + \alpha_{s+1}b_s\right)\\ &+ \frac{2\hbar U}{M}\left[s(s-1) + (N-s)(N-s-1)\right]\alpha_s - i\hbar\frac{\gamma}{2}s^2\alpha_s \end{aligned} \tag{4.11}$$

where $b_s = \sqrt{(s+1)(N-s)}$. Note that this expression does not contain a chemical potential since we will solve the Schrödinger equation for a fixed number of particles, as emphasized by the left hand side of equation (4.11). In the limit $N \gg 1$ we can replace the index s with the continuous variable $x = s/N$ which represents the (relative) occupation of the odd sites of the optical lattice. Moreover, we define the wavefunction $\psi(x = s/N) = \sqrt{N}\alpha_s$ where the $\sqrt{N}$ prefactor ensures that $\psi(x)$ is normalized, i. e.

$$\sum_{s=0}^{N} |\alpha_s|^2 = \int_0^1 |\psi(x)|^2 \, \mathrm{d}x = 1. \tag{4.12}$$

Introducing $b(x) = \sqrt{(x+h)(1-x)}$, $h = 1/N$, $\Lambda = UN/M$ and $\Gamma = N\gamma/2$, and neglecting constant shifts we can rewrite (4.11) as

$$\begin{aligned}\langle x|\hat{H}_{\text{eff}}|\psi\rangle =& -\sqrt{N}J\hbar\left[b(x-h)\psi(x-h) + \psi(x+h)b(x)\right]\\ &+ 2\sqrt{N}\hbar\Lambda x(x-1)\psi(x) - i\sqrt{N}\hbar\Gamma x^2\psi(x).\end{aligned} \tag{4.13}$$

Expanding this expression up to second order in h and defining the normalized atom imbalance $z = (N_{\rm odd} - N_{\rm even})/N = 2x - 1$, we obtain an effective non-Hermitian Hamiltonian that describes the dynamics of the two macroscopically occupied spatial modes. Specifically, we describe the evolution of the system between two quantum jumps with the effective Schrödinger equation

$$ih\frac{\mathrm{d}}{\mathrm{d}t}\psi(z,t) = H(z)\psi(z,t). \tag{4.14}$$

where the Hamiltonian $H(z)$ is

$$H(z)\psi(z) = -\,2Jh^2\frac{\mathrm{d}}{\mathrm{d}z}\left(\sqrt{1-z^2}\frac{\mathrm{d}}{\mathrm{d}z}\psi(z)\right) + \frac{1}{2}\Lambda z^2 + V(z)\psi(z) - i\Gamma\frac{(z+1)^2}{4}\psi(z) \tag{4.15}$$

and the effective potential $V(z)$ is given by

$$V(z) = -J\sqrt{1-z^2}\psi(z)\left[1 + \frac{h}{1-z^2} - \frac{h^2(1+z^2)}{(1-z^2)^2}\right]. \tag{4.16}$$

The dynamics of the spatial modes is therefore equivalent to the motion of a particle with effective mass $\sqrt{1-z^2}$ in the real potential $V(z)$ and imaginary potential $-i\Gamma(z+1)^2/4$. Using the same approximations, we find that the initial state (4.7) in the limit $N \gg 1$ reduces to the Gaussian function

$$\psi(z,0) = \left(\frac{1}{\pi b_0^2}\right)^{1/4} e^{-z^2/(2b_0^2)}. \tag{4.17}$$

describing a perfectly balanced population between the two spatial modes (i. e. $\langle \hat{N}_{\rm odd} - \hat{N}_{\rm even}\rangle = 0$) with variance $b_0^2 = 2h$. In order to give an analytic expression of $\psi(z,t)$, we take the limit of small population unbalance so the mass term becomes $\sqrt{1-z^2} \approx 1$ and we expand the potential $V(z)$ up to second order in z:

$$V(z) \approx -1 - h + \frac{1}{8}\omega^2 z^2, \qquad \omega = 2\sqrt{1 + \Lambda - h}. \tag{4.18}$$

Therefore, the dynamics of the atomic system is mapped to the evolution of a Gaussian wave packet in an harmonic potential and subjected to dissipation via the non-Hermitian term due to the measurement. Within these assumptions, the wavefunction of the system remains Gaussian at all times and it can be expressed as

$$\psi(z,t) = \left(\frac{1}{\pi b^2(t)}\right)^{1/4} \exp\left[ia(t) + \frac{izc(t) + iz^2\phi(t) - (z - z_0(t))^2}{2b^2(t)}\right]. \tag{4.19}$$

The functions $b^2(t)$, $z_0(t)$, $c(t)$, $\phi(t)$ and $a(t)$ describe the collective dynamics of the system. Specifically, $b^2(t)$ is proportional to the width of the atomic distribution, $z_0(t)$ is the mean value of the unbalance (i. e. $\langle \hat{N}_{\text{odd}} - \hat{N}_{\text{even}} \rangle$) while $c(t)$ and $\phi(t)$ are phase differences between superfluid states with different populations. Moreover, $\mathrm{Re}\,[a(t)]$ describes the global phase of the wavefunction and $\mathrm{Im}\,[a(t)]$ its norm. Importantly, all these functions are real with the exception of $a(t)$ which is complex. Finally, from the Schrödinger equation (4.14) we obtain the differential equations that dictate the evolution of $b^2(t)$, $z_0(t)$, $c(t)$, $\phi(t)$ and $a(t)$. Specifically, one can prove that

$$\dot{(b^2)} = 8hJ\phi - \frac{\Gamma}{2h}b^4 \tag{4.20}$$

$$\dot{\phi} = -\frac{J\omega^2}{4h}b^2 - \frac{\Gamma}{2h}b^2\phi + \frac{4hJ}{b^2}(1 + \phi^2) \tag{4.21}$$

$$\dot{z_0} = -\frac{\Gamma}{2h}b^2(1 + z_0) + \frac{2hJ}{b^2}(2z_0\phi + c) \tag{4.22}$$

$$\dot{c} = -\frac{\Gamma}{2h}b^2 c + \frac{4hJ}{b^2}(\phi c - 2z_0) \tag{4.23}$$

Because of the dissipation, the norm of the wavefunction is not conserved and it is decreasing according to $\exp\left(-2\,\mathrm{Im}\left[a(t)\right]\right)$ where

$$\mathrm{Im}\left(\dot{a}\right) = \frac{\Gamma}{4h}\left[\left(1+z_0\right)^2 + \frac{b^2}{2}\right], \tag{4.24}$$

which determines when a photon escapes the cavity and a quantum jump occurs.

It has been shown that Equations (4.20-4.23) can be solved analytically introducing the auxiliary variables $p = (1-i\phi)/b^2$ and $q = (z_0 + ic/2)/b^2$ [90]. Substituting in (4.20-4.23), the four equations describing the dynamics of the atomic state reduce to two differential equations:

$$-2Jh^2p^2 + \left(\frac{J\omega^2}{8} - \frac{i\Gamma}{4}\right) + \frac{ih}{2}\frac{\mathrm{d}p}{\mathrm{d}t} = 0 \tag{4.25}$$

$$4Jh^2pq - \frac{i\Gamma}{2} - ih\frac{\mathrm{d}q}{\mathrm{d}t} = 0. \tag{4.26}$$

Defining, $\zeta^2 = 1 - i2\Gamma/(J\omega^2)$ and making use of standard integrals, one can prove that the solution of the first equation is

$$p(t) = \frac{\zeta\omega}{4h}\frac{\left[\zeta\omega + 4hp(0)\right]e^{i2\zeta\omega t} - \left[\zeta\omega - 4hp(0)\right]}{\left[\zeta\omega + 4hp(0)\right]e^{i2\zeta\omega t} + \left[\zeta\omega - 4hp(0)\right]}. \tag{4.27}$$

Furthermore, the equation that determines the evolution of $q(t)$ can be solved noting that (4.26) can be rewritten as

$$\frac{\mathrm{d}}{\mathrm{d}t}\left(Iq\right) = -\frac{\Gamma}{2h}I. \tag{4.28}$$

where the integrating factor I is given by

$$I = \exp\left[i4h\int p(t)\mathrm{d}t\right] \tag{4.29}$$

$$= [\zeta\omega + 4hp(0)]\, e^{i\zeta\omega t} + [\zeta\omega - 4hp(0)]\, e^{-i\zeta\omega t} \tag{4.30}$$

so that $q(t)$ is given by

$$q(t) = \frac{1}{2h\zeta\omega} \frac{A}{(\zeta\omega + 4hp(0))\, e^{i\zeta\omega t} + (\zeta\omega - 4hp(0))\, e^{-i\zeta\omega t}} \tag{4.31}$$

$$\begin{aligned} A = i\Gamma \left[(\zeta\omega + 4hp(0))\, e^{i\zeta\omega t} - (\zeta\omega - 4hp(0))\, e^{-i\zeta\omega t} \right], \\ +4h\zeta^2\omega^2 q(0) - i8h\Gamma p(0). \end{aligned} \tag{4.32}$$

Finally, from these solutions we can extract the physical observables of equations (4.20-4.23) as $b^2(t) = 1/\operatorname{Re}[p(t)]$, $\phi(t) = -\operatorname{Im}[p(t)] / \operatorname{Re}[p(t)]$, $z_0(t) = \operatorname{Re}[q(t)] / \operatorname{Re}[p(t)]$ and $c(t) = 2\operatorname{Im}[q(t)] / \operatorname{Re}[p(t)]$.

Instead of focusing on the full solution, here we give a qualitative description of the dynamics generated by these equations. Specifically,we compute the eigenvalues of the Jacobian matrix of the system (4.20-4.23) in its stationary points and we study the behavior of the solution around these points. Setting the left hand side of the systems (4.20-4.23) or (4.25-4.26) to zero, we find that there is only one physical critical point. Defining the parameter

$$\alpha = \sqrt{-\frac{1}{2} + \frac{1}{2}\sqrt{\frac{4\Gamma^2}{J^2\omega^4} + 1}} \tag{4.33}$$

one can prove that

$$b^2(\infty) = \frac{4hJ\omega\alpha}{\Gamma} \tag{4.34}$$

$$\phi(\infty) = \frac{J\omega^2\alpha^2}{\Gamma} \tag{4.35}$$

$$z_0(\infty) = -1 + \frac{1}{2\alpha^2 + 1} \tag{4.36}$$

$$c(\infty) = \frac{4\Gamma}{J\omega^2(2\alpha^2+1)}. \tag{4.37}$$

Note that these expressions can be obtained also by taking the limit $t \to \infty$ of the exact solutions (4.27) and (4.31). We then calculate the Jacobian matrix $\mathcal{J}$ by differentiating each equation in (4.20-4.23) with respect to all the dynamical variables, i. e.

$$\mathcal{J} = \begin{bmatrix} \frac{\partial(\dot{b^2})}{\partial b^2} & \frac{\partial(\dot{b^2})}{\partial \phi} & \frac{\partial(\dot{b^2})}{\partial z_0} & \frac{\partial(\dot{b^2})}{\partial c} \\ \frac{\partial\dot{\phi}}{\partial b^2} & \frac{\partial\dot{\phi}}{\partial \phi} & \frac{\partial\dot{\phi}}{\partial z_0} & \frac{\partial\dot{\phi}}{\partial c} \\ \frac{\partial\dot{z_0}}{\partial b^2} & \frac{\partial\dot{z_0}}{\partial \phi} & \frac{\partial\dot{z_0}}{\partial z_0} & \frac{\partial\dot{z_0}}{\partial c} \\ \frac{\partial\dot{c}}{\partial b^2} & \frac{\partial\dot{c}}{\partial \phi} & \frac{\partial\dot{c}}{\partial z_0} & \frac{\partial\dot{c}}{\partial c} \end{bmatrix} \tag{4.38}$$

$$= \begin{bmatrix} -\frac{b^2\Gamma}{h} & 8hJ & 0 & 0 \\ -\frac{4hJ\left(1+\phi^2\right)}{b^2} - \frac{2\phi\Gamma+J\omega^2}{4h} & \frac{8hJ\phi}{b^2} - \frac{b^2\Gamma}{2h} & 0 & 0 \\ -\frac{2hJ(c+2\phi z_0)}{b^2} - \frac{\Gamma(1+z_0)}{2h} & \frac{4hJz_0}{b^2} & \frac{4hJ\phi}{b^2} - \frac{b^2\Gamma}{2h} & \frac{2hJ}{b^2} \\ -\frac{4hJ(c\phi-2z_0)}{b^2} - \frac{\Gamma c}{2h} & \frac{4hJc}{b^2} & -\frac{8hJ}{b^2} & \frac{4hJ\phi}{b^2} - \frac{b^2\Gamma}{2h} \end{bmatrix}. \tag{4.39}$$

The eigenvalues of this matrix when evaluated at the stationary point $P = (b^2, \phi, z_0, c)$ defined by (4.34-4.37) allow to study the stability of the solutions of the differential equations (4.20-4.23) without having to calculate an exact solution. Specifically, we find that the eigenvalues of $\mathcal{J}$ in the critical point are

$$\lambda_{1,2} = \pm\frac{i\Gamma}{\omega\alpha} - J\omega\alpha \qquad \text{and} \qquad \lambda_{3,4} = \pm\frac{2i\Gamma}{\omega\alpha} - 2J\omega\alpha. \tag{4.40}$$

Since all of them have a non-positive real part, P is a stable critical point. Therefore, the evolution of the system in the large time limit will tend to damped oscillations around the stationary point with frequency $\Omega = 2\Gamma/(\omega\alpha)$ and decay time $\Delta t_d = 1/(2J\omega\alpha)$. The ratio between the measurement strength Γ and the tunneling amplitude J determines if the oscillatory behavior is under- or over-damped. The predictions of this analytic model agree quantitatively with the dynamics described by (4.11) only if the population imbalance between the two spatial modes is small. Despite this, we find that this simple

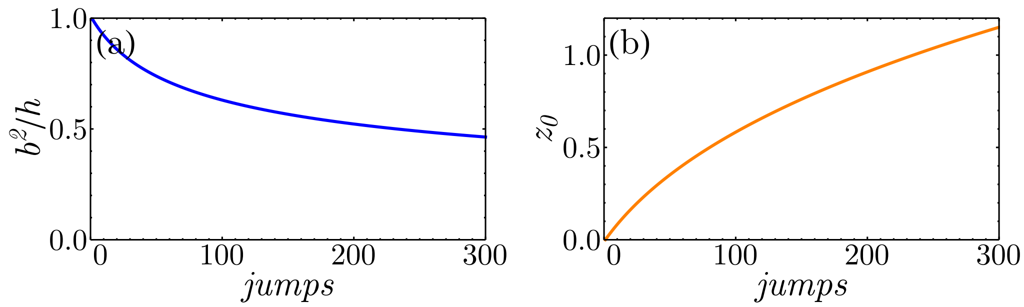

Fig. 4.3 Effect of the quantum jumps on the atomic observables neglecting the effective non-Hermitian dynamics. The uncertainty associated to the number of atoms in each spatial mode decreases (a) while the system prefers configurations with larger imbalance between odd and even sites (b).

formulation captures the qualitative behavior of b^2 and z_0 and helps to explain the emergence of the collective oscillations between odd and even sites.

The quantum jumps substantially contribute to the evolution of the atomic state and drastically alter the dynamics described by (4.20-4.23). Their effect can be included in the model by expanding the jump operator $\hat{a}_1 = C(z+1)/2$ around the peak of the Gaussian wavefunction (4.19) as

$$\frac{(1+z)}{2} \approx \frac{1}{2} \exp\left[\ln(1+z_0) + \frac{z-z_0}{(1+z_0)} - \frac{(z-z_0)^2}{2(1+z_0)^2}\right]. \tag{4.41}$$

Using this expression, we compute the effect of the jumps on the functions $b^2(t)$, $z_0(t)$, $c(t)$ and $\phi(t)$ and we obtain a set of equations that determines the change in initial condition for (4.20-4.23) due to the detection of one photon

$$b^2 \to \frac{b^2(1+z_0)^2}{(1+z_0)^2+b^2} \tag{4.42}$$

$$\phi \to \frac{\phi(1+z_0)^2}{(1+z_0)^2+b^2} \tag{4.43}$$

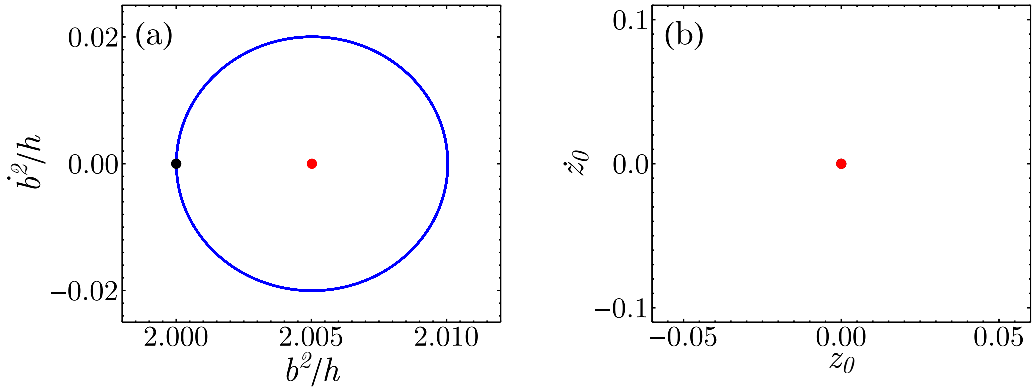

Fig. 4.4 Close orbits around the stable point for the width of the atomic distribution $(b^2, \dot{b^2})$ (a) and the population imbalance $(z_0, \dot{z}_0)$ (b) in a single trajectory setting $\Gamma = 0$ and without jumps. The black point marks the initial state ($b^2 = 2h$, $z_0 = 0$) while the red one marks the stationary point. Panel (b) does not show any dynamics since the initial state and the stationary point coincide.

$$z_0 \to z_0 + \frac{b^2(1+z_0)}{(1+z_0)^2 + b^2} \tag{4.44}$$

$$c \to \frac{c(1+z_0)^2}{(1+z_0)^2 + b^2}. \tag{4.45}$$

Neglecting the non-Hermitian dynamics, these equations imply that each quantum jump tends to squeeze the width of the atomic distribution while it increases the atom imbalance between odd and even sites (see Figure 4.3). As a consequence, the measurement process decreases the uncertainty in the population of the spatial modes and the atomic state becomes a product of two superfluid states with well-defined atom number. In the next paragraphs, we will discuss how the quantum jumps compete with the effective non-unitary dynamics, leading to the creation of states where the atomic population collectively oscillates between odd and even sites.

4.3.2 Case $J = 0$

We first start by considering the case when the atomic tunneling is much slower than the measurement and J can be neglected (see Chapter 3). Within this assumption, the evolution of the system between two quantum jumps is solely determined by the non-Hermitian dynamics which, together with the quantum jumps, decreases the variance of the population imbalance between odd and even sites. Therefore, the final state of the system is a product of two superfluids with a well-defined number of atoms for each quantum trajectory and the behavior of $b(t)$ is almost deterministic [42]. However, the imbalance between odd and even sites is not the same for each quantum trajectory since it is determined by the specific sequence of quantum jumps. In fact, the photodetections or the non-Hermitian decay dominates the dynamics of z_0 in opposite regimes: the first effect is predominant if the occupation in the odd sites is large while the second one is favored by a large occupation of the even sites. In each quantum trajectory, these two phenomena balance each other and, in the long time limit, z_0 reaches a stationary value which follows the Gaussian probability distribution defined by the initial state (4.17), favoring states with small population difference between odd and even sites.

4.3.3 Case $J \neq 0$

If the tunneling amplitude J cannot be neglected, the detection process competes with the usual atomic dynamics. We first consider the weak measurement limit $\Gamma \ll J$ so that we can describe the evolution of the system between two quantum jumps setting $\Gamma \approx 0$ in (4.20-4.23). From the stability analysis we find that the stable point of the system is $b(\infty) \approx 4h/\omega$ and $z_0(\infty) \approx 0$ while the eigenvalues of the Jacobian matrix are purely imaginary, i. e. $\lambda_{1,2} = \pm iJ\omega$ and $\lambda_{3,4} = \pm 2iJ\omega$. Therefore, in the absence of quantum jumps, the solutions of (4.20-4.23) are oscillating around the stable point without damping (see Figure 4.4). The photodetections perturb this regular oscillations and drive the system quasi-periodically, leading to giant oscillations in the population of the spatial modes. Specifically, the quantum jumps tend to increase the value of z_0 according to (4.42-4.45) and consequently, the radius of the oscillations in the $(z_0, \dot{z}_0)$ plane is increasing if a jump happens when $z_0 > 0$ while it is decreasing when $z_0 < 0$. Importantly, these two processes do not happen with the same rate because the probability for the emission of a photon in the time interval δt depends on the atomic state and it is given by

$$p_{\text{jump}} = \frac{\Gamma}{2h}\left[(1+z_0)^2 + \frac{b^2}{2}\right]\delta t. \tag{4.46}$$

Therefore, jumps that increase the radius of the oscillations happen more often and increase the amplitude of the oscillations of $z_0(t)$ (see Figure 4.5). In order to confirm this prediction, we now turn to the full measurement problem. Taking into account the non-Hermitian dynamics in the differential equations for $b(t)$ and $z(t)$, the radius of the orbits shown in Figure 4.4 decreases exponentially. Therefore, we can identify three different time scales in the evolution of the system:

(i) the oscillation frequency $\Omega = 2\Gamma/(\omega\alpha)$,

(ii) the damping time $\Delta t_d = 1/(2J\omega\alpha)$,

(iii) the average time interval between two quantum jumps $\Delta t_j = 2h/\Gamma$.

The ratios between these quantities determine which process is dominating the physics of the system. Considering again the weak measurement regime ($\Gamma \ll J$) but taking into account the terms depending on Γ in equations (4.20-4.23), we find that both $b(t)$ and $z_0(t)$ oscillate around the stationary point with decreasing radius. In this limit, one has $\Omega\Delta t_d \approx J\omega^2/\Gamma \gg 1$, indicating that the system behaves like an under-damped oscillator (Figure 4.6). Importantly, there are many photocounts during each oscillation ($\Omega\Delta t_j \approx \Gamma h/(J\omega^3) \ll 1$) and the quantum jumps can counteract the damping, driving

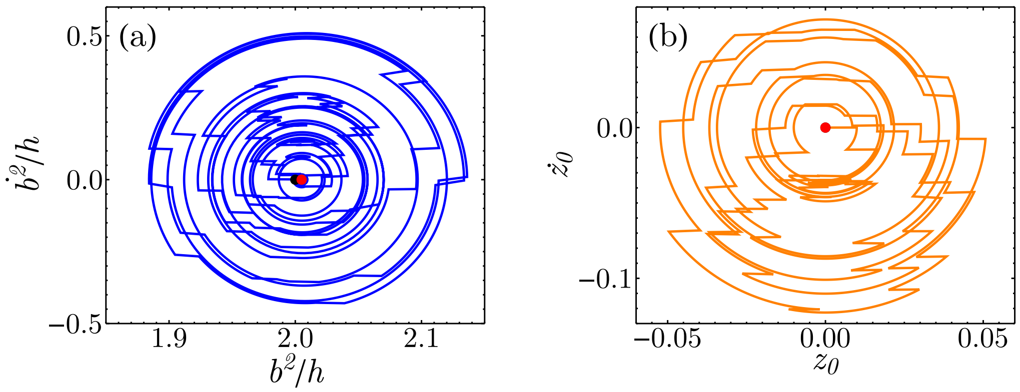

Fig. 4.5 Oscillations of $(b^2, \dot{b^2})$ (a) and $(z_0, \dot{z}_0)$ (b) in a single quantum trajectory setting $\Gamma = 0$ and applying jumps according to the exact diagonalization solution (4.9). The black point represents the initial state ($b^2 = 2h$, $z_0 = 0$) while the red one marks the stationary point. The solutions rotate around the stable point with increasing amplitude. Note that the jumps are from right to left for b^2 while they are from left to right for z_0.

the atomic system towards states with high population imbalance. In order to prove this, we describe the *average* effect of a quantum jump on the width of the atomic distribution and the relative imbalance as

$$\delta b^2 = \Delta b^2 \, p_{\text{jump}} \qquad \text{and} \qquad \delta z_0 = \Delta z_0 \, p_{\text{jump}} \tag{4.47}$$

where Δb^2 and Δz_0 are the effect of a single jump on b^2 and z_0 computed using (4.42) and (4.44). From these expressions we find that the average photocurrent affects b^2 and z_0 as

$$\frac{\delta b^2}{\delta t} = -\frac{\Gamma}{2h} b^4(t) \left[1 - \frac{1}{2} \frac{b^2(t)}{(z_0(t)+1)^2 + b^2(t)} \right] \tag{4.48}$$

$$\frac{\delta z_0}{\delta t} = \frac{\Gamma}{2h} b^2(t)(z_0(t)+1) \left[1 - \frac{1}{2} \frac{b^2(t)}{(z_0(t)+1)^2 + b^2(t)} \right]. \tag{4.49}$$

Note that these equations are consistent with the case $J = 0$: the measurement process decreases the width of the atomic distribution and, once b^2 reaches its stationary value

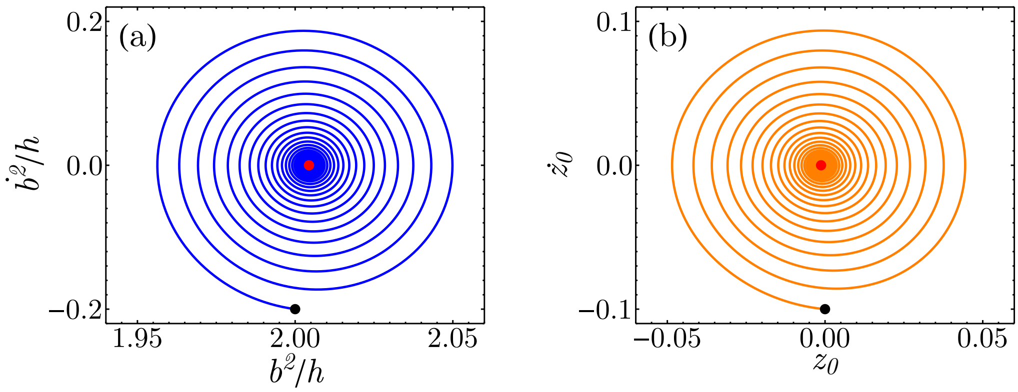

Fig. 4.6 Under-damped oscillations of $(b^2, \dot{b^2})$ (a) and $(z_0, \dot{z}_0)$ (b) in a single quantum trajectory in the weak measurement regime ($\Gamma = 0.001J$) without quantum jumps. The black point represents the initial state ($b^2 = 2h$, $z_0 = 0$) while the red one marks the stationary point.

($b^2 = 0$), the unbalance between odd and even sites becomes a constant. We compare the exponential damping towards the stable point to the effect of the jumps described by (4.48) and (4.49). Specifically, solving these equations at first order in b^2 we find

$$z_{0,\mathrm{jumps}}(t) = -1 + [1 + z_0(0)]\, \mathrm{e}^{\frac{b^2 \Gamma t}{2h}} . \tag{4.50}$$

The exponent in this expression should be compared with the one describing the exponential decay of $z_0(t)$. In the weak measurement regime, the evolution between two quantum jumps follows

$$z_0(t) = \frac{1}{2}\mathrm{e}^{-\frac{\Gamma}{\omega}t}\left[c(0)\sin(J\omega t) + 2z_0(0)\cos(J\omega t)\right] . \tag{4.51}$$

Therefore, the difference between the exponents in (4.50) and (4.51) is

$$\Gamma\left(\frac{b^2}{2h} - \frac{1}{\omega}\right), \tag{4.52}$$

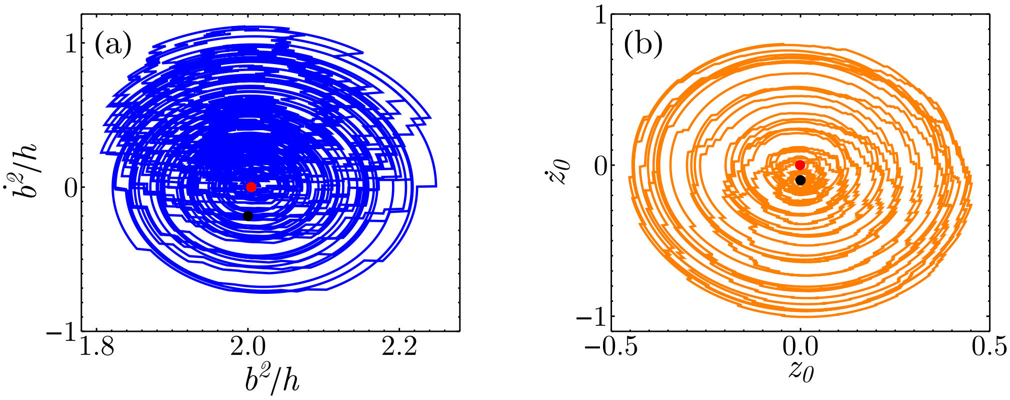

Fig. 4.7 Full conditional dynamics of $(b^2, \dot{b^2})$ (a) and $(z_0, \dot{z}_0)$ (b) of a single trajectory in the weak measurement regime ($\Gamma = 0.001J$). The black point represents the starting point ($b^2 = 4h$, $z_0 = 0$) while the red one marks the stationary point.

which, since $\omega = 2\sqrt{(1-h)}$ and $b^2 \sim 2h$, is positive. This confirms that the jumps increase the amplitude of the oscillations driving the system away from the stable point (Figure 4.7).

In order to estimate the behavior of the imbalance in the large time limit taking into account both the effective dynamics and the quantum jumps, we compute analogous equations to (4.48) and (4.49) for the phases ϕ and c, and we incorporate them in the system (4.20-4.23). Expanding the resulting expressions at first order in h we find

$$\dot{(b^2)} = 8hJ\phi - \frac{\Gamma}{h}b^4 \tag{4.53}$$

$$\dot{\phi} = -\frac{J\omega^2}{4h}b^2 - \frac{\Gamma}{h}b^2\phi + \frac{4hJ}{b^2}(1+\phi^2) \tag{4.54}$$

$$\dot{z}_0 = \frac{2hJ}{b^2}(2z_0\phi + c) \tag{4.55}$$

$$\dot{c} = -\frac{\Gamma}{h}b^2c + \frac{4hJ}{b^2}(\phi c - 2z_0). \tag{4.56}$$

In the large time limit, the width of the atomic distribution becomes constant since the squeezing due to the measurement and the spreading due to the tunneling balance each other so that $(\dot{b^2}) = 0$ and $\dot{\phi} = 0$. Rearranging the equation for $z_0(t)$ in this limit we find

$$\ddot{z}_0 = -\omega^2 z_0, \tag{4.57}$$

i. e. the population oscillates between the spatial modes without decaying (Figure 4.7).

If the measurement dominates the dynamics, i. e. $\Gamma \gg J$, the non-Hermitian dynamics dominates the evolution between two quantum jumps, In this case, the coordinates of the stationary point in this regime are $b^2(\infty) = 4h\sqrt{J/\Gamma}$ and $z_0(\infty) = -1 + J\omega^2/(2\Gamma)$, i. e. the width of the atomic distribution is extremely squeezed while the odd sites of the lattice tend to be empty. Importantly, the evolution of the system is not oscillatory since the equations of motions around the stable point resemble an over-damped oscillator as the eigenvalues of the Jacobian matrix are $\lambda_{1,2} = \pm i\sqrt{J\Gamma} - \sqrt{J\Gamma}$ and $\lambda_{3,4} = \pm 2i\sqrt{J\Gamma} - 2\sqrt{J\Gamma}$. In other words, the period of an oscillation around the stable point and the damping time are approximately the same ($\Omega\Delta t_d \approx 1 + J\omega^2/(2\Gamma)$, see Figure 4.8). As we described in the previous paragraphs, the quantum jumps decrease the width of the atomic distribution even further and the full dynamics of $b(t)$ is not qualitatively different from the one determined by the differential equation (4.20). In contrast, the evolution of the imbalance $z_0(t)$ is heavily affected by the photodetections, as illustrated in Figure 4.9. Specifically, we compare the dynamics due to the quantum jumps (4.51) to the one due to the differential equation (4.22):

$$z_0(t) = \frac{1}{2}\mathrm{e}^{-\sqrt{J\Gamma}t}\left[c(0)\sin(\sqrt{J\Gamma}t) + 2z_0(0)\cos(\sqrt{J\Gamma}t)\right]. \tag{4.58}$$

Taking the difference between the two exponents we obtain

$$\Gamma\left(\frac{b^2}{2h} - \frac{1}{\sqrt{J\Gamma}}\right) \tag{4.59}$$

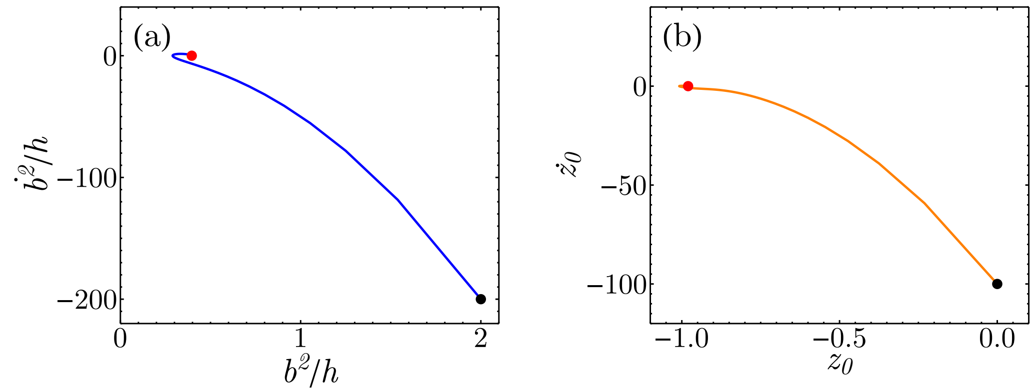

Fig. 4.8 Over-damped oscillations of $(b^2, \dot{b^2})$ (a) and $(z_0, \dot{z_0})$ (b) of a single trajectory in the strong measurement regime ($\Gamma = 100J$). The black point represents the starting point ($b^2 = 4h$, $z_0 = 0$) while the red one marks the stationary point.

which is always positive, implying that the quantum jumps dominate the dynamics of the system taking z_0 away from its stationary point.

4.3.4 Effect of detector efficiency

The oscillatory dynamics we presented in the previous sections requires that all the photons leaving the optical cavity are successfully recorded by the detector, i. e. $\eta = 1$ where η is the detection efficiency. Nevertheless, the effects we described in this Chapter can be observed even if $\eta < 1$ provided that enough photons are detected for each oscillation period so that it is possible to estimate the photocurrent. Figure 4.10 illustrates this by showing the conditional dynamics of the atomic system for different detection efficiencies when the measurement addresses the population of the odd lattice sites $\hat{a}_1 = C\hat{N}_{\text{odd}}$.

If the detector is not ideal, it is not possible to describe the conditional dynamics of the system by applying the quantum trajectory technique to the atomic wavefunction. Specifically, if some photons are "missed" by the detector, the quantum state of the system becomes mixed and needs to be described by the density matrix $\hat{\rho}$ [190] and the stochastic master equation (SME) we presented in §3.3.1. The physical quantity that is

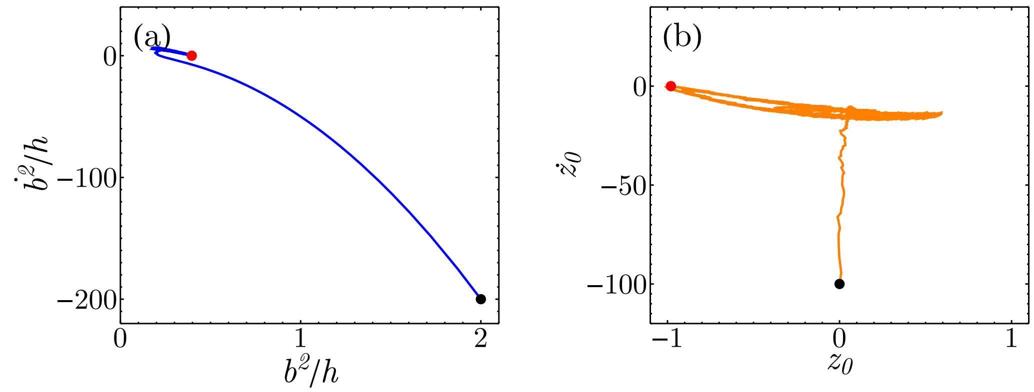

Fig. 4.9 Full conditional dynamics of $(b^2, \dot{b^2})$ (a) and $(z_0, \dot{z_0})$ (b) of a single trajectory in the strong measurement regime ($\Gamma = 100J$). The black point represents the starting point ($b^2 = 4h$, $z_0 = 0$) while the red one marks the stationary point.

directly accessible in the experiments is $N_{ph}(t)$, i.e. the number of photons recorded by the detector up to time t. Importantly, this function is related to the jump operator and, in the limit where the timescale of the atomic dynamics is much slower than the typical interval between two photocounts, can be expressed as

$$\frac{\mathrm{d}N_{ph}}{\mathrm{d}t} = \eta\langle\hat{c}^\dagger\hat{c}\rangle(t), \tag{4.60}$$

where the symbol $\langle\hat{O}\rangle$ represents the expectation value of the operator $\hat{O}$ on a single realization of the SME. Equation (4.60) allows us to estimate the minimum efficiency required for distinguishing the long-range oscillations induced by the measurement backaction. If the population of the odd sites of the optical lattices oscillates in time, the number of photons recorded by the detector should show a growing “staircase” behavior with a characteristic time $2\pi/J$ (see panel 2 of Figure 4.10). We can use this peculiar shape to identify the value of $\langle N_{\text{odd}}\rangle$: the tread corresponds to the times when $\langle N_{\text{odd}}\rangle \sim 0$ while the riser coincide with $\langle N_{\text{odd}}\rangle \sim N$. Therefore, if the detection efficiency allows to clearly resolve each step, the measurement backaction makes the atoms oscillate between odd and even sites retrieving the phenomena that we described in the previous sections.

More quantitatively, defining $N_e(t)$ as the number of photons escaping the cavity, the value of $N_{ph}(t)$ follows a Bernoulli process with probability η so that $\mathrm{E}[N_{ph}(t)] = \eta N_e(t)$ and $\mathrm{Var}[N_{ph}(t)] = \eta(1-\eta)N_e(t)$. Importantly, the detection scheme we consider does not address single site properties since the measurement-induced spatial modes scatter light collectively. For this reason, the photocurrent $\eta\langle \hat{c}^\dagger \hat{c}\rangle$ scales as the square of the number of atoms loaded in the optical lattice. This property is crucial and highlights the fact that the oscillatory behavior of the atomic population is not a consequence of the detection of a *single* photon but relies on many collective scattering events. Comparing the variance of $N_{ph}(t)$ to the number of detected photons in a single oscillation period, we estimate that the oscillatory dynamics is present if $\eta \gtrsim J/\gamma N^2$, making the effects we described robust with respect to detection inefficiency.

4.3.5 Stochastic differential equations and measurement

In Section 4.3.1 we investigated the conditional evolution of the atomic system by analyzing the effect of the non-Hermitian dynamics and the stochastic process described by the quantum jumps separately. However, it is possible to reach the same conclusions by treating these two effects in the same (stochastic) differential equation. Specifically, from the SSE (3.17) and the Itô table (3.12), we find a generalization of the Ehrenfest theorem for the conditional evolution of the observable $\hat{O}$

$$\mathrm{d}\langle\hat{O}\rangle(t) = \left(\frac{\langle\hat{c}^\dagger\hat{O}\hat{c}\rangle}{\langle\hat{c}^\dagger\hat{c}\rangle} - \langle\hat{O}\rangle\right)\mathrm{d}N(t) + \left(i\langle\left[\hat{H},\hat{O}\right]\rangle - \frac{1}{2}\langle\left\{\hat{c}^\dagger\hat{c},\hat{O}\right\}\rangle + \langle\hat{O}\rangle\langle\hat{c}^\dagger\hat{c}\rangle\right)\mathrm{d}t \tag{4.61}$$

where the expectation values on the right hand side are computed at time t and $[\cdot,\cdot]$ ($\{\cdot,\cdot\}$) is the (anti)commutator [65]. Considering a probe that addresses the population of the odd sites, we can follow the evolution of the system by computing the expectation values of the number of atoms occupying the mode ($\hat{N}_{\mathrm{odd}}$), the atomic current between odd and even sites ($\hat{\Delta}$) and their fluctuations $\sigma_{AB} = \langle\hat{A}\hat{B} + \hat{B}\hat{A}\rangle/2 - \langle\hat{A}\rangle\langle\hat{B}\rangle$. From

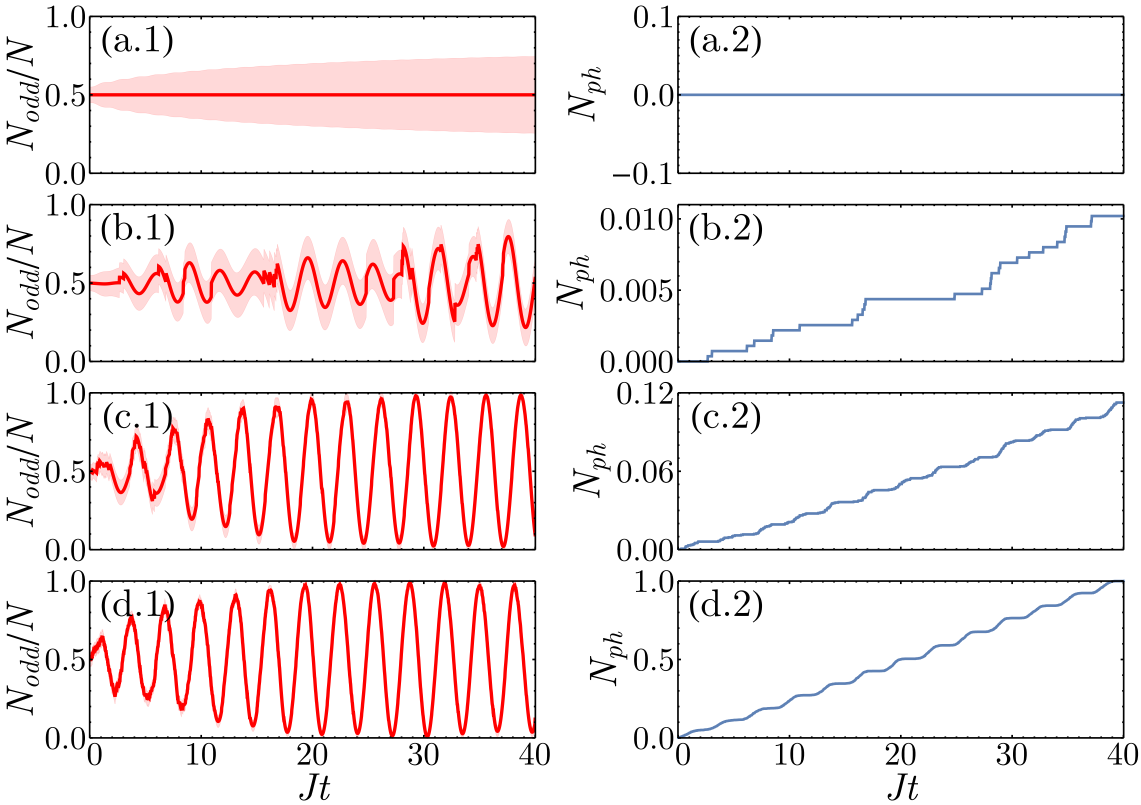

Fig. 4.10 Conditional dynamics measuring $N_{\rm odd}$ for different detection efficiency obtained solving the SME for different efficiencies ($\eta = 0, 0.01, 0.1, 1$ for the panels (a), (b), (c), (d) respectively). Panels (1): atomic population of the odd sites. Panels (2): number of photons detected N_{ph} (normalized to the case $\eta = 1$). The shaded area in the panels (1) represents the fluctuations $\sigma = \sqrt{\mathrm{Tr}\left(\hat{\rho}\hat{N}_{\rm odd}^2\right) - \mathrm{Tr}\left(\hat{\rho}\hat{N}_{\rm odd}\right)^2}$. Oscillations in the atomic population can be directly observed in the behavior of $N_{ph}(t)$. For zero efficiency (no detector), no oscillations develop, while for finite efficiency the oscillations exist. ($N = 100$, $\gamma/J = 0.01$)

equation (4.61) we find

$$\mathrm{d}\langle \hat{N}_{\rm odd}\rangle = \mathrm{d}N\left[\frac{\langle \hat{N}_{\rm odd}^3\rangle}{\langle \hat{N}_{\rm odd}^2\rangle} - \langle \hat{N}_{\rm odd}\rangle\right] + \mathrm{d}t\left[-J\langle\hat{\Delta}\rangle - \gamma\left(\langle \hat{N}_{\rm odd}^3\rangle - \langle \hat{N}_{\rm odd}\rangle\langle \hat{N}_{\rm odd}^2\rangle\right)\right] \tag{4.62}$$

$$\begin{aligned}\mathrm{d}\langle\hat{\Delta}\rangle =& \mathrm{d}N\left[\frac{\langle \hat{N}_{\rm odd}\hat{\Delta}\hat{N}_{\rm odd}\rangle}{\langle \hat{N}_{\rm odd}^2\rangle} - \langle\hat{\Delta}\rangle\right] + \mathrm{d}t\Bigg[-2J\left(N - 2\langle \hat{N}_{\rm odd}\rangle\right) \\ &-\frac{\gamma}{2}\left(\langle \hat{N}_{\rm odd}^2\hat{\Delta}\rangle + \langle\hat{\Delta}\hat{N}_{\rm odd}^2\rangle - \langle\hat{\Delta}\rangle\langle \hat{N}_{\rm odd}\rangle\right)\Bigg]\end{aligned} \tag{4.63}$$

$$\begin{aligned}
\mathrm{d}\sigma_N^2 =&\mathrm{d}N\left[\frac{\langle\hat{N}_{\mathrm{odd}}^4\rangle\langle\hat{N}_{\mathrm{odd}}^2\rangle-\langle\hat{N}_{\mathrm{odd}}^3\rangle^2}{\langle\hat{N}_{\mathrm{odd}}^2\rangle}-\sigma_N^2\right]\\
&+\mathrm{d}t\Big[-J\left(\langle\hat{N}_{\mathrm{odd}}\hat{\Delta}\rangle+\langle\hat{\Delta}\hat{N}_{\mathrm{odd}}\rangle-2\langle\hat{\Delta}\rangle\langle\hat{N}_{\mathrm{odd}}\rangle\right)\\
&-\frac{\gamma}{2}\left(2\langle\hat{N}_{\mathrm{odd}}^4\rangle-4\langle\hat{N}_{\mathrm{odd}}\rangle\langle\hat{N}_{\mathrm{odd}}^3\rangle-2\langle\hat{N}_{\mathrm{odd}}^2\rangle^2+4\langle\hat{N}_{\mathrm{odd}}^2\rangle\langle\hat{N}_{\mathrm{odd}}\rangle^2\right)\Big] \qquad (4.64)\\
\mathrm{d}\sigma_\Delta^2 =&\mathrm{d}N\left[\frac{\langle\hat{N}_{\mathrm{odd}}\hat{\Delta}^2\hat{N}_{\mathrm{odd}}\rangle\langle\hat{N}_{\mathrm{odd}}^2\rangle-\langle\hat{N}_{\mathrm{odd}}\hat{\Delta}\hat{N}_{\mathrm{odd}}\rangle^2}{\langle\hat{N}_{\mathrm{odd}}^2\rangle}-\sigma_\Delta^2\right]\\
&+\mathrm{d}t\Big[4J\left(\langle\hat{N}_{\mathrm{odd}}\hat{\Delta}\rangle+\langle\hat{\Delta}\hat{N}_{\mathrm{odd}}\rangle-2\langle\hat{\Delta}\rangle\langle\hat{N}_{\mathrm{odd}}\rangle\right)\\
&-\frac{\gamma}{2}\Big(\langle\hat{N}_{\mathrm{odd}}^2\hat{\Delta}^2\rangle+\langle\hat{\Delta}^2\hat{N}_{\mathrm{odd}}^2\rangle-2\langle\hat{\Delta}\rangle(\langle\hat{N}_{\mathrm{odd}}^2\hat{\Delta}\rangle+\langle\hat{\Delta}\hat{N}_{\mathrm{odd}}^2\rangle)\\
&-2\langle\hat{N}_{\mathrm{odd}}^2\rangle(\langle\hat{\Delta}^2\rangle-2\langle\hat{\Delta}\rangle^2)\Big)\Big] \qquad (4.65)\\
\mathrm{d}\sigma_{\Delta N} =&\mathrm{d}N\left[\frac{\langle\hat{N}_{\mathrm{odd}}\hat{\Delta}\hat{N}_{\mathrm{odd}}^2\rangle\langle\hat{N}_{\mathrm{odd}}^2\rangle-\langle\hat{N}_{\mathrm{odd}}\hat{\Delta}\hat{N}_{\mathrm{odd}}\rangle\langle\hat{N}_{\mathrm{odd}}^3\rangle}{\langle\hat{N}_{\mathrm{odd}}^2\rangle}-\sigma_{\Delta N}\right]+\\
&+\mathrm{d}t\Big[-J\left(\langle\hat{\Delta}^2\rangle-\langle\hat{\Delta}\rangle^2+4\langle\hat{N}_{\mathrm{odd}}\rangle^2-4\langle\hat{N}_{\mathrm{odd}}^2\rangle\right)\\
&-\frac{\gamma}{2}\Big(\langle\hat{N}_{\mathrm{odd}}^2\hat{\Delta}\hat{N}_{\mathrm{odd}}\rangle+\langle\hat{\Delta}\hat{N}_{\mathrm{odd}}^3\rangle-2\langle\hat{\Delta}\rangle\langle\hat{N}_{\mathrm{odd}}^3\rangle+\\
&-\langle\hat{N}_{\mathrm{odd}}\rangle(\langle\hat{N}_{\mathrm{odd}}^2\hat{\Delta}\rangle+\langle\hat{\Delta}\hat{N}_{\mathrm{odd}}^2\rangle)-2\langle\hat{N}_{\mathrm{odd}}^2\rangle(\langle\hat{\Delta}\hat{N}_{\mathrm{odd}}\rangle-2\langle\hat{\Delta}\rangle\langle\hat{N}_{\mathrm{odd}}\rangle)\Big)\Big] \qquad (4.66)
\end{aligned}$$

where the probability of a jump in a small time interval δt is given by

$$p_{\mathrm{jump}}=\delta t\gamma\langle\hat{N}_{\mathrm{odd}}^2\rangle. \qquad (4.67)$$

The system (4.62-4.65) is not closed since each equation depends on the expectation values of higher moments of $\hat{N}_{\mathrm{odd}}$ and $\hat{\Delta}$. However, we can give an approximate closed formulation of these equations by assuming that $\langle\hat{N}_{\mathrm{odd}}\rangle$ and $\langle\hat{\Delta}\rangle$ are classical Gaussian variables so that all their moments can be expressed as a function of their mean and variance (for example $\langle\hat{N}_{\mathrm{odd}}^3\rangle\approx\langle\hat{N}_{\mathrm{odd}}\rangle^3+3\langle\hat{N}_{\mathrm{odd}}\rangle\sigma_N^2$). Similarly to Section 4.3.1, we focus on the large particle number limit $N\gg1$ so that it is possible to neglect the variance of $\hat{N}_{\mathrm{odd}}$ with respect to its squared value, i. e. $\sigma_N^2/\langle\hat{N}_{\mathrm{odd}}\rangle^2\sim1/N\sim0$. Taking into account these approximations, equations (4.62-4.65) simplify greatly and can be rewritten as

$$\mathrm{d}\langle \hat{N}_{\mathrm{odd}}\rangle = \frac{2\sigma_N^2}{\langle \hat{N}_{\mathrm{odd}}\rangle}\mathrm{d}N - \left(J\langle\hat{\Delta}\rangle + 2\gamma\langle \hat{N}_{\mathrm{odd}}\rangle\sigma_N^2\right)\mathrm{d}t \tag{4.68}$$

$$\mathrm{d}\langle\hat{\Delta}\rangle = \frac{2\sigma_{\Delta N}}{\langle \hat{N}_{\mathrm{odd}}\rangle}\mathrm{d}N - 2\left[J\left(N - 2\langle \hat{N}_{\mathrm{odd}}\rangle\right) + \gamma\langle \hat{N}_{\mathrm{odd}}\rangle\sigma_{\Delta N}\right]\mathrm{d}t \tag{4.69}$$

$$\mathrm{d}\sigma_N^2 = -\frac{2\sigma_N^4}{\langle \hat{N}_{\mathrm{odd}}\rangle^2}\mathrm{d}N - 2\left(J\sigma_{\Delta N} + \gamma\sigma_N^4\right)\mathrm{d}t \tag{4.70}$$

$$\mathrm{d}\sigma_\Delta^2 = -\frac{2\sigma_{\Delta N}^2}{\langle \hat{N}_{\mathrm{odd}}\rangle^2}\mathrm{d}N - 2\left(4J\sigma_{\Delta N} + \gamma\sigma_{\Delta N}^2\right)\mathrm{d}t \tag{4.71}$$

$$\mathrm{d}\sigma_{\Delta N} = \frac{2\sigma_{\Delta N}\sigma_N^2}{\langle \hat{N}_{\mathrm{odd}}\rangle^2}\mathrm{d}N + \left[J(4\sigma_N^2 - \sigma_\Delta^2) - 2\gamma\sigma_N^2\sigma_{\Delta N}\right]\mathrm{d}t \tag{4.72}$$

where the jump probability is given by $p_{\mathrm{jump}} = \delta t\gamma\langle \hat{N}_{\mathrm{odd}}\rangle^2$. The deterministic terms in the equations for $\langle \hat{N}_{\mathrm{odd}}\rangle$ and σ_N^2, i. e. the ones proportional to the time increment dt, coincide with the differential equations we obtained in Section 4.3.1 using the mean field approximation. Specifically, we retrieve equations (4.20) and (4.22) by setting $\sigma_N^2 = 2N^2b^2$ and $\langle \hat{N}_{\mathrm{odd}}\rangle = N(1+z_0)$. This confirms that the two different approaches we considered are consistent and lead to the same behavior for the collective variables addressed by the measurement. The main advantage of the system (4.68-4.72) is that it allows us to describe the quantum jumps and the non-Hermitian dynamics in a single equation. We can use these expressions for gaining insight in the conditional evolution of the atomic system. In order to discuss the behavior of a "typical" quantum trajectory, we focus on the equations for the atomic imbalance $\langle \hat{N}_{\mathrm{odd}}\rangle$ and the current $\langle\hat{\Delta}\rangle$ in the limit where the number of photons recorded by the detector can be approximated by a continuous function, i. e. the time interval between two photocounts is much smaller than the timescale of the atomic dynamics. If this is the case, we can rewrite the Itô increment as $\mathrm{d}N = \langle \mathrm{d}N\rangle - \langle \mathrm{d}N\rangle + \mathrm{d}N = \gamma\langle \hat{N}_{\mathrm{odd}}\rangle^2\mathrm{d}t + \sqrt{\gamma}\langle \hat{N}_{\mathrm{odd}}\rangle\mathrm{d}W$ where dW is a Wiener increment representing the fluctuations in the photocounts around the average value [11, 100, 190]. Substituting this expression in (4.68)-(4.73) we find

$$\mathrm{d}\langle \hat{N}_{\mathrm{odd}}\rangle = -J\langle\hat{\Delta}\rangle \mathrm{d}t + 2\sqrt{\gamma}\sigma_N^2 \mathrm{d}W \tag{4.73}$$

$$\mathrm{d}\langle\hat{\Delta}\rangle = -2J\left(N - 2\langle \hat{N}_{\mathrm{odd}}\rangle\right)\mathrm{d}t + 2\sqrt{\gamma}\sigma_{\Delta N}\mathrm{d}W. \tag{4.74}$$

$$\mathrm{d}\sigma_N^2 = -2\left(J\sigma_{\Delta N} + 2\gamma\sigma_N^4\right)\mathrm{d}t - \frac{2\sqrt{\gamma}\sigma_N^4}{\langle \hat{N}_{\mathrm{odd}}\rangle}\mathrm{d}W. \tag{4.75}$$

$$\mathrm{d}\sigma_\Delta^2 = -4\left(2J\sigma_{\Delta N} + \gamma\sigma_{\Delta N}^2\right)\mathrm{d}t - \frac{2\sqrt{\gamma}\sigma_{\Delta N}^2}{\langle \hat{N}_{\mathrm{odd}}\rangle}\mathrm{d}W. \tag{4.76}$$

$$\mathrm{d}\sigma_{\Delta N} = J\left(4\sigma_N^2 - \sigma_\Delta^2\right)\mathrm{d}t + \frac{2\sqrt{\gamma}\sigma_{\Delta N}\sigma_N^2}{\langle \hat{N}_{\mathrm{odd}}\rangle}\mathrm{d}W. \tag{4.77}$$

Neglecting the fluctuations in the photocounts, the equations for $\langle \hat{N}_{\mathrm{odd}}\rangle$ and $\langle\hat{\Delta}\rangle$ describe the evolution of an harmonic oscillator and confirm the emergence of the oscillatory behavior for the population of the odd sites of the lattice. Note that these oscillations are present even without measurement but here their behavior is fundamentally different: in the absence of continuous monitoring the amplitude of the oscillations is proportional to the atom imbalance of the initial state and its probability distribution tends to spread, i. e. the value of σ_N^2 increases in time. In contrast, here we observe that the uncertainty in the occupation of the spatial modes (σ_N^2) decreases in time (as suggested by equation (4.75)) and that full-exchange of atoms between the two spatial modes is possible even starting with a perfectly balanced state. An alternative formulation of equations (4.73)-(4.77) can be obtained by rewriting them using the Stratonovich formalism:

$$\frac{\mathrm{d}}{\mathrm{d}t}\langle \hat{N}_{\mathrm{odd}}\rangle = -J\langle\hat{\Delta}\rangle - \gamma\frac{\mathrm{d}}{\mathrm{d}t}\sigma_N^4 + 2\sqrt{\gamma}\sigma_N^2\xi(t) \tag{4.78}$$

$$\frac{\mathrm{d}}{\mathrm{d}t}\langle\hat{\Delta}\rangle = -2J\left(N - 2\langle \hat{N}_{\mathrm{odd}}\rangle\right) - \gamma\frac{\mathrm{d}}{\mathrm{d}t}\sigma_{\Delta N}^2 + 2\sqrt{\gamma}\sigma_{\Delta N}\xi(t) \tag{4.79}$$

$$\frac{\mathrm{d}}{\mathrm{d}t}\sigma_N^2 = \frac{-2\left(J\sigma_{\Delta N} + 2\gamma\sigma_N^4\right) + \gamma\sigma_N^4\frac{\mathrm{d}}{\mathrm{d}t}\frac{1}{\langle \hat{N}_{\mathrm{odd}}\rangle^2} - \frac{2\sqrt{\gamma}\sigma_N^8}{\langle \hat{N}_{\mathrm{odd}}\rangle}\xi(t)}{1 - 2\gamma\frac{\sigma_N^2}{\langle \hat{N}_{\mathrm{odd}}\rangle^2}} \tag{4.80}$$

$$\frac{\mathrm{d}}{\mathrm{d}t}\sigma_\Delta^2 = -4\left(2J\sigma_{\Delta N} + \gamma\sigma_{\Delta N}^2\right) + \gamma\frac{\mathrm{d}}{\mathrm{d}t}\frac{\sigma_{\Delta N}^4}{\langle \hat{N}_{\mathrm{odd}}\rangle^2} - \frac{2\sqrt{\gamma}\sigma_{\Delta N}^2}{\langle \hat{N}_{\mathrm{odd}}\rangle}\xi(t) \tag{4.81}$$

$$\frac{\mathrm{d}}{\mathrm{d}t}\sigma_{\Delta N} = \frac{J\left(4\sigma_N^2 - \sigma_\Delta^2\right) - \gamma\sigma_{\Delta N}\frac{\mathrm{d}}{\mathrm{d}t}\frac{\sigma_N^4}{\langle\hat{N}_{\mathrm{odd}}\rangle^2} + \frac{2\sqrt{\gamma}\sigma_{\Delta N}\sigma_N^2}{\langle\hat{N}_{\mathrm{odd}}\rangle}\xi(t)}{1 + \gamma\frac{\sigma_N^4}{\langle\hat{N}_{\mathrm{odd}}\rangle^2}} \tag{4.82}$$

where $\xi(t)$ is a Wiener process. Combining Eq. (4.78) and (4.79), we find that the dynamics of the number of atoms in the odd sites can be described as a forced harmonic oscillator:

$$\frac{\mathrm{d}^2}{\mathrm{d}t^2}\langle\hat{N}_{\mathrm{odd}}\rangle = 2J^2\left(N - 2\langle\hat{N}_{\mathrm{odd}}\rangle\right) + F \tag{4.83}$$

where the forcing term is given by

$$F = \gamma\left(J\frac{\mathrm{d}}{\mathrm{d}t}\sigma_{\Delta N}^2 - \frac{\mathrm{d}^2}{\mathrm{d}t^2}\sigma_N^4\right) + 2\sqrt{\gamma}\left[\frac{\mathrm{d}}{\mathrm{d}t}\left(\sigma_N^2\xi(t)\right) - \sigma_{\Delta N}\xi(t)\right]. \tag{4.84}$$

Therefore, the measurement introduces a quasi-periodic stochastic force F that drives the system towards larger imbalance, increasing the amplitude of the oscillations of $\langle\hat{N}_{\mathrm{odd}}\rangle$.

4.4 Beyond non-interacting bosons

The analytic model we introduced in the previous sections can be applied successfully for describing the conditional dynamics of a system of non-interacting bosons loaded in an optical lattice. In §4.2 we showed that it is possible to incorporate interactions in this model by approximating the local on-site repulsion of the Bose-Hubbard model with an effective interaction between the spatial modes defined by the measurement scheme. However, in current experimental setups the interaction between the atoms is indeed local and this property is often fundamental for observing several interesting phenomena, from the superfluid-Mott insulator quantum phase transition to superconductivity. For these reasons, we will now consider an alternative method for solving the conditional dynamics of an ultracold gas.

As we have seen in the previous Chapter, the quantum trajectory formalism allows to describe the dynamics of a quantum system subjected to continuous monitoring by performing a stochastic evolution of its quantum state. It is relatively easy to perform this task when considering single-particle systems since it is possible to represent the wavefunction of the system as a state vector and propagate it in time according to the effective Schrödinger equation (3.19). For example, considering one atom in an optical lattice with M lattice sites, one can store its quantum state using a vector with M complex numbers and generate the conditional dynamics by modeling the Hamiltonian $\hat{H}_{\text{eff}}$ with an $M \times M$ matrix. Although this approach provides an immediate physical representation of the measurement process, it is particularly challenging to use it when dealing with many-body physics. In the past decades, several efficient methods have been developed for studying these systems such as Quantum Monte Carlo and variational methods [149]. Nevertheless, in most cases, these algorithms allow only to calculate ground state properties of the atomic system and to compute its phase diagram and are not suitable for computing the conditional evolution of the quantum state in a single experimental realization. A notable exception to this are the methods based on the Density Matrix Renormalization Group [172] where the wavefunction of the system is modeled using a clever variational ansatz based on Matrix Product States which allows to calculate its conditional dynamics applying the so-called time-evolving block decimation algorithm. However, this technique relies on the fact that the Hamiltonian of the system under study is contains only short-range interactions leading to entanglement of limited extent. This poses strong limitations in applying these methods to many-body systems coupled to quantum light: because of the global coupling between the cavity modes and the atoms, the light field introduces an effective long-range interaction between distant lattice sites which is reflected in the non-Hermitian term of $\hat{H}_{\text{eff}}$. This is the main reason why performing numerical calculations of our system for large atom numbers is really difficult and highly efficient methods developed for solving condensed matter systems fail.

Because of these limitations, we computed the conditional dynamics of many-body systems using the exact diagonalization (ED) technique. This approach is particularly convenient since it allows to directly solve the Schrödinger equation (3.19) even if long-range interactions are present. On the other hand, it is possible to apply ED only to relatively small systems since the dimensionality of the Hilbert space grows exponentially with the number of atoms. Therefore, we will now focus on the case of one-dimensional systems. Importantly, the results we will present are applicable in any number of dimensions and for an arbitrary system size. The dimensionality of the system affects key properties of the ground state such as quantum critical points and decay of atomic correlations. However, in this thesis the ground state represents only a realistic initial condition and the long-range correlations are dominated by the effect of the nonlocal nature of the measurement. Therefore, the results that we will present do not strictly depend on the number of spatial dimensions but on the geometry and symmetry of the measurement scheme. The only exception is represented by the behavior of 1D fermions: This differs from any other dimension since atoms with the same spin cannot pass each other.

4.4.1 Fermi systems

We now focus on the case of fermions[2] and we assume that the dynamics of the system in the absence of measurement is described by the one dimensional Fermi-Hubbard Hamiltonian *with fixed particle number*. The first step for applying ED is to choose a suitable basis for expressing the Hamiltonian of the system and its quantum state. Since the measurement scheme we propose is sensitive to linear combinations of local quantities

[2] A description of how to implement ED for bosonic systems is given in [90]

(e. g. the number of atoms occupying the odd sites of the optical lattice), we use the Fock states as a basis for the Hilbert space. This choice is particularly convenient for several reasons. Firstly, it allows to index each Fock state with a binary number. For example, considering a chain with 4 sites filled with 2 $\uparrow$ and 1 $\downarrow$ fermion, we can write a Fock state as

$$|\psi\rangle = \hat{f}^\dagger_{2\downarrow}\hat{f}^\dagger_{1\uparrow}\hat{f}^\dagger_{3\uparrow}|0\rangle = |0010\rangle_\downarrow|0101\rangle_\uparrow \quad \Longrightarrow \quad 00100101. \tag{4.85}$$

Secondly, the basis states are eigenstates of the measurement operator and therefore it is possible to compute its expectation values using element-wise vector operations (the jump operator $\hat{c}$ is diagonal). Finally, it is very easy to generate the Hamiltonian matrix of the system by using bit-wise logical operations. For example, if $a_\uparrow$ and $a_\downarrow$ are two binary numbers representing two Fock states for the $\uparrow$ and $\downarrow$ fermionic species, the interaction energy between them can be calculated by applying the logical operator AND to corresponding bits of $a_\uparrow$ and $a_\downarrow$. In general, we build all the indices of the basis set for the Hilbert space of an atomic chain with L lattice sites as follows:

(i) input the number of $\uparrow$ and $\downarrow$ fermions ($N_\uparrow$ and $N_\downarrow$) and the length of the Fermi-Hubbard chain M;

(ii) generate all the possible $M-$bits binary numbers such that $N_\uparrow$ or $N_\downarrow$ bits are set to 1 while the others are set to 0;

(iii) given the binary numbers $a_\uparrow$ and $a_\downarrow$ describing two $\uparrow$ and $\downarrow$ Fock states, we express them in base 10 and obtain the two labels $I_\uparrow$ and $I_\downarrow$. These two indices can be combined together as

$$I = 2^L I_\downarrow + I_\uparrow \tag{4.86}$$

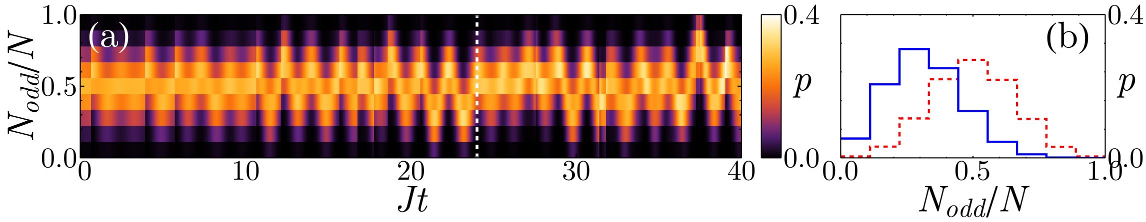

Fig. 4.11 Oscillatory dynamics induced by the measurement process. Measurement of $\hat{N}_{\text{odd}}$ for fermions leads to oscillations in $P(N_{\text{odd}})$, though not as clearly defined as for bosons because of Pauli blocking. Panels (a) illustrates the full probability distribution for all times while panels (b) focuses on the time indicated by the dashed vertical line (blue) and the initial state (Fermi Sea, red). ($\gamma/J = 0.01$, $M = 8$ sites, $N_\uparrow = N_\downarrow = 4$ fermions, $J_{jj} = 1$ if j is odd and 0 otherwise).

in order to uniquely identify each state of the basis set. Moreover, this gives a fast and convenient way to "translate" states into indices and vice versa. For example, the index I can be stored as

```
I(i + (n-1)*D) = 2^L * Id(n) + Iu(i);
```

where `D=dim(Iu)`.

After generating the basis set, we compute the Hamiltonian matrix of the system by using bit-wise operations on the state indices. Moreover, we usually use the ground state of the system as the initial state for the conditional dynamics since this is a realistic starting point and a reference for explaining the measurement-induced effect. This can be computed by diagonalizing the Hamiltonian matrix (without the non-Hermitian term) using the Lanczos algorithm. The code we developed for simulating the quantum trajectories is available at the address http://github.com/gambero88/quantum_trajectories.

In contrast to bosons, it is not possible to formulate a simple analytic description of the conditional evolution of a system of non-interacting fermions subjected to quantum measurement. Focusing on the case where the light scattering probes the number of atoms occupying the odd sites of the optical lattice, we apply ED in order to generate quantum trajectories. Again, the measurement setups defines two spatial modes and induces an oscillatory dynamics between them (Figure 4.11). However, for non-interacting fermions the peak of the probability distribution of $\hat{N}_{\text{odd}}$ is not as squeezed as the bosonic case and the oscillations are not as well-defined. This is not surprising and it is a consequence of the Pauli exclusion principle: since atoms of the same spin species cannot overlap, this prevents the measurement from squeezing $\hat{N}_{\text{odd}}$ and inducing regular oscillations. Moreover, while the initial ground state is a product of $\uparrow$ and $\downarrow$ wave functions (Slater determinants), the photons leaking from the cavity introduce an effective interaction between two spin components and the state becomes entangled by measurement. The dynamics of a one-dimensional fermionic system strongly depends on the spatial profile of the measurement operator. For example, if only the central part of the lattice is illuminated (diffraction maximum) the atom transfer between the modes induced by the measurement is suppressed as the presence of an atom at the edges of the illuminated area completely forbids the atomic tunneling between the two modes, greatly decreasing the fluctuations of the measurement operator.

4.4.2 Competition between tunneling, measurement and interactions

If the interaction energy U is different from zero, the conditional dynamics of the atomic system changes since the measurement process competes with both the tunneling term J and the on-site interaction. In general, different quantum trajectories have a different time evolution and even states with similar expectation values of $\hat{D}$ can have minimal overlap. Therefore it is not possible to derive a phase diagram that describes the properties of the atomic state as a function of U, J and γ. However, even though each quantum trajectory is determined stochastically, we can analyze distinct features that are common to all of them. For example, the uncertainty in the measured operator $\hat{D}$ is only a function of the parameters in the Hamiltonian. Therefore, by taking the ensemble average of $\sigma_D^2 = \langle \hat{D}^2 \rangle - \langle \hat{D} \rangle^2$ over several quantum trajectories, i. e. $\mathrm{E}[\sigma_D^2]$, we can characterize the squeezing of the atomic distribution due to measurement. Importantly, it is not possible to access this quantity by solving the master equation for the density matrix. This is because the uncertainty in the final state is very large and each trajectory is characterized by a different sequence of quantum jumps so that

$$\mathrm{Var}\left[\hat{D}\right] = \mathrm{E}\left[\hat{D}^2\right] - \mathrm{E}\left[\hat{D}\right]^2 \neq \mathrm{E}\left[\sigma_D^2\right]. \tag{4.87}$$

In other words, the master equation addresses the variance of the average value of $\hat{D}$ over the trajectories ensemble ($\mathrm{Var}\left[\hat{D}\right]$) and not the squeezing of a single trajectory conditioned to the measurement outcome. In this section we show results for the measurement of $\hat{D} = \hat{N}_{\mathrm{odd}}$, which is robust to photon losses. Specifically, we compute the width of the atomic distribution ($\langle \sigma_D^2 \rangle_{\mathrm{traj}}$) in the limit $t \to \infty$, when its value does not change significantly in time even if the atomic imbalance is not constant. Moreover, we use the ground state of the system as initial state since this is a realistic starting point and a reference for explaining the measurement-induced dynamics.

For bosons (Figure 4.12a), the number fluctuations σ_D^2 calculated in the ground state decrease monotonically for increasing U, reflecting the superfluid - Mott insulator quantum phase transition: for large interactions the atoms tend to localize and therefore σ_D^2 drops to zero. However, if the system is subjected to continuous monitoring the number fluctuations behave very differently and $\langle \sigma_D^2 \rangle_{\mathrm{traj}}$ varies non-monotonically. For weak interaction, the fluctuations are strongly squeezed below those of the ground state; then they quickly increase, reach their maximum and subsequently decrease as the interaction becomes stronger. It has been shown [90] that this peculiar effect can be explained by looking at the dynamics of single trajectories (cf. Figure 4.13). For small values of U/J, the population imbalance between odd and even sites oscillates and its

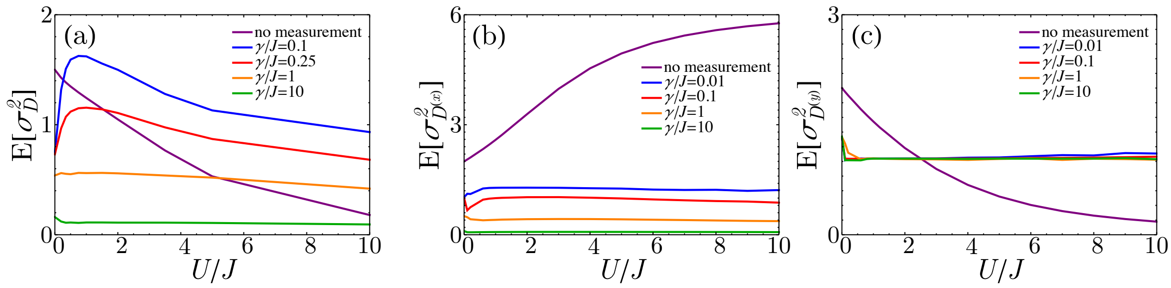

Fig. 4.12 Atom number fluctuations demonstrating the competition of global measurement with local interaction and tunneling. Number variances are averaged over many trajectories. Error bars are too small to be shown ($\sim 1\%$), which emphasizes the fundamental nature of the squeezing. (a), Bose-Hubbard model with repulsive interaction. The fluctuations of the atom number at odd sites $\hat{N}_{\text{odd}}$ in the ground state without a measurement decrease as U/J increases, reflecting the transition between the superfluid and Mott insulator phases. For the weak measurement, $\langle\sigma_D^2\rangle_{\text{traj}}$ is squeezed below the ground state value, but then increases and reaches its maximum as the atom repulsion prevents oscillations and makes the squeezing less effective. In the strong interacting limit, the Mott insulator state is destroyed and the fluctuations are larger than in the ground state. (100 trajectories, $N = L = 6$, $J_{jj} = 1$ if j is odd and 0 otherwise.) (b),(c), Fermionic Hubbard model with attractive interaction; fluctuations of the total atom number at odd sites $\hat{D}_x = \hat{N}_{\uparrow\text{odd}} + \hat{N}_{\downarrow\text{odd}}$ (b) and of the magnetization at odd sites $\hat{D}_y = \hat{M}_{\text{odd}} = \hat{N}_{\uparrow\text{odd}} - \hat{N}_{\downarrow\text{odd}}$ (c). Without measurement, the interaction favors formation of doubly occupied sites so the density fluctuations in the ground state are increasing while the magnetization ones are decreasing. The measurement creates singly occupied sites decreasing the density fluctuations and increasing the magnetization ones, which manifests the break-up of fermion pairs by measurement. (100 trajectories, $L = 8$, $N_\uparrow = N_\downarrow = 4$, $J_{jj} = 1$ if j is odd and 0 otherwise.)

uncertainty is squeezed by the measurement as described in §4.3.1. However, when such oscillations reach maximal amplitude the local atomic repulsion spreads the atomic distribution and prevents the formation of states with large atom number in one of the two modes (Figure 4.12a). Since the interaction is a nonlinear term in the atomic dynamics, states with different imbalance oscillate with different frequencies and the measurement is not able to squeeze $\hat{N}_{\text{odd}}$ as efficiently as in the non-interacting case. This behavior in the weak measurement and weak interaction limit is in contrast with what the effective two-sites model introduced in the previous section predicts (in a double well fluctuations are monotonically decreasing with U. This model cannot capture this behavior since it does not take into account the local nature of the interactions, modeling them with an effective coupling between all the atoms in different modes. In other words, the effective double well approximation treated in §4.2 is only valid in the $N \gg 1$ limit which suggests that this difference is due to the fact that in a double well with a large occupancy the population transfer is sequential, i.e. atoms transfer one by one from one well to the other, steadily increasing the total interaction energy as $\langle \hat{n}_i^2 \rangle$. On the other hand, in a lattice the transfer of an atom from one spatial mode to the other is a collective excitation that increases the energy by KU, where K is the number sites in one mode. This is an increase by a factor of K compared to a single particle-hole excitation pair. Therefore, such collective transfer of atoms can be only observed in a lattice where the measurement addresses the system globally.

For strong interactions, the ground state of the system is characterized by very small number fluctuations. Even though the interactions and the measurement tend to squeeze the fluctuations if considered separately, their competition with the tunneling processes lead to an increase of the uncertainty in the atom number and the destruction of the Mott insulator phase. This has been explained by investigating the effect of the photocounts on the particle-hole excitations that are present on top of the Mott state for finite values of the interaction parameter U [90]. Specifically, the first-order expansion of the ground state of the system is given by

$$|\Psi_{J/U}\rangle = \left[1 + \frac{J}{U}\sum_{\langle i,j\rangle}\hat{b}_i^\dagger\hat{b}_j\right]|\Psi_0\rangle \tag{4.88}$$

where $|\Psi_0\rangle$ is the Mott insulator state and the second term represents a uniform distribution of particle-hole excitation pairs across the lattice. These excitations are amplified by each photodetection: considering a lattice with unit filling and $K \gg 1$, the atomic state after m quantum jumps becomes $\hat{c}^m|\Psi_{J/U}\rangle \propto |\Psi_{J/U}\rangle + |\Phi_m\rangle$ where

$$|\Phi_m\rangle = \frac{2^m J}{KU}\sum_{i\,\mathrm{odd}}\left(\hat{b}_i^\dagger b_{i-1} - \hat{b}_{i-1}^\dagger\hat{b}_i - \hat{b}_{i+1}^\dagger\hat{b}_i + \hat{b}_i^\dagger\hat{b}_{i+1}\right)|\Psi_0\rangle. \tag{4.89}$$

Since in the weak measurement regime the non-Hermitian term in the effective Hamiltonian can be neglected with respect to the local atomic dynamics, this is a good approximation for the state of the system. Because of the exponential growth of the excitations, even a small number of photocounts destroys the Mott insulator state very quickly. This process cannot be avoided provided that the initial state of the system has finite fluctuations.

For fermions (Figure 4.13b,c), the ground state of the attractive Hubbard model in the strong interacting regime contains mainly doubly occupied sites (pairs) and empty sites as the attraction favors these configurations. Therefore, in the absence of measurement, the fluctuations in the atom population $\hat{D}^{(x)} = \hat{N}_{\uparrow\mathrm{odd}} + \hat{N}_{\downarrow\mathrm{odd}}$ ($\sigma^2_{D^{(x)}}$) increase with U/J while the ones in the magnetization $\hat{D}^{(y)} = \hat{M}_{\mathrm{odd}} = \hat{N}_{\uparrow\mathrm{odd}} - \hat{N}_{\downarrow\mathrm{odd}}$ ($\sigma^2_{D^{(y)}}$) decrease because singly occupied sites become more improbable. The measurement induces two different kinds of dynamics using the same mode functions since, depending on the light polarization, we can address either the total population, or both total population and magnetization. In the first case (Figure 4.13b,c), the weak measurement quickly squeezes

$\sigma^2_{D(x)}$, but destroys the pairs. This is because both tunneling and quantum jumps do not distinguish between singly or doubly occupied sites. Figure 4.13c illustrates such a measurement-induced breakup: the initial state contains mainly even values of $\hat{N}_{\text{odd}}$, corresponding to a superposition of empty and doubly occupied lattice sites. As time progresses and photons are scattered from the atoms, the variance $\sigma^2_{D(x)}$ is squeezed and unpaired fermions are free to tunnel across the lattice allowing odd values for $\hat{N}_{\text{odd}}$. In contrast, if both density and magnetization are probed, the measurement process reduces both their fluctuations and, as a result, the lifetime of doubly occupied sites is largely increased. In this case, the conditional dynamics of the system inhibits the tunneling of single fermions as they are allowed to move across the optical lattice only in pairs with opposite spin. In both cases, the dynamics of the system is not a result of the projective quantum Zeno effect (here measurement is weak) but is a manifestation of the squeezing of the atomic population and magnetization of the two macroscopically occupied modes.

Increasing the measurement strength, its backaction becomes more important until it is more significant than the local dynamics. If $\gamma \gg J$, the detection process freezes the state of the system in an eigenstate of the jump operator. In this case, the measurement is able to squeeze the fluctuations of the atomic state well below the ones of the ground state. This effect is the same for both bosons and fermions. However, it is particularly difficult to observe this when probing the magnetization of a fermionic system. This is due to the degeneracy of the jump operator: in analogy to the effects described in Chapter 3, the measurement tends to project the atomic state to a configuration characterized by a well-defined value of $\hat{M}^2_{\text{odd}}$, i. e. a “magnetization cat state” with two components with opposite values M and $-M$. Therefore, the quantity $\mathrm{E}\left[\sigma^2_{D(y)}\right]$ it is not good for representing the squeezing of the system because, instead of measuring the width of the probability distribution of the magnetization around one of the two peaks, it is sensitive to the distance between them. In order to mitigate this problem, we compute

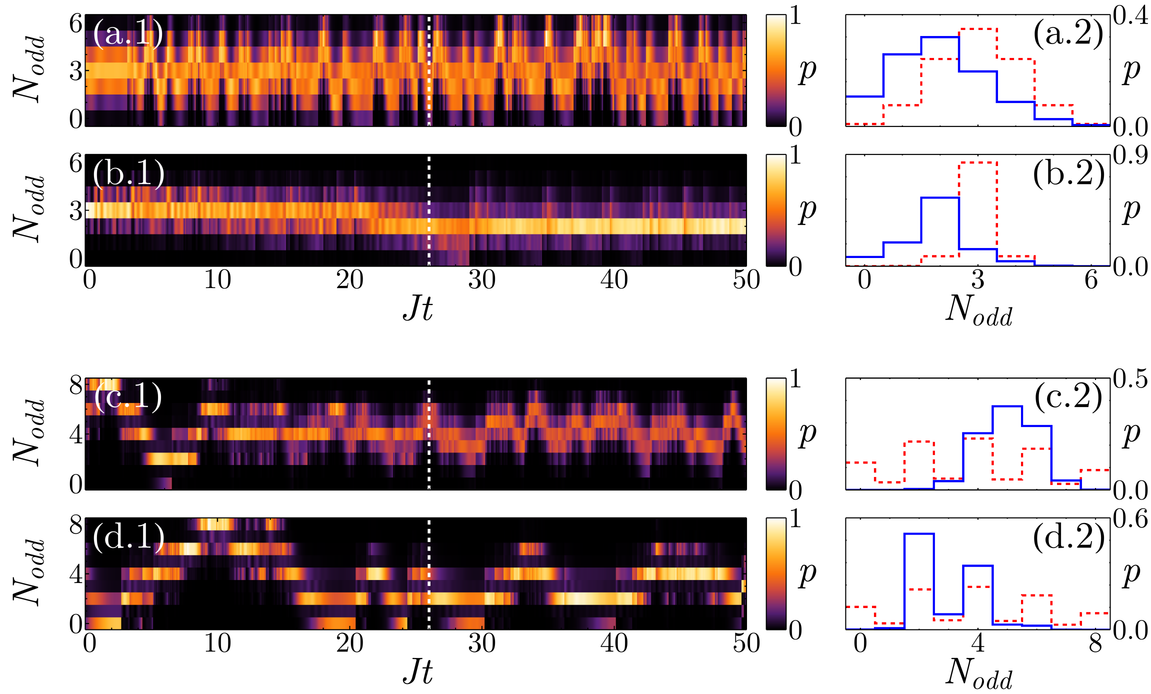

Fig. 4.13 Conditional dynamics of the atom-number distributions at odd sites illustrating competition of the global measurement with local interaction and tunneling (single quantum trajectories, initial states are the ground states). (a), Weakly interacting bosons: the on-site repulsion prevents the formation of well-defined oscillations in the population of the mode. As states with different imbalance evolve with different frequencies, the squeezing due to the measurement is not as efficient as one observed in the non-interacting case ($N = L = 6$, $U/J = 1$, $\gamma/J = 0.1$, $J_{jj} = 1$ if j is odd and 0 otherwise). (b), Strongly interacting bosons: oscillations are completely suppressed and the number of atoms in the mode is rather well-defined, although less squeezed than in the Mott insulator. ($N = L = 6$, $U/J = 10$, $\gamma/J = 0.1$, $J_{jj} = 1$ if j is odd and 0 otherwise).(c), Attractive fermionic Hubbard model in the strong interaction limit. Measuring only the total population at odd sites $\hat{D}_x = \hat{N}_{\uparrow\text{odd}} + \hat{N}_{\downarrow\text{odd}}$ quickly creates singly occupied sites, demonstrating measurement-induced break-up of fermion pairs ($L = 8$, $N_\uparrow = N_\downarrow = 4$, $U/J = 10$, $\gamma/J = 0.1$, $J_{jj} = 1$ if j is odd and 0 otherwise). (d), The same as in (c), but with added measurement of the magnetization at odd sites $\hat{D}_y = \hat{M}_{\text{odd}} = \hat{N}_{\uparrow\text{odd}} - \hat{N}_{\downarrow\text{odd}}$. This protects the doubly occupied sites, thus, demonstrating protection of fermion pairs by measurement. The distribution of N_{odd} vanishes for odd numbers, implying that the fermions tunnel only in pairs. Simulations for 1D lattice.

the ensemble average of $\sigma^2_{|D^{(y)}|} = \langle \left(\hat{D}^{(y)}\right)^2 \rangle - \langle \left|\hat{D}^{(y)}\right| \rangle^2$. Although this quantity is perfectly acceptable for estimating the squeezing of the magnetization if the two peaks are far apart, it is not very accurate if $M \sim 0$ or in small systems.

In the strong measurement regime, the quantum jumps freeze the collective quantities probed by the light and the populations of different spatial modes decorrelate. Nevertheless, dynamical processes are not completely suppressed and can still take place [90, 110]. In the quantum Zeno limit of projective measurement, i. e. $\gamma \to \infty$ tunneling between lattice sites belonging to different modes would be completely inhibited. However, if γ/J is large but finite we observe the following effects. First, the evolution between nearest neighbors *within* each mode is basically unperturbed by the measurement process and it is determined by the usual tunneling. Importantly, by engineering the light mode functions, it is possible to forbid part of this first-order dynamics and select which processes participate in the quantum Zeno dynamics. Therefore, one can design the Zeno subspace of the Hilbert space where the system evolves. Second, tunneling *between* different spatial modes is possible only via higher-order, long-range correlated tunneling events that preserve the eigenvalue of the $D-$operator. In other words, atoms tunnel across distant sites of the lattice via a virtual state and they behave as delocalized correlated pairs. It has been shown that the strong measurement regime can be modeled with an non-Hermitian Hamiltonian which allows to describe the atomic dynamics when the state of the system is confined in a single Zeno subspace [90, 92, 110].

4.5 Extensions for multimode photonic systems

In this Chapter we focused on multimode dynamics of ultracold atoms. However, it is reasonable to ask a question, whether the idea of combining the multimode unitary dynamics and quantum backaction of measurement can be extended to other systems. Recently, significant effort has been made in the development of purely photonic systems with multiple path interferometers, which are one of the setups promising for applications in quantum technologies. A possible realization consists of multiple interconnected fibers, the so called photonic circuits or photonic chips [77, 176]. Indeed, quantum walks [54] have been already discussed in the contexts of both ultracold atoms in optical lattices and single photons propagating and interfering in a multiple path interferometer. Both systems are the candidates for realizations of quantum simulations and quantum computation protocols.

The tunneling of atoms in an optical lattice can be analogous to the propagation of photons in the waveguides and their transmission and reflection at beamsplitters (waveguide couplers). Already current technologies allow using single photons and photon pairs as input states for multiple waveguides [176]. The Boson sampling is considered as a realization of essentially multimode quantum interference of bosons during their unitary evolution (i.e. the propagation through the photonic system).

The detection of photons can be considered in several ways. On the one hand, the non-destructive detection of photons is indeed very difficult to implement. Nevertheless some research is being carried out, which makes it reasonable to expect at least some progress in the future. First, parametric down conversion produces pairs of entangled photons or beams. The detection of an idler beam represents a QND measurement of the signal beam [190]. The use of photon pairs is already consistent with current systems [176]. Second, a QND method of photodetection was realized using a cavity QED system [154]. It indeed remains a challenge to integrate various elements together. On the other hand, as several photons participate in the interference, even the standard detection of a small number of them, while being destructive, can be also considered as a non-fully projective measurement as the rest of photons continue to evolve after some photons are detected. For example, the photon subtraction technique was already shown to produce interesting nonclassical states of light and quantum correlations [140]. One can draw an analogy with ultracold atoms for the case of two BECs: when the small number of atoms is destructively detected after the matter-wave interference, the remaining atoms develop the phase coherence between two condensates due to the projection of quantum state [36]. Thus, while being an experimental challenge, the fully photonic realization of the competition between measurement backaction and unitary dynamics can lead to interesting developments in quantum technologies.

4.6 Discussion

In this Chapter, we proved that the quantum backaction of a global measurement can efficiently compete with standard local processes in strongly correlated systems. This introduces a physically novel source of competition in research on quantum many-body systems. The competition becomes efficient due to the ability to spatially structure the global measurement at a microscopic scale comparable to the lattice period, without the need for single site addressing. The extreme tunability of the setup we considered allows to vary the spatial profile of the measurement operator, effectively tailoring the long-range entanglement and long-range correlations present in the system. The competition between the global backaction and usual atomic dynamics leads to the production of spatially multimode macroscopic superpositions which exhibit large-scale oscillatory dynamics and could be used for quantum information and metrology. We formulated an effective model for the dynamics of this mode in a single quantum trajectory, mapping each spatial mode to a single "well" and describing its properties in term of collective variables. We presented an analytic model that captures the emergence of large-scale collective oscillations with increasing amplitude for the case where only two spatial modes are present. Using the quantum trajectory formalism, we found that the measurement backaction drives the system away from its stationary point and behaves as a quasi-periodic force acting on the atoms. We confirmed our finding by formulating an alternative description in terms of stochastic differential equations for the evolution of collective atomic observables. In the limit where the time interval between two photocounts is much smaller than the timescale of the atomic dynamics and the fluctuations in the photocount can be neglected, the atomic population of one of the modes evolve as an harmonic oscillator driven by a stochastic force. Moreover, we addressed the effect of measurement in other physical systems beyond non-interacting bosons. We showed the possibility of measurement-induced break-up and protection of strongly interacting fermion pairs. Importantly, these effects emerge from the *weak* interaction between photons and atoms and it is not necessary to achieve the strong coupling regime between them (each photon is scattered only once).

The measurement scheme described in this Chapter has been recently realized [87, 98] and the phenomena that we predicted can be observed in these setups. Several experiments succeeded in implementing part of our proposal: light scattered from ultracold atoms in an optical lattice (without a cavity) has been detected [127, 188] and ultracold bosons have been trapped in an optical cavity (without an optical lattice) [17, 171, 191]. Moreover, the effect of measurement backaction on atomic system has been observed in the context of single-atom [141] and multi-particle quantum Zeno effect [15]. Because it relies on off-resonant scattering, the monitoring scheme we propose is not sensitive to the detailed level structure of the system. This makes it applicable to a vast range of quantum objects such as molecules (including biological ones) [114], ions [19], atoms in multiple cavities [25, 74, 138, 139, 147, 189], semiconductor [182], multimode cavities [63, 88] or superconducting [58] qubits.

Chapter 5

Measurement-induced magnetic order and density modulations in ultracold Fermi gases in optical lattices[1]

The study of quantum gases trapped in optical lattice potentials is a truly multidisciplinary field [103]. The experimental realization of Hamiltonians typical of condensed matter physics such as the Hubbard model allows to study intriguing many-body effects typical of Fermi systems such as high temperature superconductivity and quantum magnetism. The latter one is particularly challanging to observe with ultracold atomic systems because of the extreme cooling it requires in order to create quantum states with very low entropy which exhibit antiferromagnetic (AFM) correlations. Nevertheless, recent experiments succeeded in realizing these states and investigated the effect of lattice geometry and dimensionality on the magnetic correlations of the ground state of the Hubbard model [66, 73]. In these setups, the presence of AFM ordering is revealed

[1]The results presented in this chapter are published in [109].

by averaging the results of time-of-flight images over many different experimental runs and the atomic cloud is irremediably destroyed after the detection takes place. In this Chapter, we focus on the effect of measurement backaction in Fermi systems and we show that by globally coupling the atoms to the light modes of an optical cavity it is possible to engineer quantum states with density and magnetization ordering, even in the absence of atomic interactions. Moreover, the detection of the photons escaping the cavity allows to observe the formation of such long-range correlations in real-time. We demonstrate that collective light scattering is crucial for establishing these effects and we compare our approach to similar works based on local addressing [47, 84, 192]. Importantly, the approach we describe in this Chapter is solely based on the measurement backaction and does not rely on the effective cavity potential which can lead to self-organization [32, 33, 94, 144, 155, 174], including that of fermions [38, 85, 145]. This opens new possibilities for studying the dynamics of strongly correlated materials and the effect of magnetic ordering on superconducting states [126] as the methods we will describe could be used for imprinting magnetic correlations on states with superconducting properties.

5.1 Monitoring Fermi systems

In this Chapter, we focus on the conditional dynamics of a Fermi system subjected to continuous monitoring. Specifically, we focus on the case where the atomic evolution in the absence of the detection process is described by the Hubbard Hamiltonian (4.3). Moreover, in analogy to the previous Chapter, we focus on the case of well-localized atoms so that the annihilation operator for the light field inside the optical cavity depends solely on the local density and it is given by

$$\hat{a}_1 = \sum_{\sigma=\uparrow,\downarrow} C_\sigma J_{ii} \hat{n}_{i\sigma} \qquad \text{where} \qquad C_\sigma = \frac{U_{10} a_{0\sigma}}{\Delta_p + i\kappa}. \tag{5.1}$$

As we have illustrated in §2.2.3, the polarization of the probe beam defines which linear combination of the $\uparrow$ and $\downarrow$ are addressed by the measurement scheme. For example, if the probe laser is circularly polarized (L or R), the measurement process is sensitive only to one of the two spin species ($\hat{a}_1 = C_L \hat{D}^{(\uparrow)}$ or $\hat{a}_1 = C_R \hat{D}^{(\downarrow)}$). Furthermore, considering the case of linearly polarized probe, the photons escaping the optical cavity carry information about the atomic density $\hat{\rho}_i = \hat{n}_{i\uparrow} + \hat{n}_{i\downarrow}$ and the magnetization $\hat{m}_i = \hat{n}_{i\uparrow} - \hat{n}_{i\downarrow}$ so that the annihilation operators for the cavity field are proportional to $\hat{D}^{(x)} = \sum_{i=1} J_{ii} \hat{\rho}_i$ (x-polarized light) and $\hat{D}^{(y)} = \sum_{i=1} J_{ii} \hat{m}_i$ (y-polarized light).

In the following sections, we focus mainly on two different geometric configurations for the measurement that partition the lattice in two spatial modes. The first one addresses the difference in occupation between odd and even lattice sites ($\hat{D}_\sigma = \hat{N}_{\sigma,\text{odd}} - \hat{N}_{\sigma,\text{even}}$) and is implemented using traveling or standing waves and detecting the scattered photons in the diffraction minimum orthogonal to the direction of the probe beam. This corresponds to the case where the cavity is placed along the lattice direction (i. e. $\theta_1 = 0$) and the probe beam is perpendicular to them (i. e. $\theta_0 = \pi/2$) so that $J_{ii} = (-1)^i$. The second scheme we consider probes the number of atoms at the odd sites ($\hat{D}_\sigma = \hat{N}_{\sigma,\text{odd}}$). It is realized with standing waves ($u_i(\mathbf{r}) = \cos(\mathbf{k}_i \cdot \mathbf{r})$), crossed at such angles to the lattice that $\mathbf{k}_0 \cdot \mathbf{r}$ is equal to $\mathbf{k}_1 \cdot \mathbf{r}$ and shifted such that the even sites are placed in the maxima of the light interference pattern, while the even sites are positioned at the interference zeros and do not scatter light, so that $J_{ii} = 1$ for i odd while $J_{ii} = 0$ for i even.

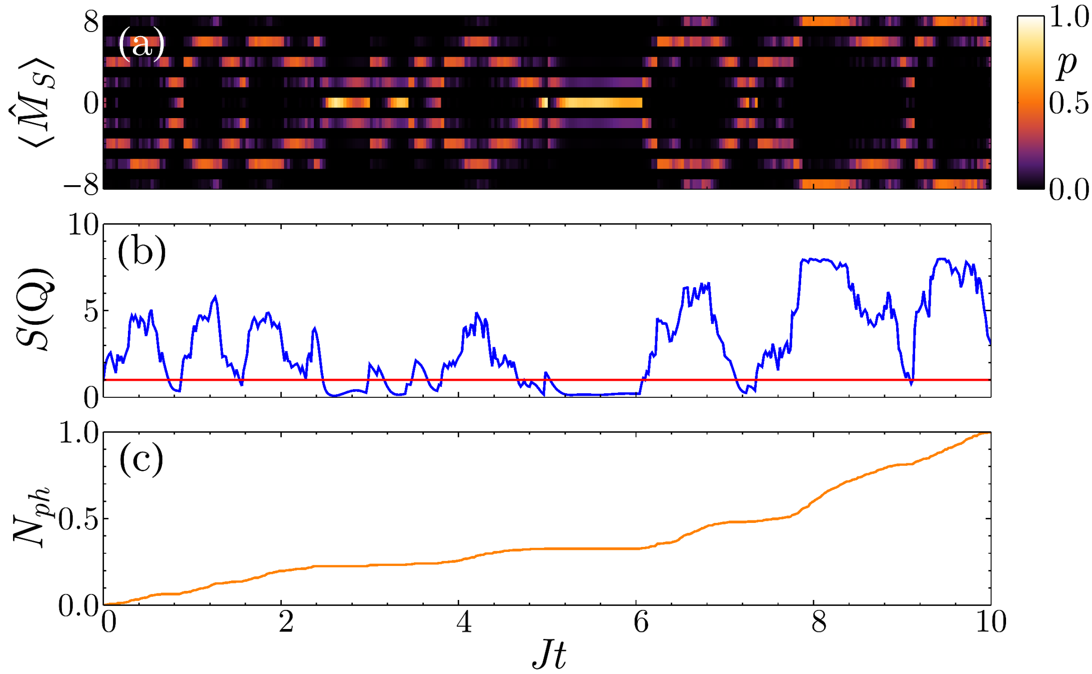

Fig. 5.1 Measurement-induced AFM order in a single experimental run. (a) The probability distribution of the staggered magnetization $\langle \hat{M}_s \rangle$ presents two strong peaks as the state of the system is in a quantum superposition analogous to a Schrödinger cat state. (b) Comparison between the magnetic structure factor $S(\mathbf{Q})$ for the ground state (red) and the conditional dynamics (blue), confirming the presence of AFM order. (c) Number of detected photons as a function of time (normalized to one). The derivative of this curve (photocount rate) is proportional to $S(\mathbf{Q})$. ($\gamma/J = 1$, $U/J = 0$, $N_\uparrow = N_\downarrow = 4$, $L = 8$)

5.2 Measurement-induced antiferromagnetic ordering

We first focus on non-interacting fermions with two spin components at half filling ($N_\uparrow = N_\downarrow = M/2$) and we detect the light scattered in the diffraction minimum. In this case, the ground state of the system is the Fermi Sea $|FS\rangle$ where only single particle states with $k < k_\text{F}$ are occupied (k_F being the Fermi wavevector) and the density and magnetization are uniform across the lattice. We use this state as a reference point, assuming that the atomic system is initialized in its ground state before the measurement take place. The monitoring process perturbs this state and induces AFM correlations that can drive the atomic state to a superposition of the Neel states $|\uparrow\downarrow\uparrow\downarrow ....\rangle$ and $|\downarrow\uparrow\downarrow\uparrow ....\rangle$. In contrast to previous works [32, 33, 38, 85, 94, 144, 145, 155, 174], this state emerges as a consequence of the competition between measurement backaction and atomic tunneling in a single quantum trajectory and does not rely on the cavity potential. Probing the atomic system with linearly polarized light along the y axis, the annihilation operator describing the photons escaping the cavity is $\hat{a}_1 = C\sum_{i=1}(-1)^i\hat{m}_i = C(\hat{M}_{\text{even}} - \hat{M}_{\text{odd}}) \equiv C\hat{M}_s$ so the measurement is directly addressing the staggered magnetization of the atomic system. Moreover, the photon number operator $\hat{a}_1^\dagger\hat{a}_1$ does not depend on the sign of $\hat{M}_s$ and therefore does not distinguish between states with opposite magnetization profile. Consequently, the conditional dynamics preserves $\langle\hat{M}_s\rangle$ and the local magnetization remains the same as the ground state ($\langle m_i\rangle = 0$ for all i). In analogy to section §3.2.1, the quantum jumps tend to suppress states that do not present AFM correlations since the application of $\hat{c}$ on the atomic state completely vanishes its components with $\langle\hat{M}_s^2\rangle = 0$. Therefore, the detection process modifies the probability distribution of $\langle\hat{M}_s\rangle$, making it bimodal with two symmetric peaks around $\langle\hat{M}_s\rangle = 0$ that reflect the degeneracy of $\hat{a}_1^\dagger\hat{a}_1$. The evolution of such peaks depends on the ratio γ/J which determines whether the dynamics is dominated by the quantum jumps or by the usual tunneling processes. Specifically, in the strong measurement regime ($\gamma \gg J$) the detection process freezes $\langle\hat{M}_s^2\rangle$ to a specific value stochastically determined by a particular series of quantum jumps. However, if $\gamma \ll J$ the measurement cannot inhibit the dynamics and the tunneling of atoms across the optical lattice leads to an oscillatory behavior, that, in the case of bosons, can be described analytically (see §4.3).

The presence of AFM correlations in the quantum state resulting from the conditional dynamics is revealed by computing the magnetic structure factor

$$S(\mathbf{q}) = \frac{1}{M}\sum_{i,j} e^{i\mathbf{q}\cdot(\mathbf{r}_i-\mathbf{r}_j)}\left(\langle \hat{m}_i\hat{m}_j\rangle - \langle \hat{m}_i\rangle\langle \hat{m}_j\rangle\right). \tag{5.2}$$

Monitoring this quantity for each quantum trajectory, we find that the measurement induces a strong peak at $\mathbf{q} = \mathbf{Q} = \pi/d$ and creates an AFM state (Fig. 5.1). Importantly, the value of $S(\mathbf{Q})$ is directly accessible to the experiments since the probability for a photon to escape the optical cavity in a (small) time interval $\mathrm{d}t$ is proportional to $\langle \hat{c}^\dagger\hat{c}\rangle \mathrm{d}t$. This allows to observe the formation of AFM ordering in real-time by simply computing the photocount rate. Note that the emergence of these intriguing quantum states is stochastic and varies depending on the specific quantum trajectory, i. e. a single experimental set of photodetections. However, thanks to the photons escaping from the cavity, it is possible to precisely determined when the AFM correlations are established and any subsequent dynamics can be frozen by increasing the depth of the optical lattice. The resulting state can then be used for more advanced studies with applications to quantum simulations and quantum information. In contrast to condensed matter systems or usual cold atoms experiments where a strong repulsion between the atoms is necessary for establishing AFM order, our measurement scheme allows to obtain these states even for non-interacting fermions. Furthermore, the spatial period of the correlations imprinted by the measurement can be tuned changing the scattering angle and may lead to the realization of states with more complex spatial modulations of the magnetization. Therefore, global light scattering will help to simulate effects of long-range interactions in Fermi systems which are inaccessible in contemporary setups based on optical lattices with classical light.

Considering the case of interacting fermions, we show that addressing only one of the two spin species affects the global density distribution and induces AFM correlations.

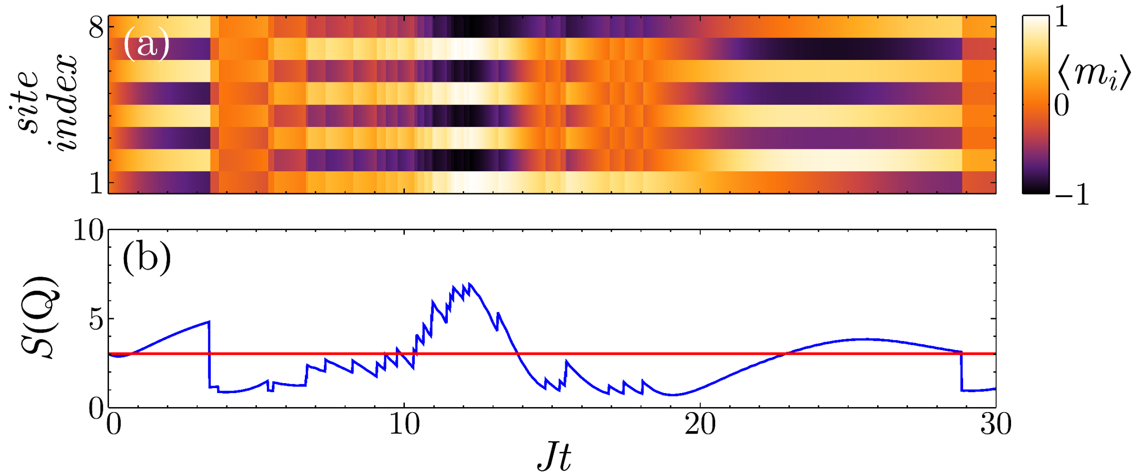

Fig. 5.2 Measurement-induced AFM order in a single experimental run for repulsive fermions. (a) The measurement process creates a modulation in the local magnetization, which is not present in the ground state. (b) Comparison between magnetic structure factor $S(\mathbf{Q})$ for the ground state (red) and the conditional dynamics (blue), confirming the enhancement of AFM correlations. ($\gamma/J = 0.1$, $U/J = 20$, $N_\uparrow = N_\downarrow = 4$, $L = 8$)

Specifically, we consider the measurement operator $\hat{D}_L = \hat{N}_{\mathrm{odd}\uparrow}$, which probes only one spin species using circularly polarized light, and we focus on the strongly repulsive limit $U = 20J$. The detection process is sensitive only to the spin-$\uparrow$ density and therefore induces a periodic modulation of the spatial distribution of this species, favoring either odd or even lattice sites. However, since the two different spins are coupled by the repulsive interaction, spin-$\downarrow$ atoms are also affected by the measurement and tend to occupy the lattice sites that are not occupied by the spin-$\uparrow$ atoms, enhancing the AFM correlations of the ground state. Importantly, in this case the AFM character of the atomic state is visible in the local magnetization (Fig. 5.2) since the photon number operator can distinguish between states with opposite values of $\langle \hat{M}_s \rangle$. The presence of a single peak in the probability distribution of $\langle \hat{M}_s \rangle$ makes this scheme more robust to decoherence due photon losses than detecting the scattered light in the diffraction minimum.

5.3 Measurement-induced density ordering

We now turn to non-interacting polarized fermions, i. e. all the atoms are in the same spin state and the atomic Hamiltonian only describes tunneling processes between neighboring lattice sites. The effective dynamics emerging by measuring $\hat{c} \propto \hat{N}_{\text{odd}}$ modulates the atomic density across the lattice and depends on the ratio γ/J. If the measurement is weak, the atoms periodically oscillate between odd and even sites so that $\langle \hat{N}_{\text{odd}} - \hat{N}_{\text{even}} \rangle \neq 0$, i. e. a state where a density wave with the period of the lattice is established. Such configuration is usually a consequence of finite range interactions [76] and it has been observed in solid state systems [128] and molecules in layer geometries [21]. Here, in contrast, the atoms do not interact but the cavity coupling with all the lattice sites mediates an effective interaction between them. Note that global quantum nondemolition measurements have been already proposed for molecules in low dimensions [114], which can link these fields even closer. Observing the photons leaving the cavity allows us to continuously monitor the state of the atoms, precisely determining when the density wave is established without need of external feedback [78, 142, 186]. If $\gamma \gg J$, the amplitude of the density wave remains constant on a timescale larger than $1/J$. Importantly, the fluctuation of the expectation value of the $\hat{N}_{\text{odd}}$ are strongly suppressed even if the on-site atomic density is not well-defined. This is a consequence of the global addressing of our measurement scheme: the jump operator does not distinguish between different configurations having the same $\hat{N}_{\text{odd}}$. This property is crucial for establishing correlations between distant lattice sites (Figure 5.3). Local [47] or fixed-range [13] addressing destroys coherence between different lattice sites and tends to project the atomic state to a single Fock state, failing to establish a density wave with a well-defined spatial period. Furthermore, the spatial period of the long-range correlations imprinted by the global measurement can be easily tuned changing the scattering angle. We illustrate this by considering the coefficients $J_{ii} = [1,\ 1/2,\ 0,\ 1/2,\ 1,\ 1/2,\ 0...]$ which can be obtained using

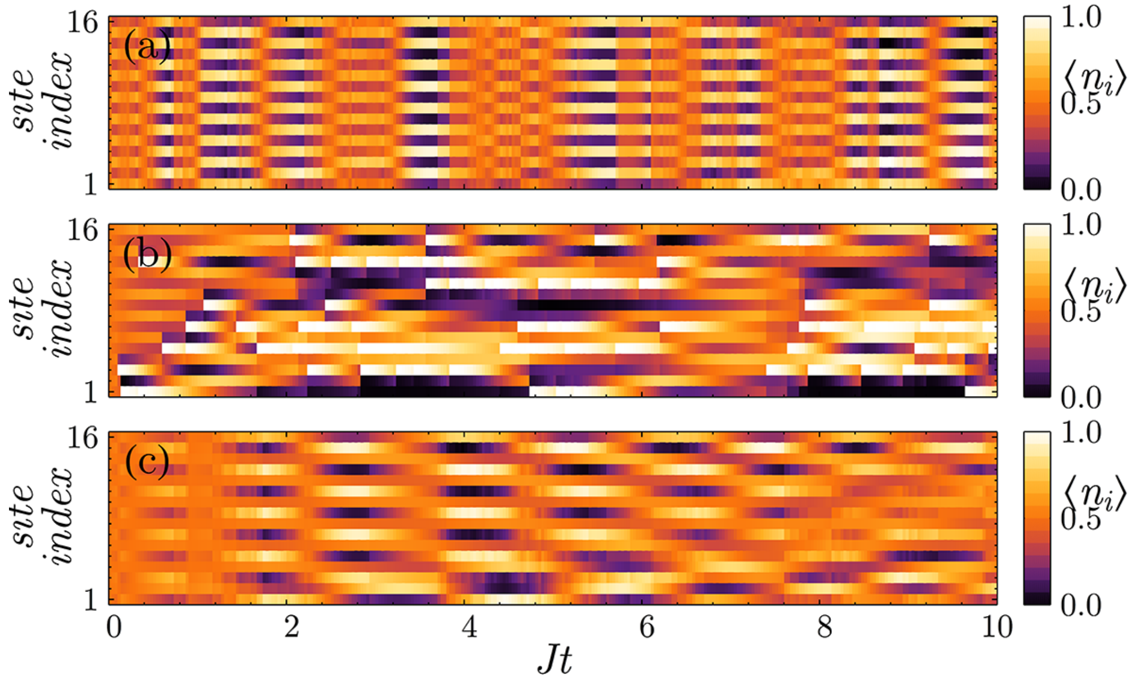

Fig. 5.3 Conditional evolution of the local density in a single experimental run probing the optical lattice with (a,c) global and (b) local addressing illuminating the odd lattice sites. (a) The atomic population collectively oscillates between the two modes defined by the measurement establishing a spatial periodic modulation with period $2d$. (b) The measurement process suppresses the local fluctuations independently for each lattice site.(c) Changing the detection angle it is possible to tune the spatial period of the oscillations, establishing a density wave with period $3d$ ($\gamma/J = 1$, $U/J = 0$, $N = N_\uparrow = 8$, $L = 16$)

standing waves crossing the lattice at an angle such that $\mathbf{k}_{1,0} \cdot \mathbf{r} = \pi/4$. With this scheme, the measurement partitions the lattice in $R = 3$ non-overlapping spatial modes and leads to the emergence of density modulations with period $3d$ (Figure 5.3c).

The measurement backaction changes the structure of the atomic state taking the system away from its ground state. The specific form of the excitations on top of the Fermi Sea depends on the spatial structure of the jump operator $\hat{c}$ and, changing the spatial profile of J_{ii}, allows us to select which momentum states are affected by the measurement process. Defining $A_\mathbf{k}$ to be the Fourier transform of $A_i = \sqrt{2\kappa} C J_{ii}$, one has

$$\hat{c} = \sum_{\mathbf{k},\mathbf{p}\in BZ} A_{\mathbf{p}} \hat{f}^\dagger_{\mathbf{k}} \hat{f}_{\mathbf{k}+\mathbf{p}}, \tag{5.3}$$

where BZ indicates the first Brillouin zone. If $A_{\mathbf{k}}$ presents a narrow peak around $\mathbf{k} = 0$, i. e. the measurement probes the number of atoms rather homogeneously in an extended region of the lattice ($J_{ii} \sim$ const), the detection process creates particles and holes only on the Fermi surface, which is the typical scenario in conventional condensed matter systems. In contrast to this, the setup we propose allows us to probe states that are deep in the Fermi Sea: if $\hat{c} \propto \hat{N}_{\mathrm{odd}}$ one has $A_{\mathbf{k}} \propto \delta(\mathbf{k}) + \delta(\mathbf{k}+\mathbf{Q})$ and the resulting jump operator is

$$\hat{c} \propto \sum_{\mathbf{k}\in BZ} \hat{f}^\dagger_{\mathbf{k}} \hat{f}_{\mathbf{k}} + \hat{f}^\dagger_{\mathbf{k}} \hat{f}_{\mathbf{k}+\mathbf{Q}}. \tag{5.4}$$

Applying this expression on the ground states leads to $\hat{c}|FS\rangle \propto N|FS\rangle/2 + |\Phi\rangle$ where

$$|\Phi\rangle = \sum_{\mathbf{k}:|\mathbf{k}+\mathbf{Q}|<k_{\mathrm{F}}} \hat{f}^\dagger_{\mathbf{k}} \hat{f}_{\mathbf{k}+\mathbf{Q}} |FS\rangle \tag{5.5}$$

and $\langle\Phi|FS\rangle = 0$. Therefore, the detection process creates particle-hole excitations with momenta that are symmetric around the wavevector $\mathbf{Q}/2$ and are not necessarily confined around k_{F}. This symmetry is reflected in the occupation of the single particle states (Figure 5.4b) and can be better understood defining $\hat{\beta}_{\mathbf{k}} = (\hat{f}_{\mathbf{k}} + \hat{f}_{\mathbf{k}+\mathbf{Q}})/\sqrt{2}$ and rewriting the jump operator as $\hat{c} = \sum_{\mathbf{k}\in RBZ} \hat{\beta}^\dagger_{\mathbf{k}} \hat{\beta}_{\mathbf{k}}$ where RBZ is the reduced Brillouin zone. Therefore, the measurement tends to freeze the number of particle-hole excitations with wavevectors that are symmetric superposition around $\mathbf{Q}/2$.

The emergence of long-range entanglement makes the numerical solution of the conditional dynamics in a single quantum trajectory an extremely challenging problem which is difficult to solve efficiently even with methods such as Matrix Product States (MPS) [172]. While, in general, the system dynamics for small and large particle numbers can be indeed different [119], here we confirm our findings on larger systems by formulating a mean field theory for the stochastic evolution of single particle occupation number $n_{\mathbf{k}} = \langle \hat{f}^\dagger_{\mathbf{k}} \hat{f}_{\mathbf{k}} \rangle$ and the order parameter $\alpha_{\mathbf{k}} = \langle \hat{f}^\dagger_{\mathbf{k}} \hat{f}_{\mathbf{k+Q}} \rangle$. We describe the evolution of $n_{\mathbf{k}}$ and $\alpha_{\mathbf{k}}$ using generalization of the Ehrenfest theorem presented in section § 4.3.5. Identifying the operator $\hat{O}$ in equation (4.61) as $\hat{O} = \hat{f}^\dagger_{\mathbf{p}} \hat{f}_{\mathbf{q}}$, the terms entering the stochastic differential equation (SDE) (4.61) are given by

$$\begin{aligned}\left[\hat{H}_a, \hat{O}\right] =& \sum_{\mathbf{k}} \left[\epsilon(\mathbf{k}) \hat{f}^\dagger_{\mathbf{k}} \hat{f}_{\mathbf{k}}, \hat{f}^\dagger_{\mathbf{p}} \hat{f}_{\mathbf{q}}\right] \\ =& \left[\epsilon(\mathbf{p}) - \epsilon(\mathbf{q})\right] \hat{f}^\dagger_{\mathbf{p}} \hat{f}_{\mathbf{q}}\end{aligned} \tag{5.6}$$

$$\begin{aligned}\left\{\hat{c}^\dagger \hat{c}, \hat{O}\right\} =& \sum_{\mathbf{r},\mathbf{s}} \left\{\hat{f}^\dagger_{\mathbf{r}} \hat{f}_{\mathbf{r+Q}} \hat{f}^\dagger_{\mathbf{s}} \hat{f}_{\mathbf{s+Q}}, \hat{f}^\dagger_{\mathbf{p}} \hat{f}_{\mathbf{q}}\right\} \\ =& 2\hat{f}^\dagger_{\mathbf{p}} \hat{f}_{\mathbf{q}} + 2\sum_{\mathbf{r}} \hat{f}^\dagger_{\mathbf{p}} \hat{f}^\dagger_{\mathbf{r}} \hat{f}_{\mathbf{r}} \hat{f}_{\mathbf{q}} + 2\sum_{\mathbf{r}} \hat{f}^\dagger_{\mathbf{p-Q}} \hat{f}^\dagger_{\mathbf{r}} \hat{f}_{\mathbf{r+Q}} \hat{f}_{\mathbf{q}} + \\ & 2\sum_{\mathbf{r}} \hat{f}^\dagger_{\mathbf{p}} \hat{f}^\dagger_{\mathbf{r}} \hat{f}_{\mathbf{r+Q}} \hat{f}_{\mathbf{q+Q}} + 2\sum_{\mathbf{r},\mathbf{s}} \hat{f}^\dagger_{\mathbf{r}} \hat{f}^\dagger_{\mathbf{s}} \hat{f}^\dagger_{\mathbf{p}} \hat{f}_{\mathbf{q}} \hat{f}_{\mathbf{s+Q}} \hat{f}_{\mathbf{r+Q}}\end{aligned} \tag{5.7}$$

$$\begin{aligned}\hat{c}^\dagger \hat{c} =& \sum_{\mathbf{r},\mathbf{s}} \hat{f}^\dagger_{\mathbf{r}} \hat{f}_{\mathbf{r+Q}} \hat{f}^\dagger_{\mathbf{s}} \hat{f}_{\mathbf{s+Q}} \\ =& \sum_{\mathbf{r}} \hat{f}^\dagger_{\mathbf{r}} \hat{f}_{\mathbf{r}} + \sum_{\mathbf{r},\mathbf{s}} \hat{f}^\dagger_{\mathbf{r}} \hat{f}^\dagger_{\mathbf{s}} \hat{f}_{\mathbf{s+Q}} \hat{f}_{\mathbf{r+Q}}\end{aligned} \tag{5.8}$$

$$\begin{aligned}\hat{c}^\dagger \hat{O} \hat{c} =& \sum_{\mathbf{r},\mathbf{s}} \hat{f}^\dagger_{\mathbf{r}} \hat{f}_{\mathbf{r+Q}} \hat{f}^\dagger_{\mathbf{p}} \hat{f}_{\mathbf{q}} \hat{f}^\dagger_{\mathbf{s}} \hat{f}_{\mathbf{s+Q}} \\ =& \hat{f}^\dagger_{\mathbf{p+Q}} \hat{f}_{\mathbf{q+Q}} + \sum_{\mathbf{r}} \hat{f}^\dagger_{\mathbf{p+Q}} \hat{f}^\dagger_{\mathbf{r}} \hat{f}_{\mathbf{r+Q}} \hat{f}_{\mathbf{q}} + \sum_{\mathbf{r}} \hat{f}^\dagger_{\mathbf{r}} \hat{f}^\dagger_{\mathbf{p}} \hat{f}_{\mathbf{q+Q}} \hat{f}_{\mathbf{r+Q}} + \\ & \sum_{\mathbf{r}} \hat{f}^\dagger_{\mathbf{r}} \hat{f}^\dagger_{\mathbf{p}} \hat{f}_{\mathbf{q}} \hat{f}_{\mathbf{r}} - \sum_{\mathbf{r},\mathbf{s}} \hat{f}^\dagger_{\mathbf{r}} \hat{f}^\dagger_{\mathbf{s}} \hat{f}^\dagger_{\mathbf{p}} \hat{f}_{\mathbf{q}} \hat{f}_{\mathbf{s+Q}} \hat{f}_{\mathbf{r+Q}}.\end{aligned} \tag{5.9}$$

As expected, the SDE describing the evolution of $\langle \hat{f}^\dagger_{\mathbf{p}} \hat{f}_{\mathbf{q}} \rangle$ depends on the expectation value of higher correlation functions and, therefore, generates a system of equation that is not closed. In order to give an approximate solution, we apply a mean field treatment to these expressions decoupling the terms with more than two operators as we did in

Chapter 2. Specifically, we compute the expectation values as follows:

$$\langle \hat{f}^\dagger_{\mathbf{a}}\hat{f}^\dagger_{\mathbf{b}}\hat{f}_{\mathbf{c}}\hat{f}_{\mathbf{d}}\rangle \approx \langle \hat{f}^\dagger_{\mathbf{a}}\hat{f}_{\mathbf{d}}\rangle\langle \hat{f}^\dagger_{\mathbf{b}}\hat{f}_{\mathbf{c}}\rangle - \langle \hat{f}^\dagger_{\mathbf{a}}\hat{f}_{\mathbf{c}}\rangle\langle \hat{f}^\dagger_{\mathbf{b}}\hat{f}_{\mathbf{d}}\rangle \tag{5.10}$$

$$\begin{aligned}\langle \hat{f}^\dagger_{\mathbf{a}}\hat{f}^\dagger_{\mathbf{b}}\hat{f}^\dagger_{\mathbf{c}}\hat{f}_{\mathbf{d}}\hat{f}_{\mathbf{e}}\hat{f}_{\mathbf{f}}\rangle \approx{}& \langle \hat{f}^\dagger_{\mathbf{a}}\hat{f}_{\mathbf{f}}\rangle\langle \hat{f}^\dagger_{\mathbf{b}}\hat{f}_{\mathbf{e}}\rangle\langle \hat{f}^\dagger_{\mathbf{c}}\hat{f}_{\mathbf{d}}\rangle - \langle \hat{f}^\dagger_{\mathbf{c}}\hat{f}_{\mathbf{d}}\rangle\langle \hat{f}^\dagger_{\mathbf{a}}\hat{f}_{\mathbf{e}}\rangle\langle \hat{f}^\dagger_{\mathbf{b}}\hat{f}_{\mathbf{f}}\rangle - \\ & \langle \hat{f}^\dagger_{\mathbf{a}}\hat{f}_{\mathbf{f}}\rangle\langle \hat{f}^\dagger_{\mathbf{b}}\hat{f}_{\mathbf{d}}\rangle\langle \hat{f}^\dagger_{\mathbf{c}}\hat{f}_{\mathbf{e}}\rangle - \langle \hat{f}^\dagger_{\mathbf{b}}\hat{f}_{\mathbf{e}}\rangle\langle \hat{f}^\dagger_{\mathbf{a}}\hat{f}_{\mathbf{d}}\rangle\langle \hat{f}^\dagger_{\mathbf{c}}\hat{f}_{\mathbf{f}}\rangle + \\ & \langle \hat{f}^\dagger_{\mathbf{a}}\hat{f}_{\mathbf{d}}\rangle\langle \hat{f}^\dagger_{\mathbf{b}}\hat{f}_{\mathbf{f}}\rangle\langle \hat{f}^\dagger_{\mathbf{c}}\hat{f}_{\mathbf{e}}\rangle + \langle \hat{f}^\dagger_{\mathbf{a}}\hat{f}_{\mathbf{e}}\rangle\langle \hat{f}^\dagger_{\mathbf{b}}\hat{f}_{\mathbf{d}}\rangle\langle \hat{f}^\dagger_{\mathbf{c}}\hat{f}_{\mathbf{f}}\rangle\end{aligned} \tag{5.11}$$

where we assumed $\langle \hat{f}_{\mathbf{p}}\hat{f}_{\mathbf{q}}\rangle = \langle \hat{f}^\dagger_{\mathbf{p}}\hat{f}^\dagger_{\mathbf{q}}\rangle = 0$. Defining $s_{\mathbf{q}} = n_{\mathbf{q}} + n_{\mathbf{q+Q}} + \alpha_{\mathbf{q}} + \alpha_{\mathbf{q+Q}}$ and $x_{\mathbf{q}} = 1 + \sum_{\mathbf{k}\neq\mathbf{q}} s_{\mathbf{k}}$, after a rather tedious calculation, we find

$$\langle\left\{\hat{f}^\dagger_{\mathbf{q}}\hat{f}_{\mathbf{q}}, \hat{c}^\dagger\hat{c}\right\}\rangle \approx -\gamma x_{\mathbf{q}}\left[2n_{\mathbf{q}} + \alpha_{\mathbf{q}} + \alpha_{\mathbf{q+Q}} - 2\left(\alpha_{\mathbf{q}} + n_{\mathbf{q}}\right)\left(\alpha_{\mathbf{q+Q}} + n_{\mathbf{q}}\right)\right] \tag{5.12}$$

$$\langle\left\{\hat{f}^\dagger_{\mathbf{q}}\hat{f}_{\mathbf{q+Q}}, \hat{c}^\dagger\hat{c}\right\}\rangle \approx -\gamma x_{\mathbf{q}}\left[2\alpha_{\mathbf{q}} + n_{\mathbf{q}} + n_{\mathbf{q+Q}} - 2\left(\alpha_{\mathbf{q}} + n_{\mathbf{q}}\right)\left(n_{\mathbf{q+Q}} + \alpha_{\mathbf{q}}\right)\right] \tag{5.13}$$

$$\langle\left[\hat{H}_a, \hat{f}^\dagger_{\mathbf{q}}\hat{f}_{\mathbf{q}}\right]\rangle = 0 \tag{5.14}$$

$$\langle\left[\hat{H}_a, \hat{f}^\dagger_{\mathbf{q}}\hat{f}_{\mathbf{q+Q}}\right]\rangle = -2J\alpha_{\mathbf{q}}\left[\cos\left(\mathbf{q}+\mathbf{Q}\right) - \cos\left(\mathbf{q}\right)\right] \tag{5.15}$$

$$\langle\hat{c}^\dagger\hat{f}^\dagger_{\mathbf{q}}\hat{f}_{\mathbf{q}}\hat{c}\rangle \approx \frac{1}{2}\left[\langle\left\{\hat{f}^\dagger_{\mathbf{q}}\hat{f}_{\mathbf{q}}, \hat{c}^\dagger\hat{c}\right\}\rangle - \gamma(n_{\mathbf{q}} - n_{\mathbf{q+Q}})\right] \tag{5.16}$$

$$\langle\hat{c}^\dagger\hat{f}^\dagger_{\mathbf{q}}\hat{f}_{\mathbf{q+Q}}\hat{c}\rangle \approx \frac{1}{2}\left[\langle\left\{\hat{f}^\dagger_{\mathbf{q}}\hat{f}_{\mathbf{q+Q}}, \hat{c}^\dagger\hat{c}\right\}\rangle - \gamma(\alpha_{\mathbf{q}} - \alpha_{\mathbf{q+Q}})\right] \tag{5.17}$$

$$\langle\hat{c}^\dagger\hat{c}\rangle \approx \frac{\gamma}{4}\left[2\sum_{\mathbf{q}} s_{\mathbf{q}} + \left(\sum_{\mathbf{q}} s_{\mathbf{q}}\right)^2 - \sum_{\mathbf{q}} s^2_{\mathbf{q}}\right] \tag{5.18}$$

Using these expressions in (4.61), we obtain a closed system of N SDE that can be solved numerically. Solving the conditional evolution of $n_{\mathbf{k}}$ and $\alpha_{\mathbf{k}}$ in a single quantum trajectory, we find that the emergence of density modulations is confirmed even in large systems.

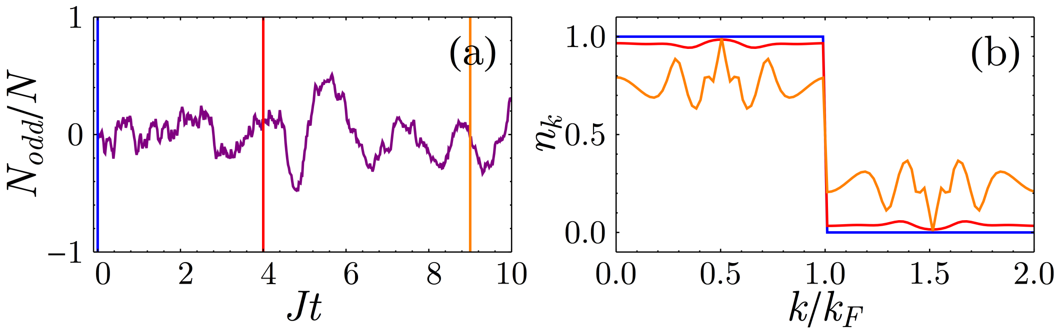

Fig. 5.4 Solution of the mean field equations for a single experimental run. (a) The measurement imprints a density modulation on the atomic state as the number of atoms occupying the odd sites oscillates. (b) Occupation of the single particle momentum states for different times showing that the creation of particle-hole excitations is symmetric around k_F. Different colors represent different times with reference to panel (a) ($\gamma/J = 0.05$, $U/J = 0$, $N = 50$, $L = 100$)

5.4 Discussion

In this Chapter, we have shown that measurement backaction on ultracold Fermi gases can be used for realizing intriguing quantum states characterized by a periodic spatial modulation of the density and the magnetization. We have demonstrated that this spatial structure is a consequence of the global nature of the coupling between atoms and light. The competition between measurement backaction and usual dynamics determined by the tunneling enables the study of quantum magnetism without requiring extreme cooling or strong interactions between the atoms. Our method enables the possibility to engineer otherwise low entropy states (i.e. with small number of defects). Importantly, the formation of magnetic states can be observed in real-time by measuring the photocurrent leaving the optical cavity, without the need of destructive techniques such as time-of-flight imaging. Additionally, it might be possible to engineer feedback control to stabilise a desired correlated quantum many-body state (see Chapter 6). This opens new possibility for studying the effect of magnetic ordering on superconducting states [126]. Moreover, the setup we presented is extremely flexible and, by tuning the spatial profile of the measurement operator, allows to realize different macroscopic quantum superpositions with applications ranging from quantum information to quantum technologies. It may be promising to extend recent phase-space methods [82] to fermionic systems [41, 159] and to investigate the effect of measurement on atomic systems with higher spin. Although light scattering into the cavity constitute an additional source of heating and decoherence for the atoms, the effects described in this work can be observed in present experimental setups [87, 98] since the life time of the important states is large enough and its dynamics can be probed [97]. Moreover, ultracold bosons have been successfully trapped in optical cavities without a lattice [31, 97, 191] and light scattered from ultracold atoms loaded in an optical lattice without a cavity has been detected [127, 188]. Finally, Bragg spectroscopy of a cloud of ultracold bosons coupled to vacuum field of a cavity [97] and measurement-induced creation of Schrödinger cat states involving few thousand atoms [112] have been recently reported.

Chapter 6

Quantum optical feedback control for creating strong correlations in many-body systems[1]

In the previous chapters, we have seen how the measurement backaction affects the conditional dynamics of a many-body atomic system subjected to continuous monitoring. We illustrated this effect in several contexts and we showed how one can exploit this phenomenon for engineering quantum states characterized by large-scale oscillatory dynamics or magnetic and density order. Although the evolution of these interesting states can be observed in real-time by looking at the photons escaping the optical cavity, a common feature of these examples is that their dynamics is stochastic and depends on the exact sequence of photocounts recorded by the detector. In this Chapter we show that combining the effects arising from measurement backaction and feedback, it is possible to realize in real-time [168] stable strongly correlated many-body states such as density waves, NOON, and antiferromagnetic states (even in the absence of atomic interactions), which are important for simulating analogous condensed matter systems and have

[1]The results presented in this chapter are accepted for publication in [108].

applications in quantum information. In contrast to recent proposals [78, 79, 100, 142], where measurements are performed at optimized moments in time or the specific series of quantum jumps is approximated with a continuous signal, we control the quantum state of the system by modulating the system parameters in a single quantum trajectory depending on the outcome of quantum weak measurement. Quantum optical control allows us not only create, but also tune the stationary and dynamical parameters of the many-body states (e.g. the particle imbalance and oscillation frequency).

6.1 Conditional dynamics of the atomic state in presence of feedback

Classical devices rely on feedback loops for stabilizing and rescaling the output signal around a predetermined value. The generalization of these schemes to the quantum world must take into account one of the most fundamental manifestations of quantum mechanics: each time a detection is performed, the state of the system changes because of the measurement backaction. In analogy with the previous chapters, we focus on the conditional evolution of an ultracold atomic gas loaded in an optical lattice coupled to the quantized light modes of an optical cavity. The quantum state of the atoms can be probed in real-time by recording the photons leaking from the cavity. In this Chapter, we add another layer of complexity to this system as we use the information from the photodetections for applying feedback to the system changing the amplitude of the lasers that form the optical lattice. Depending on the feedback gain, it is possible to stabilize interesting quantum states and obtain a deterministic evolution.

We focus on a system of atoms (bosons or fermions) in an optical lattice that are described by the Hamiltonian $\hat{H}_a$ [see (4.2) and (4.3)] in the absence of interactions so that $U = 0$. Within these assumptions, the free atomic dynamics in the absence of measurement is solely determined by the tunneling processes between nearest neighbors sites of the optical lattice. As we have seen in §3.3, the most general formulation of the quantum trajectories formalism is in terms of the density matrix $\hat{\pi}(t)$ which evolves following the stochastic differential equation

$$\mathrm{d}\hat{\pi}(t) = \left(\mathrm{d}N(t)\mathcal{G}[\hat{c}] - \mathrm{d}t\mathcal{H}\left[i\hat{H}_a + \tfrac{1}{2}\hat{c}^\dagger\hat{c}\right]\right)\hat{\pi}(t) \tag{6.1}$$

where $\mathcal{G}[\dots]$ and $\mathcal{H}[\dots]$ are the non-linear superoperators

$$\mathcal{G}[\hat{w}]\,\hat{\pi} = \frac{\hat{w}\hat{\pi}\hat{w}^\dagger}{\mathrm{Tr}[\hat{w}\hat{\pi}\hat{w}^\dagger]} - \hat{\pi} \tag{6.2}$$

$$\mathcal{H}[\hat{w}]\,\hat{\pi} = \hat{w}\hat{\pi} + \hat{\pi}\hat{w}^\dagger - \mathrm{Tr}\left[\hat{w}\hat{\pi} + \hat{\pi}\hat{w}^\dagger\right]\hat{\pi}. \tag{6.3}$$

and $\mathrm{Tr}\left[\hat{O}\right]$ is the trace of $\hat{O}$. If we identify the jump operator $\hat{c}$ with the annihilation operator for the cavity mode, we can define the photocurrent measured by the detector as $I(t) = \mathrm{d}N/\mathrm{d}t$. In a single quantum trajectory, this expression coincides with a sequence of Dirac-δ functions at the specific times when photons are emitted. Nevertheless, it is natural to use this quantity for altering the parameters of the system and consequently affect its dynamics since $I(t)$ is directly available experimentally. In this Chapter, we will use the photocurrent $I(t)$ to modulate the depth of the optical lattice, effectively changing the tunneling amplitude J. Other options could include modifying the intensity of the probe beam, the length of the optical cavity or the cavity decay loss rate κ. In general, using the current $I(t)$ to act on the atomic system will change the evolution of its density matrix $\hat{\pi}(t)$ and this change does not depend only on the value of $I(t)$ at the time t but also on all the times preceding t. In other words, there is a *functional* relation between the change in $\hat{\pi}(t)$ due to the feedback and the current $I(t)$ in the interval $[0, t)$.

Therefore, the most general expression for the effect of feedback on $\hat{\pi}(t)$ is

$$\left[\dot{\hat{\pi}}(t)\right]_{\text{fb}} = \mathcal{U}\left[t, I_{[0,t)}\right]\hat{\pi}(t) \tag{6.4}$$

where $I_{[0,t)}$ represents the photocurrent recorded at all times from $t = 0$ to t and the superoperator $\mathcal{U}[\dots]$ is a functional of $I_{[0,t)}$. In order to include this term in (6.1), we specialize to the case of a linear functional $\mathcal{U}[\dots]$ so that the feedback evolution is

$$\left[\dot{\hat{\pi}}(t)\right]_{\text{fb}} = \int_0^\infty h(s)I(t-s)\mathcal{K}\hat{\pi}(t)\mathrm{d}s \tag{6.5}$$

where $h(s)$ is a response function representing the delay between the photocurrent and the application of the feedback and $\mathcal{K}$ is a so-called Liouville superoperator, i. e. it can be expressed as

$$\mathcal{K}\hat{\pi}(t) = -i\left[\hat{H}_a, \hat{\pi}\right] + \sum_{k=1}^{K}\mathcal{D}\left[\hat{L}_k\right]\hat{\pi}(t) \tag{6.6}$$

where $\left\{\hat{L}_k\right\}$ are arbitrary operators and

$$\mathcal{D}\left[\hat{L}_k\right]\hat{\pi} = \hat{L}_k\hat{\pi}\hat{L}_k^\dagger - \tfrac{1}{2}\left(\hat{L}_k\hat{L}_k^\dagger\hat{\pi} + \hat{\pi}\hat{L}_k^\dagger\hat{L}_k\right). \tag{6.7}$$

Further simplifying the problem, we assume the system does not maintain any memory about past values of the photocurrent and the feedback acts on the system with a fixed delay τ so that $h(s) = \delta(s-\tau)$. Thus, equation (6.5) reduces to

$$\left[\dot{\hat{\pi}}(t)\right]_{\text{fb}} = I(t-\tau)\mathcal{K}\hat{\pi}(t). \tag{6.8}$$

Computing the differential $\left[\mathrm{d}\dot{\hat{\pi}}(t)\right]_{\text{fb}}$ and incorporating it in the SME (6.1) is non-trivial problem because of the peculiar properties of the stochastic differential $\mathrm{d}N$. In order to do so, it is necessary to compute the Taylor expansion of $[\hat{\pi}(t+\mathrm{d}t)]_{\mathrm{fb}}$ at *all* orders as

$$[\hat{\pi}(t+\mathrm{d}t)]_{\mathrm{fb}} = \exp\left(\mathrm{d}t\frac{\partial}{\partial s}\right)[\hat{\pi}(s)]_{\mathrm{fb}}\Big|_{s=t}. \tag{6.9}$$

This expression can be evaluated by noting that, for a real physical system, there is finite correlation time over which the noise term $I(t-\tau)$ remains relatively constant and it is not really given by a sequence of δ functions [190]. Therefore, we can evolve $[\hat{\pi}(s)]_{\mathrm{fb}}$ while keeping $I(t-\tau)$ constant so that

$$\frac{\mathrm{d}}{\mathrm{d}s}[\hat{\pi}(s)]_{\mathrm{fb}}\Big|_{s=t} = \frac{\mathrm{d}N(t-\tau)}{\mathrm{d}t}\mathcal{K}\hat{\pi}(s)\Big|_{s=t}. \tag{6.10}$$

Inserting this expression in (6.9), we find

$$[\hat{\pi}(t+\mathrm{d}t)]_{\mathrm{fb}} = \exp\left[\mathrm{d}N(t-\tau)\mathcal{K}\right]\hat{\pi}(t). \tag{6.11}$$

This equation allow us to calculate the SME describing the evolution for the density matrix $\hat{\pi}$ subjected to both measurement and feedback. Crucially, such an equation must take into account the fact that the feedback must always act *after* the measurement. Therefore, the value of $\hat{\pi}(t+\mathrm{d}t)$ after both measurement and feedback take place is

$$\hat{\pi}(t+\mathrm{d}t) = \exp\left[\mathrm{d}N(t-\tau)\mathcal{K}\right]\Big\{1+\mathrm{d}N(t)\mathcal{G}[\hat{c}] - \mathrm{d}t\mathcal{H}\Big[i\hat{H}_a + \tfrac{1}{2}\hat{c}^\dagger\hat{c}\Big]\Big\}\hat{\pi}(t). \tag{6.12}$$

Finally, we focus on the case $\tau \to 0$ where there is no delay between the detection of a photon and the application of the feedback loop. By taking this limit and applying the properties of the increment $\mathrm{d}N$ we find that (6.1) becomes

$$\mathrm{d}\hat{\pi}(t) = \Big\{\mathrm{d}N(t)\Big[e^{\mathcal{K}}\left(\mathcal{G}[\hat{c}]+1\right)-1\Big] - \mathrm{d}t\mathcal{H}\Big[i\hat{H}_a + \tfrac{1}{2}\hat{c}^\dagger\hat{c}\Big]\Big\}\hat{\pi}(t). \tag{6.13}$$

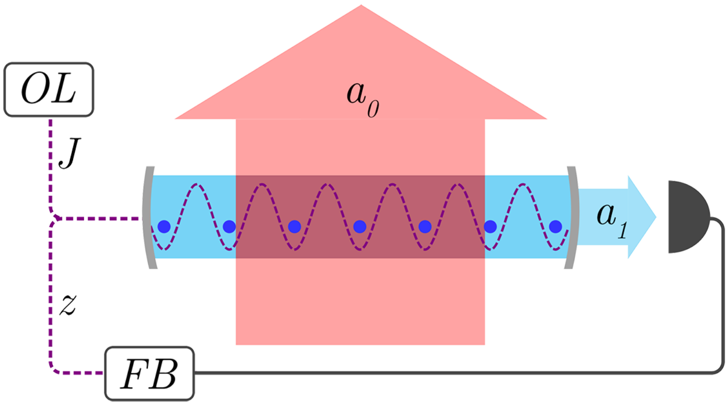

Fig. 6.1 Experimental setup. Ultracold atoms are loaded in an optical lattice (OL) inside an optical cavity and probed with a coherent light beam (mode a_0). The cavity enhances the light scattered orthogonally to a_0 and the photons escaping it are detected (mode $\hat{a}_1$). Depending on the measurement outcome, a feedback (FB) loop with gain z is applied for modulating the depth of the optical lattice.

In this Chapter, we consider the case where the feedback loop instantaneously changes the depth of the atomic potential, effectively modulating the value of the tunneling amplitude J depending on the photocount rate (Figure 6.1). Within these hypotheses, the superoperator $\mathcal{K}$ acts on the density matrix as

$$\mathcal{K}\hat{\rho} = i[z\hat{H}_0, \hat{\rho}] \tag{6.14}$$

where the parameter z describes the feedback strength. Assuming perfect detection efficiency and that the initial state of the system is in a pure state, we solve the master equation (6.13) by simulating individual quantum trajectories. The evolution of the system is determined by the stochastic process described by the quantum jump operator $\hat{d} = \sqrt{2\kappa}\mathrm{e}^{iz\hat{H}_0}\hat{c}$ and the non-Hermitian Hamiltonian $\hat{H}_{\text{eff}} = \hat{H}_a - i\hbar\hat{d}^\dagger\hat{d}/2$. In other words, $\hat{H}_{\text{eff}}$ generates the dynamics of the atomic system in between two consecutive photoemissions and, when a photon escapes the optical cavity, the jump operator $\hat{d}$ is applied to the atomic wavefunction. Note that $\hat{d}$ describes both the effects of measurement backaction ($\hat{c}$) and the feedback loop ($\mathrm{e}^{-iz\hat{H}_0}$). Adopting the notation of Chapter 4, we characterize the strength of the measurement process with the ratio γ/J where $\gamma = \kappa|C|^2$: this quantity determines if the dynamics of the system in the absence of feedback is dominated by the tunneling or by the quantum jumps.

In the following sections we will apply these ideas to the case of a one-dimensional optical lattice. We focus on two different detection schemes which lead to the same number of spatial modes (see §2.2.2). If the light modes are standing waves and their interference pattern has nodes at the odd sites of the lattice, one has $J_{jj} = 0$ for odd and $J_{jj} = 1$ for even sites. In this configuration, the measurement probes the number of atoms occupying the even sites of the lattice and induces the formation of two spatial modes defined by lattice sites with different parity. The same mode structure can be obtained considering traveling or standing waves such that the wave vector of the cavity ($\mathbf{k}_1$) is along the lattice direction and the wavevector of the probe ($\mathbf{k}_0$) is orthogonal to it so that $(\mathbf{k}_0 - \mathbf{k}_1) \cdot \mathbf{r}_j = \pi j$. This configuration corresponds to detecting the photons that are scattered in the diffraction minimum at 90° and $J_{jj} = (-1)^j$.

6.2 Feedback-stabilized density waves and antiferromagnetic ordering

We first consider non-interacting bosons and demonstrate that the feedback process can be used for targeting specific quantum states even in the weak measurement regime ($\gamma \ll J$). Collecting the photons scattered in the diffraction minimum, the detection scheme probes the population imbalance between the odd and even sites of the lattice ($\hat{c} \propto \hat{N}_{\text{odd}} - \hat{N}_{\text{even}}$). Importantly, since the intensity of the scattered light is $\hat{a}_1^\dagger \hat{a}_1$, the measurement is not sensitive to the sign of the imbalance and the atomic state remains in a superposition of states with opposite imbalance (Schrödinger cat state). In order to analyze the conditional evolution of the system, we focus on the Fourier Transform (FT)

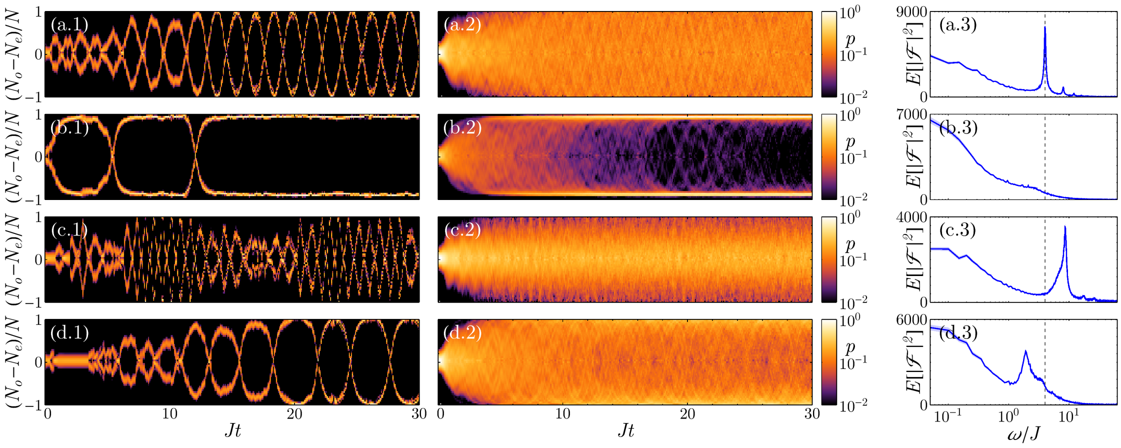

Fig. 6.2 Probability distribution of $\hat{N}_{\text{odd}} - \hat{N}_{\text{even}}$ for single quantum trajectories (Panels 1) and averages over 200 trajectories (Panels 2) for different values of the feedback gain z. Panel 3 shows the power spectrum of $\langle \hat{N}_{\text{odd}} - \hat{N}_{\text{even}} \rangle$ averaged over 200 trajectories. In the absence of feedback [Panel (a), $z = 0$] the oscillations of the population of the odd sites are visible only in a single trajectory. For $z > z_c$ [Panel (b), $z = 1.23z_c$] the imbalance between odd and even sites is frozen for each quantum trajectory and $E\left[|\mathcal{F}|^2\right]$ does not have a strong peak, indicating that $\hat{N}_{\text{odd}} - \hat{N}_{\text{even}}$ does not oscillate. For $z < z_c$ the frequency of the oscillations can be tuned above [Panel (c) $z = -4z_c$] or below [Panel (d) $z = 0.8z_c$] the frequency defined by the tunnelling amplitude J. Again, the oscillatory dynamics is visible only in a single quantum trajectory and the average probability distribution spreads quickly. ($N = 100$, $\gamma/J = 0.02$, $J_{jj} = (-1)^j$, $z_c = 0.0025$)

of the square population difference:

$$F(\omega) = \int \langle (\hat{N}_{\text{odd}} - \hat{N}_{\text{even}})^2 \rangle e^{-i\omega t} \text{d}t. \tag{6.15}$$

This quantity is directly accessible in the experiments since $\langle (\hat{N}_{\text{odd}} - \hat{N}_{\text{even}})^2 \rangle$ is proportional to the photocurrent $\langle \hat{a}_1^\dagger \hat{a}_1 \rangle$. In the absence of feedback, the effect of the measurement is to induce the giant oscillations in the atomic population that we analyzed in Chapter 4 (Figure 6.2a). Moreover, we can calculate their frequency by looking at eventual peaks in $F(\omega)$. Note that the phase of such oscillations varies randomly between different quantum trajectories and therefore the ensemble average $\text{E}[F(\omega)]$ does not allow to describe the typical dynamics in a single realization. However, by taking the power spectrum of $F(\omega)$ and then computing its expectation value over many trajectories, i. e. $\mathrm{E}[|F(\omega)|^2]$, the relative phase difference between different experimental runs disappears. Therefore, by studying the behavior of $\mathrm{E}[|F(\omega)|^2]$ it is to determine the average oscillation frequency and remove the "noise" that characterizes the conditional dynamics in a single trajectory. As expected, if the feedback is not present ($z = 0$), $\mathrm{E}[|F(\omega)|^2]$ has a strong peak at $\omega = 4J$ indicating that the oscillation frequency is determined by the tunneling amplitude.

Considering now the case when feedback is applied to the system, we find that there is a critical value for the parameter z_c which defines two different dynamical regimes: if $z < z_c$ the expectation value $\langle(\hat{N}_{\text{odd}} - \hat{N}_{\text{even}})^2\rangle$ oscillates while if $z > z_c$ the imbalance reaches a steady state value that is deterministically defined by the parameter z itself (Figure 6.2). We explain this effect by looking at the effect of feedback on atoms: defining Δt_n to be the time interval between the $(n-1)-$th and $n-$th quantum jump, the state of the system after N_{ph} photocounts is

$$|\psi(t; N_{ph})\rangle \propto \prod_{n=2}^{N_{ph}} \left[\mathrm{e}^{-i\hat{H}_{\text{eff}}\Delta t_n} \mathrm{e}^{iz\hat{H}_a} \hat{c}\right] \mathrm{e}^{-i\hat{H}_{\text{eff}}\Delta t_1} |\psi(0)\rangle \tag{6.16}$$

where $|\psi(0)\rangle$ is the initial state of the system. In the weak measurement regime ($\gamma \ll J$), we can focus on the terms depending linearly on Δt_n or z and neglect the commutator between $\hat{H}_{\text{eff}}$ and $\hat{H}_a$ since it scales as $\Delta t_n z$, thus

$$\mathrm{e}^{-i\hat{H}_{\text{eff}}\Delta t_n} \mathrm{e}^{iz\hat{H}_a} \approx \mathrm{e}^{-i(\Delta t_n - z)\hat{H}_a - \hbar \hat{c}^\dagger \hat{c} \Delta t_n/2}. \tag{6.17}$$

Therefore, the parameter z defines an effective timescale which competes with the tunneling and the measurement processes. We find that it is possible to formulate a simple description of the dynamics of the atomic system by comparing the value of z to the average time interval between two consecutive quantum jumps, i. e. $\overline{\Delta t} = 1/(2\gamma\langle\hat{D}^\dagger\hat{D}\rangle)$.

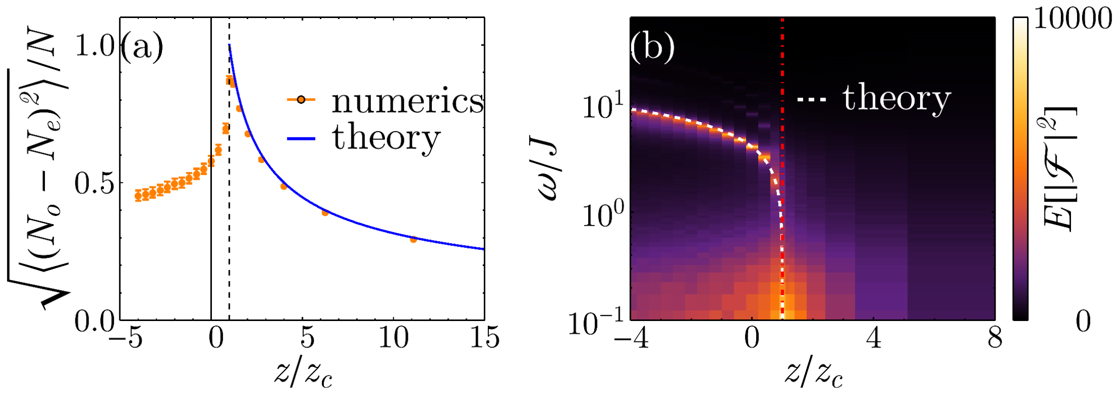

Fig. 6.3 Effects of measurement and feedback detecting the photons scattered in the diffraction minimum. Panel (a): Imbalance between odd and even sites as a function of the feedback strength. There is a very good agreement between the numerical results and the analytic expression derived in text. Panel (b): average power spectrum as a function of the feedback strength. The value of $E\left[|\mathcal{F}|^2\right]$ presents a strong peak for $z < z_c$, indicating that the trajectories are characterized by an oscillatory dynamics. The vertical dashed line marks $z = z_c$. ($N = 100$, $\gamma/J = 0.02$, $J_{jj} = (-1)^j$, $z_c = 0.0025$)

Specifically, if $\Delta t_n \approx \overline{\Delta t} = z$, the feedback completely inhibits the tunneling described by the Hamiltonian $\hat{H}_a$ and the dynamics of the system is determined by the "decay" term in $\hat{H}_{\text{eff}}$. In this case, there are only two processes which contribute to the evolution of the system: the non-Hermitian dynamics (which tends to suppress the atom imbalance) and the quantum jumps (which drive the system towards large $\langle(\hat{N}_{\text{odd}} - \hat{N}_{\text{even}})^2\rangle$). In the large time limit, these two effects balance each other and the system reaches a steady state where the probability distribution of $\hat{N}_{\text{odd}} - \hat{N}_{\text{even}}$ has two narrow peaks at opposite values. This regime is somehow analogous to the one we described in Chapter 3 (where the atomic dynamics was neglected) and to the strong measurement regime (quantum Zeno effect) [92, 93]. However, in these cases the system is confined to a quantum state that is an eigenvector of the jump operator whose eigenvalue is determined stochastically and ultimately depends on the initial state of the system. In contrast, here the introduction of a feedback loop allows us to deterministically select the final state of the system by tuning the value of z. Defining $\langle \hat{D}^\dagger \hat{D} \rangle_T$ as the target imbalance one wants to obtain, the corresponding feedback gain realizing this specific configuration is $z = 1/(2\gamma \langle \hat{D}^\dagger \hat{D} \rangle_T)$ [see Figure 6.3(a)]. Moreover, the target steady state is reached independently from the initial state of the system.

Since the value of the population imbalance between odd and even sites cannot exceed the total number of atoms, the maximum possible value for $\langle \hat{D}^\dagger \hat{D} \rangle_T$ is N^2. This defines a critical z under which the condition $\overline{\Delta t} = z$ cannot be fulfilled, $z_c = 1/(2\gamma N^2)$. As a consequence, for $z < z_c$ the state of the system does not reach a steady state and the measurement backaction establishes an oscillatory dynamics.

Following the approach presented in Chapter 4, we find that carefully choosing the feedback gain it is possible to tune the frequency of the oscillations of $\langle (\hat{N}_{\text{odd}} - \hat{N}_{\text{even}})^2 \rangle$ according to $\omega = 4\sqrt{1 - z/z_c}$ [see Figure 6.3(b)]. Again, these oscillations are visible only analyzing single quantum trajectory and are not visible in the average probability distribution. The presence of two peaks in the probability distribution $\langle \hat{N}_{\text{odd}} - \hat{N}_{\text{even}} \rangle$ makes this measurement setup susceptible to decoherence due to photon losses [116]. However, this scheme can be made more robust by illuminating only the odd sites of the lattice so that $\hat{c} \propto \hat{N}_{\text{odd}}$. In this case, the measurement operator probes the occupation of the odd sites and its probability distribution has only one strong peak.

We now turn to non-interacting fermions and we focus on the case where the system is probed using linearly polarized light so that the jump operator is sensitive to the staggered magnetization $\hat{M}_S = \hat{M}_{\text{odd}} - \hat{M}_{\text{even}}$. If feedback is not present, the measurement backaction leads to quantum states characterized by antiferromagnetic ordering, as described in Chapter 5. However, these correlations follow an oscillatory dynamics and cannot be selected deterministically since they are a result of the competition between local tunneling processes and the (stochastic) quantum jumps. In analogy to the bosonic case, introducing a feedback loop allows us to obtain antiferromagnetic states with a

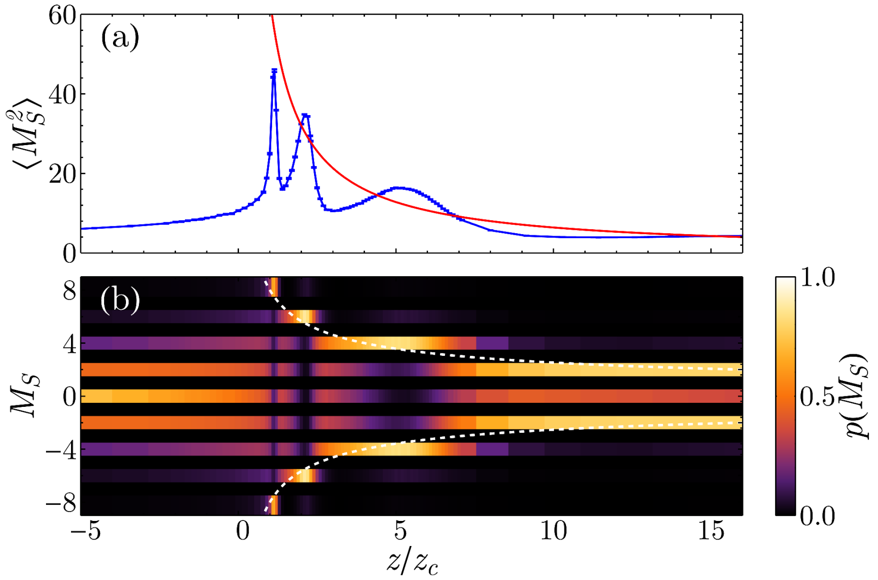

Fig. 6.4 Effects of measurement and feedback probing the staggered magnetization in a fermionic system. (a): square of the staggered magnetization as a function of the feedback strength (blue line) compared to the analytic formula (red line) for a fermionic system. Note that the two curves do not have the same behavior because the analytic solution assumes that $\hat{M}_S$ is a continuous variable while the numerical simulations are performed on a small system where $\hat{M}_S$ assumes only discrete values. Panel (b): steady state value of the probability distribution of $\hat{M}_S$ as a function of the feedback strength. The dashed line represents the theoretical prediction. The feedback loop stabilizes antiferromagnetic correlations. ($N_\uparrow = N_\downarrow = 4$, $\gamma/J = 1$, $J_{jj} = (-1)^j$, $z_c = 1/128$)

predetermined staggered magnetization in each single quantum trajectory even in the absence of many-body interactions. Again, there is a critical value of the gain z which sharply divides two regimes. If $z > z_c$ the system reaches a steady state such that $\langle \hat{M}_S \rangle = \sqrt{1/(2\gamma z)}$ for each quantum trajectory. In contrast, if $z < z_c$ the value of $\langle \hat{M} \rangle_S$ is not stationary and taking its expectation over many quantum trajectories we find that, on average, the atomic state does not present antiferromagnetic order. Figure 6.4 illustrates this effect by showing the average over many realizations of the expectation value of the staggered magnetization and its probability distribution in the large time limit as a function of the feedback gain. Note that the predicted value for $\hat{M}_S$ agrees with the numerical results only qualitatively. This is because the analytic solution $\langle\hat{M}_S\rangle = \sqrt{1/(2\gamma z)}$ treats the staggered magnetization as a continuous variable while when performing a simulation on a small system only some discrete values of $\langle\hat{M}_S\rangle$ are possible. This effect is not surprising and it is rather analogous to previous works where the discreteness of the matter field leads to spectra with multiple peaks [28, 60, 123].

6.3 Discussion

In this Chapter, we demonstrated that the feedback control and optical measurement backaction can be used for engineering quantum states with long-range correlations which can be tuned by changing the spatial structure of the jump operator. We illustrated this by considering the case where the measurement induces two macroscopically occupied spatial modes and the feedback loop can stabilize interesting quantum phases such as supersolid-like states (i.e. the density waves with long-range matter-wave coherence) and states with antiferromagnetic correlations, depending on the value of the feedback gain z. This parameter determines the strength of the feedback loop and its net effect is to modulate the tunneling amplitude J according to the measurement outcome. Experimentally, this can be achieved by changing the depth of the optical lattice V_0 in [29]

$$J = \frac{4E_R}{\sqrt{\pi}}\left(\frac{V_0}{E_R}\right)^{3/4}\exp\left(-2\sqrt{\frac{V_0}{E_R}}\right) \tag{6.18}$$

where E_R the recoil energy. Importantly, since the critical value of z scales as $1/(\gamma N^2)$ the effects described in this work can be observed by weakly perturbing V_0, changing the optical lattice depth by slightly modifying the intensity of the lasers. For example, assuming $V_0/E_R \sim 10$ and considering $z \sim 10^{-2}$, one needs to change the ratio V_0/E_R by a factor $\sim 5 \cdot 10^{-3}$. Moreover, the light-atom coupling regime we considered has been recently realized in two different experimental setups [87, 98]. Finally, these phenomena are not specific to ultracold atomic systems but the same ideas can be applied to superconducting qubits [138, 139, 147, 189], molecules [114], optomechanical arrays [12, 140], arrays of optical resonators [125], Rydberg [170, 193] and other polaritonic and spin excitations [9, 30] and even purely photonic systems with multiple path interference [24, 54, 134, 136, 176]. Moreover, the phenomena we described in this Chapter could also be observed in conventional condensed matter systems in the regime of ultra-strong light matter interactions. These include 2D electron gases in THz metamaterials [194] and light-induced high-Tc superconductivity in conventional materials [45, 126, 132]. Engineering the effects we presented in real solid state systems opens the possibility of realizing hybrid devices for quantum technologies [95] in the near future.

Summary and Conclusions

In this thesis, we focused on the effects emerging by treating light as a quantum variable when it is coupled to a many-body atomic system. Specifically, we considered the case of an ultracold atomic system coupled to the quantized light modes of an optical cavity. Because of this coupling, light and matter become entangled, leading to the vast range of novel phenomena that we presented in this work. Firstly, we showed that by observing the photons leaking form the cavity it is possible to perform a QND measurement of the atomic variables. The quantum correlations of the atomic state are imprinted onto the light field and this property can be exploited for distinguishing different quantum states. As a consequence, the angular distribution of the intensity of the scattered light does not coincide with the classical diffraction pattern but contains a quantum addition. We illustrated this effect by considering the case of an ultracold Fermi gas. Depending on the polarization of the probe beam, the scattered photons give access to the fluctuations of local magnetization of the atomic cloud. This quantity is directly related to the presence of Cooper pairs in the ultracold gas since the strong attraction between atoms with opposite spin leads to smaller fluctuations of the magnetization. Therefore, by observing the scattered light one can distinguish between different ground states of the atomic system without recurring to destructive techniques such as time-of-flight imaging.

Secondly, we demonstrated that the light field inside the optical cavity mediates an effective synthetic inter-atomic interaction. This new coupling between the atoms does not depend on fundamental processes, making it extremely suitable for realizing quantum simulations of many-body systems with long-range interactions. We showed that the spatial profile of this effective interaction can be tuned by changing the relative position of probe beam and cavity modes, giving several examples that go beyond what can be obtained using complex systems such as polar molecules and Rydberg atoms.

Thirdly, we proved that measurement backaction constitutes an additional dynamical term in the evolution of many-body systems which competes with the usual short-range processes described by local interactions and tunneling between neighboring lattice sites. Moreover, we showed that its effect greatly depends on the spatial profile of the measurement operator which can be engineered on a scale comparable to the lattice spacing without the need of single-site resolution. Because of the global nature of the coupling between light and atoms, the measurement preserves long range entanglement and correlations. In the case of bosons, we presented an effective analytic model that describes the conditional evolution of the system and we demonstrated that the detection process induces macroscopic oscillations of the atomic population across the optical lattice. We analyze this dynamics in details and we confirmed that the effects we describe can be observed even if the efficiency of the detector is not ideal. For fermions, we presented different measurement schemes which lead to both the break up and protection of strongly interacting fermionic pairs. Furthermore, we explain how to exploit the competition between measurement backaction and tunneling for creating interesting quantum states characterized by antiferromagnetic and density correlations. Comparing our approach to other works based on local addressing, we show that the global coupling between light and atoms is crucial for obtaining these novel effects.

Finally, we conclude this work by illustrating how the effective stochastic dynamics induced by continuously monitoring the atomic system can be stabilized with the aid of quantum feedback. By modulating the depth of the optical lattice depending on the number of photons leaking from the optical cavity, it is possible to create Schrödinger cat states and imprint magnetic or density correlations on the atomic state in a deterministic way.

Although here we focussed on a system of ultracold atoms loaded in an optical lattice, the effects we described can be generalized to other physical systems where the measurement backaction can compete with the usual unitary dynamics. For example, the phenomena we presented could be observed in purely photonic systems with multiple path interferometers known as photonic chips or photonic circuits [77, 105, 136, 176]. In these systems, single photons can propagate across multiple paths, generating dynamics which is analogous to the tunneling of atoms in an optical lattices. Moreover, the propagation of the photons that can be easily controlled by tuning the reflection and transmission coefficients of the beam splitters or waveguide couplers, allows to implement feedback [134] on the system. Such setups are within the reach of current experiments where single photons and photonic pairs have been successfully used as input states for multiple waveguides [176]. The effects demonstrated in such photonic systems include quantum walks [51, 54] and boson sampling [176].

The non-destructive detection of photons is very difficult to implement and it is certainly a challenge for current experiments. However, there are some techniques which allow to perform this task. For example, measuring an idler beam arising from the creation of pairs of entangled photons or beams via parametric down conversion represents a QND measurement of the signal beam [190]. Moreover, such a setup is consistent with current experiments involving photon pairs [176]. Another possibility for realizing QND of photons is to use a cavity QED system [154]. If the number of photons participating in the multiple-path interference is not too small, the usual destructive detection of few of them can be considered as a measurement that is not fully projective since the surviving photons continue to propagate. This is analogous to the creation of nonclassical states of light and quantum correlations using photon subtraction [140].

In conclusion, we demonstrated that applying quantum optical methods to the study of ultracold gases greatly enriches their physics introducing novel processes and methods for engineering quantum states. The effects we described in this thesis rely on off-resonant light scattering and are therefore non-sensitive to the detailed electronic structure of the atomic system. Therefore, the phenomena and the methods we presented can be applied to a vast range of quantum systems such as molecules (including biological ones) [114], ions [19], atoms in multiple cavities [25, 74, 138, 139, 147, 189], semiconductor [182], multimode cavities [63, 88] or superconducting [58] qubits. This highlights even further the multidisciplinarity of the results presented in this thesis making them promising for applications in future quantum technologies.

References

[1] "A little bit, better," *Economist*, June 20th 2015. [Online]. Available: http://www.economist.com/news/science-and-technology/21654566-after-decades-languishing-laboratory-quantum-computers-are-attracting

[2] J. Abo-Shaeer, C. Raman, J. Vogels, and W. Ketterle, "Observation of vortex lattices in Bose-Einstein condensates," *Science*, vol. 292, no. 5516, pp. 476–479, 2001.

[3] M. Abramowitz and I. A. Stegun, *Handbook of mathematical functions: with formulas, graphs, and mathematical tables*. Courier Corporation, 1964, vol. 55.

[4] F. C. Aguilar, A. F. Ho, and J. Ruostekoski, "Optical signatures of antiferromagnetic ordering of fermionic atoms in an optical lattice," *Physical Review X*, vol. 4, no. 3, p. 031036, 2014.

[5] S. Al-Assam, S. R. Clark, D. Jaksch, and TNT Development team, "Tensor Network Theory Library." [Online]. Available: www.tensornetworktheory.org

[6] A. Altland and B. D. Simons, *Condensed matter field theory*. Cambridge University Press, 2010.

[7] M. Anderson, J. Ensher, M. Matthews, C. Wieman, and E. Cornell, "Observation of Bose-Einstein Condensation in a Dilute Atomic Vapor," *Science*, vol. 269, p. 14, 1995.

[8] M. Andrews, C. Townsend, H.-J. Miesner, D. Durfee, D. Kurn, and W. Ketterle, "Observation of interference between two Bose condensates," *Science*, vol. 275, no. 5300, pp. 637–641, 1997.

[9] G. Angelatos and S. Hughes, "Polariton waveguides from a quantum dot chain in a photonic crystal waveguide: an architecture for waveguide quantum electrodynamics," *Optica*, vol. 3, no. 4, pp. 370–376, 2016.

[10] Y. Ashida and M. Ueda, "Diffraction-Unlimited Position Measurement of Ultracold Atoms in an Optical Lattice," *Physical Review Letters*, vol. 115, no. 9, p. 095301, 2015.

[11] Y. Ashida and M. Ueda, "Multi-Particle Quantum Dynamics under Continuous Observation," *arXiv preprint arXiv:1510.04001*, 2015.

[12] M. Aspelmeyer, T. J. Kippenberg, and F. Marquardt, "Cavity optomechanics," *Reviews of Modern Physics*, vol. 86, no. 4, p. 1391, 2014.

[13] C. Ates, B. Olmos, W. Li, and I. Lesanovsky, “Dissipative Binding of Lattice Bosons through Distance-Selective Pair Loss,” *Physical Review Letters*, vol. 109, no. 23, p. 233003, 2012.

[14] S. Baier, M. Mark, D. Petter, K. Aikawa, L. Chomaz, Z. Cai, M. Baranov, P. Zoller, and F. Ferlaino, “Extended Bose-Hubbard models with ultracold magnetic atoms,” *Science*, vol. 352, no. 6282, pp. 201–205, 2016.

[15] G. Barontini, L. Hohmann, F. Haas, J. Estève, and J. Reichel, “Deterministic generation of multiparticle entanglement by quantum Zeno dynamics,” *Science*, vol. 349, no. 6254, pp. 1317–1321, 2015.

[16] M. Bartenstein, A. Altmeyer, S. Riedl, S. Jochim, C. Chin, J. H. Denschlag, and R. Grimm, “Crossover from a molecular Bose-Einstein condensate to a degenerate Fermi gas,” *Physical Review Letters*, vol. 92, no. 12, p. 120401, 2004.

[17] K. Baumann, C. Guerlin, F. Brennecke, and T. Esslinger, “Dicke quantum phase transition with a superfluid gas in an optical cavity,” *Nature*, vol. 464, pp. 1301–1306, 2010.

[18] J.-S. Bernier, D. Poletti, and C. Kollath, “Dissipative quantum dynamics of fermions in optical lattices: A slave-spin approach,” *Physical Review B*, vol. 90, no. 20, p. 205125, 2014.

[19] R. Blatt and C. F. Roos, “Quantum simulations with trapped ions,” *Nature Physics*, vol. 8, pp. 277–284, 2012.

[20] I. Bloch, “Ultracold quantum gases in optical lattices,” *Nature Physics*, vol. 1, no. 1, pp. 23–30, 2005.

[21] J. K. Block, N. T. Zinner, and G. M. Bruun, “Density wave instabilities of tilted fermionic dipoles in a multilayer geometry,” *New Journal of Physics*, vol. 14, no. 10, p. 105006, 2012.

[22] T. Bourdel, L. Khaykovich, J. Cubizolles, J. Zhang, F. Chevy, M. Teichmann, L. Tarruell, S. Kokkelmans, and C. Salomon, “Experimental study of the BEC-BCS crossover region in lithium 6,” *Physical Review Letters*, vol. 93, no. 5, p. 050401, 2004.

[23] C. C. Bradley, C. Sackett, J. Tollett, and R. G. Hulet, “Evidence of Bose-Einstein condensation in an atomic gas with attractive interactions,” *Physical Review Letters*, vol. 75, no. 9, p. 1687, 1995.

[24] B. Brecht, D. V. Reddy, C. Silberhorn, and M. Raymer, “Photon temporal modes: a complete framework for quantum information science,” *Physical Review X*, vol. 5, no. 4, p. 041017, 2015.

[25] L. Bretheau, P. Campagne-Ibarcq, E. Flurin, F. Mallet, and B. Huard, “Quantum dynamics of an electromagnetic mode that cannot contain N photons,” *Science*, vol. 348, no. 6236, pp. 776–779, 2015.

[26] J. W. Britton, B. C. Sawyer, A. C. Keith, C.-C. J. Wang, J. K. Freericks, H. Uys, M. J. Biercuk, and J. J. Bollinger, "Engineered two-dimensional Ising interactions in a trapped-ion quantum simulator with hundreds of spins," *Nature*, vol. 484, no. 7395, pp. 489–492, 2012.

[27] M. Brune, S. Haroche, J. Raimond, L. Davidovich, and N. Zagury, "Manipulation of photons in a cavity by dispersive atom-field coupling: Quantum-nondemolition measurements and generation of Schrödinger cat states," *Physical Review A*, vol. 45, no. 7, p. 5193, 1992.

[28] M. Brune, F. Schmidt-Kaler, A. Maali, J. Dreyer, E. Hagley, J. Raimond, and S. Haroche, "Quantum Rabi oscillation: A direct test of field quantization in a cavity," *Physical Review Letters*, vol. 76, no. 11, p. 1800, 1996.

[29] H. Büchler, G. Blatter, and W. Zwerger, "Commensurate-incommensurate transition of cold atoms in an optical lattice," *Physical Review Letters*, vol. 90, no. 13, p. 130401, 2003.

[30] C. Budroni, G. Vitagliano, G. Colangelo, R. J. Sewell, O. Gühne, G. Toth, and M. Mitchell, "Quantum Nondemolition Measurement Enables Macroscopic Leggett-Garg Tests," *Physical Review Letters*, vol. 115, no. 20, p. 200403, 2015.

[31] S. Bux, H. Tomczyk, D. Schmidt, P. W. Courteille, N. Piovella, and C. Zimmermann, "Control of matter-wave superradiance with a high-finesse ring cavity," *Physical Review A*, vol. 87, p. 023607, 2013.

[32] S. F. Caballero-Benitez and I. B. Mekhov, "Quantum properties of light scattered from structured many-body phases of ultracold atoms in quantum optical lattices," *New Journal of Physics*, vol. 17, no. 12, p. 123023, 2015.

[33] S. F. Caballero-Benitez and I. B. Mekhov, "Quantum optical lattices for emergent many-body phases of ultracold atoms," *Physical Review Letters*, vol. 115, no. 24, p. 243604, 2015.

[34] S. F. Caballero-Benitez and I. B. Mekhov, "Bond order via light-induced synthetic many-body interactions of ultracold atoms in optical lattices," *New Journal of Physics*, vol. 18, no. 11, p. 113010, 2016.

[35] S. F. Caballero-Benitez, G. Mazzucchi, and I. B. Mekhov, "Quantum simulators based on the global collective light-matter interaction," *Physical Review A*, vol. 93, p. 063632, 2016.

[36] Y. Castin and J. Dalibard, "Relative phase of two Bose-Einstein condensates," *Physical Review A*, vol. 55, no. 6, p. 4330, 1997.

[37] W. Chen and P. Meystre, "Cavity QED characterization of many-body atomic states in double-well potentials: Role of dissipation," *Physical Review A*, vol. 79, no. 4, p. 043801, 2009.

[38] Y. Chen, Z. Yu, and H. Zhai, "Superradiance of Degenerate Fermi Gases in a Cavity," *Physical Review Letters*, vol. 112, p. 143004, 2014.

[39] C. Chin, M. Bartenstein, A. Altmeyer, S. Riedl, S. Jochim, J. H. Denschlag, and R. Grimm, “Observation of the pairing gap in a strongly interacting Fermi gas,” *Science*, vol. 305, no. 5687, pp. 1128–1130, 2004.

[40] A. J. Daley, “Quantum trajectories and open many-body quantum systems,” *Advances in Physics*, vol. 63, no. 2, pp. 77–149, 2014.

[41] B. Dalton, B. Garraway, J. Jeffers, and S. Barnett, “Grassmann phase space theory and the Jaynes-Cummings model,” *Annals of Physics*, vol. 334, pp. 100–141, 2013.

[42] D. A. Dalvit, J. Dziarmaga, and R. Onofrio, “Measurement-induced squeezing of a Bose-Einstein condensate,” *Physical Review A*, vol. 65, no. 3, p. 033620, 2002.

[43] K. B. Davis, M.-O. Mewes, M. R. Andrews, N. Van Druten, D. Durfee, D. Kurn, and W. Ketterle, “Bose-Einstein condensation in a gas of sodium atoms,” *Physical Review Letters*, vol. 75, no. 22, p. 3969, 1995.

[44] B. DeMarco and D. S. Jin, “Onset of Fermi degeneracy in a trapped atomic gas,” *Science*, vol. 285, no. 5434, pp. 1703–1706, 1999.

[45] S. Denny, S. Clark, Y. Laplace, A. Cavalleri, and D. Jaksch, “Proposed parametric cooling of bilayer cuprate superconductors by terahertz excitation,” *Physical Review Letters*, vol. 114, no. 13, p. 137001, 2015.

[46] C. D’Errico, E. Lucioni, L. Tanzi, L. Gori, G. Roux, I. P. McCulloch, T. Giamarchi, M. Inguscio, and G. Modugno, “Observation of a disordered bosonic insulator from weak to strong interactions,” *Physical Review Letters*, vol. 113, no. 9, p. 095301, 2014.

[47] S. Diehl, A. Micheli, A. Kantian, B. Kraus, H. Büchler, and P. Zoller, “Quantum states and phases in driven open quantum systems with cold atoms,” *Nature Physics*, vol. 4, no. 11, pp. 878–883, 2008.

[48] J. S. Douglas, H. Habibian, C.-L. Hung, A. Gorshkov, H. J. Kimble, and D. E. Chang, “Quantum many-body models with cold atoms coupled to photonic crystals,” *Nature Photonics*, vol. 9, no. 5, pp. 326–331, 2015.

[49] K. Eckert, A. Sanpera, M. Lewenstein, E. Polzik *et al.*, “Quantum polarization spectroscopy of ultracold spinor gases,” *Physical Review Letters*, vol. 98, no. 10, p. 100404, 2007.

[50] K. Eckert, O. Romero-Isart, M. Rodriguez, M. Lewenstein, E. S. Polzik, and A. Sanpera, “Quantum Non-Demolition Detection of Strongly Correlated Systems,” *Nature Physics*, vol. 4, no. 1, pp. 50–54, 2008.

[51] T. Eichelkraut, C. Vetter, A. Perez-Leija, H. Moya-Cessa, D. N. Christodoulides, and A. Szameit, “Coherent random walks in free space,” *Optica*, vol. 1, no. 4, pp. 268–271, 2014.

[52] T. J. Elliott, W. Kozlowski, S. Caballero-Benitez, and I. B. Mekhov, “Multipartite entangled spatial modes of ultracold atoms generated and controlled by quantum measurement,” *Physical Review Letters*, vol. 114, no. 11, p. 113604, 2015.

[53] T. J. Elliott, G. Mazzucchi, W. Kozlowski, S. F. Caballero-Benitez, and I. B. Mekhov, "Probing and Manipulating Fermionic and Bosonic Quantum Gases with Quantum Light," *Atoms*, vol. 3, no. 3, pp. 392–406, 2015.

[54] F. Elster, S. Barkhofen, T. Nitsche, J. Novotnỳ, A. Gábris, I. Jex, and C. Silberhorn, "Quantum walk coherences on a dynamical percolation graph," *Scientific Reports*, vol. 5, p. 13495, 2015.

[55] B. Everest, M. R. Hush, and I. Lesanovsky, "Many-body out-of-equilibrium dynamics of hard-core lattice bosons with nonlocal loss," *Physical Review B*, vol. 90, no. 13, p. 134306, 2014.

[56] P. Facchi and S. Pascazio, "Quantum Zeno dynamics: mathematical and physical aspects," *Journal of Physics A: Mathematical and Theoretical*, vol. 41, p. 52, 2009.

[57] S. Fernández-Vidal, G. De Chiara, J. Larson, and G. Morigi, "Quantum ground state of self-organized atomic crystals in optical resonators," *Physical Review A*, vol. 81, no. 4, p. 043407, 2010.

[58] J. M. Fink, R. Bianchetti, M. Baur, M. Göppl, L. Steffen, S. Filipp, P. J. Leek, A. Blais, and A. Wallraff, "Dressed Collective Qubit States and the Tavis-Cummings Model in Circuit QED," *Physical Review Letters*, vol. 103, no. 8, p. 083601, 2009.

[59] F. Fröwis and W. Dür, "Measures of macroscopicity for quantum spin systems," *New Journal of Physics*, vol. 14, no. 9, p. 093039, 2012.

[60] J. Gambetta, A. Blais, D. I. Schuster, A. Wallraff, L. Frunzio, J. Majer, M. H. Devoret, S. M. Girvin, and R. J. Schoelkopf, "Qubit-photon interactions in a cavity: Measurement-induced dephasing and number splitting," *Physical Review A*, vol. 74, no. 4, p. 042318, 2006.

[61] C. Gardiner and P. Zoller, *Quantum noise: a handbook of Markovian and non-Markovian quantum stochastic methods with applications to quantum optics*. Springer Science & Business Media, 2004, vol. 56.

[62] H. Gimperlein, S. Wessel, J. Schmiedmayer, and L. Santos, "Ultracold atoms in optical lattices with random on-site interactions," *Physical Review Letters*, vol. 95, no. 17, p. 170401, 2005.

[63] S. Gopalakrishnan, B. L. Lev, and P. M. Goldbart, "Emergent crystallinity and frustration with Bose-Einstein condensates in multimode cavities," *Nature Physics*, vol. 5, no. 11, pp. 845–850, 2009.

[64] A. V. Gorshkov, J. Otterbach, M. Fleischhauer, T. Pohl, and M. D. Lukin, "Photon-photon interactions via Rydberg blockade," *Physical Review Letters*, vol. 107, no. 13, p. 133602, 2011.

[65] E. M. Graefe, H. J. Korsch, and A. E. Niederle, "Mean-field dynamics of a non-hermitian bose-hubbard dimer," *Phys. Rev. Lett.*, vol. 101, p. 150408, 2008.

[66] D. Greif, G. Jotzu, M. Messer, R. Desbuquois, and T. Esslinger, "Formation and Dynamics of Antiferromagnetic Correlations in Tunable Optical Lattices," *Physical Review Letters*, vol. 115, no. 26, p. 260401, 2015.

[67] M. Greiner, O. Mandel, T. Esslinger, T. W. Hänsch, and I. Bloch, "Quantum phase transition from a superfluid to a Mott insulator in a gas of ultracold atoms," *Nature*, vol. 415, no. 6867, pp. 39–44, 2002.

[68] M. Greiner, C. Regal, J. Stewart, and D. Jin, "Probing pair-correlated fermionic atoms through correlations in atom shot noise," *Physical Review Letters*, vol. 94, no. 11, p. 110401, 2005.

[69] H. Habibian, A. Winter, S. Paganelli, H. Rieger, and G. Morigi, "Bose-glass phases of ultracold atoms due to cavity backaction," *Physical Review Letters*, vol. 110, no. 7, p. 075304, 2013.

[70] H. Habibian, A. Winter, S. Paganelli, H. Rieger, and G. Morigi, "Bose-glass phases of ultracold atoms due to cavity backaction," *Physical Review Letters*, vol. 110, no. 7, p. 075304, 2013.

[71] K. Hammerer, K. Mølmer, E. S. Polzik, and J. I. Cirac, "Light-matter quantum interface," *Physical Review A*, vol. 70, no. 4, p. 044304, 2004.

[72] S. Haroche and J.-M. Raimond, *Exploring the Quantum: Atoms, Cavities, and Photons*. Oxford University Press, 2006.

[73] R. Hart, P. Duarte, T. Yang, and X. Liu, "Observation of antiferromagnetic correlations in the Hubbard model with ultracold atoms," *Nature Letters*, vol. 519, no. 7542, p. 211, 2015.

[74] M. Hartmann, F. Brandao, and M. B. Plenio, "Strongly interacting polaritons in coupled arrays of cavities," *Nature Physics*, vol. 2, pp. 849–855, 2006.

[75] P. Hauke, R. J. Sewell, M. W. Mitchell, and M. Lewenstein, "Quantum control of spin correlations in ultracold lattice gases," *Physical Review A*, vol. 87, no. 2, p. 021601, 2013.

[76] J. Hirsch, "Charge-density-wave to spin-density-wave transition in the extended Hubbard model," *Physical Review Letters*, vol. 53, no. 24, pp. 2327–2330, 1984.

[77] A. Holleczek, O. Barter, A. Rubenok, J. Dilley, P. B. R. Nisbet-Jones, G. Langfahl-Klabes, G. D. Marshall, C. Sparrow, J. L. O'Brien, K. Poulios, A. Kuhn, and J. C. F. Matthews, "Quantum Logic with Cavity Photons From Single Atoms," *Physical Review Letters*, vol. 117, no. 2, p. 023602, 2016.

[78] D. Ivanov and T. Ivanova, "Feedback-enhanced self-organization of atoms in an optical cavity," *Journal of Experimental and Theoretical Physics Letters*, vol. 100, no. 7, pp. 481–485, 2014.

[79] D. A. Ivanov, T. Y. Ivanova, and I. B. Mekhov, "Incoherent quantum feedback control of collective light scattering by Bose-Einstein condensates," *arXiv preprint arXiv:1601.02230*, 2016.

[80] T. Y. Ivanova and D. Ivanov, "Quantum measurement of collective atomic position in optical lattice," *Optics Communications*, vol. 272, no. 1, pp. 148–153, 2007.

[81] D. Jaksch, C. Bruder, J. I. Cirac, C. W. Gardiner, and P. Zoller, "Cold bosonic atoms in optical lattices," *Physical Review Letters*, vol. 81, no. 15, p. 3108, 1998.

[82] J. Javanainen and J. Ruostekoski, "Emergent classicality in continuous quantum measurements," *New Journal of Physics*, vol. 15, no. 1, p. 013005, 2013.

[83] B. Julia-Diaz, E. Torrontegui, J. Martorell, J. G. Muga, and A. Polls, "Fast generation of spin-squeezed states in bosonic Josephson junctions," *Physical Review A*, vol. 86, no. 6, p. 063623, 2012.

[84] J. Kaczmarczyk, H. Weimer, and M. Lemeshko, "Dissipative preparation of antiferromagnetic order in the Fermi-Hubbard model," *New Journal of Physics*, vol. 18, no. 9, p. 093042, 2016.

[85] J. Keeling, M. J. Bhaseen, and B. D. Simons, "Fermionic Superradiance in a Transversely Pumped Optical Cavity," *Physical Review Letters*, vol. 112, p. 143002, 2014.

[86] K. V. Kepesidis and M. J. Hartmann, "Bose-Hubbard model with localized particle losses," *Physical Review A*, vol. 85, no. 6, p. 063620, 2012.

[87] J. Klinder, H. Keßler, M. R. Bakhtiari, M. Thorwart, and A. Hemmerich, "Observation of a superradiant Mott insulator in the Dicke-Hubbard model," *Physical Review Letters*, vol. 115, no. 23, p. 230403, 2015.

[88] A. J. Kollár, A. T. Papageorge, K. Baumann, M. A. Armen, and B. L. Lev, "An adjustable-length cavity and Bose-Einstein condensate apparatus for multimode cavity QED," *New Journal of Physics*, vol. 17, no. 4, p. 043012, 2015.

[89] M. Koschorreck, M. Napolitano, B. Dubost, and M. Mitchell, "Quantum nondemolition measurement of large-spin ensembles by dynamical decoupling," *Physical Review Letters*, vol. 105, no. 9, p. 093602, 2010.

[90] W. Kozlowski, "Competition between Weak Quantum Measurement and Many-Body Dynamics in Ultracold Bosonic Gases," Ph.D. dissertation, University of Oxford, 2016.

[91] W. Kozlowski, S. F. Caballero-Benitez, and I. B. Mekhov, "Probing matter-field and atom-number correlations in optical lattices by global nondestructive addressing," *Physical Review A*, vol. 92, no. 1, p. 013613, 2015.

[92] W. Kozlowski, S. F. Caballero-Benitez, and I. B. Mekhov, "Non-hermitian dynamics in the quantum zeno limit," *Physical Review A*, vol. 94, p. 012123, 2015.

[93] W. Kozlowski, S. F. Caballero-Benitez, and I. B. Mekhov, "Quantum State Reduction by Matter-Phase-Related Measurements in Optical Lattices," *TBP in Scientific Reports, arXiv preprint arXiv:1605.06000*, 2016.

[94] S. Krämer and H. Ritsch, "Self-ordering dynamics of ultracold atoms in multicolored cavity fields," *Physical Review A*, vol. 90, no. 3, p. 033833, 2014.

[95] G. Kurizki, P. Bertet, Y. Kubo, K. Mølmer, D. Petrosyan, P. Rabl, and J. Schmiedmayer, "Quantum technologies with hybrid systems," *Proceedings of the National Academy of Sciences*, vol. 112, no. 13, pp. 3866–3873, 2016.

[96] T. Lahaye, C. Menotti, L. Santos, M. Lewenstein, and T. Pfau, "The physics of dipolar bosonic quantum gases," *Reports on Progress in Physics*, vol. 72, no. 12, p. 126401, 2009.

[97] R. Landig, F. Brennecke, R. Mottl, T. Donner, and T. Esslinger, "Measuring the dynamic structure factor of a quantum gas undergoing a structural phase transition," *Nature Communications*, vol. 6, 2015.

[98] R. Landig, L. Hruby, N. Dogra, M. Landini, R. Mottl, T. Donner, and T. Esslinger, "Quantum phases from competing short- and long-range interactions in an optical lattice," *Nature*, vol. 532, no. 7600, pp. 476–479, 2016.

[99] J. Larson, B. Damski, G. Morigi, and M. Lewenstein, "Mott-insulator states of ultracold atoms in optical resonators," *Physical Review Letters*, vol. 100, no. 5, p. 050401, 2008.

[100] M. D. Lee and J. Ruostekoski, "Classical stochastic measurement trajectories: Bosonic atomic gases in an optical cavity and quantum measurement backaction," *Physical Review A*, vol. 90, no. 2, p. 023628, 2014.

[101] Y.-R. Lee, M.-S. Heo, J.-H. Choi, T. T. Wang, C. A. Christensen, T. M. Rvachov, and W. Ketterle, "Compressibility of an ultracold Fermi gas with repulsive interactions," *Physical Review A*, vol. 85, no. 6, p. 063615, 2012.

[102] J. Léonard, A. Morales, P. Zupancic, T. Esslinger, and T. Donner, "Supersolid formation in a quantum gas breaking continuous translational symmetry," *arXiv preprint arXiv:1609.09053*, 2016.

[103] M. Lewenstein, A. Sanpera, and V. Ahufinger, *Ultracold atoms in optical lattices. Simulating quantum many-body systems.* Oxford: Oxford University Press. xiv, 479 p., 2012.

[104] K. Madison, F. Chevy, W. Wohlleben, and J. Dalibard, "Vortex formation in a stirred Bose-Einstein condensate," *Physical Review Letters*, vol. 84, no. 5, p. 806, 2000.

[105] R. P. Marchildon and A. S. Helmy, "Dispersion-enabled quantum state control in integrated photonics," *Optica*, vol. 3, no. 3, pp. 243–251, 2016.

[106] C. Maschler, I. B. Mekhov, and H. Ritsch, "Ultracold atoms in optical lattices generated by quantized light fields," *The European Physical Journal D*, vol. 46, no. 3, pp. 545–560, 2008.

[107] M. R. Matthews, B. P. Anderson, P. Haljan, D. Hall, C. Wieman, and E. Cornell, "Vortices in a Bose-Einstein condensate," *Physical Review Letters*, vol. 83, no. 13, p. 2498, 1999.

[108] G. Mazzucchi, S. F. Caballero-Benitez, D. A. Ivanov, and I. B. Mekhov, "Quantum optical feedback control for creating strong correlations in many-body systems," *Optica*, vol. 3, no. 11, pp. 1213–1219, 2016.

[109] G. Mazzucchi, S. F. Caballero-Benitez, and I. B. Mekhov, "Quantum measurement-induced antiferromagnetic order and density modulations in ultracold Fermi gases in optical lattices," *Scientific Reports*, vol. 6, p. 31196, 2016.

[110] G. Mazzucchi, W. Kozlowski, S. F. Caballero-Benitez, T. J. Elliott, and I. B. Mekhov, "Quantum measurement-induced dynamics of many-body ultracold bosonic and fermionic systems in optical lattices," *Physical Review A*, vol. 93, no. 2, p. 023632, 2016.

[111] G. Mazzucchi, W. Kozlowski, S. F. Caballero-Benitez, and I. B. Mekhov, "Collective dynamics of multimode bosonic systems induced by weak quantum measurement," *New Journal of Physics*, vol. 18, no. 7, p. 073017, 2016.

[112] R. McConnell, H. Zhang, J. Hu, S. Ćuk, and V. Vuletić, "Entanglement with negative Wigner function of almost 3,000 atoms heralded by one photon," *Nature*, vol. 519, no. 7544, pp. 439–442, 2015.

[113] J. Meineke, J.-P. Brantut, D. Stadler, T. Müller, H. Moritz, and T. Esslinger, "Interferometric measurement of local spin fluctuations in a quantum gas," *Nature Physics*, vol. 8, no. 6, pp. 454–458, 2012.

[114] I. B. Mekhov, "Quantum non-demolition detection of polar molecule complexes: dimers, trimers, tetramers," *Laser Physics*, vol. 23, p. 015501, 2013.

[115] I. B. Mekhov and H. Ritsch, "Quantum optics with quantum gases," *Laser Physics*, vol. 19, no. 4, pp. 610–615, 2009.

[116] I. B. Mekhov and H. Ritsch, "Quantum optics with quantum gases: Controlled state reduction by designed light scattering," *Physical Review A*, vol. 80, no. 1, p. 013604, 2009.

[117] I. B. Mekhov and H. Ritsch, "Quantum nondemolition measurements and state preparation in quantum gases by light detection," *Physical Review Letters*, vol. 102, no. 2, p. 020403, 2009.

[118] I. B. Mekhov and H. Ritsch, "Quantum optical measurements in ultracold gases: Macroscopic Bose-Einstein condensates," *Laser Physics*, vol. 20, no. 3, pp. 694–699, 2010.

[119] I. B. Mekhov and H. Ritsch, "Atom state evolution and collapse in ultracold gases during light scattering into a cavity," *Laser Physics*, vol. 21, no. 8, pp. 1486–1490, 2011.

[120] I. B. Mekhov and H. Ritsch, “Quantum optics with ultracold quantum gases: towards the full quantum regime of the light-matter interaction,” *Journal of Physics B: Atomic, Molecular and Optical Physics*, vol. 45, no. 10, p. 102001, 2012.

[121] I. B. Mekhov, C. Maschler, and H. Ritsch, “Light scattering from ultracold atoms in optical lattices as an optical probe of quantum statistics,” *Physical Review A*, vol. 76, no. 5, p. 053618, 2007.

[122] I. B. Mekhov, C. Maschler, and H. Ritsch, “Cavity-enhanced light scattering in optical lattices to probe atomic quantum statistics,” *Physical Review Letters*, vol. 98, no. 10, p. 100402, 2007.

[123] I. B. Mekhov, C. Maschler, and H. Ritsch, “Probing quantum phases of ultracold atoms in optical lattices by transmission spectra in cavity quantum electrodynamics,” *Nature Physics*, vol. 3, no. 5, pp. 319–323, 2007.

[124] B. Mihaila, S. Gaudio, K. B. Blagoev, A. V. Balatsky, P. B. Littlewood, and D. L. Smith, “Density and spin response functions in ultracold fermionic atom gases,” *Physical Review Letters*, vol. 95, no. 9, p. 090402, 2005.

[125] M. Minkov and V. Savona, “Haldane quantum Hall effect for light in a dynamically modulated array of resonators,” *Optica*, vol. 3, no. 2, pp. 200–206, 2016.

[126] M. Mitrano, A. Cantaluppi, D. Nicoletti, S. Kaiser, A. Perucchi, S. Lupi, P. Di Pietro, D. Pontiroli, M. Riccò, S. R. Clark, D. Jaksch, and A. Cavalleri, “Possible light-induced superconductivity in K_3C_{60} at high temperature,” *Nature*, vol. 530, pp. 461–464, 2016.

[127] H. Miyake, G. A. Siviloglou, G. Puentes, D. E. Pritchard, W. Ketterle, and D. M. Weld, “Bragg Scattering as a Probe of Atomic Wave Functions and Quantum Phase Transitions in Optical Lattices,” *Physical Review Letters*, vol. 107, no. 17, p. 175302, 2011.

[128] D. E. Moncton, J. D. Axe, and F. J. DiSalvo, “Neutron scattering study of the charge-density wave transitions in $2H-\mathrm{TaSe}_2$ and $2H-\mathrm{NbSe}_2$,” *Physical Review B*, vol. 16, pp. 801–819, 1977.

[129] M. G. Moore, O. Zobay, and P. Meystre, “Quantum optics of a Bose-Einstein condensate coupled to a quantized light field,” *Physical Review A*, vol. 60, pp. 1491–1506, 1999.

[130] T. Müller, B. Zimmermann, J. Meineke, J.-P. Brantut, T. Esslinger, and H. Moritz, “Local observation of antibunching in a trapped Fermi gas,” *Physical Review Letters*, vol. 105, no. 4, p. 040401, 2010.

[131] D. Nagy, G. Szirmai, and P. Domokos, “Self-organization of a Bose-Einstein condensate in an optical cavity,” *The European Physical Journal D*, vol. 48, no. 1, pp. 127–137, 2008.

[132] D. Nicoletti, E. Casandruc, Y. Laplace, V. Khanna, C. R. Hunt, S. Kaiser, S. Dhesi, G. Gu, J. Hill, and A. Cavalleri, “Optically induced superconductivity in striped $La2-xBa_xCuO_4$ by polarization-selective excitation in the near infrared,” *Physical Review B*, vol. 90, no. 10, p. 100503, 2014.

[133] A. Niederle and H. Rieger, “Bosons in a two-dimensional bichromatic quasiperiodic potential: Analysis of the disorder in the Bose-Hubbard parameters and phase diagrams,” *Physical Review A*, vol. 91, no. 4, p. 043632, 2015.

[134] T. Nitsche, F. Elster, J. Novotnỳ, A. Gábris, I. Jex, S. Barkhofen, and C. Silberhorn, “Quantum Walks with Dynamical Control: Graph Engineering, Initial State Preparation and State Transfer,” *New Journal of Physics*, vol. 18, no. 6, p. 063017, 2016.

[135] B. Olmos, D. Yu, Y. Singh, F. Schreck, K. Bongs, and I. Lesanovsky, “Long-range interacting many-body systems with alkaline-earth-metal atoms,” *Physical Review Letters*, vol. 110, no. 14, p. 143602, 2013.

[136] D. Oren, Y. Shechtman, M. Mutzafi, Y. C. Eldar, and M. Segev, “Sparsity-based recovery of three-photon quantum states from two-fold correlations,” *Optica*, vol. 3, no. 3, pp. 226–232, 2016.

[137] J. Otterbach, M. Moos, D. Muth, and M. Fleischhauer, “Wigner crystallization of single photons in cold Rydberg ensembles,” *Physical Review Letters*, vol. 111, no. 11, p. 113001, 2013.

[138] A. Palacios-Laloy, F. Mallet, F. Nguyen, P. Bertet, D. Vion, D. Esteve, and A. N. Korotkov, “Experimental violation of a Bell/’s inequality in time with weak measurement,” *Nature Physics*, vol. 6, no. 6, pp. 442–447, 2010.

[139] G. Paraoanu, “Generalized partial measurements,” *Europhysics Letters*, vol. 93, no. 6, p. 64002, 2011.

[140] M. Paternostro, “Engineering nonclassicality in a mechanical system through photon subtraction,” *Physical Review Letters*, vol. 106, no. 18, p. 183601, 2011.

[141] Y. S. Patil, S. Chakram, and M. Vengalattore, “Measurement-Induced Localization of an Ultracold Lattice Gas,” *Physical Review Letters*, vol. 115, no. 14, p. 140402, 2015.

[142] M. K. Pedersen, J. J. W. H. Sorensen, M. C. Tichy, and J. F. Sherson, “Many-body state engineering using measurements and fixed unitary dynamics,” *New Journal of Physics*, vol. 16, no. 11, p. 113038, 2014.

[143] C. J. Pethick and H. Smith, *Bose-Einstein condensation in dilute gases*. Cambridge university press, 2002.

[144] F. Piazza and H. Ritsch, “Self-Ordered Limit Cycles, Chaos, and Phase Slippage with a Superfluid inside an Optical Resonator,” *Physical Review Letters*, vol. 115, no. 16, p. 163601, 2015.

[145] F. Piazza and P. Strack, "Umklapp Superradiance with a Collisionless Quantum Degenerate Fermi Gas," *Physical Review Letters*, vol. 112, p. 143003, 2014.

[146] H. Pichler, A. Daley, and P. Zoller, "Nonequilibrium dynamics of bosonic atoms in optical lattices: Decoherence of many-body states due to spontaneous emission," *Physical Review A*, vol. 82, no. 6, p. 063605, 2010.

[147] J.-M. Pirkkalainen, S. Cho, J. Li, G. Paraoanu, P. Hakonen, and M. Sillanpää, "Hybrid circuit cavity quantum electrodynamics with a micromechanical resonator," *Nature*, vol. 494, no. 7436, pp. 211–215, 2013.

[148] T. Pohl, H. R. Sadeghpour, and P. Schmelcher, "Cold and ultracold Rydberg atoms in strong magnetic fields," *Physics Reports*, vol. 484, no. 6, pp. 181–229, 2009.

[149] L. Pollet, "Recent developments in quantum Monte Carlo simulations with applications for cold gases," *Reports on Progress in Physics*, vol. 75, no. 9, p. 094501, 2012.

[150] D. Porras and J. I. Cirac, "Quantum manipulation of trapped ions in two dimensional Coulomb crystals," *Physical Review Letters*, vol. 96, no. 25, p. 250501, 2006.

[151] J.-M. Raimond, C. Sayrin, S. Gleyzes, I. Dotsenko, M. Brune, S. Haroche, P. Facchi, and S. Pascazio, "Phase space tweezers for tailoring cavity fields by quantum Zeno dynamics," *Physical Review Letters*, vol. 105, no. 21, p. 213601, 2010.

[152] J.-M. Raimond, P. Facchi, B. Peaudecerf, S. Pascazio, C. Sayrin, I. Dotsenko, S. Gleyzes, M. Brune, and S. Haroche, "Quantum Zeno dynamics of a field in a cavity," *Physical Review A*, vol. 86, no. 3, p. 032120, 2012.

[153] C. Regal, M. Greiner, and D. S. Jin, "Observation of resonance condensation of fermionic atom pairs," *Physical Review Letters*, vol. 92, no. 4, p. 040403, 2004.

[154] A. Reiserer, S. Ritter, and G. Rempe, "Nondestructive detection of an optical photon," *Science*, vol. 342, no. 6164, pp. 1349–1351, 2013.

[155] H. Ritsch, P. Domokos, F. Brennecke, and T. Esslinger, "Cold atoms in cavity-generated dynamical optical potentials," *Reviews of Modern Physics*, vol. 85, no. 2, p. 553, 2013.

[156] G. Roati, C. D?Errico, L. Fallani, M. Fattori, C. Fort, M. Zaccanti, G. Modugno, M. Modugno, and M. Inguscio, "Anderson localization of a non-interacting Bose-Einstein condensate," *Nature*, vol. 453, no. 7197, pp. 895–898, 2008.

[157] B. Rogers, M. Paternostro, J. F. Sherson, and G. De Chiara, "Characterization of Bose-Hubbard models with quantum nondemolition measurements," *Physical Review A*, vol. 90, no. 4, p. 043618, 2014.

[158] O. Romero-Isart, M. Rizzi, C. Muschik, E. Polzik, M. Lewenstein, and A. Sanpera, "Quantum memory assisted probing of dynamical spin correlations," *Physical Review Letters*, vol. 108, no. 6, p. 065302, 2012.

[159] L. E. Rosales-Zárate and P. Drummond, "Probabilistic Q-function distributions in fermionic phase-space," *New Journal of Physics*, vol. 17, no. 3, p. 032002, 2015.

[160] T. Roscilde, M. Rodriguez, K. Eckert, O. Romero-Isart, M. Lewenstein, E. Polzik, and A. Sanpera, "Quantum polarization spectroscopy of correlations in attractive fermionic gases," *New Journal of Physics*, vol. 11, no. 5, p. 055041, 2009.

[161] J. Ruostekoski, *Lecture Notes in Physics: Directions in Quantum Optics.* Springer, 2001.

[162] T. Rybarczyk, B. Peaudecerf, M. Penasa, S. Gerlich, B. Julsgaard, K. Mølmer, S. Gleyzes, M. Brune, J. Raimond, S. Haroche *et al.*, "Forward-backward analysis of the photon-number evolution in a cavity," *Physical Review A*, vol. 91, no. 6, p. 062116, 2015.

[163] L. Sanchez-Palencia and M. Lewenstein, "Disordered quantum gases under control," *Nature Physics*, vol. 6, no. 2, pp. 87–95, 2010.

[164] C. Sanner, E. J. Su, A. Keshet, R. Gommers, Y.-i. Shin, W. Huang, and W. Ketterle, "Suppression of density fluctuations in a quantum degenerate Fermi gas," *Physical Review Letters*, vol. 105, no. 4, p. 040402, 2010.

[165] C. Sanner, E. J. Su, A. Keshet, W. Huang, J. Gillen, R. Gommers, and W. Ketterle, "Speckle imaging of spin fluctuations in a strongly interacting Fermi gas," *Physical Review Letters*, vol. 106, no. 1, p. 010402, 2011.

[166] C. Sanner, E. J. Su, W. Huang, A. Keshet, J. Gillen, and W. Ketterle, "Correlations and pair formation in a repulsively interacting Fermi gas," *Physical Review Letters*, vol. 108, no. 24, p. 240404, 2012.

[167] S. Sarkar, S. Langer, J. Schachenmayer, and A. J. Daley, "Light scattering and dissipative dynamics of many fermionic atoms in an optical lattice," *Physical Review A*, vol. 90, no. 2, p. 023618, 2014.

[168] C. Sayrin, I. Dotsenko, X. Zhou, B. Peaudecerf, T. Rybarczyk, S. Gleyzes, P. Rouchon, M. Mirrahimi, H. Amini, M. Brune *et al.*, "Real-time quantum feedback prepares and stabilizes photon number states," *Nature*, vol. 477, no. 7362, pp. 73–77, 2011.

[169] F. Schäfer, I. Herrera, S. Cherukattil, C. Lovecchio, F. Cataliotti, F. Caruso, and A. Smerzi, "Experimental realization of quantum Zeno dynamics," *Nature Communications*, vol. 5, p. 3194, 2014.

[170] P. Schauß, J. Zeiher, T. Fukuhara, S. Hild, M. Cheneau, T. Macrì, T. Pohl, I. Bloch, and C. Gross, "Crystallization in Ising quantum magnets," *Science*, vol. 347, no. 6229, pp. 1455–1458, 2015.

[171] D. Schmidt, H. Tomczyk, S. Slama, and C. Zimmermann, "Dynamical Instability of a Bose-Einstein Condensate in an Optical Ring Resonator," *Physical Review Letters*, vol. 112, no. 11, p. 115302, 2014.

[172] U. Schollwöck, "The density-matrix renormalization group," *Reviews of Modern Physics*, vol. 77, pp. 259–315, 2005.

[173] F. Schreck, L. Khaykovich, K. Corwin, G. Ferrari, T. Bourdel, J. Cubizolles, and C. Salomon, "Quasipure Bose-Einstein condensate immersed in a Fermi sea," *Physical Review Letters*, vol. 87, no. 8, p. 080403, 2001.

[174] S. Schütz, S. B. Jäger, and G. Morigi, "Thermodynamics and dynamics of atomic self-organization in an optical cavity," *Physical Review A*, vol. 92, no. 6, p. 063808, 2015.

[175] A. Signoles, A. Facon, D. Grosso, I. Dotsenko, S. Haroche, J.-M. Raimond, M. Brune, and S. Gleyzes, "Confined quantum Zeno dynamics of a watched atomic arrow," *Nature Physics*, vol. 5, pp. 715–719, 2014.

[176] J. B. Spring, B. J. Metcalf, P. C. Humphreys, W. S. Kolthammer, X.-M. Jin, M. Barbieri, A. Datta, N. Thomas-Peter, N. K. Langford, D. Kundys *et al.*, "Boson sampling on a photonic chip," *Science*, vol. 339, no. 6121, pp. 798–801, 2013.

[177] P. Strack and S. Sachdev, "Dicke quantum spin glass of atoms and photons," *Physical Review Letters*, vol. 107, no. 27, p. 277202, 2011.

[178] N. Syassen, D. M. Bauer, M. Lettner, T. Volz, D. Dietze, J. J. Garcia-Ripoll, J. I. Cirac, G. Rempe, and S. Dürr, "Strong Dissipation Inhibits Losses and Induces Correlations in Cold Molecular Gases," *Science*, vol. 320, pp. 1329–1331, 2008.

[179] S. Szigeti, M. Hush, A. Carvalho, and J. Hope, "Continuous measurement feedback control of a Bose-Einstein condensate using phase-contrast imaging," *Physical Review A*, vol. 80, no. 1, p. 013614, 2009.

[180] L. Tarruell, D. Greif, T. Uehlinger, G. Jotzu, and T. Esslinger, "Creating, moving and merging Dirac points with a Fermi gas in a tunable honeycomb lattice," *Nature*, vol. 483, no. 7389, pp. 302–305, 2012.

[181] M. Tinkham, *Introduction to superconductivity.* Courier Corporation, 1996.

[182] B. Trauzettel, D. V. Bulaev, D. Loss, and G. Burkards, "Spin qubits in graphene quantum dots," *Nature Physics*, vol. 3, pp. 192–196, 2007.

[183] A. G. Truscott, K. E. Strecker, W. I. McAlexander, G. B. Partridge, and R. G. Hulet, "Observation of Fermi pressure in a gas of trapped atoms," *Science*, vol. 291, no. 5513, pp. 2570–2572, 2001.

[184] I. Vidanović, D. Cocks, and W. Hofstetter, "Dissipation through localized loss in bosonic systems with long-range interactions," *Physical Review A*, vol. 89, no. 5, p. 053614, 2014.

[185] B. Vlastakis, G. Kirchmair, Z. Leghtas, S. E. Nigg, L. Frunzio, S. M. Girvin, M. Mirrahimi, M. H. Devoret, and R. J. Schoelkopf, "Deterministically encoding quantum information using 100-photon Schrödinger cat states," *Science*, vol. 342, no. 6158, pp. 607–610, 2013.

[186] A. C. J. Wade, J. F. Sherson, and K. Mølmer, "Squeezing and Entanglement of Density Oscillations in a Bose-Einstein Condensate," *Physical Review Letters*, vol. 115, p. 060401, 2015.

[187] F. Weig and W. Zwerger, "Optical detection of a BCS transition of lithium-6 in harmonic traps," *Europhysics Letters*, vol. 49, no. 3, p. 282, 2000.

[188] C. Weitenberg, P. Schauß, T. Fukuhara, M. Cheneau, M. Endres, I. Bloch, and S. Kuhr, "Coherent Light Scattering from a Two-Dimensional Mott Insulator," *Physical Review Letters*, vol. 106, no. 21, pp. 2–5, 2011.

[189] T. White, J. Mutus, J. Dressel, J. Kelly, R. Barends, E. Jeffrey, D. Sank, A. Megrant, B. CampBell, Y. Chen *et al.*, "Violating the Bell-Leggett-Garg inequality with weak measurement of an entangled state," *NPJ Quantum Information*, vol. 2, p. 15022, 2016.

[190] H. M. Wiseman and G. J. Milburn, *Quantum measurement and control.* Cambridge University Press, 2009.

[191] M. Wolke, J. Klinner, H. Kessler, and A. Hemmerich, "Cavity cooling below the recoil limit," *Science*, vol. 337, pp. 85–87, 2012.

[192] W. Yi, S. Diehl, A. Daley, and P. Zoller, "Driven-dissipative many-body pairing states for cold fermionic atoms in an optical lattice," *New Journal of Physics*, vol. 14, no. 5, p. 055002, 2012.

[193] J. Zeiher, R. van Bijnen, P. Schauß, S. Hild, J.-y. Choi, T. Pohl, I. Bloch, and C. Gross, "Many-body interferometry of a Rydberg-dressed spin lattice," *Nature Physics*, vol. advance on., 2016.

[194] Q. Zhang, M. Lou, X. Li, J. L. Reno, W. Pan, J. D. Watson, M. J. Manfra, and J. Kono, "Collective non-perturbative coupling of 2D electrons with high-quality-factor terahertz cavity photons," *Nature Physics*, vol. 12, no. 11, pp. 1005–1011, 2016.

[195] M. W. Zwierlein, J. R. Abo-Shaeer, A. Schirotzek, C. H. Schunck, and W. Ketterle, "Vortices and superfluidity in a strongly interacting Fermi gas," *Nature*, vol. 435, no. 7045, pp. 1047–1051, 2005.

[196] M. Zwierlein, C. Stan, C. Schunck, S. Raupach, A. Kerman, and W. Ketterle, "Condensation of pairs of fermionic atoms near a Feshbach resonance," *Physical Review Letters*, vol. 92, no. 12, p. 120403, 2004.